DISSERTATION

MODIFICATIONS OF IMAGING SPECTROSCOPY METHODS FOR INCREASED SPATIAL AND TEMPORAL CONSISTENCY: A CASE STUDY OF CHANGE IN LEAFY SPURGE DISTRIBUTION BETWEEN 1999 AND 2001 IN THEODORE ROOSEVELT NATIONAL PARK, NORTH DAKOTA

Submitted by

Kathleen Burke Dudek

Forest, Rangeland, and Watershed Stewardship Department

In partial fulfillment of the requirements

For the Degree of Doctor of Philosophy

Colorado State University

Fort Collins, Colorado

Summer 2006

COLORADO STATE UNIVERSITY

May 1, 2006

WE HEREBY RECOMMEND THAT THE DISSERTATION PREPARED UNDER OUR SUPERVISION BY KATHLEEN BURKE DUDEK ENTITLED MODIFICATIONS OF IMAGING SPECTROSCOPY METHODS FOR INCREASED SPATIAL AND TEMPORAL CONSISTENCY: A CASE STUDY OF CHANGE IN LEAFY SPURGE DISTRIBUTION BETWEEN 1999 AND 2001 IN THEODORE ROOSEVELT NATIONAL PARK, NORTH DAKOTA BE ACCEPTED AS FULFILLING IN PART REQUIREMENTS FOR THE DEGREE OF DOCTOR OF PHILOSOPHY.

Committee on Graduate Work

Adviser

Department Head

ABSTRACT OF DISSERTATION

MODIFICATIONS OF IMAGING SPECTROSCOPY METHODS FOR INCREASED SPATIAL AND TEMPORAL CONSISTENCY: A CASE STUDY OF CHANGE IN LEAFY SPURGE DISTRIBUTION BETWEEN 1999 AND 2001 IN THEODORE ROOSEVELT NATIONAL PARK, NORTH DAKOTA

From the early 1800's, when leafy spurge (*Euphorbia esula* L.) was first introduced into North America, it has spread throughout the northern Great Plains where it is currently a significant management concern. Accurate, rapid location is critical for economical control of this noxious weed, while repeatable measurements are necessary for successful temporal monitoring of infestations. Leafy spurge has been located using imaging spectroscopy (hyperspectral remote sensing) in the past, but the development and dissemination of standardized mapping procedures that produce consistent multi-temporal maps has been absent. In this study Airborne Visible/Infrared Imaging Spectrometer (AVIRIS) data, collected in 1999 and 2001 over Theodore Roosevelt National Park, North Dakota, were used to locate leafy spurge. Mapping strategies were developed that improved the consistency of maps over time and space, increasing their suitability for monitoring change in spurge.

Commercial software and algorithms were used to process the AVIRIS imagery. Published image-preprocessing methods, mapping algorithms, as well as field and image-derived spectral libraries were tested to determine which were most successful for consistent, repeatable mapping of leafy spurge over time and space. Best results were obtained using: 1) NDVI masking; 2) cross-track illumination correction; 3) an image-derived spectral library; and 4) the mixture-tuned matched filtering (MTMF) algorithm. The application of the algorithm was modified to standardize processing and to eliminate threshold decisions; the image-derived spectral library was also refined to eliminate additional variability in the spurge maps. The image-processing

protocol appears to be consistent and reliable both temporally and spatially. Primary (spurge dominant), secondary (spurge non-dominant), and fraction maps were produced, as well as area-wide vegetation maps.

Map accuracies were analyzed with three independent reference data sets (points, polygons, and grids) using standard confusion matrices as well as regression between field-measured percent spurge and image-derived matched filter ("abundance") scores. To accommodate offset between imagery and reference points, accuracies were recalculated after applying a majority filter, and after applying buffers ranging from 1-5 pixels wide around the classified data. The similar accuracy values of identical ground areas mapped from adjacent flight lines, as well as good visual correspondence, indicated that the mapping method produced consistent maps. Overall accuracy of area-wide spurge maps varied from 39% to 82%. Registration problems accounted for some of this variability. Some validation data and methods were more appropriate for assessing the detailed maps of small, fragmented patches of leafy spurge as well. Different mapping strategies produced very different spurge maps, another source of accuracy variation. Validation data for hyperspectral remote sensing should be carefully selected. Accuracy based on standard confusion matrices was sensitive to: 1) registration offsets between field and image locations; 2) modification of analytical methods; and 3) quality of the reference data.

The vegetation maps of identical areas produced from adjacent flight lines varied when the difference in sensor viewing angles was at a maximum. Less spurge was classified at the highest viewing angles, regardless of viewing direction. Initial corrections for cross-track illumination differences were insufficient to entirely eliminate the effects of viewing geometry on the spurge classifications. Higher order corrections appeared to model the cross-track variation more closely. The first order correction may account for the discrepancies in the classification between high and low view angles. Overall accuracy was only 1% higher with the second and third order corrections; user's accuracy was 13% higher, however, and the visual correspondence between maps and reference data improved with the higher order corrections. Better modeling of

cross-track variation improved the consistency of the spurge classifications where differences were related to sensor viewing angle.

Regional patterns of change in spurge, as well as some localized trends, were evident based on differenced primary, present/absent maps. Post-classification change detection indicated a 41% decrease in leafy spurge within the park, and 36% in the surrounding National Grasslands, private range, and agricultural land between 1999 and 2001. The change in spurge fraction was calculated, but pixel-by-pixel change detection was difficult to interpret due to misalignment between multi-temporal images and slight shifts in the position of the flight lines between 1999 and 2001.

The leafy spurge change maps produced from consistent multi-temporal maps will be valuable for land managers tasked with monitoring leafy spurge, as well as assessing the effect of different biological and chemical controls in order to optimize the management of leafy spurge on a regional scale.

Kathleen Burke Dudek
Forest, Rangeland, and Watershed Stewardship Department
Colorado State University
Fort Collins, CO 80523
Summer 2006

ACKNOWLEDGEMENTS

I would like to acknowledge and thank my committee members, Drs. Ray Hunt, George Beck, and Melinda Laituiri for their guidance and support, and particularly my advisor, Dr. Michael Lefsky, who graciously "absorbed" me mid-project following the retirement and moves of several committee members. I would also like to thank Dr. Roger Hoffer for introducing me to the remote sensing field, my colleague Ray Kokaly for many helpful discussions, and Gerry Anderson (ARS), Steve Hager (NPS), and Carol Mladinich, Karl Brown, and Susan Stitt (USGS) for assistance and access to the AVIRIS data.

Friends and family, near and far, provided invaluable encouragement. I would especially like to thank my mom Anne Burke, my husband Ed, and daughters Sara and Amanda, for their love and support over the course of this project.

Finally, I would like to thank my mentor, colleague and friend Dr. Ralph Root, my best friend Kathy, mother-in-law Mary Ellen, and my dad John Burke, all of whom passed away during the course of this project. Their wonderful words of support and encouragement have stayed with me and prodded me along, even after they were gone.

TABLE OF CONTENTS

LIST OF FIGURES

LIST OF TABLES

CHAPTER 1

INTRODUCTION AND BACKGROUND: THE LEAFY SPURGE PROBLEM

INTRODUCTION

Imaging spectroscopy, or hyperspectral remote sensing, has been used predominantly for research-oriented studies. Recently there has been increased interest in exploiting this technology to address applied problems. The applied work has lagged behind in part due to the complex interactive processing that hyperspectral imagery requires, and the associated steep learning curve. Land managers that stand to benefit from the technology may be aware of the potential advantages of imaging spectroscopy for ecological monitoring, but are often not well versed in hyperspectral processing and analysis. Current processing methods require specialized training or extensive experience in remote sensing in order to determine the most appropriate methods to use, to make informed decisions during interactive processing, and to determine whether results are realistic and accurate. Land managers working in and around Theodore Roosevelt National Park, North Dakota (THRO), have been interested in exploring imaging spectroscopy as a potential tool for temporal monitoring of the invasive weed, leafy spurge (*Euphorbia esula* L.). This invasive is a serious ecological and economic problem in the northern Great Plains States and Prairie Provinces of Canada (Bangsund et al., 1993; Beck, 1996; Leitch et al., 1994; Wallace et al., 1992).

Leafy spurge background/history. Leafy spurge was introduced into North America from Eastern Europe in the early 1800's from immigrant seed stocks, soil in ship ballast, and cereal/grass seed introductions (Dunn, 1985). This aggressive perennial weed has since spread through at least 30 states and all Canadian provinces except Newfoundland. Leafy spurge is currently a major concern of ranchers, farmers, and land managers in the northern plains and

prairies of the United States and Canada where it has spread at an alarming rate over the last 50 years (Watson, 1985).

Leafy spurge in THRO. Infestation of Theodore Roosevelt National Park began in the late 1960's. By 1970 leafy spurge occupied 13 ha within the park, and by 1993, 704 to 1700 ha, or roughly 4-10% of the Park was infested (Anderson et al., 1996; O'Neill et al., 2000). Although other alien species have invaded the park, leafy spurge is the invasive weed with the greatest potential for damage to native ecosystems, and the control of this weed is currently the primary management concern within the park (Andrascik, 1994; Root et al., 2002).

The leafy spurge problem. Once established, leafy spurge can form extensive, dense monocultures (Figure 1.1), out-competing all other vegetation (Callihan et al., 1990). Expansion of the weed is exacerbated by the rapid rate of spread, and possible allelopathic characteristics of leafy spurge (Steenhagen, 1977; Manners, 1983; Galitz, 1994; Messersmith et al., 1985). Patch expansion, for example, averages 0.6 to 1.8 m/yr in undisturbed areas, while higher rates of up to 6 m/yr are reported where soil has been tilled or otherwise disturbed (Watson, 1985; Galitz, 1994). The horizontal roots of single plants are estimated to spread up to 5 m diameter per year (Selleck et al., 1962; Lym, 1998). These persistent, deep, rhizotomous roots contain large nutrient reserves that can sustain the plant for years (Sisk and Tysdal-Sisk, 2000; Lym, 1998). Roots can grow to depths of 8 m (~ 26 ft) or more, where they can tap water reserves that are inaccessible to more shallow-rooted plants during periods of drought stress (Lajeunesse et al., 1997; Galitz, 1994). Hardy, water tolerant seeds are easily disseminated via "explosive" dispersal up to 5 m (Lym and Messersmith, 1984), and are transported aerially, as well as by streams, animals, birds, insects, and humans. Seeds can remain viable in soil up to eight years, and the weed is easily established in nearly all soil types (Sisk and Tysdal-Sisk, 2000). Leafy spurge grows in diverse environments, ranging from semiarid zones to shallow aquatic marshes, open sun or shaded understory, and both northern and southern slope exposures (Callihan et al., 1990; Galitz, 1994). This weed is a perennial species that is among the earliest emergent plants in spring, giving leafy spurge an additional competitive advantage (Lajeunesse et al., 1997).

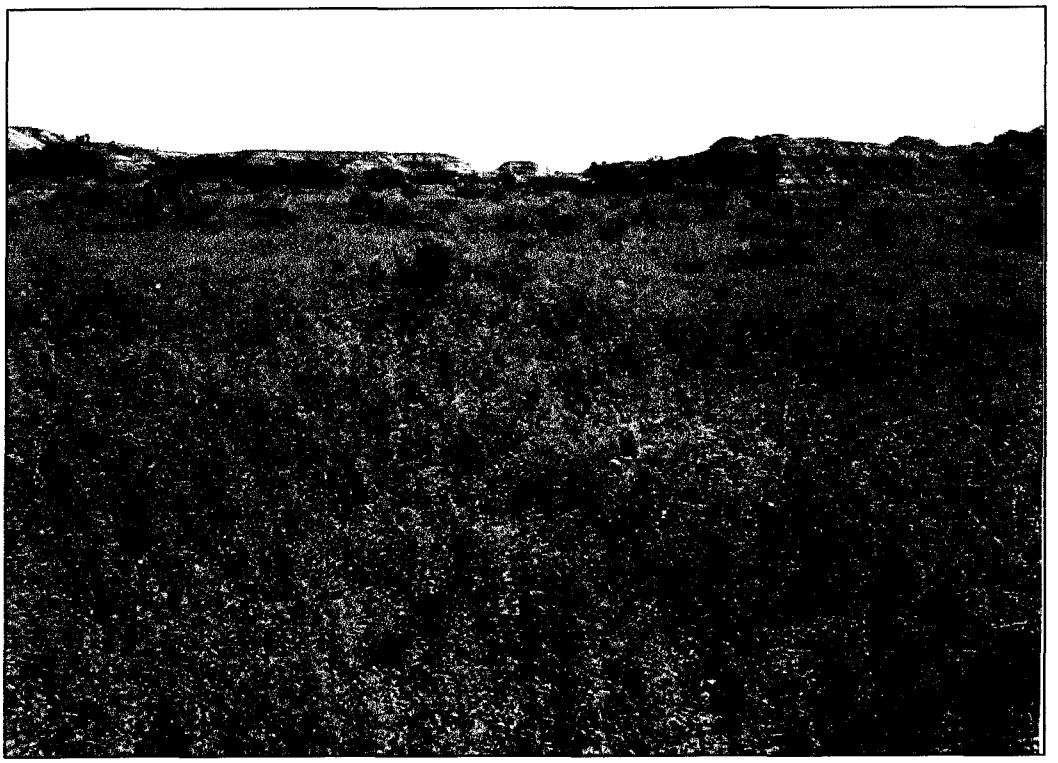

Figure 1.1. Leafy spurge monoculture. View is to the south, southeast over the "no man's land" region of THRO, showing nearly total replacement of native grasses and forbs by leafy spurge. The characteristic yellow-green bracts are well-developed in this photograph.

Economic impacts. Leafy spurge acreage has doubled every 10 years, and in some cases every five years over the past 30 years in parts of the Northern Great Plains (Wallace et al., 1992; Anderson et al., 2000), with a corresponding reduction of cattle carrying capacity of infested rangeland anywhere from 50% to 100% loss of carrying capacity (Beck, 1996). An 80% leafy spurge infestation can result in 100% loss of carrying capacity, rendering the land essentially useless for forage (Leitch et al., 1994). Callihan et al. (1990) reported annual estimated losses to the cattle and hay industries in the U.S. to be $7 million, in spite of annual expenditures of approximately $10 million to control leafy spurge. Others have estimated total direct and indirect impacts of leafy spurge in the northern Great Plains region to be in excess of several tens of millions of dollars (Wallace et al., 1992).

Health implications. The entire plant contains a milky latex substance that can irritate skin and can cause blindness in humans with direct eye contact. If ingested it acts as an irritant, emetic, and purgative, which can result in weakness or death in cattle. Leafy spurge also contains euphorbon, an alkaloid that is toxic to cattle and is known to be a co-carcinogen (Callihan et al., 1990; Lym, 1998).

Ecological impacts. The loss of native plant diversity as leafy spurge establishes monocultures is considered a potential threat to native wildlife, and may alter natural soil and surface water characteristics and quality as well (Bangsund et al., 1993). Following infestation by leafy spurge in THRO, localized extinction of some rarer species, as well as a reduction in cover of common native species, was noted (Cogan and Butler, 1999; Andrascik, 1994).

Leafy spurge control. Several states list this species as one of the top ten most noxious weeds (Van Bruggen, 1992), a designation that requires legally mandated control by landowners and land managers of federal protected lands (Lajeunesse, 1997; Andrascik, 1994). Control of leafy spurge is very difficult, but is best accomplished using well-coordinated integrated pest management strategies (Lym and Zollinger, 1995). This involves a combination of treatments that are tailored to the specific environment (i.e., rangeland, agricultural, or "wildland", including forests, recreation areas, wilderness, meadow, riparian and lacustrine banks, etc.). The treatments generally include various combinations of physical, chemical, and biological control

agents. Examples include tillage, mowing, watering and limiting over-grazing to encourage competitive grass growth, various herbicides with optimally-timed application (which depends on the type of chemical used), grazing by sheep and goats, and release of flea beetles and other insects that feed on the roots and foliage of leafy spurge (Wallace et al., 1992). Leafy spurge can recover from almost any control effort (Beck, 1996), therefore successful management requires a combination of control methods applied minimally over 4-5 years, followed by ongoing monitoring. Elimination of leafy spurge is particularly difficult in national parks and other protected lands where control methods are somewhat restricted. Established infestations are generally not economically feasible to control, although this depends on the relative value of the infested land. Efforts are often focused, therefore, on preventing new smaller infestations from becoming established (Chicoine et al., 1985).

Leafy spurge control efforts in THRO. Biological and chemical methods have been used in an attempt to control the weed in THRO (Andrascik, 1994; Root et al., 2002; Anderson et al., 2003). Flea beetles are the natural control agent in eastern Europe, the native habitat of leafy spurge. Several species of flea beetles, including *Aphthona lacertosa*, *Aphthona nigriscutis*, and *Aphthona flava* have been imported, propagated, and released in THRO and the surrounding grasslands and range, beginning with small-scale releases in 1987 (Andrascik, 1994). The gall midge (*Spurgia esulae*) is another biological control agent that has been released in the area (Lym and Zollinger, 1995). The chemical agents 2,4-D and picloram (Tordon), have been applied to localized heavy infestations (THRO Natural History Page; Lym and Zollinger, 1995). Tracking the success of the different control agents based on the change in spatial distribution of the weed over time is necessary for cost-effective management of the weed. Control strategies have been successful in some areas of the park, yet leafy spurge continues to spread rapidly in other regions within and surrounding the park. In some areas of the park the infested acreage has doubled in 5 years, in spite of aggressive control efforts (Anderson et al., 1999). In addition, the likelihood or rate of return to successfully treated areas is currently unclear. Greatest success with control is realized if the infestation is treated within the first years of establishment (Lajeunesse et al., 1997).

In order to successfully track leafy spurge both spatially and temporally, timely location of nascent patches, as well as ongoing monitoring of established and treated patches is necessary. Monitoring methods ideally should cover large areas accurately, rapidly, and economically, and be repeatable over time and space. In addition, the analytical techniques that are employed should be unambiguous and standardized. This weed is difficult to monitor over large areas, however, in part due to the wide range of ecological niches it can inhabit.

Remote sensing to monitor leafy spurge. Remote sensing is effective for rapidly acquiring data over large inaccessible areas, and is therefore well suited to monitoring landscapes. Several types of remotely acquired data have been used to monitor land cover over THRO (Kokaly et al., 2001c; Anderson et al., 1997; Everitt et al., 1995) and other areas that have been infested with leafy spurge (Elliston and Miller, 1987; Myhre, 1987). Each type of sensor has advantages and disadvantages, including tradeoffs in spectral and spatial resolution, repeatability, cost, availability, reliability, and accuracy. Aerial and satellite-borne sensors have been used with some success for mapping vegetation at community and species levels (Everitt et al., 1992; 1993; Gausman et al., 1977; Graetz et al., 1983; Tueller, 1982), as well as for identification of certain invasive species (Anderson et al., 1993; Dewey et al., 1991; Everitt et al., 1994). The ability to differentiate the weed from associated plant species that are often spectrally similar is critical for monitoring leafy spurge.

Aerial photography use and limitations. Aerial photography has been used to produce vegetation maps, including distribution of leafy spurge over THRO and other infested areas (Birdsall et al., 1995; Miller and Elliston, 1987; Myhre, 1983; Dalsted et al., 1988). Aerial campaigns from both 1993 and 1998 were used specifically over THRO and the surrounding grasslands to monitor the distribution of the weed and the progress of control efforts over time (Anderson et al., 1999). The use of aerial photographs for mapping has some limitations, however. Maps from 1993 over THRO were produced from 1:10,000 and 1:15,000 scale photographs (Anderson et al., 1996). The resolution of the photographs was as fine as 0.3 m, however small stands or areas with leafy spurge density less than 25% were not detectable. Dalsted et al. (1988) evaluated the accuracy of photo-interpreted maps of leafy spurge that were

produced from imagery collected at several resolutions, and determined that very low altitude imagery, collected at 457 m (1500 ft), was required to produce maps with 80% accuracy for leafy spurge identification. Within-canopy shadowing, shadowing from other types of vegetation, soil background with high reflectance, leafy spurge interspersed with other herbaceous species or partially obscured by brush and trees, limited bract development, and deeply incised topography all contributed to the inability to detect small, sparse leafy spurge stands with aerial photography (Anderson et al., 1995; Anderson et al., 1996). Only established, dense stands could be delineated from the photographs. Either photography with finer spatial resolution or imagery with enhanced spectral resolution is required to locate smaller, nascent patches of leafy spurge. Similar requirements are necessary for monitoring subtle change in distribution over time, and the success of different control methods. Photography at the necessary large scale and with sufficient aerial coverage would be prohibitively expensive for large-area surveys and monitoring. Additional drawbacks to photo-interpreted maps include the requirement for many photos and labor-intensive manual interpretation. It is difficult to automate change detection with aerial photography, which would require digitizing, geo-referencing, and mosaicing many photographs to obtain sufficient aerial coverage. An additional problem with photo-interpreted maps is the difficulty correlating changes between dates due to the subjective analysis of different photo-interpreters. This can lead to significant temporal inconsistencies in maps and errors in change detection (Root et al., 2002; DiPietro et al., 2002; Birdsall et al, 1995; Birdsall et al., 1997). Several of the above limitations could be resolved by using other remote sensing systems, including digital broad and narrow band optical sensors.

Imaging spectroscopy to monitor spurge. Imaging spectroscopy has been used successfully to map some plant species (see Chapter 2 and included references). This type of data is unique by virtue of the narrow, contiguous bands that record radiance data within the optical region of the spectrum, allowing materials to be differentiated based on subtle, narrow absorption features, as well as subtle differences in the overall shape of spectral curves throughout the full spectral range of the sensors. In this way, very subtle differences in

reflectance may be detected that are not evident visually on standard color or color-infrared photography, or on imagery collected from broad-band multi-spectral scanners.

Potential problems with hyperspectral monitoring of spurge. Although many of the imaging spectroscopy studies have shown that certain plant species can be identified remotely, quantitative accuracy results, including both producer's and user's accuracies, were typically not included. Some studies have reported a correlation to ground reference data for the species of interest, but have not included information regarding user's accuracy (i.e., they have not reported over-classification errors). Early test maps produced during this study indicated significant problems with over-classification of leafy spurge, while known occurrences of leafy spurge appeared to be correctly represented on the maps. From a management perspective, omission error for spurge would be the greatest concern, and should be minimized. Significant commission errors, however, will also compromise the interpretation of results and subsequent control operations. The primary issue is not whether leafy spurge can be detected with imaging spectroscopy, but rather can over-classification of the weed be minimized, while still correctly mapping fragmented, small, or sparse patches. To be effective operationally, maps produced from remotely sensed data should be as accurate as possible, in terms of both producer's and user's accuracies. Producer's accuracy indicates how well the map captured all the material on the ground, or what percentage of the spurge reference data was omitted from the map (omission error), while user's accuracy is an indication of the quantity of the material on the map that is actually the same material on the ground, or how frequently other material on the ground was incorrectly mapped as leafy spurge (commission error) (Lillesand and Kiefer, 2000). For effective monitoring it is critical to minimize omission errors (i.e., it is crucial to locate all areas of leafy spurge, including new and low density patches). Ideally, commission errors would be minimized as well in order to avoid erroneously mapping other species as leafy spurge. From a management perspective, however, over-classification is not as critical as under-classifying and missing areas of leafy spurge that require treatment.

For imaging spectroscopy to be an effective temporal management tool, high precision (i.e., repeatable and reliable results both temporally and spatially) is required in addition to high

accuracy (Birdsall et al., 1997). High-precision mapping ideally would require only nominal ground surveys if the mapping was completed using a detailed, standardized processing protocol that is insensitive to the interpretive input of the image analyst, or requires guiding with ground reference data.

OBJECTIVES

AVIRIS images, obtained over THRO in 1999 and 2001, were used to determine whether hyperspectral data are reliable for mapping leafy spurge, and whether the data are appropriate for accurately detecting change in the distribution of the invasive weed over a 2-year period. Specific objectives of this study included:

1) selecting a processing stream that yields the most accurate leafy spurge maps with respect to both omission and commission errors;

2) refining the processing methods to increase automation and standardization in order to improve consistency of maps for more successful multi-temporal analyses;

3) testing the applicability and suitability of using multi-spectral accuracy techniques for analyses of maps produced from hyperspectral data;

4) producing leafy spurge change maps for delivery to THRO managers to facilitate tracking and treatment of the weed.

The ultimate goal of this study was to develop a temporally consistent, more automated, less subjective and interactive processing stream. It should be portable over time and space, using only commercially available software and algorithms to produce accurate maps of leafy spurge infestations to facilitate weed management decisions. Issues or problems that are encountered when transitioning from experimental to applied hyperspectral remote sensing were specifically addressed.

To streamline, refine, and automate current processing, standard hyperspectral mapping methods were tested and modified within a commercially available software package, the Environment for Visualizing Images (ENVI). Specific objectives for the refinement included: decreasing the influence of analyst decisions or bias; decreasing the need for expert knowledge

or advanced training; decreasing the needed ground support or reference data; and decreasing the need for conclusive *a priori* knowledge of the target endmember spectrum. Realizing these objectives would facilitate the production of accurate and consistent multi-temporal maps, and would avoid misinterpretations due to apparent change (e.g., changes that are a reflection of differences in processing rather than real land cover change). The intent of this work was to develop specific strategies to facilitate and streamline analysis, and eliminate interactive steps that require in-depth knowledge of the ground to guide processing decisions. If the need for advanced training or experience can be minimized, imaging spectroscopy could become a more widespread tool for ecological and other applied work.

CHAPTER 2

HYPERSPECTRAL LITERATURE REVIEW: THEORY, APPLICATIONS, AND THE AVIRIS SENSOR

HISTORY OF IMAGING SPECTROSCOPY

The early development of imaging spectroscopy can be traced to an experimental profiling spectroradiometer that was used in orbit on the space shuttle in 1981 (Goetz, 1989). This test bolstered interest in the nascent imaging spectrometer program at NASA JPL. The Airborne Imaging Spectrometer (AIS) was the first high spectral resolution imaging spectrometer to be developed from this program (Vane et al., 1984; Goetz et al., 1985). This planar array detector was a one-dimensional profiler that covered a range from 1.2-2.4 μm. This was first flown in 1983 as a "proof of concept" test sensor (van der Meer, 1999). The relative success of this sensor for mineralogical mapping was justification for the development of a more advanced sensor, the Airborne Visible Infrared Imaging Spectrometer (AVIRIS). This is a whisk-broom sensor, with detectors arranged in a line array that allows simultaneous collection of 224-spectral band, co-registered images (Green et al., 1998). This was designed to be a well-calibrated instrument that could be used for routine collection of imagery for many applications (van der Meer, 1999). The sensor was first flown in 1987, and currently remains operational. Both AIS and AVIRIS were developed by NASA JPL for research purposes. In the last 10 to 15 years, however, a host of other hyperspectral sensors have been developed by government agencies and commercial enterprises. Several of these are no longer operational, or funding was rescinded, while others have been successfully operating and upgraded over the last several years. Currently AVIRIS, HyMap, Probe-1, AISA, and CASI (Compact Airborne Spectrographic Imager) are most commonly used. The Hyperion sensor, a proof of concept space-borne optical hyperspectral imager, is carried on the Earth Observation-1 (EO-1) platform that was launched in

2000. This is the first orbiting hyperspectral instrument available to research scientists, and has lasted well beyond its intended operational life. This sensor is still functional and is being run in an extended mission for which tasked data requests can be made (http://eo1.usgs.gov/hyperion.php).

ADVANTAGES OF HYPERSPECTRAL

The term hyperspectral has been applied to imaging spectrometers because they allow "over-determined sampling" (Boardman and Green, 2000), i.e., there tends to be correlation between many of the contiguous bands. Due to this correlation, many of these bands are considered redundant by some authors (Price, 1997). Others consider the large number of bands to be critical to the success of these sensors for detailed materials mapping (Boardman and Green, 2000). The goal of over-sampling is to obtain sufficient data to discriminate similar, but unique absorption features in different materials. The narrow, 5-20 nm, contiguous bands of hyperspectral sensors allow sampling of spectral characteristics of materials at a level that, following calibration, approaches the quality of spectral measurements that are obtained with laboratory spectrometers (Clark and Swayze, 1996). With these sensors, materials that display unique absorption features can be isolated and differentiated that would otherwise be masked using broad-band, discontinuous-sampling sensors. With imaging spectrometers it is possible to discriminate between very similar, but still unique materials, because the data are more detailed, and closely spaced unique diagnostic features of different materials can be differentiated. Similar materials can be distinguished due to a combination of the development and refinement of more sophisticated algorithms for extracting information, and the increased signal-to-noise ratio (SNR) that has accompanied the upgrade of airborne hyperspectral sensors (Figure 2.1) (Clark and Swayze, 1996; Asner, 2004). Data with higher signal-to-noise ratio (SNR) have allowed finer, more subtle features to be distinguished. The ability to discriminate between minerals, for example, is directly proportional to SNR, and the current high SNR has allowed the creation of mineral maps that are considered more complex and detailed than most standard geologic maps that have been published (Clark and Swayze, 1996). Even when very subtle changes within

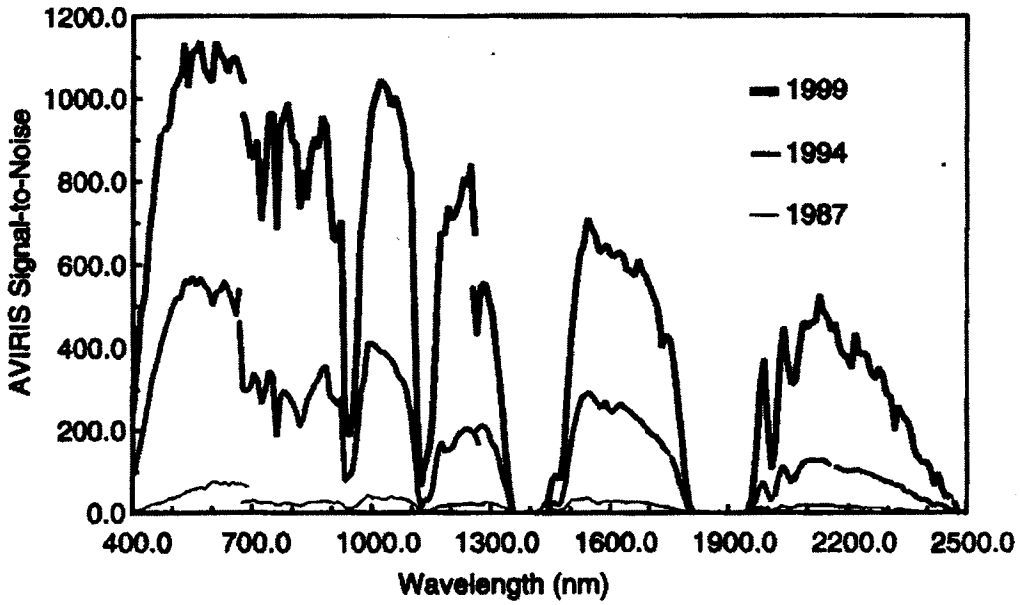

Figure 2.1. Change in signal to noise ratio (SNR) of AVIRIS between 1987 and 1999. Figure from Asner, 2004.

single ions alter absorption features, the differences can be detected if the SNR is sufficiently high. Presumably, then, these sensors should also allow better discrimination of subtle, and possibly significant, spectral differences between vegetation species and/or assemblages. This assumes that the natural variation in spectra from a single species can be distinguished from inter-species spectral variability.

BACKGROUND: CAUSES OF ABSORPTIONS

Diagnostic absorption features that form the basis of imaging spectroscopy are the expression of the interaction between matter and energy (Hunt, 1980). The absorption features result from energy transitions in molecules that are caused by either electronic transitions or molecular vibrations. The electronic effects are seen predominantly at shorter wavelengths, from UV into the NIR up to about 1μm. These include crystal field effects, color centers, band gap/conduction bands, and charge transfer between ions (Gaffey et al., 1993; Clark, 1995; Clark, 1999; Hunt, 1980). Vibrational effects dominate in the infrared region, particularly the 2-2.5 μm range. In reflectance spectroscopy within the optical infrared region of the electromagnetic spectrum, these vibrations generally involve overtones or combinations of fundamental bending or stretching vibrations that occur primarily at longer wavelengths (Curan, 1989; Gaffey et al., 1993; Hunt, 1980; Kokaly and Clark, 1999). Photons entering a material supply the energy that causes these electronic or vibrational effects, which occur at specific wavelengths that are determined by the molecular structure and chemical composition of the material. Energy consumed in these electronic or vibrational processes results in a decrease in the energy available for reflection at these wavelengths, which is manifested as an absorption feature or dip in reflected energy.

The absorption features may display characteristic shapes, depths, and widths that are unique due to the structural and chemical characteristics of materials (Clark, 1999). These features are typically characterized by the wavelength of maximum absorption, and the full width of the feature measured at ½ the maximum depth of the feature (FWHM) (Figure 2.2). Depth is measured from the "shoulder" of the feature, the point where the individual feature breaks from

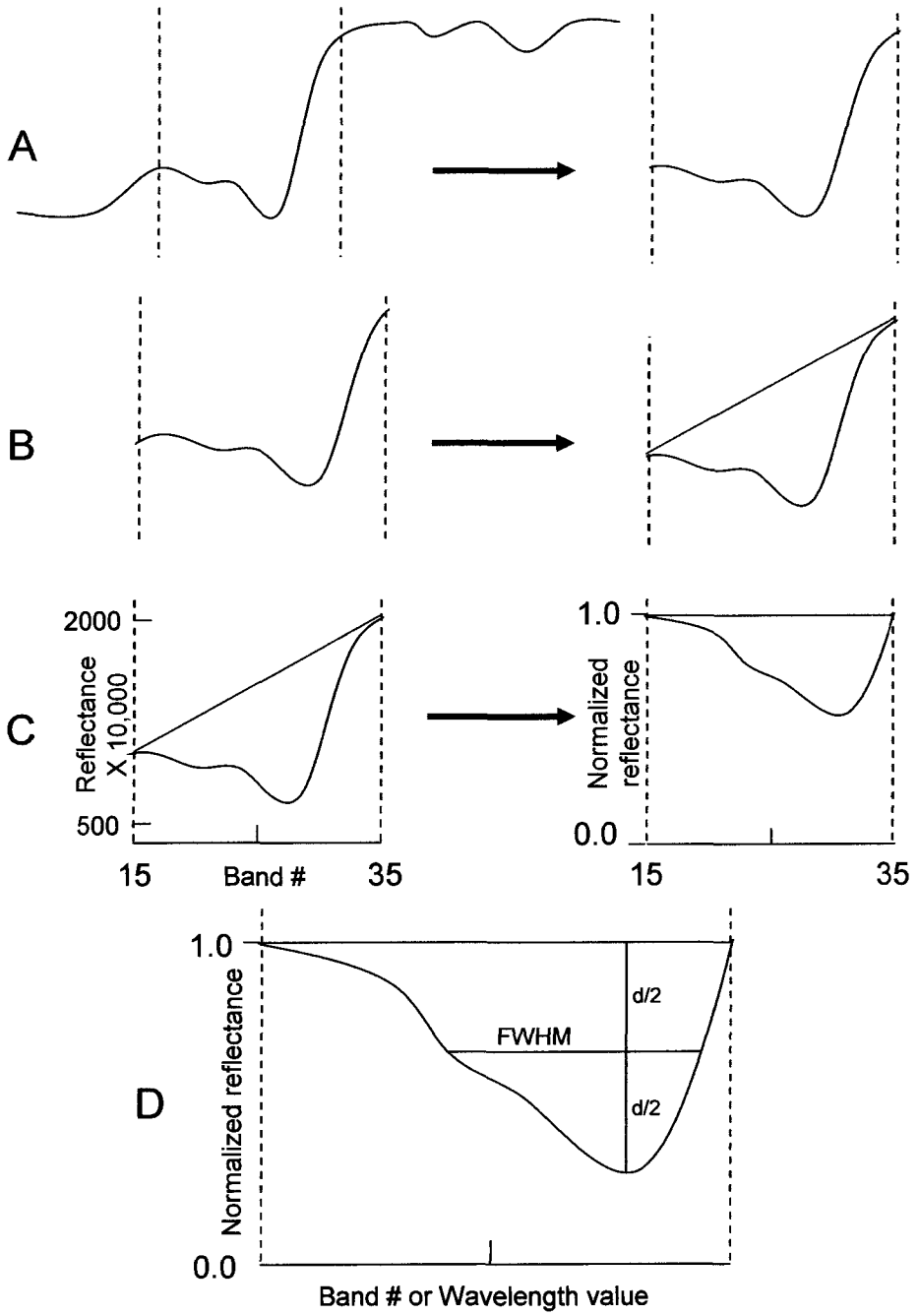

Figure 2.2. Full width at half maximum depth (FWHM) of an isolated absorption feature. The FWHM is derived from the following steps: a spectral subset is created to isolate the feature of interest (A); a continuum is added between the two "shoulders" of the feature (red line in B); the continuum is removed by dividing the continuum reflectance value (for each band) by the reflectance value of the spectrum of the absorption feature (for each band) (C). The wavelength of maximum depth is located, the maximum depth is divided in half, and the width of the feature is measured at the ½ depth to give the full width at half maximum depth of the absorption feature (D).

the continuum, where the continuum represents a much broader diagnostic general background reflectance across the full wavelength range of the sensor (Ingle, 1988). The FWHM of absorption features for most solid earth materials is greater than the 5-10 nm bandwidth of most hyperspectral sensors, typically between 20-40 nm (van der Meer, 1999; Goetz, 1989). Theoretically, therefore, if materials exhibit absorption features, they can be detected with imaging spectrometers. This assumes that the sensor has a sufficiently high signal-to-noise ratio (SNR), a sufficiently broad spectral range to include a diagnostic feature, sufficient abundance of the material within a given pixel to be detected, and that the absorption feature for the pure material itself is strong enough to be detected (Clark, 1995).

IMAGING SPECTROSCOPY DEFINED

When the reflectance spectra of materials are tied to the spatial distribution or coordinates of the materials, this becomes the unique combination that defines imaging spectroscopy. A visual representation of surface materials is organized in a 2-dimensional spatial array of reflectance of the material or mixture within each pixel. For each pixel, the reflectance of materials in 224 distinct wavelength regions can be displayed simultaneously, and represents the third dimension that is often associated with imaging spectroscopy, and that is represented in the standard, three-dimensional hyperspectral cube (Figure 2.3). Plotting the reflectance of all wavelength bands reconstructs a nearly continuous spectral reflectance curve throughout the optical region of the electromagnetic spectrum. This is referred to as the "Z-profile" in ENVI software. The combination of spectroscopy and imaging is also referred to as imaging spectrometry, hyperspectral remote sensing, or hyperspectral imaging.

APPLICATIONS, GENERAL

During the early development of imaging spectroscopy the initial focus was on exploitation of well-defined, unique spectral features that are associated with certain minerals. Early geologic applications included clay-mineral mapping and mapping of alteration minerals that are indicative of acidic drainage (Goetz and Rowan, 1981; Goetz et al., 1985; Hutsinpillar, 1988;

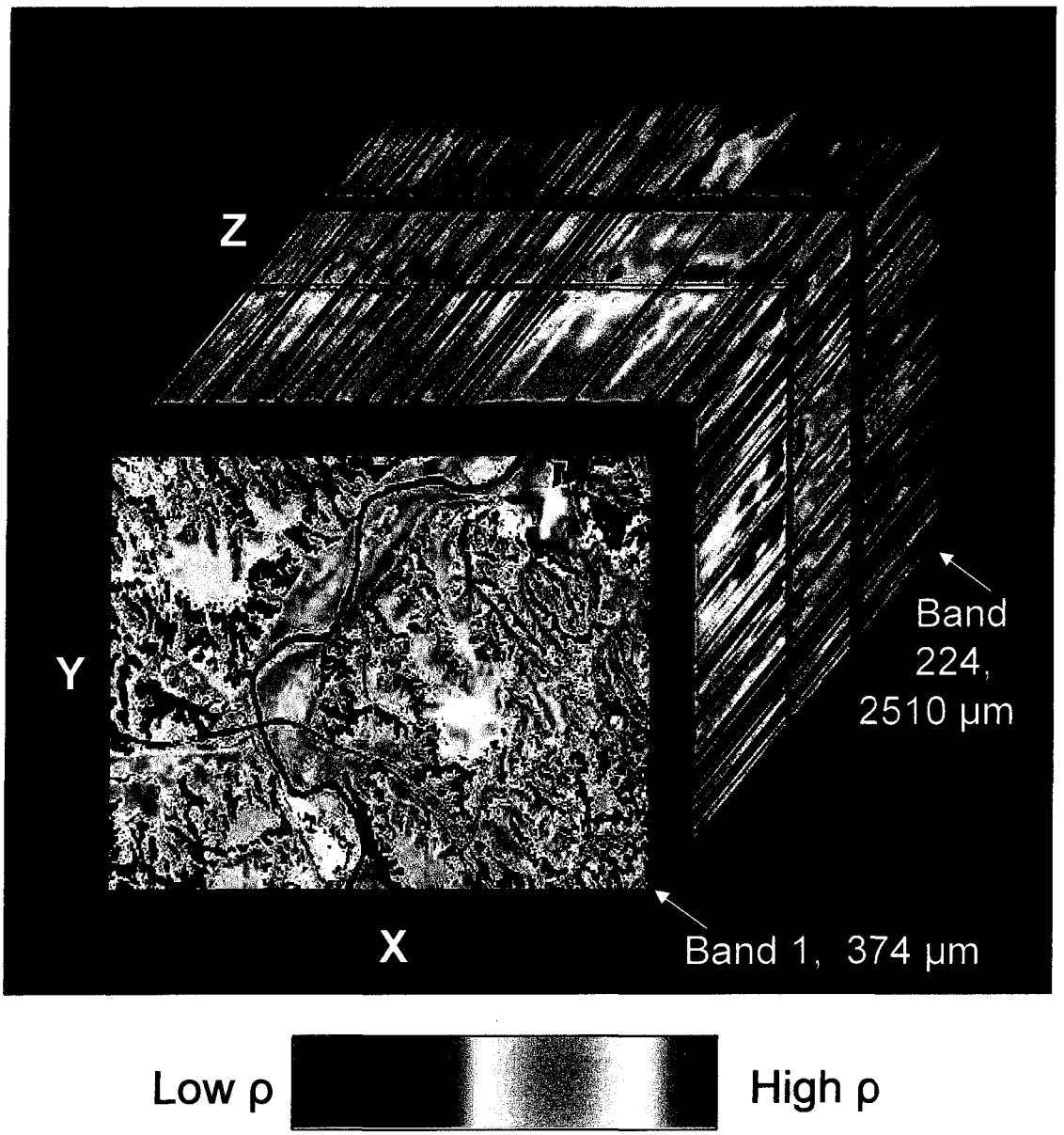

Figure 2.3. 3-D, hyperspectral image cube. Subset from image collected over THRO in 2001. X, Y define pixel location, Z dimension shows the general magnitude of the spectral response (in this image, reflectance, ρ) for each of the 224 wavelength bands. Image is displayed with bands: 45 at 769 nm (red); 35 at 674 nm (green); and 20 at 558 nm (blue). Non-vegetated areas that were excluded from the analysis are masked (black) and show no spectral response in this figure.

King et al., 1995; Kruse, 1988; Swayze et al., 1996; Farrand and Harsanyi, 1993; Vane and Goetz, 1993). Over the last decade, the use of this technology has expanded to include many urban, atmospheric, agricultural, forestry, ecological, snow and ice hydrology, hazards, coastal and inland waters, and other natural resources investigations (Green et al., 1998). Specific examples are included in Table 2.1. A wide range of vegetation studies have been completed as well (see following sections).

FEASIBILITY STUDIES BASED ON FIELD/LABORATORY SPECTROSCOPY

Laboratory and field spectroscopy have been used in feasibility studies for potential applications of remote imaging spectroscopy in many different disciplines. Diverse examples include the identification of contaminated soil in floodplains (Kooistra et al., 2001), paleoseismic trench stratigraphy (Ragona et al., 2003), and locating potential archeological sites within the cryosphere (Clarke et al., 2003). Laboratory and field spectroscopy have also been used in vegetation studies to address the potential of remote imaging spectrometers for studying and monitoring vegetation.

Some of these plant investigations were experimental and performed under controlled laboratory conditions, while others examined the spectral characteristics of vegetation in natural field settings. Species discrimination, detecting vegetation stress, and evaluating the palatability of leaves for marsupials (Dury et al., 2001) are examples of field-based vegetation research. Many projects attempted to establish a relationship between variation in foliar chemistry (either natural or manipulated experimentally) and unique spectral characteristics. Biophysical characteristics of canopies (i.e., leaf area index (LAI), leaf angle distribution (LAD), or biomass) that were derived from field spectra have also been correlated to traditional field measurements of these characteristics.

A long-standing goal of remote sensing is the identification of individual species or vegetation assemblages. Laboratory and field spectroscopy have demonstrated that many plant species display subtle but unique variation in reflectance that may be diagnostic for specific vegetation, or minimally allow vegetation within some environments to be differentiated. The

Natural and anthropogenic hazardous materials: Natural asbestos deposits Contamination from vermiculite mine Swelling soils Salt-affected soils Acid mine drainage Surface land mines; mine affected areas associated with buried land mines	 Swayze et al., 2004 Clark et al., 2003 Chabrillat et al., 2000 Whiting and Ustin, 1999; Ben-Dor et al., 2002; Metternicht and Zinck, 2003 Hauff et al., 2003 Dalton et al., 1998 Swayze et al., 1998 Anger, 2003
Natural hazard assessment Rock weathering and landslides Hyrothermal alteration and risk of volcanic mass-wasting	 Riaza et al., 2001 Crowley and Zimbelman, 1997
Hydrologic and water quality studies Fluvial turbidity and sediment transport Snow area and grain size for climate and hydrology Toxic phytoplankton blooms Eutrophication of waterways Estuarine wetland characterization and monitoring Coral reef health Mapping stream habitats and depth	 Wass et al., 1997 Painter et al., 2003 Sathyendranath et al., 1997 Karaska et al., 2004 Dalton et al., 2004 Kruse, 2003 Legeiter et al., 2004; Marcus et al., 2003
Urban applications Road conditions Urban land cover identification	 Herold et al., 2004 Herold and Roberts, 2004; Kruse et al., 2004
Characterization of geothermal systems	Kennedy-Bowdoin et al., 2003
Earth analogs for Mars research	Guiness et al, 2003; Farrand et al., 2004
Fire temperature tracking during forest fires September 11 World Trade Center fire temperature estimates	Gao et al., 1993; Green, 1996 Clark et al., 2001; Green et al., 2002

Table 2.1. Example hyperspectral studies and citations (see text for description of example vegetation projects and citations).

hope with these field/laboratory studies is that diagnostic spectra can be identified, which can be used in libraries for supervised mapping of species with remote sensor data. This assumes that the spectra are universally unique, which may not be valid in all cases.

Species have been successfully discriminated using field spectroscopy. In a study by Van Aardt and Wynne (2001), for example, stepwise discriminant analysis, canonical discriminant analysis, and normal discriminant analysis of field spectra were used to differentiate between field spectra that were collected over six associated southern tree species. In a similar field study, Schmidt and Skidmore (2003) successfully discriminated between coastal wetland species based on spectral characteristics.

Early (pre-visual) detection of vegetation stress is another goal of remote sensing. Experimental field studies using spectroscopy have produced some promising results. Carter (1993) and Carter and Miller (1994) induced stress in vegetation by applying different herbicide treatments to evaluate whether stress responses could be detected in reflectance spectra, and whether stress-related spectral responses varied with the source of the stressing agent, or with species. Smith et al. (2004) correlated vegetation stress, that was induced by experimental exposure to gas, to derivative ratios calculated from spectral reflectance curves to determine whether it may be feasible to use hyperspectral remote sensing for detection of gas leaks near pipelines, based on early detection of stress in the surrounding vegetation.

The relationship between both natural and experimentally induced chemical variability (i.e., Dungan et al., 1996), measured with standard laboratory wet chemical analyses, and the corresponding spectral response of vegetation have been examined using a variety of methods. Empirical relationships between leaf chlorophyll, water, lignin, cellulose, and nitrogen concentrations and the spectral characteristics of vegetation have been established with statistical methods.

Laboratory measurements of foliar chemistry have also been used to develop general models of leaf optical properties, that may be used to predict leaf and optical properties based on spectral data. Curan et al. (1992), for example, attempted to correlate the concentration of a number of chemical constituents in fresh whole leaves, including chlorophyll, protein, starch,

sugar, and water, to the derivative reflectance of selected wavelength bands from the visible and NIR. Band selection was based on stepwise regression, and the equation that was generated from the regression was tested as a general method for estimating foliar chemistry composition and concentration. Kokaly and Clark (1999) and Kokaly (2000) completed detailed laboratory analyses of dried leaves that correlated chemical analyses with spectral characteristics in an effort to identify the physical basis for differences in spectra (i.e., specific nitrogen-containing bonds in plant proteins). They used continuum removal (Ingle, 1988) and normalization of specific absorption features in conjunction with stepwise multiple regression to identify specific bands within absorption features that were correlated to plant chemistry. Their analyses included numerous species from several locations. This was an early investigation into the possibility of developing a general algorithm for estimating nitrogen content from the reflectance spectra of dried vegetation. Jacquemond and Baret (1990) used the relationship between laboratory-measured foliar chemistry and spectral response to develop and then refine (Jacquemond et al., 1996) a radiative transfer model (PROSPECT) that can be inverted to derive leaf biochemical properties based on remote measurements of reflectance and transmittance.

NIR/red ratios and the first derivative values of field spectral measurements have been compared to laboratory measured chlorophyll concentrations to determine which method provides a better estimate of chlorophyll content in reservoirs (Han and Rundquist, 1997). These authors determined that the ratio was not a useful predictor of chlorophyll. The first derivative was more closely correlated with actual chlorophyll measurements, but the correlation varied with wavelength. This was a preliminary investigation to evaluate the potential of imaging spectroscopy for evaluating trophic status of water bodies for water quality assessment.

Field-based spectral measurements at the canopy level have also been correlated with biophysical properties such as LAI, LAD, and biomass. Hurcom et al. (1996) used factor analysis to decompose canopy spectra into "factors" that were believed to represent critical variables affecting spectral response, in hopes of eventually separating or modeling spectrally mixed vegetation signatures into groups representing differences in biophysical characteristics, rather than standard vegetation classes (i.e., species).

Asner (1998) completed detailed field studies regarding the effect of isolated canopy components (i.e., green foliage, standing litter, and woody stems) on field spectral measurements. He also identified the portions of the optical region where each of these components exhibited the greatest effect. Canopy properties were also isolated to determine the relative impact on spectral characteristics. LAI and LAD variation produced the largest effects, except in areas where vegetation was sparse. In these areas percent vegetation cover and soil reflectance significantly affected spectra as well.

Several authors have extended their field spectroscopy research to include temporal changes in vegetation chemistry, and the correlation to temporal variation in spectra. For example, Asrar et al. (1989) measured the diurnal and seasonal (phenological) spectral response of vegetation within a tallgrass prairie ecosystem. The study included analysis of diurnal characteristics as a function of canopy structure as well (specifically erectophile versus planophile responses, with planophiles generally exhibiting more uniform spectral responses in the visible through mid IR). They correlated field-measured spectra with simulated spectral responses based on a radiative transfer model. The model correctly simulated diurnal responses, but the modeled seasonal responses varied from those measured in the field. Laba et al. (2005) used a derivative analysis (first, second, and higher order derivatives) of field spectra collected periodically over a single growing season to determine whether optimal dates for discriminating invasive wetland plant species could be identified. Seasonal differences were noted, with best discrimination between species when spectral measurements were collected in August. These results are site-specific, however, and it is unlikely that they can be generally applied to other locations.

Many of these laboratory and field studies were successful, while the results from others were not as promising. Species discrimination and stress detection were successful under the conditions presented. The results of extraction of biochemical and biophysical parameters were more variable. Analytical methods used in these studies varied and could account for some of the inconsistent results. In general, however, correlation between leaf-level measurements and spectral response was stronger than correlation between canopy measurements and spectral

response. At the canopy level, there are additional confounding factors, including multiple scattering, and non-linear mixing within the canopy. Field measurements of parameters such as LAI may be more variable than leaf chemical concentrations that are analyzed in the lab. As a result it can be difficult to model canopy reflectance accurately enough to be suitable for generalized models that can be applied to different species, seasons, and ecosystems.

The unique difficulties associated with transitioning from field measurements to airborne or spaceborne sensors and monitoring often were not addressed in the field projects. Atmospheric effects, sensor quality, and spectral resolution (relative to field spectrometers) may limit successful scaling up for some applications. It can be difficult to extrapolate field analyses to remote systems due to the coarser spatial resolution of imaging spectrometers. Mixed spectral signatures within individual pixels from the remote imagery adds complexity to remote analyses, and difficulties with precise geo-location of the remote data, or accurately co-locating reference data and imagery could limit some applications as well.

APPLICATIONS OF REMOTE IMAGING SPECTROSCOPY TO TERRESTRIAL VEGETATION

Remote sensing of vegetation, loosely termed "ecological" remote sensing (Asner, 1998; Curran, 2001) can be challenging due to variation in the proportion of individual species, structure of the canopy, ratio of live versus senescent vegetation, and plant health or stress. These factors add variability to canopy level spectral measurements and increase the complexity of identifying plant species characteristics with certainty (Asner and Lobell, 2000). Detailed plant mapping is also difficult due to temporal differences in spectral response that are related to diurnal, seasonal, and phenological changes. In addition, the spectral response of plants is sensitive to illumination and sensor view angles (Schott, 1997). Plants can exhibit complex, non-linearly mixed spectral signatures resulting from the combination of live vegetation, litter, soil, and shadow, and multiple scattering within the canopy (Ray and Murray, 1996). Additional unique characteristics of a species or individual plant are imparted by microscopic structure, macroscopic leaf structure and area, as well as plant canopy structure, which add a complex additional dimension to the final spectral response received by a sensor (Asner, 1998; Asner et al., 1998a).

In spite of the difficulties in scaling up to landscape-scale imaging spectroscopy, many unique vegetation applications have been successful. Because plants are principally composed of the same chemical components, however, the spectral response of diverse plant species and assemblages is generally very similar and successful segregation of vegetation requires differentiating between subtle differences in overall spectral response curves. This requires high quality spectral data with minimal noise. Instruments such as AVIRIS have been increasingly successful for vegetation mapping and ecological studies (Asner, 2004; Green et al., 1998).

In general, the ecological hyperspectral literature has been dominated by investigations in four broad categories: crops and precision agriculture; invasive species mapping; forest/wildland mapping, including species differentiation; and the development of techniques for deriving biochemical and biophysical attributes of vegetation canopies from spectral characteristics. Identification of species and characterization of vegetation health status can be used directly to facilitate management of crops, rangeland, and forests. The derivation of biochemical and biophysical characteristics are initial steps that are required to build and implement models that can be used in a predictive capacity in more complex ecological models of global chemical exchange between land surface and atmosphere for monitoring regional to global environmental change.

Agriculture. The advantage of hyperspectral imagery for monitoring crops is the potential for early and rapid identification of localized problems, such as insect damage or water/nutrients stress, which can be specifically targeted and mitigated. This is a more economical and ecologically sound approach to agricultural management than generalized applications of fertilizers, herbicides, and water. Fitzgerald et al. (2002) used spectral mixture analysis of AVIRIS imagery to detect spider mite damage in cotton crops, to assist in precision application of miticide treatments that were restricted to the infested vegetation. Champagne et al. (2003) used a spectral derivative curve-fitting model for the estimation (and validation) of water content in crops. Reliable plant liquid water maps would allow water resources to be conserved by selectively watering only where needed. Differentiating crops species and locating stressed vegetation was also completed using imaging spectroscopy (Clark et al., 1995). Ericson et al.

(2004) used a combination of field and remote imagery to improve localized estimates of stand loss and defoliation in maize, an important capability for farmers and the insurance industry.

Invasive species. Several studies have used imaging spectroscopy to identify invasive plant species. Iceplant and jubata grass (Underwood et al., 2002) and arundo (giant cane), as well as the associated vegetation communities (DiPietro et al., 2002) have been successfully mapped with AVIRIS data. Leafy spurge has been the target of several investigations. Glenn et al. (2005) mapped large, dense patches of leafy spurge during two consecutive seasons. Hunt and Parker Williams (2004) and Parker Williams and Hunt (2002a; 2002b; 2004) examined different techniques for mapping leafy spurge (i.e., MTMF, SAM, minimum distance classifier, and various vegetation indices) as well as different sensors (AVIRIS, Landsat, and SPOT). They showed that hyperspectral data processed using techniques developed specifically for hyperspectral mapping produced significantly improved spurge maps. Root et al. (2002) compared leafy spurge maps that were produced using low-altitude airborne (CASI), high-altitude airborne (AVIRIS), and satellite borne (Hyperion) hyperspectral data in an effort to establish whether a single sensor was optimal for spurge detection in terms of spatial resolution, economy, and repeatability for temporal monitoring purposes. Dudek et al. (2002; 2003; 2004) and Dudek (2005) compared the effects of preprocessing steps and different mapping algorithms on the resulting leafy spurge maps, to investigate optimal approaches to use for mapping leafy spurge.

Forest/wildland mapping. Imaging spectroscopy has also been used successfully for differentiating species in environments such as forest and wetlands. Viers et al. (2002) successfully discriminated between riparian species using AVIRIS imagery. Martin et al. (1998) used transformed divergence (Jensen, 1996) to select optimal bands from "first difference" reflectance spectra for separating forest spectral classes. The selected bands were used to map species, including pure and mixed stands of deciduous and conifer species within mixed forests in the northeastern United States. Kokaly et al. (1998) differentiated forest species, as well as broad stand-age categories using AVIRIS data collected over Yellowstone National Park. In conjunction with this project they also mapped distinctive hot spring biota (bacteria and algae) that were associated with different aqueous chemical systems. Foster and Townsend (2002)

used classification trees (for species) and regression trees (for total basal area) to evaluate the effects of phenology and topography on discriminating between three dominant forest species in the central Appalachian Mountains.

Biochemical and biophysical attributes of vegetation. In several studies the correlation between laboratory measurements of foliar chemistry and spectral characteristics of remote hyperspectral imagery was examined to determine whether predictable relationships exist between these that could be used to estimate the measurements solely from remote imagery. For example, Kupiec et al. (1993) calculated the correlation between laboratory measurements of chlorophyll concentration and the first derivative of reflectance from each AVIRIS wavelength band, in an effort to select an optimal band (based on highest r^2) for estimating chlorophyll content from imaging spectroscopy. Similarly, Martin and Aber (1993) used a multiple linear regression of the first derivative of reflectance data from AVIRIS against field measurements of vegetation chemistry to select optimal wavelengths for predicting foliar nitrogen. The estimates from spectral data were used as input to an ecosystem model to predict carbon balance in the forests ecosystem under study. They discovered, however, that the optimal wavelengths that were selected with the multiple regression varied by location.

Ustin et al. (1998) compared ground-based measurements of chaparral canopy water content to canopy water estimates derived from spectral measurements taken at leaf, canopy and landscape (image) scales, to evaluate the reliability of image-derived plant liquid water estimates, an important component in wildfire risk-assessment models. Roberts et al. (1998) used AVIRIS data and a modified multiple endmember selection technique (MESMA: multiple endmember spectral mixture analysis) to derive canopy liquid water maps. In addition they produced water vapor maps, maps of green vegetation (GV), non-photosynthetic vegetation (NPV), soil and shade fraction, as well as species maps to improve characterization of wildland fire fuels. These products were linked to fuel models that were used in turn as input to fire spread models to improve prediction of fire hazard in the Santa Monica Mountains of southern California. Dennison and Roberts (2003) built on this research by using multi-temporal AVIRIS to determine the effect

of seasonal and phenological variation on the endmembers that were selected for species (fuel) mapping with the MESMA technique.

Canopy biophysical measurements (from laboratory and field) were also correlated with remote spectra to define general relationships for use in canopy reflectance models. Lee and Cohen (2002) compared LAI measurements from AVIRIS and Landsat ETM+, which were derived by regression of field measured LAI, against spectral response. AVIRIS showed better correlation, but only for specific wavelength bands. Meroni et al. (2004) input hyperspectral measurements to a canopy reflectance model (SAIL: Verhoef, 1984) coupled with a leaf optical properties model (PROSPECT: Jacquemoud and Baret, 1990) and inverted the models to predict LAI. Gamon et al. (2002) used indices derived from AVIRIS spectra (i.e., photochemical reflectance index, NDVI, NDWI, chlorophyll index) in conjunction with derived biophysical measurements (fAPAR, PAR, APAR, light use efficiency) to produce models to assess photosynthetic and respiratory carbon flux over fragmented landscapes.

Roberts et al. (1998) tracked the change in liquid water content that was measured in the laboratory with standard analytical chemistry techniques and the estimated liquid water content based on spectral measurements collected in the field and with AVIRIS imagery over a *Populus* clone plantation during a 4-year period. Measurements were collected over trees from one to six years old. The intent of this project was to examine the potential of using liquid water estimates from remote hyperspectral data as an alternative to NDVI for estimating LAI over densely forested areas in which NDVI values saturate and show little change with increasing LAI values above approximately 3. This field study was proposed after an earlier remote sensing project showed significant change in remotely measured liquid water over forest canopies that showed little change in NDVI. AVIRIS-derived canopy liquid water estimates were compared with temporal changes in LAI (from the field) to determine whether a linear relationship was seen between spectrally measured liquid water and LAI. They determined that the AVIRIS-derived liquid water matched the measured changes, while NDVI did not vary significantly, and proposed that the remotely measured liquid water could provide an alternative to NDVI for estimating LAI.

Additional vegetation applications of imaging spectroscopy. Recent studies have combined spectral data with additional techniques to improve exploitation of the high spectral resolution imagery. For example, Schmidt et al. (2004) improved the accuracy and speed at which saltmarsh vegetation maps were produced in the Netherlands by using a rule-based expert system to combine airborne hyperspectral vegetation maps with terrain data from the field and radar altimetry. Asner et al. (2003) used field spectroscopy to derive "endmember bundles" that were used in a spectral mixture analysis in conjunction with a textural analysis of multispectral (Landsat) data to establish a relationship between subpixel vegetation/non-photosynthetic vegetation/soil fractions and inter-pixel textural variation in deforested regions of Brazil.

Imaging spectroscopy of vegetation has been used to support research in other fields, for example, geologic exploration and mapping. Rowan et al. (1998) used AVIRS imagery to distinguish between chestnut oaks growing over unaltered terrain versus those growing over silicified, hydrothermally altered rocks, to supplement conventional geologic mapping for mineral resources. Gold and silver deposits were known to be associated with some of these hydrothermally altered rocks. Some previously unknown hydrothermal deposits were located with this method. Martini and Silver (2002) used hyperspectral imagery and aerial photography to map tree kills that were induced by magmatic CO_2 emissions over an active volcanic zone, and suggested that the spatial orientation of the kill zones appeared to be related to subsurface geologic structure in the region.

Summary/conclusions regarding ecological remote sensing literature. The projects described above provide a representative sample of major current and potential ecological applications of hyperspectral remote sensing. These studies have expanded and improved understanding of the potential of this type of remote sensing. Most of these studies were exploratory and focused on testing imaging spectroscopy for discriminating new or novel materials. These were useful tests for potential applications of imaging spectroscopy. In the above examples, however, a variety of processing and analytical methods were used, as well as different spectral subsets or bands. Because of this it is difficult to determine whether inconsistency in results stems from the processing method or the application. For species

identification, practical issues regarding the consistency of identification over time, space, or under different viewing geometry have not been sufficiently addressed, although there are exceptions (i.e., Kennedy et al., 1997). A quantitative assessment of map accuracy to determine whether the derived maps are accurate or consistent was not reported in many of these studies.

An area that has not been widely tested with hyperspectral imagery is temporal monitoring of land cover classes (change detection). Although the hope for biochemical and biophysical modeling is to track temporal variation in biomass, etc. within an ecosystem, traditional change detection of covertype classes has not been done, in spite of the fact that imaging spectroscopy has successfully mapped vegetation to the species level in some environments, and has potential for producing detailed species change maps. Hyperspectral remote sensing may prove to be very useful for tracking changes in dominant species or species fractions that can provide an early indication of significant changes within ecosystems. Monitoring the expansion or control of invasive species over time is particularly suited to hyperspectral analysis, but temporal studies in this field based on hyperspectral data are lacking. There are few investigations in the literature regarding the consistency of hyperspectral covertype maps over time, or studies that address problems that are encountered when using imaging spectroscopy for multi-temporal, management-oriented research. The development of consistent methods for producing and analyzing species maps from imaging spectroscopy would advance this type of application.

THE AVIRIS SENSOR

Data collection. For this study multi-temporal AVIRIS data was collected in the summers of 1999 and 2001, close to peak bloom stage for leafy spurge. AVIRIS has been monitored and upgraded over the last 15 years by NASA JPL (Green et al., 1998), and is the standard to which other imaging spectrometers are typically compared. A particularly critical factor in the improvement of AVIRIS has been the increase in signal-to-noise ratio (SNR) from early values of 80 to 150 (depending on the wavelength sensitivity of the detector) to current values in excess of 1100 (Asner, 2004). This was accomplished primarily by applying

increasingly sophisticated methods for removing atmospheric noise, and converting from 8 bit to 12 bit data (Clark and Swayze, 1996). As more noise has been eliminated, subtle features and differences in materials that were previously undetectable are now within the detectable range and stand out above the noise of the instrument.

Sensor and platform characteristics (Johnson and Green, 1995; Green et al., 1998; AVIRIS Data Facility web page). The AVIRIS sensor covers a wavelength range of 380 to 2500 nm with 224 detectors or "bands", each sensitive to a different narrow bandwidth, and offset from each adjacent band by approximately 10 nm. This results in nearly continuous coverage of reflectance characteristics within the reflective optical range. The sensor is composed of four separate spectrometers, the A spectrometer covering a nominal range of 400-700 nm, B from 700-1300 nm, C 1300-1900 nm, and D from 1900-2500 nm, although there is slight overlap of band coverage between each spectrometer. For visible wavelengths, the detectors are composed of silicon, and indium-antimonide is used for the detectors in the infrared region. AVIRIS is a whisk-broom (cross-track) mirror scanner, with a 30 degree swath total, 15 degrees each side of nadir. This results in a maximum of 614 samples or cross-track pixels. Currently 12-bit data encoding is used.

The data is collected from both high and low altitude aircraft. High altitude data has approximately 20 m spot size, yielding approximately 17 m pixel resolution, a 10.5 to 11 km swath width, and variable length flight lines, where the limits are imposed by data volume restrictions (up to 16GB). The number of flight lines can be reduced to increase the length of individual flight lines, and vice versa. Runs (flight lines) can range in number from 1 to 15, with each run composed of 1 to 40 scenes. Each scene or "cube" is stored in 512-line blocks that are approximately 10 km long.

The high altitude platform is an ER-2, a U2 jet modified for additional cargo capacity, which flies at approximately 20 km altitude, at 734 km/hr. The low altitude data is collected using a Twin Otter aircraft platform, typically flying at approximately 4 km altitude and 130 km/hr speed. The combination of altitude with a 2 km swath width results in approximately 4 m pixel resolution for low altitude collections.

Data costs have been in the range of $64,000/flight line, plus an additional $6000/flight hour. The analog data is pre-processed by JPL for delivery as digital radiance values.

CHAPTER 3

LITERATURE REVIEW AND DESCRIPTION OF GENERAL TECHNIQUES FOR HYPERSPECTRAL PROCESSING

INTRODUCTION

Because of the voluminous and detailed spectral information that is gathered from terrestrial imaging spectrometers, new methods for better exploiting these data have been developed that are unique from the standard classification methods that are used for processing data from multi-spectral scanners. In addition, because of the enhanced ability to discriminate subtle spectral differences, it is necessary to apply rigorous atmospheric corrections and other preprocessing steps to the data. Atmospheric correction has often been ignored in single-date, multi-spectral analyses, and generally is undertaken primarily to normalize multi-spectral data before multi-temporal analyses.

PREPROCESSING

CALIBRATION

Atmospheric calibration (or atmospheric correction) is a critical requirement for successful and complete exploitation of imaging spectroscopy. To use these data, spectral features that are due to atmospheric absorptions and scattering must be removed to correctly isolate the spectral characteristics of the surface materials. Similar to multi-spectral imagery, calibration of hyperspectral data is required to normalize the data between dates prior to change detection. It is also required to correct for variation in solar illumination and viewing geometries, as well as fluctuating detector performance that will otherwise mask the reflectance characteristics of the surface (Lunetta, 1998; Clark et al., 2002; Gao, Heidebrecht, and Goetz, 1993).

AVIRIS data are generally delivered as at-sensor radiance values that have already been corrected for instrument biases, and therefore the radiance data do not generally need to be corrected for these biases. The radiance is converted to reflectance using atmospheric radiative transfer codes that model the absorption and scattering characteristics of the atmosphere (including the solar irradiance spectrum), to correct the radiance received by the sensor for atmospheric effects, and convert radiance to reflectance. Reflectance is defined as the radiance reflected by the earth's surface (measured by AVIRIS in $W/m^2/\mu m/sr$) divided by modeled radiance reflected off a Lambertian surface for the conditions under which the image was recorded; the result yields unit-less reflectance values between 0 and 1 (Farrand and Blundell, 2004; Clark et al., 2002). These are generally multiplied by a scaling factor to convert to integers for easier processing. Many of the radiative transfer methods use the 0.94 μm and 1.14 μm water absorption bands from the image spectra to derive estimates of atmospheric water on a pixel by pixel basis. Image-wide averages for other absorbing atmospheric gases, including CO_2, O_2, and O_3, are typically calculated as a mean estimate for the entire image.

Following the conversion and correction of data to apparent reflectance with a radiative transfer model, some residual effects of atmospheric absorptions and scattering generally remain. The model is considered to give approximately an 80% correction to true reflectance because of simplifying assumptions that are used in the models regarding absorption by atmospheric gases, the solar irradiance spectrum, and variations in illumination of the target material (Clark et al., 2002). The data correction can be further refined, however, by using a mean spectrum derived from field measurements of a large, invariant, "spectrally bland" calibration site, which can be characterized spectrally in the field during collection of the remote data, and located unequivocally on the imagery. Playas, dam faces, parking lots, and cleared construction sites are examples of calibration targets that can be used. A single mean reference spectrum from all spectra collected over the calibration site is used to adjust the averaged image spectrum over the same calibration area. This additional correction step is referred to as the "single spectrum enhancement" (ACORN Quick Start Guide, 2001; Clark et al., 2002). The combination of the

modeled and field-enhanced correction is sometimes referred to as "radiative-transfer-ground-calibration (RTGC)" (Clark et al., 2002).

SPECTRAL LIBRARY SOURCES

The concept of spectral libraries is central to hyperspectral processing. A spectral library supplies representative spectra of known materials that are used in conjunction with mapping algorithms to match unknown image spectra with the known reference spectrum. The library spectra may be pure, or a mixture of materials, and the library may be a set of laboratory-measured standards, field-characterized spectra, or they can be extracted from the image itself. In many cases the library spectra are known or labeled *a priori*, but, in the case of image-derived libraries, it is possible to map materials without positive identification of the individual spectral classes before mapping.

Field derived. The field-derived library is acquired by continuously collecting spectra over target materials until a sufficient number have been obtained to average, smooth and eliminate the noise that typically occurs in individual spectra. With the field-based library, it is possible to include a library for pure materials as well as various mixtures, and have the exact field spectra corresponding to those known mixtures. In addition, the material and conditions under which the spectra were collected can be well-documented. If the area from which the spectra were collected is large it can be located on the image and the library spectra can then be directly linked to the image. The disadvantage of a field-based library, however, is that all materials and mixtures must be sampled to obtain a representative library. This is virtually impossible for complex vegetated areas.

Laboratory derived. With laboratory spectra, the exact composition of the reference sample is known, and the spectra can be collected under very stable, controlled environmental conditions. These spectra will not require correction or the collection of large numbers to minimize noise in averaged spectra, as is required with the image and field libraries. It is difficult, however, to create samples in the lab that will accurately represent the reflectance characteristics of materials at the coarser scales that are needed to match remotely collected image spectra.

This is particularly true of vegetation, where plant and canopy structure, diurnal and phenological variation, as well as underlying substrate and litter are all important contributors to the overall reflectance of vegetation. These factors are not easily reproduced in a laboratory environment.

Image derived. An advantage of using an image-derived library is that anomalies in the atmospheric correction of the image will also be incorporated into the library. With the image-derived library, problems with extrapolating from the field or laboratory spectra to the image are eliminated. Figure 3.1, for example, shows the differences in mean field-based spectral classes, collected over specific vegetation patches, and the mean spectra from the same areas that were derived from the image. In several cases, the different vegetation spectra from the image appear more similar to one another than to the field spectra from the corresponding vegetation patch. With image spectra, vegetation throughout the scene can be more completely characterized, and not limited to vegetation patches that were sampled in the field. Residual, uncorrected atmospheric effects will be minimized, because the library and image will contain the same atmospheric characteristics or anomalies. The image-derived endmember libraries are better suited to the analysis of mixed pixels, and were designed to be used with the unmixing algorithms in ENVI. The collection of spectra from the image is also more automated, and may reduce potential bias in the selection of specific vegetation patches in the field for a ground-based library. Because the purest spectra are found using computer algorithms and visualization, however (e.g., PPI and nD-Visualization, ENVI User's Guide, 2003; Chapter 4, Spectral library creation), the pixels that are selected for endmembers are unlikely to have been visited on the ground. The exact composition of the material representing the endmember is uncertain.

The construction of an image-derived spectral library from hyperspectral data has been most successful when several preprocessing steps are completed before extracting the library. These steps are intended to isolate the purest, least-mixed pixels from the image, which would best represent the spectral characteristics of unique, unmixed materials (Boardman and Kruse, 1994; Boardman et al., 1995). With this approach, each step uses a progressively smaller, more unique or purer subset from the original image, until a small group of the most spectrally unique pixels is selected and used to extract a spectral library. The library is then used to scale out and

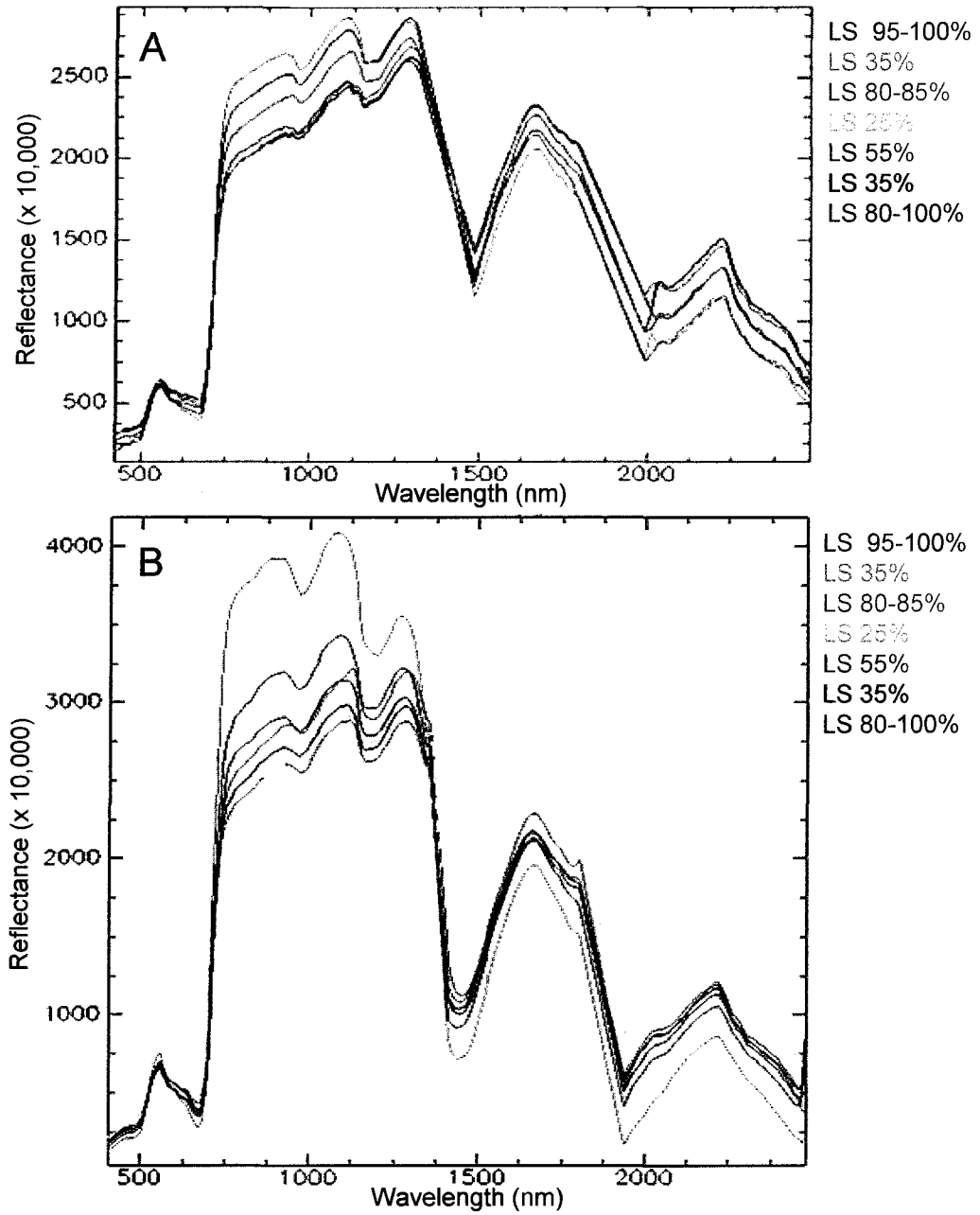

Figure 3.1. Field versus image-derived leafy spurge (LS) spectra. A: mean spectra for image pixels falling within the perimeters of the polygons defined in the field, derived from image (noise-dominated bands in the water-absorption regions centered around 1400 nm and 1900 nm have been removed, with reflectance extrapolated across the gaps); B: mean spectra within polygons collected in the field with spectrometer. Image spectra are "dampened" relative to the field spectra, with overall albedo lower, and diminished depth of absorption features, and may reflect the variable sensor viewing angles (0° to 15°) with the remote data; field spectra were collected at 0° (nadir). Scales are identical in the 2 plots. Each polygon represents a different patch density (from 20% to 100% spurge canopy cover). The equivalent polygons are color coded identically in both plots.

map the entire image by providing the training or reference information against which all other pixel spectra are matched. These include a minimum noise fraction (MNF) transformation, a pixel purity index (PPI) calculation, followed by visualization in an animated spectral plot graphics window from which the pure endmembers for the library are selected (n-D Visualization) (ENVI User's Guide, 2003).

MNF: Minimum Noise Fraction Transformation. The MNF transform is used to decrease the dimensionality and volume of the data, decrease the data noise before processing, and maximize the variance between bands to improve the chances of separating spectrally similar material, for both mapping and as a preliminary step for extracting pure pixels from the imagery to use for deriving a spectral library from the image (Research Systems, 2002).

The minimum noise fraction (MNF) transformation is equivalent to a double principal components analysis. The transform is also referred to as a noise-adjusted principal components transform (NAPC) (Lee et al., 1990; Green et al., 1988). The first transformation step is based on a noise covariance matrix that is estimated from the imagery for each pixel. The noise is de-correlated (transformed) and normalized to equalize the noise between all bands. The second step is a standard principal components transformation of the data following equalization of the noise. The second transformation de-correlates the spectral signal, then sorts the resulting eigenimages by signal-to-noise ratio (CSES, 2000). The high-numbered MNF components will be less coherent visually, and dominated by noise. To reduce both data volume and noise, these incoherent MNF components can be eliminated (ENVI User's Guide, 2003). The resulting eigenimages are an orthogonal set of maximum variance components, ordered and numbered by decreasing contribution to the total image variance.

The number of non-noisy, coherent MNF bands that are suitable for further processing is scene-dependent. The information-rich MNF bands are selected for input to the PPI algorithm. The number of coherent bands plus one (i.e., n + 1) is often accepted as the number of endmembers present within the scene, or the dimensionality of the data, and is used as a guide for determining the appropriate number of endmembers to extract from an image (Boardman, 1993; Boardman et al., 1995). The MNF is a common, but not essential transformation step,

depending on the mapping algorithm that is used. This transformation, for example, typically would not be used with a feature matching algorithm such as spectral feature fitting (SFF) because the physically interpretable characteristics of spectral absorption features are no longer evident following MNF transformation.

PPI: Pixel Purity Index. Only the coherent (non-noise) MNF bands are run through the pixel purity index (PPI) algorithm. Selected MNF-band spectra are plotted in multi-dimensional space, then iteratively projected or collapsed onto a "unit vector" that is randomly oriented in multi-dimensional space (ENVI User's Guide, 2003; Boardman and Kruse, 1994). The most spectrally extreme pixels from each random projection will occur on or near the ends of the vector. The number of times that a given pixel falls within a specified range of the ends of the vector is counted and tagged. Several thousand to several tens of thousands of random iterations are run. The output of the algorithm is a single band image where the digital number (DN) represents the number of times a particular pixel was tagged as unique or extreme. The purest pixels are at the extreme edges of the pixel cloud and will more frequently occur near the ends of the unit vector, when all pixels are projected onto the vector. The higher the DN, therefore, the more likely the pixel is to be pure, and a good endmember candidate. A threshold is used to select a set of the purest pixels which are saved as a region of interest (ROI). The ROI is used to subset these pixels from the MNF images to use in the visualization step, in which the endmember library pixels are selected (Research Systems, 2002).

N-D Visualization. The unique pixel subset is imported to the "n-Dimensional Visualizer" tool in ENVI (ENVI User's Guide, 2003; Boardman and Kruse, 1994). This is an animated, multi-dimensional graphics viewer that allows visualization of spectral scatter plots that can be randomly rotated in n-dimensional space, where n represents the number of input bands. As clusters separate in spectral space, or MNF space, clumps of pixels on the outer edges of the clusters are manually selected with an interactive ROI drawing tool, and the MNF spectra for these pixels are saved as a potential endmember group. Pixels that occur at the extreme edges of the clusters in the display are considered the least mixed and purest in the scene, and therefore the best candidates for the spectral library endmembers.

ADDITIONAL HYPERSPECTRAL PRE-PROCESSING

Other preprocessing steps are associated with hyperspectral data analysis, including for example, a cross-track illumination correction. These steps are not routinely used by image analysts. Some of these optional steps are discussed in Chapter 5 where the impacts of several preprocessing steps and mapping algorithms are compared.

MAPPING

Many approaches to mapping materials have either been developed or adapted for imaging spectroscopy. Adapted methods include, for example, artificial neural networks (ANN) (Foody, 1999). ANNs are free of assumptions regarding data normality, but the network design must be done using trial and error, which is time consuming, and because the parameters for setting up the network are controlled by the analyst, they are subjective and can have a significant impact on how well the network performs. In comparative studies, ANNs have improved calculated accuracies by a few percent over the maximum likelihood statistical classifier, but were not significantly better (Mather, 1999).

Geostatistical approaches such as cokriging and indicator kriging also do not rely on the assumption of multivariate normal data distributions, and allow spatial information to be incorporated along with the spectral data (van der Meer, 1994a; 1994b; 1996; 1999). Several studies have attempted statistical selection of "significant" channel subsets using discriminant analysis to focus processing on a reduced data set and to isolate bands that statistically allow the greatest separability between materials (i.e., Thenkabail, 2001; van Aardt and Wynne, 2001).

Other hyperspectral processing methods have been adapted from multi-spectral remote sensing. The supervised maximum-likelihood and minimum distance classifiers, as well as the unsupervised ISODATA classifier (Iterative Self-Organizing Data Analysis Technique), for example, have been used with varied success (Spruce, 2001; Spruce et al., 2002; DiPietro et al., 2002; Hunt and Parker Williams, 2004; Underwood et al., 2002). Narrow band indices are an adaptation of the band ratios and indices that have been widely used with multi-spectral data, but

represent an improvement because bands can be selected from a much larger range (Carter and Miller, 1994; Gat et al., 2000; Penn, 2001; Perry et al., 2000; Rahman et al., 2000; Thenkabail et al., 2000). The narrow bandwidths allow the hyperspectral bands to be precisely located within, or immediately adjacent to the absorption features that can be resolved with hyperspectral imagery. Although the better placement of bands may yield useful indices, only a fraction of the available data is being used, and the information that is available throughout the spectral range is not being fully exploited.

Many argue that if hyperspectral data are carefully processed, then materials are *identified* rather than statistically *discriminated.* Because of this, the methods that can best exploit the subtle differences in spectra (i.e., techniques developed specifically to analyze spectra) are most appropriate for mapping hyperspectral data. Imaging spectroscopy has evolved from, and has much in common with reflectance spectroscopy from the field of chemistry, as well as spectrometry concepts used in astronomy, suggesting that methods adapted from multi-spectral remote sensing may not be as appropriate as those adapted from the fields of signal processing and spectroscopy (Gaffey et al., 1993). This was supported by a comparison of the results of multi-spectral (minimum distance classifier) and hyperspectral (SAM or spectral angle mapping) methods that were used to map leafy spurge with hyperspectral data (Hunt and Parker Williams, 2004).

Several techniques have been developed specifically for hyperspectral processing. No single method is without disadvantages, and many of these algorithms were developed in response to weaknesses of other techniques. Examples include binary encoding (Goetz et al., 1985; Jia and Richards, 1993; Mazer et al., 1988), waveform characterization (Crowley et al., 1989; Okada and Iwashita, 1992), and CEM or constrained energy minimization (Farrand and Harsanyi, 1993; 1994; 1997). First and second derivative matching have also been used to identify and map specific materials (Martinand Aber, 1997; Wessman et al, 1989). Other strategies match the spectra of known materials directly to reflectance spectra from the remote imagery (Adams et al., 1993; Boardman, 1993; Clark et al., 1990). The matching strategies have dominated the hyperspectral literature, and represent the algorithms that have most commonly

been incorporated into commercial software for hyperspectral image processing. Matching strategies may utilize the full spectral range covered by a particular sensor, subsets of the spectrum, or specific isolated absorption features.

Within the matching techniques, two broad approaches have evolved. The first involves whole pixel matching to reference library spectra. Either complete spectra are matched, for example, as used with the spectral angle mapper (SAM) algorithm (Kruse et al., 1993a; Yuhas et al., 1992), or isolated features are used, as in spectral feature fitting (SFF) (also referred to as spectral feature matching). With SFF, specific absorption features are isolated and compared to similarly isolated features from spectral libraries of known materials and mixtures (Clark et al., 1991; Clark et al., 1995; Clark et al., 2003; Mackin et al., 1991).

The second matching approach focuses on spectral unmixing and matching to pure, "endmember" spectra (Adams et al., 1993). These are methods of sub-pixel analysis and include linear spectral mixture analysis (SMA) (Adams et al., 1993; Boardman, 1991; Settle and Drake, 1993), matched filtering (MF), mixture-tuned matched filtering (MTMF) (Boardman, 1998), and constrained energy minimization (CEM) (Farrand and Harsanyi, 1993; 1994; 1997). CEM is essentially analogous to the theoretical premises of the MTMF. More sophisticated, specialized unmixing algorithms have evolved from basic linear SMA. For example, multiple endmember spectral mixture analysis (MESMA) can determine the best set of endmembers on a pixel-by-pixel basis from a larger potential endmember set (Roberts et al., 1998). AutoSWIR (Asner and Lobell, 2000) uses a combination of "endmember bundling" and Monte Carlo unmixing to account for endmember variability and uncertainty with unmixing. These are specialized algorithms, developed to improve unmixing of vegetative land cover, and are currently unavailable in commercial software.

SAM: SPECTRAL ANGLE MAPPING

Spectral angle mapping (SAM) is an empirical approach that measures a multi-dimensional angle between the spectral vector of an unknown pixel and the vector of a known, reference spectrum. The number of dimensions of the vector is equal to the number of bands that are used in the analysis. For each reference spectrum a similarity image is produced that

indicates the match to that reference endmember, with smaller angles indicating a better, closer match. A post-classification classifier can be run using the individual rule images to produce a single-band, thematic map based on the best match (i.e., lowest angle) to an endmember or reference for each pixel. The method is relatively straightforward mathematically. An advantage of this method is that it is based on vector angle differences only. The effect of variable illumination (characterized by vector length) will be minimized as a result of the method used to calculate the difference in spectral angle. The SAM algorithm is therefore relatively insensitive to shadowing, variable illumination, or albedo differences across the landscape (Kruse et al., 1993; CSES, 2000; Farrand and Blundell, 2004). A disadvantage of SAM, however, is that it does not adequately accommodate mixed pixels. The SAM method will indicate the closest match to the library spectrum, but will not provide any measurement of fractional abundance, as unmixing methods will. It may be possible to speculate on mixtures based on the relative magnitude of reported vector angles from the similarity image; however, this is a whole pixel method, which does not quantify sub-pixel abundances (Mather, 1999). The resulting class maps cannot be fine-tuned, as with the MTMF.

SFF: SPECTRAL FEATURE FITTING

SFF is a whole pixel analysis technique that identifies materials based on comparisons of physically meaningful absorption features in a spectral library to an unknown pixel spectrum. This technique does not address mixed pixels, unless that mixture is specifically created and added to a reference spectral library.

Detailed SFF algorithms have been developed and refined predominantly by the USGS Spectroscopy Laboratory, using their in-house "Tetracorder expert system" (Clark et al., 1991; Clark et al., 1995; Clark et al., 2003). This method uses a least squares fit of unknown features to continuum-removed, reference absorption features. The continuum is a mathematical function that fits a straight line between the high points or shoulders of individual absorption features. To normalize the reflectance of individual absorption features to a common baseline, the continuum is removed by dividing the original spectrum by the continuum, resulting in values between 0 and

1, where 1 indicates the portions of the spectrum where the material spectrum and the continuum coincide (i.e., no absorption feature occurs at this location) (ENVI User's Guide, 2003).

The Tetracorder algorithm fits one or more absorption features of unknown spectra to those features in a reference library spectrum, and produces a map of the spectrally predominant material, based on best least squares fit (assuming that material was represented in the spectral library). It uses a set of user-defined rules for identification, which are based on knowledge of materials. The reference spectrum is scaled to match the image spectrum. Then a least squares fit is run, matching absorption band width, depth, symmetry, as well as wavelength of maximum depth and center wavelength. A reference spectral library is required for all materials that are to be mapped. The Tetracorder program can be modified to incorporate multiple and/or weighted features to use in the mapping.

In general, the SFF approach is limited by the incomplete characterization of all potential endmembers in a scene. In addition, the input parameters for the SFF algorithm in the commercial ENVI software cannot be modified easily, and weighting factors or combined spectral features cannot be used without programming modifications. SFF in ENVI, though similar in theory to the USGS Spectroscopy lab Tetracorder approach, uses a simpler, more generalized algorithm that does not appear to be as robust as the Tetracorder SFF method, or the ENVI unmixing algorithms. In ENVI, the spectral feature is characterized by a combination of the full width measurement at half the maximum depth of the absorption feature (FWHM) on a continuum-removed spectrum, and the wavelength of maximum absorption. Detailed variations in the shape of the feature are not characterized as well with this approach as with the Tetracorder least-squares method. With Tetracorder, mapping constraints can be modified or refined (i.e., weights for different absorption features). An advantage of SFF is the ability to work directly with physically interpretable spectra and absorption features, and differentiate classes directly using features that have a direct biophysical or other physically meaningful interpretation. In contrast, unmixing methods are generally run on MNF-transformed data, where spectra are not physically interpretable. SFF is restricted to specific portions of spectrum (i.e., specific absorption features). When the relationships between the unique absorption features and overall spectral

continuum may be critical for differentiating subtle differences between materials, this information will be excluded when mapping only uses the selected features with the SFF algorithm.

LINEAR SMA: LINEAR SPECTRAL MIXTURE ANALYSIS

An advantage of the linear spectral mixture analysis (SMA) algorithm is that it is conceptually easier to understand than some other algorithms, it accommodates subpixel mixtures of land cover, and models materials well if materials exhibit linear mixing (i.e., the reflectance is directly proportional to the fraction of that material within a mixed pixel) (Kruse et al., 1993b). The linear SMA model is based on the assumption that pixel spectra are linear mixtures or combinations of pure pixel spectra, with each "pure" spectrum weighted by the proportion of area covered by each material, essentially a weighted average (CSES, 2000). In this model, the fraction of all components must sum to 1 (to account for 100% of the pixel). No negative abundance values are allowed, nor values greater than 1. The model assumes single scattering (i.e., no multiple interaction of radiation with other materials). The number of endmembers cannot be greater than the number of input bands used in the classification. Using these assumptions, the pixel spectrum can be mathematically modeled as a product of the complete endmember library matrix and the endmember abundance vector. From the measured spectrum and the known endmember library spectra, a matrix inversion can be used to solve for the abundance of the endmember fractions within a pixel. All endmember spectra are required in order to be able to simultaneously invert the matrix and solve for all endmember fractions in each pixel, using the following format (Farrand and Blundell, 2004; Adams et al, 1993):

$$r(x,y) = M\acute{\alpha}(x,y) + n(x,y)$$

$r(x,y)$	r (the measured image spectrum) is an m x 1 vector; m = the number of bands; x and y = pixel location
$M = (u_1 \ldots . , u_p)$	M (the matrix of the complete endmember set) is an m x p matrix of spectra; m = the number of bands; p = the number of endmembers;

	u = the endmember spectrum vector (m x 1)
ά(x,y)	ά is an unknown p x 1 vector of abundances; the matrix equation is solved for ά(x,y)
n(x,y)	n is the error of the fit of each endmember spectrum, for all bands

Unmixing can give correct sub-pixel fractional abundances, however it requires that all endmembers be included for a simultaneous solution. In addition, SMA is a linear solution to what is generally a non-linear problem. Non-linear mixing is typical of most surface materials (Ray and Murray, 1996) and plants in particular display complex non-linear and interactive mixing, that is often poorly modeled with linear SMA (Borel and Gerstl, 1994). In addition, theoretical constraints on the fractional abundances with linear SMA (i.e., all fractions are required to sum to one, and no negative fractions or fractions greater than one are allowed), can be difficult to impose and rarely describe the real world.

MF: MATCHED FILTERING

The matched filter algorithm for hyperspectral processing was derived from matched filter techniques that are commonly used in the signal processing field, to isolate true signal from background noise (Boardman, 1998). The matched filter is used to determine sub-pixel abundances using a partial unmixing strategy (ENVI User's Guide, 2003; Boardman et al., 1995). The target endmembers must be selected *a priori* by the image analyst from an image-derived or field-based spectral library. The algorithm works by maximizing the response of the known target endmember, and suppressing all other material responses in a single, composite unknown background "endmember" (Boardman et al., 1995). This technique tends to produce false positives, however, because rare materials in a scene with no associated endmember tend to map as the target. This occurs commonly in real data, especially when spectral contrasts are subtle. The relative match to the known endmember is indicated for each pixel, and is generally accepted as an approximation of the sub-pixel abundances of that material. An advantage of MF is that the background endmember spectra do not need to be known when mapping a specific target material.

MTMF: MIXTURE-TUNED MATCHED FILTERING

The MTMF is a variant of the matched filter (MF) algorithm, and like the MF, was developed for use when either an incomplete set of endmembers exists for the image, or when the analyst is only concerned with mapping one or a few components of a scene (Boardman, 1998). With this algorithm a single class of interest (one endmember reference spectrum) is "matched" to each pixel spectrum in the scene. Each pixel is scored based on the degree to which it matches that endmember spectrum. All others endmembers are essentially combined as a single, suppressed background signal, as with the MF algorithm. This process is run for each endmember that is used in the algorithm. For each iteration (i.e., for each endmember), the MTMF produces both a matched filter image, a "goodness of match" measurement, and an infeasibility image, which provides a measure of the likelihood or feasibility that a pixel really represents the target material. Infeasibility is reported as "noise sigma units", with lower numbers indicating a more likely match (ENVI User's Guide, 2001). The additional infeasibility image is output for each endmember in addition to the individual matched filter images, and is used to minimize or eliminate the false positives; (Farrand and Blundell, 2004; CSES, 2000). High infeasibility values indicate that a pixel is unlikely to be a good match even with a high MF score, while low values indicate that a pixel is a feasible or likely match (if the MF score is high as well. The high infeasibility/high MF score pixels represent false positives, and can be removed. Thresholds for both the MF image and the infeasible image are established to select the pixels that will be included on a final map of a specific target endmember. These thresholds are generally selected graphically by manually outlining the region for inclusion from a plot of MF values versus infeasibility values for all pixels. The selected pixels will be in the area of the plot indicating high MF and low infeasibility. Image stretching may also be used to highlight the selected thresholds on the image. This thresholding procedure is repeated separately for each endmember in the spectral library, or any selected set of endmembers.

An advantage of this algorithm over linear SMA is the absence of mathematical restrictions on the number of endmembers that can be derived and input to the algorithm (i.e., it does not require symmetry between input pixel vector and the complete endmember matrix to

invert for all fractions simultaneously). This allows an analyst to focus on only one or a few endmembers, or a complete set of classes. Depending on the mapping objectives it may not be necessary to extract all endmembers from an image, or alternatively, as many endmembers as the image supports (contains) can be derived and mapped. Although the number of endmember classes in a scene varies (Boardman and Green, 2000), an estimated average number of endmembers in a typical natural landscape is 48 (R. Yuhas, personal communication). For example, if only 35 coherent (non-noise) transformed MNF bands are input for endmember selection, it is still possible to extract 48 or more endmembers, including many that did not plot as "extremes" in the n-d visualizer, but rather plotted as subtly distinct classes, similar, but with subtle differences from spectra of pixels plotting in close proximity. Drawbacks of the MF and MTMF algorithms include they are difficult to conceptualize, and both use interactive thresholding for creating maps, which can complicate and add subjectivity to the results.

DISCUSSION/SUMMARY

Unlike multi-spectral classification methods, most of the hyperspectral mapping algorithms do not directly produce scene-wide thematic maps, with the exception of linear SMA. Commonly, maps of specific materials of interest are produced by establishing thresholds for inclusion in a thematic class map. These thresholds are selected by the image analyst based on experience and reference data, but can be influenced by subjective decisions of the analyst. The boundary therefore can be somewhat arbitrary. The affect of threshold decisions, as well as alternatives to manual, interactive threshold selection are discussed in Chapter 5.

Although some of the more uncommon approaches to hyperspectral processing have been added to commercial image-processing software (e.g., neural networks can be run in ENVI), they are more difficult to implement, and generally are not as successful for mapping as the hyperspectral matching algorithms. ENVI software was originally written by advocates of the unmixing approach. As a result, this software has been refined and improved predominantly with a focus on hyperspectral processing, although it is now marketed as a general image-processing software package. Both unmixing and SFF algorithms have been incorporated into this software.

Because ENVI is widely available and uses a windows interface, it is more suitable for *applied* hyperspectral remote sensing analysis than specialized, in-house programs. More important than convenience, however, is the success of the method for the application at hand. For mapping leafy spurge, the matching strategies that are available in ENVI were compared to see which of these algorithms performed best for mapping spurge over time (see Chapters 5 and 6).

Few comparative studies were seen in the literature to indicate which of the processing methods produces the best maps. This absence of comparative studies, in conjunction with distinct differences between initial test maps, prompted a test of algorithms and spectral libraries, to determine which appeared to be most appropriate for mapping leafy spurge. The test maps also indicated that results varied when different preprocessing procedures were applied; therefore, in addition to testing mapping algorithms, a variety of preprocessing techniques were also analyzed to develop the most appropriate processing protocol for mapping leafy spurge (see Chapter 5).

CHAPTER 4

STUDY AREA AND GENERAL METHODS

INTRODUCTION

The invasive weed, leafy spurge, was mapped from AVIRIS imagery collected in 1999 and again in 2001. The process included procedures that were modified specifically for this study, as well as standard processing steps that are used routinely with imaging spectroscopy data. A description of these standard procedures and the study area are included below.

STUDY AREA

The study area was centered over Theodore Roosevelt National Park in southwest North Dakota. Theodore Roosevelt National Park (THRO) occupies 28,509 ha (70,447 acres) within three separate units in southwest North Dakota. The 18,680 ha (46,159 acre) South Unit, which is most heavily infested with leafy spurge, was the subject of this study (Figure 4.1).

The park is dominated by badlands topography, with rock outcrops composed of generally flat-lying bentonite, sandstone, mudstone, shale, lignite, and "scoria" (clinker) beds of Eocene through Miocene age, formations that are collectively referred to as the Fort Union Group. These rocks were carved predominantly following the last retreat of Pleistocene continental ice sheets (Biek and Gonzalez, 2001). The terrain includes fluvial environments, riparian draws, abruptly and deeply incised sedimentary rocks, buttes and plateaus. The elevation of the South Unit ranges from approximately 683 to 860 m (2240 to 2820 ft).

An estimated 500 plus planat species inhabit the Park (O'Neill et al., 2000). These are predominantly species that are typical of the northern Great Plains, but include some southwestern desert and Great Basin species, as well as isolated boreal forest species (Root et al., 2002). Leafy spurge occurs in all habitats, but the heaviest infestations normally occur within

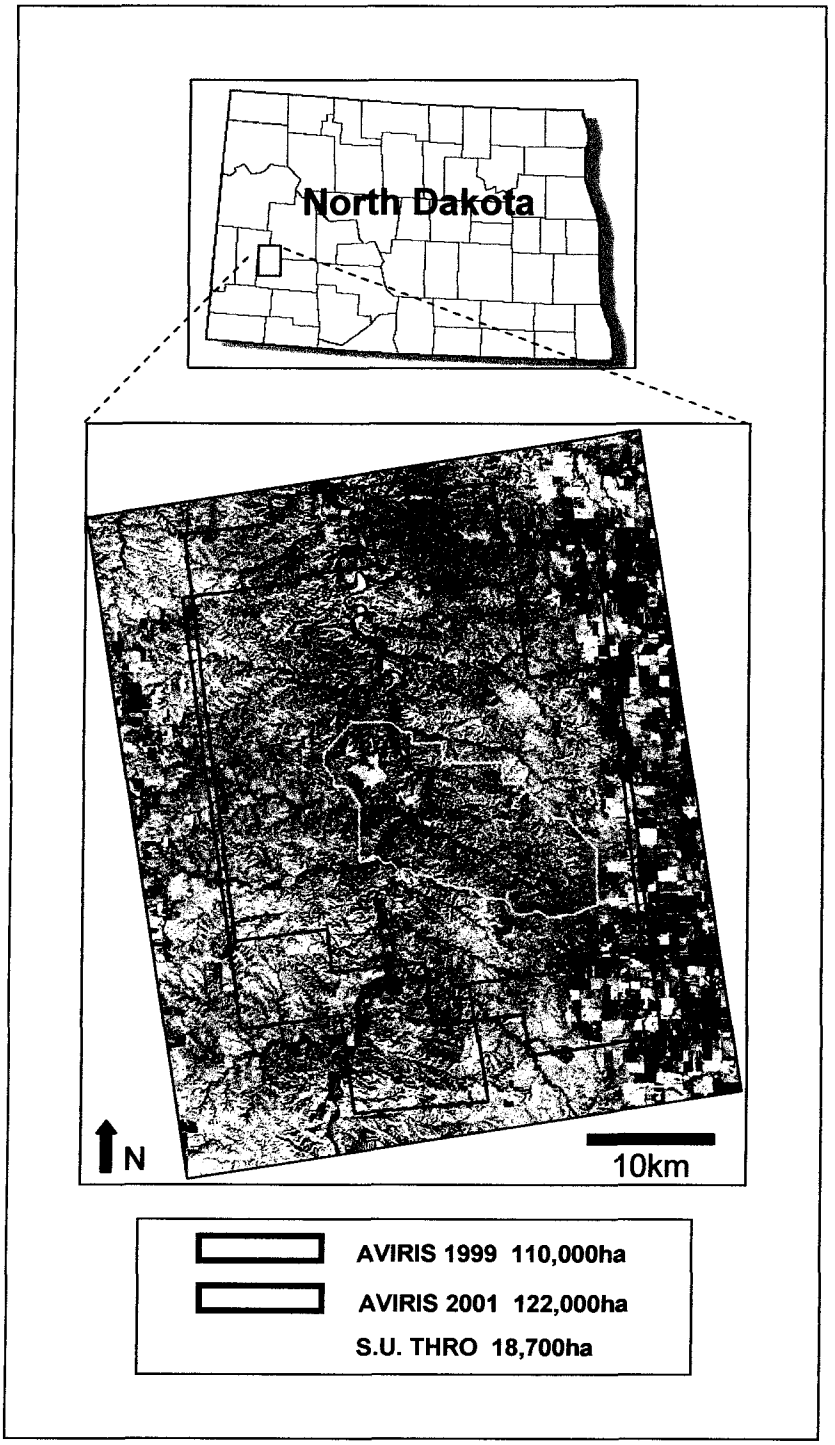

Figure 4.1. Study area: South Unit of Theodore Roosevelt National Park (THRO), ND. On the enlarged inset the coverage of the four 1999 AVIRIS flight lines is indicated in red; 2001 coverage in blue; the boundary of the South Unit (S.U.) is shown in cyan.

floodplains and riparian draws (Anderson et al., 1996).

GENERAL METHODS

The general methods included airborne data collection, field spectra collection and editing, and standard image preprocessing, including data calibration. Common preprocessing that is specific to hyperspectral imagery (minimum noise fraction (MNF) transformation, pixel purity index (PPI), and nD-visualization) were used to develop an image-derived spectral library. This was followed by mapping, target identification, georectification, and mosaicing. Leafy spurge maps for 1999 and 2001, as well as maps of the change in leafy spurge distribution between 1999 and 2001, were constructed using masking and recoding operations. Additional optional preprocessing steps that were applied included a cross-track illumination correction and an NDVI-based mask to isolate vegetation. These optional preprocessing steps, as well as other modifications of the basic mapping procedures, are discussed in Chapter 5, along with details of the classification. Accuracy assessments were run on the recoded leafy spurge maps; methods and discussion are included in Chapter 6. Change detection methods and results are discussed in Chapter 7.

DATA COLLECTION

Airborne Visible/Infrared Imaging Spectrometer (AVIRIS) data were acquired by NASA Jet Propulsion Laboratory (JPL) on 6 July, 1999 and 21 June, 2001, within the window of maximum inflorescence of leafy spurge that is accompanied by the development large, distinctive yellow-green bracts that facilitate location of the weed. Data were collected along four adjacent flight lines per date with approximately 35% sidelap over a 1100 km² (1999) or 1200 km² (2001) region of southwest North Dakota. The coverage of these flights is indicated in Figure 4.1. The flight lines were centered over the South Unit of THRO and included portions of the surrounding National Grasslands, private rangeland, and agricultural areas. Data was collected at altitudes close to 20.6 km (68,000 ft), yielding a 16.9 m pixel resolution, with individual flight lines approximately 10.5 km wide, and 28 to 40 km long.

Raw digital numbers (DN) were calibrated by JPL to at-sensor radiance using known reference target reflectors under a controlled environment (van der Meer, 1999). The imagery was adjusted for shifts in aircraft attitude, and the 2001 imagery was referenced to UTM coordinates (the AVIRIS geographical lookup tables were not available when the 1999 data were acquired). The data were delivered as a total of 35 scenes or "cubes" of radiance values for 1999 and 2001. Each cube was composed of 512 lines by 624 samples, with 224 radiance values for each pixel.

FIELD SPECTRA COLLECTION/EDITING

Vegetation spectra were collected on the ground in 2001 to use in the atmospheric calibration of the imagery, to facilitate identification of endmember spectra in the image-derived spectral libraries, to validate the quality of the atmospheric correction, and to use directly in test maps that were produced from different spectral libraries.

For spectral characterization, spurge patches were defined based on the density and homogeneity of the distribution of the plants within a patch. The spectra were collected within relatively homogeneous patches of vegetation (i.e., vegetation canopy percent cover occurring in approximately the same density and spatial distribution throughout the patch). Patches were irregularly shaped, with a minimum dimension of approximately 17 m (1 pixel) and a maximum dimension of 535 m. The number of spectral files collected per patch was roughly proportional to the patch size, and ranged from 16 to 554, with an approximate average of 500 files per hectare. Spurge canopy densities ranging from 20% to effectively 100% cover per patch were selected. Geographic coordinates of the patches were defined by continuous collection of locations using a GARMIN GPSMAP global positioning system (GPS) while circumscribing the perimeter of a selected patch. The GPS points that defined the perimeter of the patches were imported into ArcINFO to create polygon coverages and shapefiles that were used to validate the leafy spurge maps. Spectra were obtained over 13 leafy spurge patches. Spectra were also collected over homogeneous patches of a variety of associated vegetation species that are characteristic of the region. These included juniper, snowberry, sage, rabbit brush, smooth brome, little bluestem,

wheatgrass, and other grasses, as well as senescent vegetation, plant litter, and soil/litter/vegetation mixtures. Asphalt and concrete spectra were also collected to use in the atmospheric calibration of the imagery. The primary calibration site was a large, homogeneous asphalt parking lot that covered approximately 20 AVIRIS pixels; 462 integrated spectra files were collected at this site. An additional 361 files were collected with a second backup spectrometer. By averaging the large number of field spectra, noise in the reference data was reduced. Covering a large area also allows the spectra from a greater number of image pixels to be averaged, again reducing spectral noise. Noise is estimated to decrease as the square root of the number of pixels that are averaged (i.e., for spectra averaged over 16 pixels, noise will be reduced to ¼ of the original noise (Clark et al., 2002).

An Analytical Spectral Devices, Full Range (ASD FR) portable spectrometer outfitted with a laptop computer, running FieldSpec Pro software (Analytical Spectral Devices) was used for collecting the spectra. The ASD FR instrument consists of three individual spectrometers covering a wavelength range of 350 to 2500 nm with 512 detectors. The approximate sampling interval from 350-1000 nm was 1.4 nm, and increased to 2 nm between 1000 and 2500 nm.

The instrument response is very sensitive to both internal and external temperature fluctuations, wind (which can affect temperature), clouds, or other conditions affecting illumination. Because of this, the spectrometer was allowed to warm up for approximately ½ hour before the instrument was calibrated before collecting the spectral measurements. A dark current measurement was collected, as well as the radiance of a Spectralon plate. The plate provides a standardized, precise measurement of "100%" reflectance (in reality, as close to 100% as is currently available). This white reference measurement is used to calculate and adjust the reflectance of material spectra (Clark et al., 2002). The reflectance of a piece of mylar film, that displays very precise, well characterized, narrow absorption features, was also collected in the field to monitor the field performance of the instrument, and to compare the performance and comparability of the measurements from the two spectrometers that were used. The characteristic mylar absorptions can be compared to laboratory collected spectra to check for drift or other problems with the field spectrometer (Clark et al., 2002).

The spectra were collected with the spectrometer probe held in nadir orientation, extended at arm's length approximately 1.5 m above ground, and aligned toward the sun, i.e., 180° from the shadow of the operator. This effectively eliminated shadowing or interference by the field operator. Hats or other clothing with strong absorption features in the visible/IR range were avoided, if possible, to minimize interfering reflection (Figure 4.2). A sampling rate of 10 spectra per second was used. These individual spectra were averaged every 3 seconds and saved to a file. Each file, therefore, was composed of a single spectrum that represented the average of 30 individual spectra. These integrated files were collected continuously during slow traverses of a vegetation patch. The transects were spaced approximately 1 m apart, and covered the entire patch.

The THRO data were collected between 3 July and 6 July, 2001, 12-15 days following the AVIRIS flight. In all cases the ground spectral data were collected before mapping, and independent of the map results. Ground spectra were only collected on days that were cloud-free, or with only minimal clouds present toward the horizon. Bright, constant solar illumination is required to obtain quality spectra, and to avoid repeated recalibration of the field instrument during the collection. Because the instrument response is very sensitive to changing illumination, temperature, humidity, and wind, spectra were collected between 10:45 AM and 4:00 PM local daylight savings time, but predominantly as close to solar noon as was practical. Nevertheless, the instrument was frequently recalibrated during collection, from every few minutes to approximately every ½ hour depending on time of day and atmospheric conditions. This was done by rescanning the white reference plate to provide an updated measurement to reset the "100%" reflectance spectrum, which will drift over time and with changing environmental conditions.

The individual integrated ground spectra were edited with ViewSpec Pro software (Analytical Spectral Devices) to eliminate spectra that displayed significant noise, a distinct jump in reflectance values between the three individual spectrometer components, or other clearly anomalous spectra resulting from drifting spectrometer calibration, varying atmospheric conditions during data collection, white reference spectra, or other unintentionally collected non-

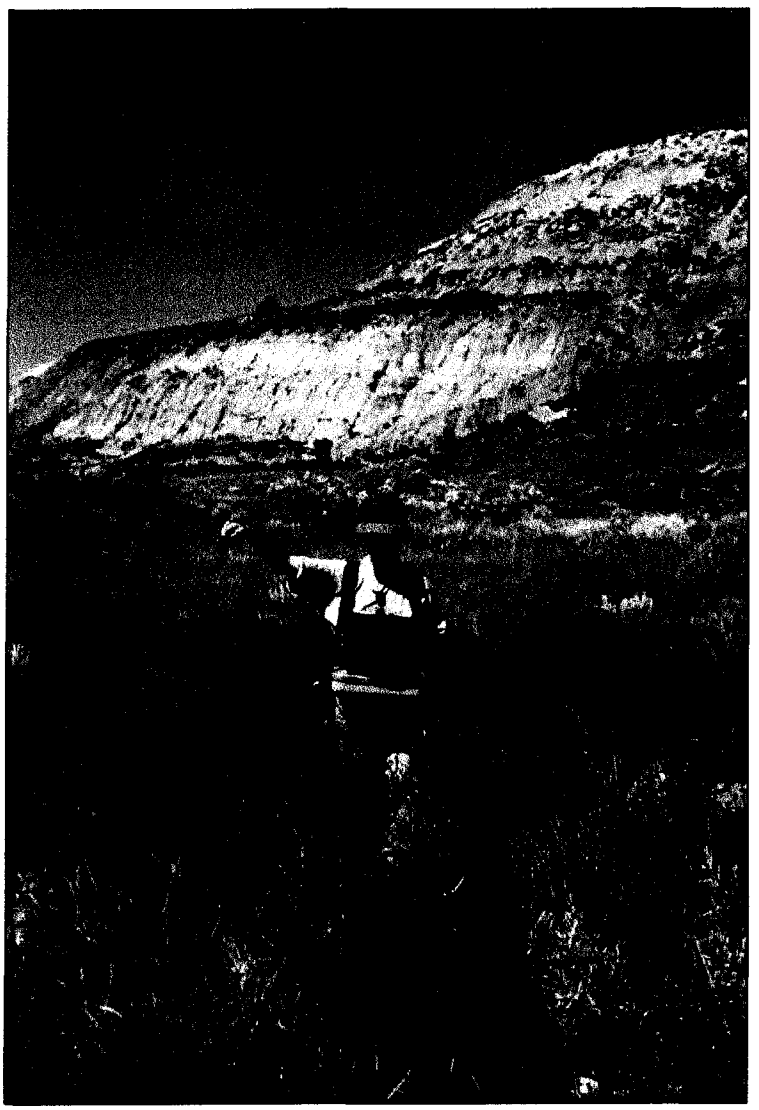

Figure 4.2. Collection of vegetation spectra with portable field spectrometer (Analytical Spectral Devices, ASD FR model, covering VNIR, SWIR I, SWIR II range).

vegetation spectra (sky, clothes, etc.). The remaining spectra were averaged for each individual patch, imported into ENVI as ASCII files, and re-sampled to match the coarser, 10 nm bandwidths of the AVIRIS sensor.

IMAGE PREPROCESSING

BAND EDITING AND IMAGE PREPARATION

The four to six data cubes in each flight line were mosaiced, leaving four flight lines per date for the remaining processing. All further processing was completed on each full flight line. Image edges were trimmed to eliminate irregular boundaries and areas of no data. The images were examined for integrity and spectral profiles were checked for anomalous detector responses to remove bad scan lines, bad bands, or other obvious spectral anomalies. The original 224 radiance bands were edited for noisy responses at both the short and long wavelength extremes of the spectral range, as well as to remove redundant bands in the overlapping region between individual spectrometers A and B.

DATA CALIBRATION

Radiance was converted to apparent reflectance using the calibration program, Atmospheric Correction Now (ACORN Quick Start Guide, 2001). The ACORN program uses a radiative transfer model and the AVIRIS measured radiance data to correct the radiance spectra for atmospheric effects and convert the measurements to reflectance (see chapter 3 for additional discussion). The correction was completed in two stages. In the first, the time, date, geographic coordinates, mean elevation, and estimated visibility parameters were supplied. The radiative transfer parameters were calculated to model then remove atmospheric absorption and scattering effects. Water vapor was determined, and corrected, on a pixel-by-pixel basis, while other absorbing gases were estimated as an average value for the entire image. The result of this first step is an approximately 80% correction to the apparent reflectance of surface materials. The remaining 20% of the variance is due to errors in the radiative transfer model, and in the estimated environmental conditions. In the second correction step, the single-spectrum

enhancement, the mean spectrum (calculated from all the field spectrometer measurements over the calibration site) was compared to the averaged, level 1-corrected image spectrum that was derived by averaging the spectra for the image pixels collected over the same calibration area. Differences between these were used to calculate correction factors to apply to the imagery to remove artifacts and anomalies that remained in the image spectra after the radiative transfer model correction (step one) was completed. In 2001, field spectra were collected during the AVIRIS data collection, as well as 2 weeks later during a Hyperion over flight. Field spectra, collected in 2000 at the same time of year, were used to calibrate the 1999 data (Root and Kokaly, in preparation).

Personnel at the USGS Spectroscopy Laboratory, Denver, CO, completed additional smoothing and extrapolation of reflectance through the 1.4 μm and 1.9 μm water absorption regions using a laboratory-measured spectrum of an asphalt sample from the calibration site.

All fractional reflectance values, to four significant figures, were converted to integers using a 10,000 multiplier. The derived atmosphere and modeled atmosphere from each flight line were used to independently correct for atmosphere in each run.

SPECTRAL LIBRARY CREATION

The algorithm used to map leafy spurge required a reference spectral library, against which the spectra of unknown image pixels could be compared and mapped. In the past, plant spectral libraries have been created from field and laboratory samples, as well as derived via unmixing from the imagery itself. Both field-based and image-derived spectral libraries were evaluated to determine which was most suitable for the leafy spurge mapping project.

FIELD-DERIVED. To create the field-based library, the edited mean field spectra (see following Spectral editing section) were imported into ENVI, convolved to match AVIRIS bandwidths, and saved as a spectral library. The final ground-based library was composed of 28 spectra, which included duplicate measurements of some of the vegetation patches when two spectrometers were used to collect spectra over a single patch (Figure 4.3).

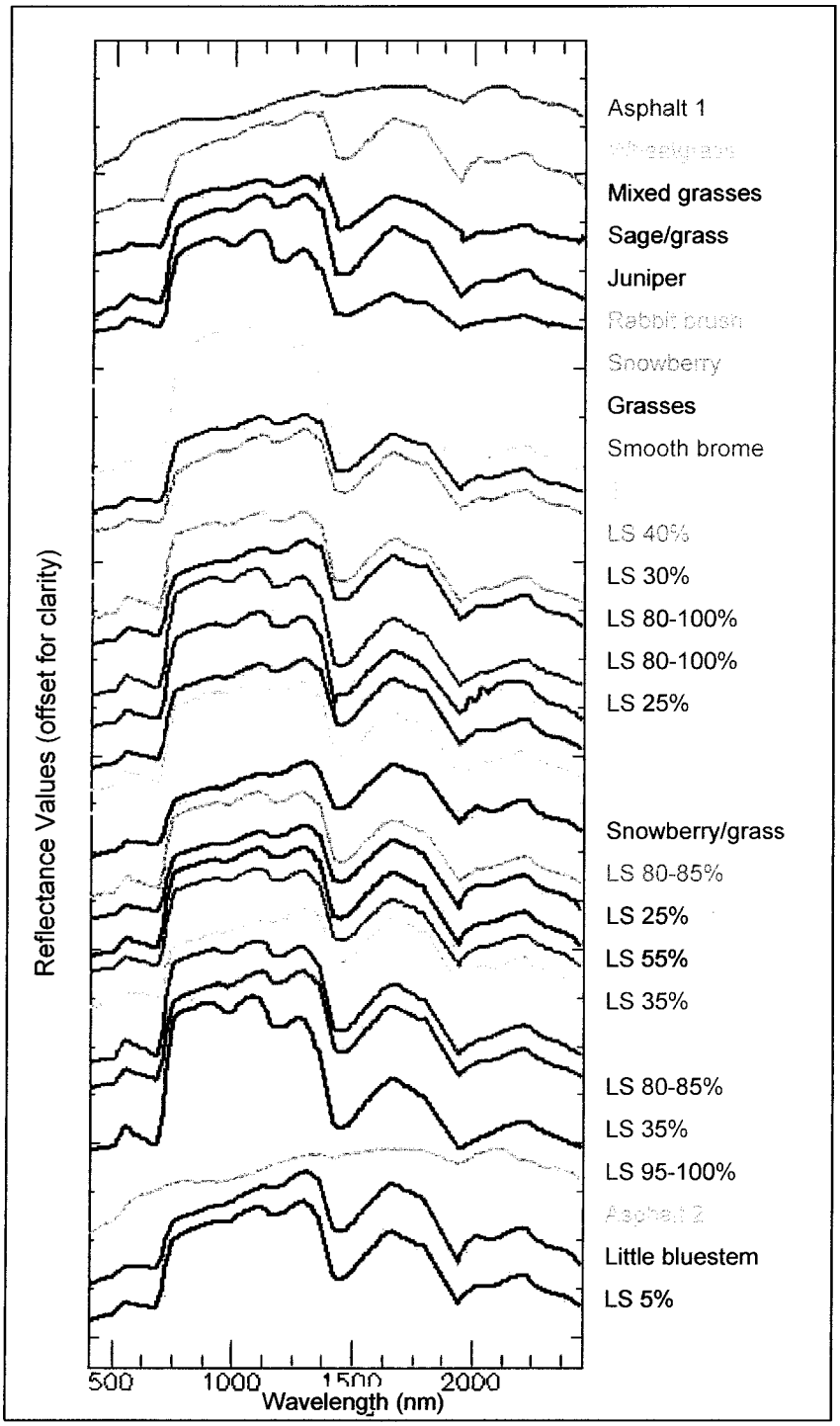

Figure 4.3. Field-derived spectral library. Derived from field measurements collected in THRO, July 2001. Includes calibration site (asphalt), leafy spurge (LS) patches ranging in density from 5% to 100% plant cover, and vegetation species that are typically associated with spurge throughout the region. Spectra collected with ASD FR field spectrometer. Spectra were edited for bad spectra, averaged, and convolved to the bandwidths of the AVIRIS sensor. Spectra are offset for clarity; tics represent a reflectance value of approximately 0.138.

IMAGE-DERIVED. The image-based library was derived using spectral unmixing techniques (Adams et al, 1993; Boardman, 1993). Specifically, a variant of the "hourglass" method (Figure 4.4) was used (Boardman and Kruse,1994; CSES, 2000). This method has been incorporated into ENVI software. With this technique, the purest pixels are isolated from the image through a number of progressive steps to isolate the endmember spectra. These were saved in a library, which is then used to scale back out to map the entire image. The general sequence of steps included: a minimum noise fraction (MNF) transformation (Green et al., 1988; Lee et al., 1990), followed by the pixel purity index algorithm (PPI) (Boardman et al., 1995), then n-dimensional visualization (Boardman and Kruse, 1994) and selection of the purest image endmember pixels (see discussion in Chapter 3). The endmember classes were edited, and added to the spectral library, where the target class was identified following mapping.

MNF band selection for image spectral library. For the THRO data, each of the eight flight lines was independently run through the MNF transformation. The number of visually coherent (e.g., information-rich) MNF bands varied somewhat between flight lines. After visual inspection of the THRO data sets, between 34 and 38 MNF bands (depending on flight line) were considered sufficiently coherent to use for further processing (Figure 4.5). The MNF band selection was supported by the corresponding eigenvalues (Figure 4.6). The eigenvalues for MNF bands greater than 34-38 were approximately one or less, which indicates that these bands represented predominantly the variance resulting from processing artifacts (from the cross-track correction), sensor noise (striping), or random signal noise.

Pixel purity index (PPI). A purer set of MNF-transformed pixels (e.g., homogeneous, unmixed pixels) was isolated using the pixel purity index step. The selected 34 to 38 MNF bands were input to the pixel purity index algorithm, to identify and tag those pixels that plotted as extreme. For each flight line, the selected set of MNF bands was run through 32,000 PPI iterations. During each iteration a randomly oriented, multi-dimensional spectral plot was projected onto a random, unit vector (Boardman et al., 1995). The pixels falling on the outer extremes of this line were tagged as unique, and the number of times that each pixel was tagged was calculated. Digital number (DN) for the resulting image represented the number of times

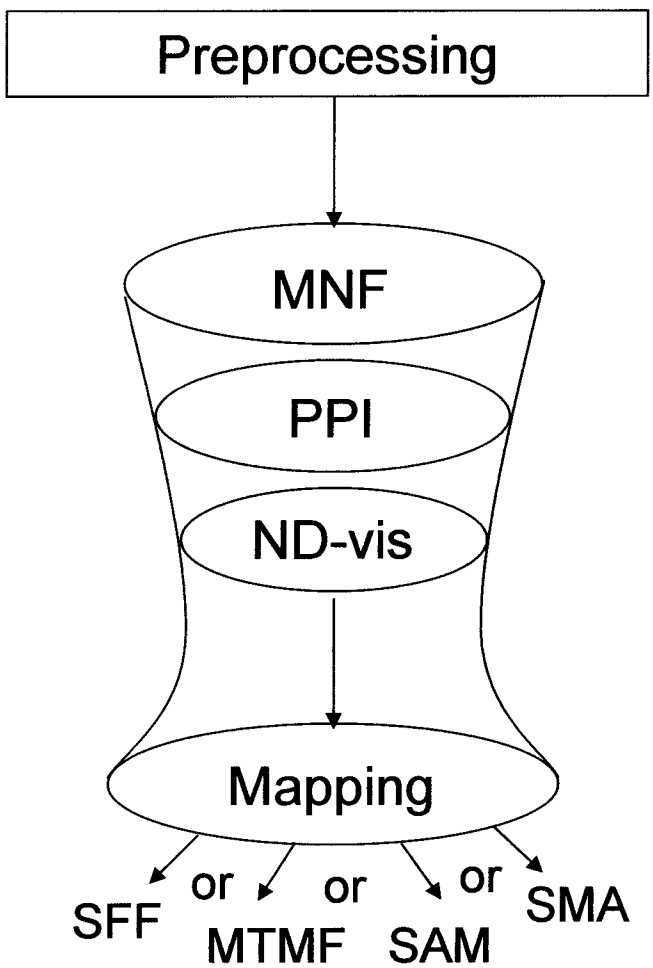

Figure 4.4. Standard "hourglass" processing. Data reduction steps completed prior to mapping are outlined: MNF transformation to reduce data volume and maximize variance between bands; PPI to select a pure set of pixels; ND-visualization to isolate endmembers for the image-derived library used for mapping (figure derived from CSES, 2000 and ENVI User's Guide, 2003.

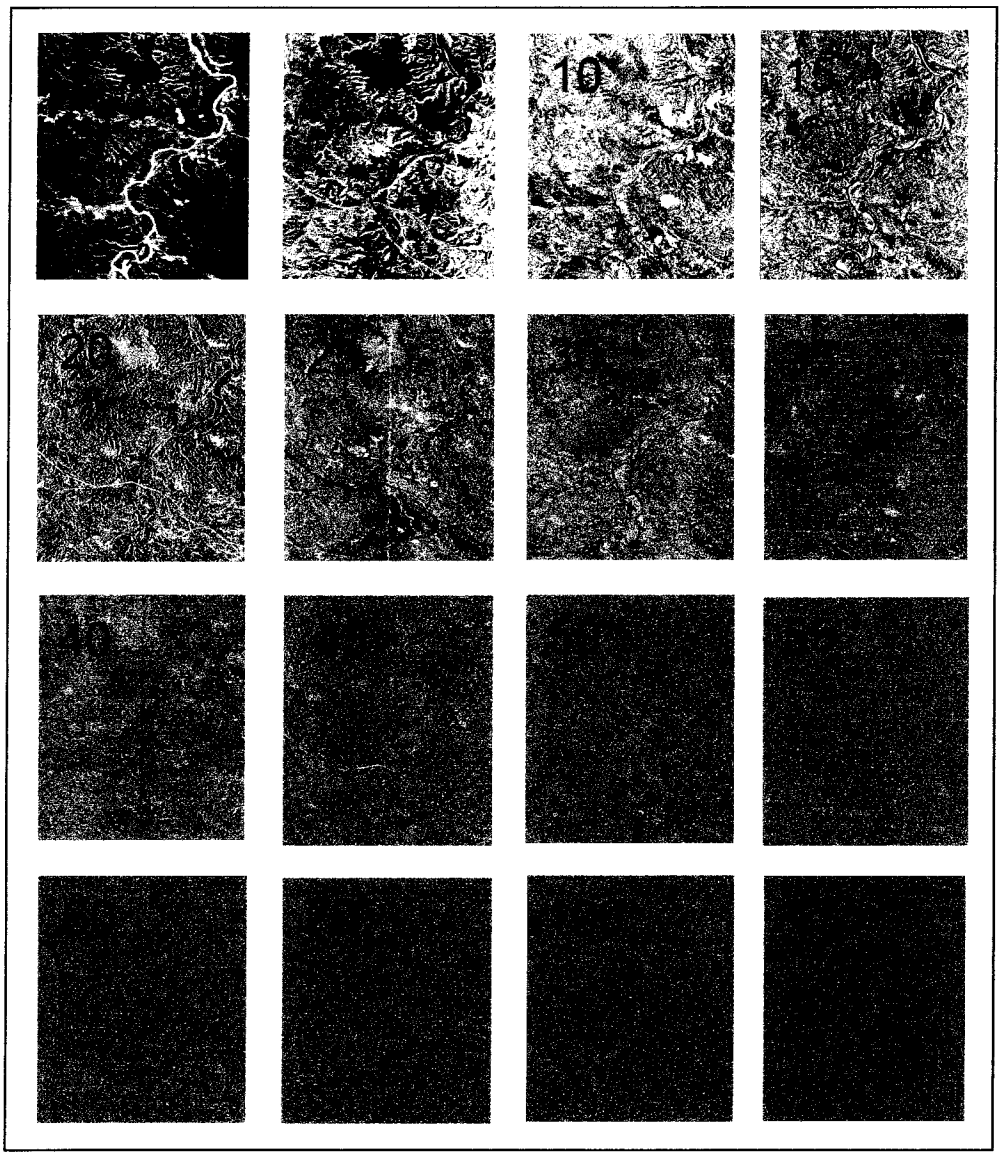

Figure 4.5. Declining image quality and increased noise with increasing MNF band number. As noise becomes dominant, coherent patterns in the image are lost. Grayscale represents the eigenvalues for each component (low, negative in black, high positive in white), where each image (MNF component) has been rotated and rescaled to maximize the variance remaining in each image. Number indicates the MNF component, ordered from 1 to 175 (maximum to minimum contribution to variance).

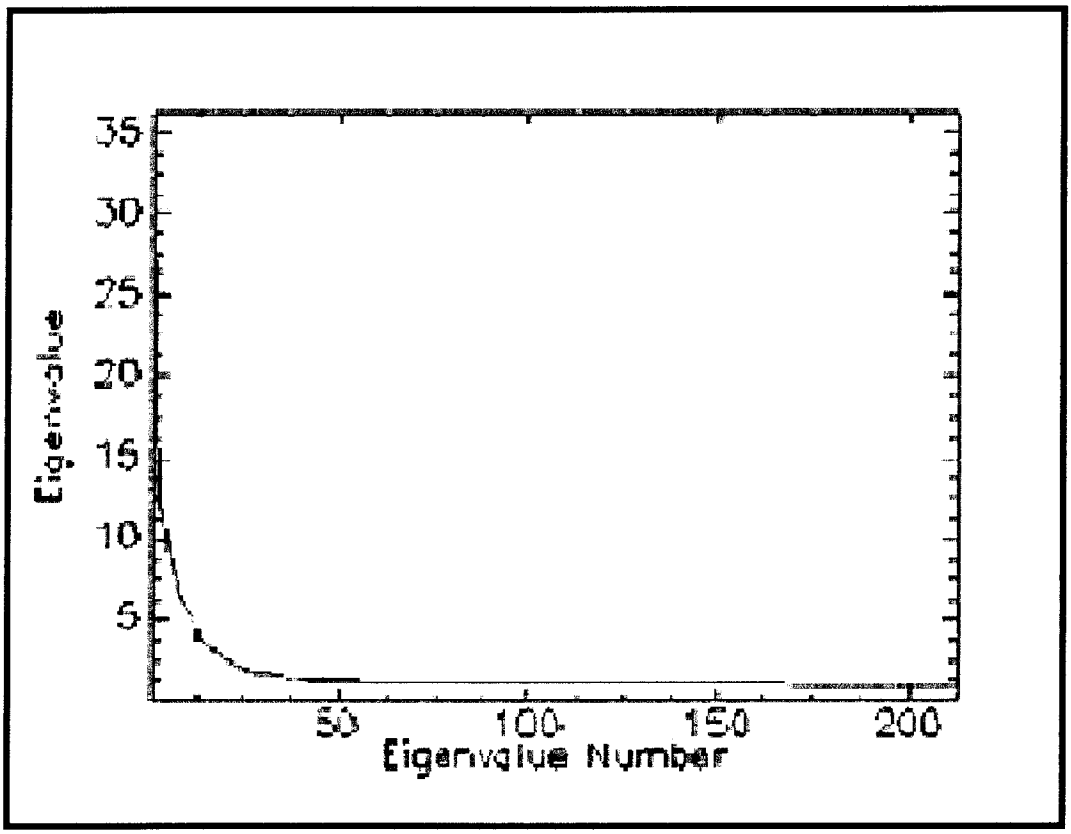

Figure 4.6. Eigenvalue graph. The example above indicates the decrease in eigenvalue that occurs with increasing MNF band number. Between MNFs 35 to 50 the MNF bands become dominated by noise, indicated by the low and constant eigenvalues, and contribute little useful information regarding true land cover variance.

each pixel was counted. Statistics were calculated for the PPI images to evaluate the count distribution. Count thresholds were established so that approximately 6000 of the most unique pixel spectra from each flight line were isolated. This required setting the minimum thresholds generally between 2 and 15, depending on flight line. A maximum threshold, ranging from 2000 to 6000 counts for the eight flight lines, was also established to eliminate anomalous pixels with extremely high counts (i.e., 24,000). Rather than representing unique land cover materials, these anomalously high counts represented pixels that were affected by edge problems, line fallout, or random pixel noise due to sensor problems that had not been eliminated during preprocessing. Water/vegetation mixed pixels, sewage ponds, and eutrophic water also displayed unusually high counts (e.g., 10,000-15,000) due to the very unique signatures compared to "normal" vegetation, and were eliminated if detected. The maximum values of 2000 to 6000 represented the upper count limit for pixels that represented unique vegetation spectra. This upper limit varied between flight lines, but was identifiable by the clear gap in counts between high values at the upper end of a relatively continuous count distribution (at 2000 to 6000) and anomalously high counts (10,000 to 24,000). The unique pixels were saved as an ROI and input to the n-D Visualizer, from which the spectral library endmembers were selected.

N-D visualization and endmember selection. The 6000 purest pixels from each flight line were input to the n-D Visualizer. Only the subsets of 34 to 38 MNF bands were used in the visualization. All other bands were dominated by noise, and considered unlikely to contain any endmember pixels.

The plots of pixels in MNF space were rotated, and pixel groups that fell outside the main pixel cloud were collected as potential endmember classes. The process was repeated as additional bands were added to the spectral viewer until all selected MNF bands had been viewed in multiple random rotations, and no more extreme clusters could reasonably be found (see Chapters 3 and 5 for additional discussion).

SPECTRAL EDITING

An inverse transformation was run on the potential endmember spectra to view interpretable spectra while editing within a given class. (The MNF spectra are difficult to compare

and edit because they do not display wavelength-dependent, physically interpretable spectral curves). If all spectra within a class were not similarly shaped or were not simply variants of the same class with slightly different albedo, the class was discarded, or the anomalous pixel was located and removed. Spectra for the remaining classes were averaged to produce a single MNF endmember spectrum for each class. These were saved in a spectral library which was again edited to eliminate redundant and therefore potentially confusing spectral classes. This reduction eliminated 10-15 endmember classes (depending on flight line), leaving approximately 50 vegetation endmembers per library, and 10-13 general cover classes, which were combined in a single library, and transformed back to MNF space prior to mapping. Separate spectral libraries were derived from each flight line, although a single spectral library from each date was used for the final, park-wide analysis (see Chapter 5).

MAPPING

The MTMF mapping algorithm, with modifications, was used to create the maps. A significant component of this study, however, included testing the suitability and success of several preprocessing steps and mapping algorithms, and refinement of the mapping procedures for multi-temporal leafy spurge monitoring. As a result, the method comparisons, selections, and refinements are presented in detail in Chapter 5.

ENDMEMBER IDENTIFICATION

Endmember identification for the leafy spurge target class was done empirically following mapping. The spurge class was identified by a combination of: 1) vector overlay of the spurge vegetation polygons that had been characterized in the field; 2) vector overlay of the leafy spurge grids that had been measured and the vegetation characterized in the field; and 3) visual comparison of unknown individual and mean spectra from image classes with field spectra of known, representative vegetation classes. Because this study was primarily concerned with mapping leafy spurge, the identification of other mapped vegetation classes was not a priority.

POST-PROCESSING

Georectification of the images was completed after mapping to avoid potential modifications to spectra that could result from pixel re-sampling during rectification. The data were geo-referenced by personnel at the USGS Rocky Mountain Mapping Center using the Geomatica/PCI OrthoEngine module (Geomatica User's Guide, 2003). Each flight line was independently processed. Between approximately 200 and 500 ground control points per flight line were collected from three-band color composite displays of each AVIRIS flight line. These were tied to UTM coordinates of identical locations on a mosaiced set of USGS digital orthophoto quadrangle maps (DOQs). A cubic spline algorithm was used to warp the AVIRIS imagery and classified maps into correct location. Overall RMS errors of less than 1 pixel (<17 m) were obtained with this method; however, individual pixel offsets of up to 5 AVIRIS pixels (~85 m) between the AVIRIS images and ground reference data were noted in some sections of the images. A similar range of offsets was noted between the georectified images from 1999 and 2001 when identical areas were compared between dates.

The classified images were joined with the mosaicing tool in ENVI by defining a seam line at slightly greater than 50% of the duplicated area contributed by each adjacent flight line, then using this to produce a subset of each classified flight line, minus the 50% overlap. The classified subsets were joined using a 20-pixel feathering distance. The overlapping coverage between 1999 and 2001 was screen digitized and saved as a region of interest (ROI) image, which was subsequently used to clip the 1999 and 2001 full thematic maps to the coincident aerial coverage for both dates prior to running the change analysis.

ACCURACY AND CHANGE MAPS

Detailed discussions of the methods that were used to evaluate map accuracy, and to produce maps of change in spurge between 1999 and 2001 are included in Chapters 6 and 7, respectively.

SUMMARY

The methods described in this chapter represent the basic procedures that are required to create a map from hyperspectral data. To produce accurate and consistent leafy spurge maps that are suitable for evaluating temporal change, however, required a more detailed analysis of specific steps within the basic procedure, as well as analysis of the most appropriate techniques to apply in cases where several methods or algorithms could be used. The method comparisons, selection, and modifications that were applied to improve multi-temporal hyperspectral mapping are described in Chapter 5.

CHAPTER 5

METHODS: COMPARISON, SELECTION, AND MODIFICATIONS

INTRODUCTION

One of the most common applications of remotely sensed data involves detecting temporal change in a landscape to evaluate and monitor ecosystem variation. With increasing pressure from anthropogenic and natural influences, monitoring changes in land use and land cover are increasingly important. Rapid, early identification of significant change is critical for intervention where detrimental or catastrophic modifications of ecosystems are occurring (Lunetta, 1998).

Remote sensing with imaging spectroscopy is one potential method for tracking subtle yet significant changes in land cover that cannot be resolved using sensors with coarse spectral resolution. This technology has been under-exploited for temporal studies. There are characteristics of hyperspectral data that present challenges when used for applied work, and applications-oriented studies have lagged behind in part due to the complex, interactive processing that hyperspectral imagery requires, as well as the associated steep learning curve. Reliable monitoring of change using imaging spectroscopy requires minimizing variation in processing methods over time, in order to produce consistent, comparable, and accurate results over time and space. Defining standardized methods will facilitate successful change detection. Ideally, applications-driven temporal monitoring should use processing methods that are easily implemented with commercial software, using readily accessible mapping algorithms. Land managers may be aware of the potential benefits of the technology for ecological monitoring, but are typically not well versed in hyperspectral processing and analysis. Several of the current processing methods require specialized training or expertise in remote sensing to determine the most appropriate methods to use, to make informed decisions during interactive processing, and to determine whether results are realistic and accurate.

Imaging spectroscopy has been used previously to map invasive species, including leafy spurge (DiPietro et al., 2002; Kokaly et al., 2001b; Kokaly et al., 2001c; O'Neill et al., 2000; Parker-Williams and Hunt, 2002; Root et al., 2002; and additional references in Chapter 2). With a few exceptions (i.e., Chen et al., 1998; Frank and Canty, 2003; Ustin et al., 1998; Garcia and Ustin, 2001; Roberts et al., 1997) imaging spectroscopy has not been used in multi-temporal or change detection work, and even fewer studies have focused on problems that are encountered with multi-temporal, airborne hyperspectral data processing. Comparative studies to determine the most appropriate and effective processing methods for specific applications are lacking (exceptions include: Clark et al., 1993; DiPietro et al., 2002; Farrand, 2001; Hunt and Parker Williams, 2004; Underwood et al., 2002), as are studies that focus on standardizing methods for consistency, automation, and repeatability over time. A variety of methods have been used to process hyperspectral data and are described in the literature (see Chapter 3), but the reports contain little discussion of the criteria that were used to select a particular method or parameter.

Most standard hyperspectral processing includes several steps that require interactive decisions on boundaries, thresholds, and appropriate inputs during the production of land cover maps. These include, for example, the appropriate number of MNF bands or the number of endmember spectra to process, thresholds for NDVI masking, and thresholds for matched filter and infeasibility scores for creating the target maps. In general, these decisions will vary with the quality and source of the reference data, and with the expertise or judgment of the image analyst, any of which could potentially impact map accuracy and consistency.

OBJECTIVES

Current hyperspectral data-processing methods were investigated and modified to evaluate whether they are sufficiently portable, and the results sufficiently reproducible for tracking changes in the distribution of the invasive weed leafy spurge (*Euphorbia esula* L.) over time. In particular, it was hoped that imaging spectroscopy would provide a means for locating small, fragmented, or nascent patches of leafy spurge, as well as provide a method to monitor subtle responses to treatments that have been applied over larger, established infestations.

In Section I of this chapter several common hyperspectral processing methods are compared and used to select the optimal processing stream for leafy spurge identification. Section II describes specific strategies and modifications that were developed to facilitate and streamline the analysis of multi-temporal AVIRIS imagery to: 1) eliminate or minimize interactive thresholding that requires in-depth knowledge of field data to guide threshold and mapping decisions; 2) increase automation and facilitate processing; 3) increase consistency of processing and results over time and space; and 4) reduce inaccuracies and/or variability in the maps that result from analyst decisions. The goal of these modifications was to produce consistent spurge maps from which change maps could be produced, and that these maps more accurately represent true change, rather than apparent change that was simply the result of different processing methods over time. This is essential for effective monitoring and management of invasive weeds over a regional scale. Land managers of infested areas could use this information to relate the change in weed distribution over time to different controls that have been applied, and to determine the most effective method(s) for managing this invasive weed. If the need for advanced training or experience can be minimized, imaging spectroscopy may become a more widespread tool for ecological and other applied work, provided that imaging spectroscopy can produce reliable identification of plants over time and space. This necessitates processing methods that are explicitly defined and repeatable, and that yield accurate and consistent results.

METHODS

Several standard hyperspectral preprocessing and mapping methods were applied to the THRO data. These are discussed in detail in Chapter 4, but include collection of the airborne data, field spectra collection and editing, and atmospheric calibration of the data to reflectance using ACORN software (ACORN Quick Start Guide, 2001). Preprocessing steps specific to hyperspectral imagery that were used to develop an image-derived spectral library included MNF transformation followed by PPI and nD-Visualization (ENVI User's Guide, 2003). These were followed by mapping, identification, georectification using a thin plate spline model (Geomatica User Guide, 2003), and mosaicing. Accuracy of the classification was assessed (Chapter 6). Leafy spurge maps for 1999

and 2001 were constructed, and from these maps of the change in leafy spurge distribution between 1999 and 2001 were produced (Chapter 7).

An area of THRO referred to as "no man's land" had been studied extensively in the field between 1998 and 2001. Because the spurge distribution on the ground within this area was well known, the area was featured in many of the map subsets that are presented in the following results.

Because this was a test of imaging spectroscopy for applied work, only off-the-shelf software and algorithms that were relatively easy to implement were used for both testing and modifications.

SECTION I: COMPARISON AND SELECTION OF IMAGE PROCESSING METHODS

INTRODUCTION

The effect of processing methods on leafy spurge classification was indicated by the distinct differences seen between initial test maps that were produced from a single data set (Figure 5.1). These maps indicated that the concentration of leafy spurge that was mapped varied dramatically depending on the pre-processing steps that were applied, the algorithm used for mapping, and threshold decisions that were made during processing. The source and quality of the spectral library also affected the results.

The variability in maps that were produced from the same data, due solely to processing differences, suggests that change maps produced from independently processed, multi-temporal hyperspectral data sets could easily include spurious results, and a misleading representation of change. Apparent change could represent an artifact of processing rather than true temporal differences in land cover. This, in turn, could lead to misinterpretation of the effect of controls, the advance and decline of infestations, and result in misdirected decisions regarding management of leafy spurge.

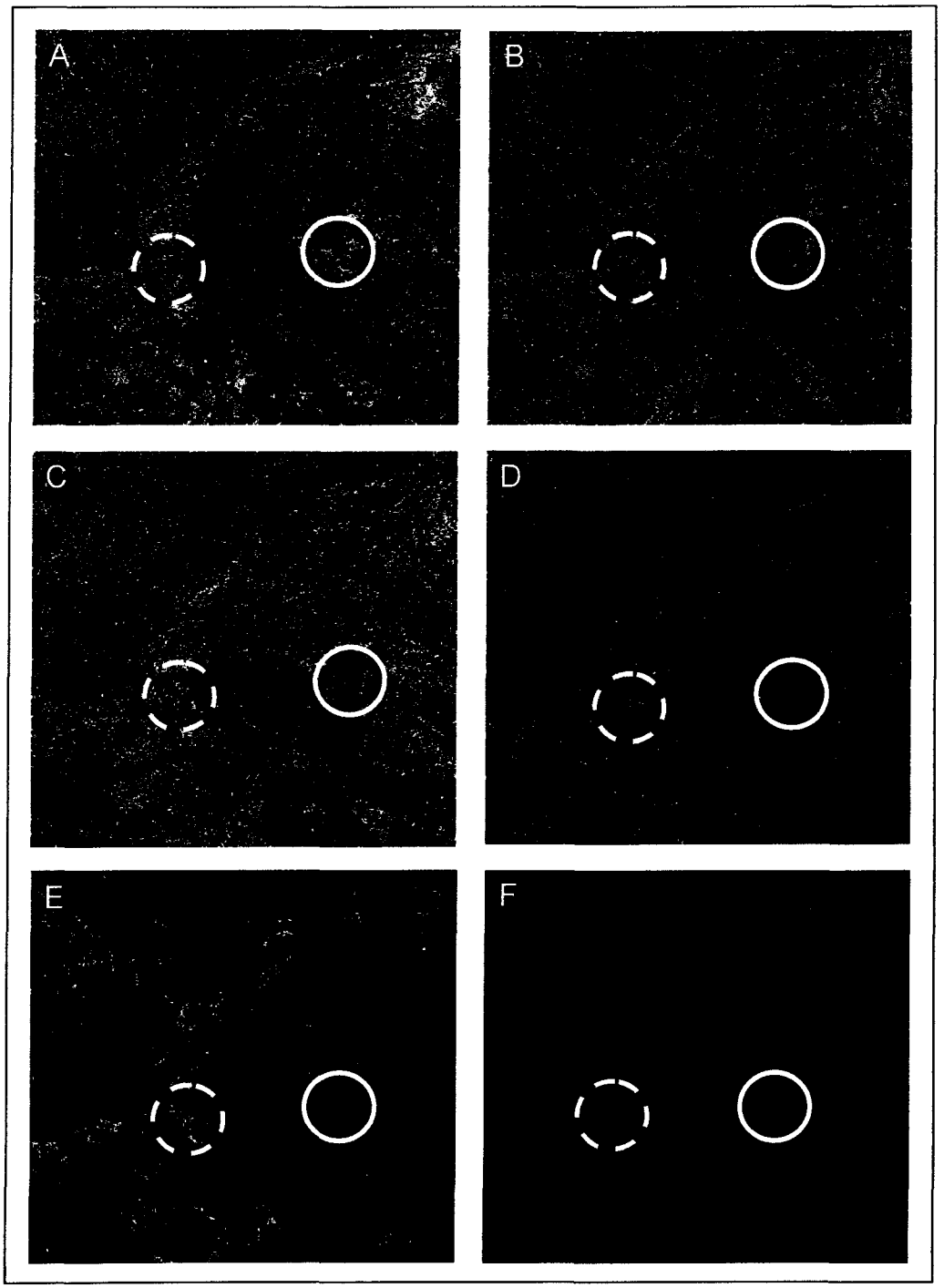

Figure 5.1. Leafy spurge test maps produced from the same data set, but with different processing methods. The same spatial subset is shown in each frame. The solid circle highlights an area verified as spurge-absent; however all mapping methods except E incorrectly mapped the vegetation as leafy spurge. All methods correctly identified leafy spurge (verified on the ground) in the area within the hatched circle; however spurge was moderately under-classified in D and E, and grossly under-classified in F. E, produced with the MTMF, was considered the most accurate overall, and was the algorithm selected as a starting point for the modifications and refinements for park-wide mapping.

COMPARISONS/TESTS

Because of the inconsistencies in the early test maps, several standard preprocessing steps and mapping algorithms, available in ENVI software, were tested and compared to determine which combination of methods was most appropriate for accurate and consistent leafy spurge identification. Two reference spectral libraries, field-based and image-derived, were also compared. Preprocessing steps that were examined included: the number of bands edited or removed before processing; cross-track illumination correction; and NDVI masking to isolate vegetation-dominated pixels. In addition, the stage at which the NDVI mask was applied relative to the cross-track correction and MNF transformation steps was tested. With the exception of a rigorous atmospheric correction, standard preprocessing steps have not been routinely recommended or applied to hyperspectral data sets, and it was unknown whether these additional preprocessing steps would improve the quality of the leafy spurge maps.

Several different mapping algorithms were evaluated, including spectral angle mapper (SAM) (Kruse et al., 1993), linear spectral mixture analysis (SMA) (Adams et al., 1993), spectral feature fitting (SFF) (Clark et al., 1990), matched filtering (MF) and mixture-tuned matched filtering (MTMF) (Boardman, 1998). These algorithms have been used for vegetation mapping in the past, and represent the more widely used methods seen in the hyperspectral literature. For applied vegetation mapping the unmixing algorithms have been used most commonly, however, the spectral feature fitting (SFF) and spectral angle mapper (SAM) matching algorithms have also been used successfully to differentiate plant materials (Root et al., 2002; O'Neill et al., 2000; Kokaly et al., 2001c). Specialized algorithms (i.e., MESMA and endmember bundling) are not currently available within commercial software packages, and were not included in this analysis. The algorithms that were developed specifically for processing imaging spectroscopy data are reviewed in greater detail in Chapter 3.

Test classifications were run on a single full flight line (flight line 1 from 2001). In each test, a single step was varied, while holding all other variables constant, to isolate the effect of each of the individual preprocessing steps, different mapping algorithms, or source of the spectral library (field or image). Map quality was either calculated using standard error matrices, or

assessed visually using several key diagnostic areas to select the best overall methods. Because each variable was tested separately, the results and discussion of each modification are included immediately following the presentation and description of the modification.

BAND EDITING

The 2001 THRO AVIRIS data contained anomalous spikes within specific bands, which occurred randomly in many of the individual pixel spectra. These anomalies were related to problems with several detectors in the AVIRIS sensor in 2001, as well as error introduced by interpolation of data values at the convergence of spectrometers 1 and 2 within the sensor this same year (R. Green, personal communication, 2003). The largest spikes, both positive and negative, occurred in the bands centered at 645 nm and 655 nm, which fell within the chlorophyll absorption feature in the visible region of the spectrum (Figure 5.2 A), and within the NIR plateau in the 1078 nm band (Figure 5.3 A). The two visible bands were adjacent to one another within the chlorophyll absorption feature and were considered especially problematic because subtle differences within the chlorophyll feature are important for differentiating vegetation characteristics. Test maps were processed from data containing the bands, and again after they were removed. It was unknown whether spurge maps would improve with these bands removed altogether, thereby losing information from critical bands within this feature, or whether it was preferable to include these bands during subsequent processing and risk the potential negative impact of sporadic band anomalies on the extraction of image endmembers or the separation of plant species.

It is often recommended that hyperspectral data be run through an MNF transform to segregate useful information from noise, with the mapping then completed on a spectral subset that includes only the non-noisy, MNF-transformed bands (RSI, 2002). For this study, the MNF transform was used to test whether the "noisy" band anomalies could be minimized through a series of steps that included: MNF transformation; spectral subsetting to eliminate the MNF components that represented dominantly noise; and inverse transformation back to the original, untransformed data format. If band anomalies could be eliminated with this method, the complete

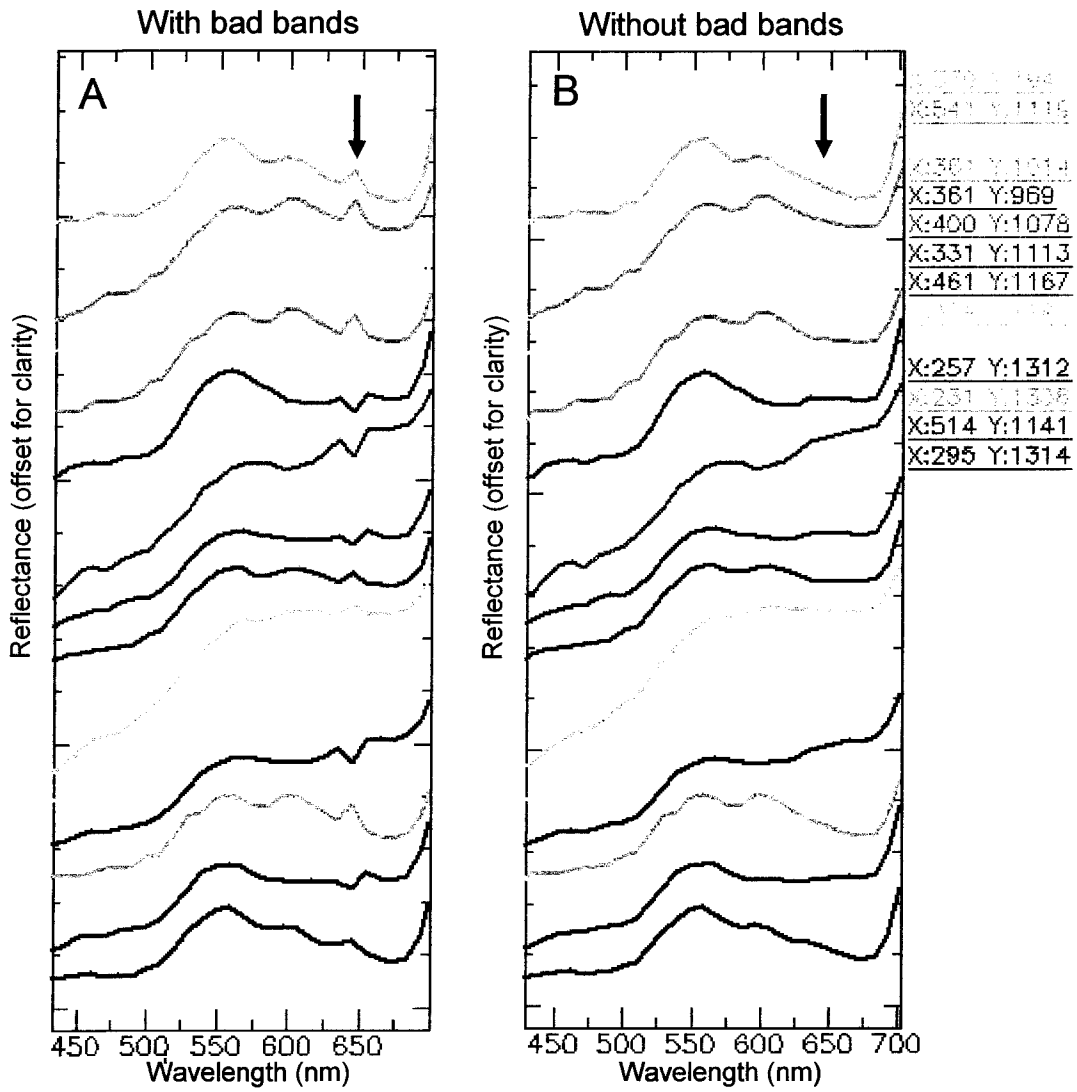

Figure 5.2. Chlorophyll absorption feature (visible region) before and after removal of band anomalies. A: Randomly selected pixel spectra containing bad bands within the chlorophyll-absorption feature shown by the sharp spikes in reflectance (both positive and negative, see arrow). B: identical pixel spectra after the bands were eliminated, showing the extrapolation of reflectance across the bands that were eliminated (see arrow).

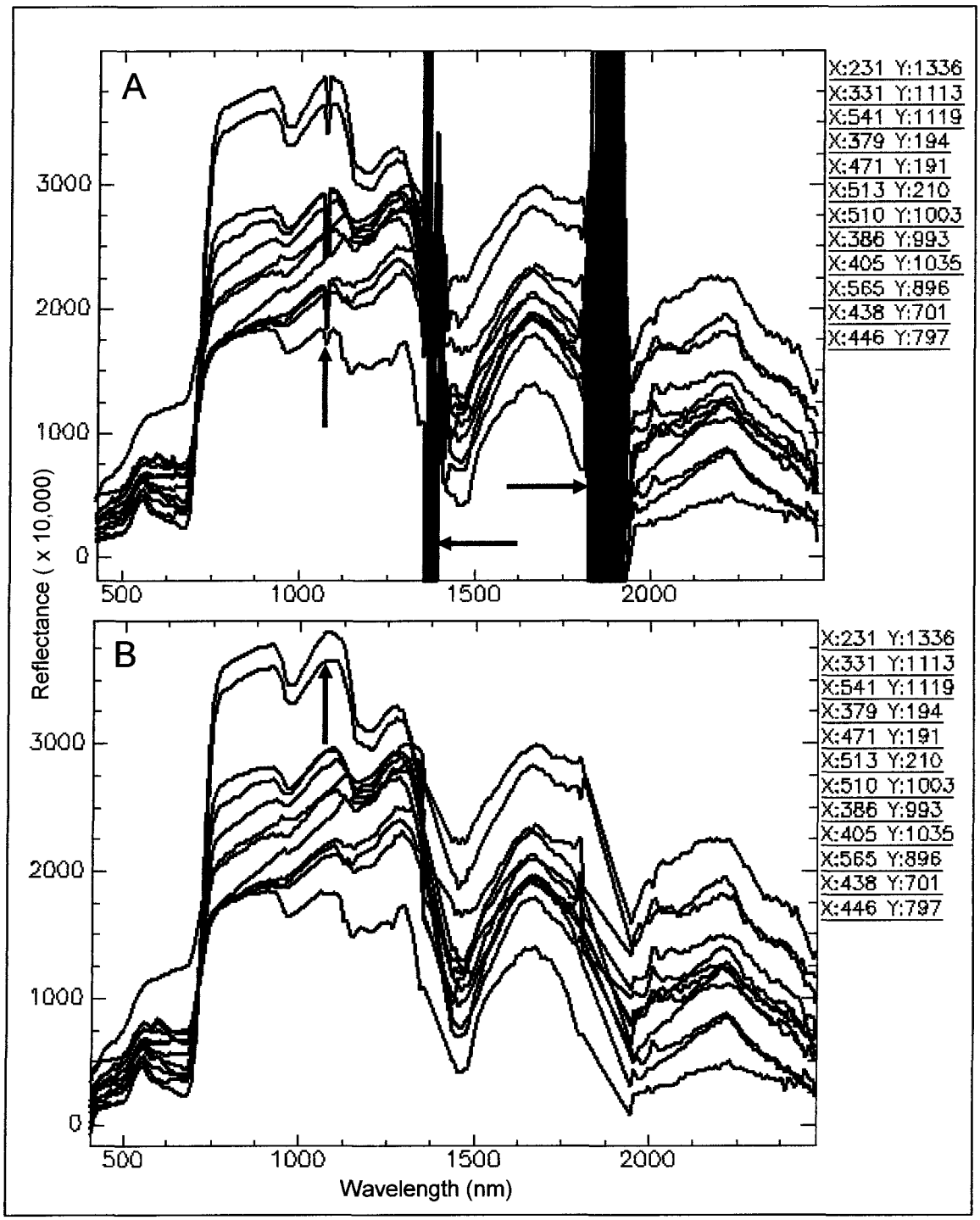

Figure 5.3. Effects of band removal over full spectral range. Example of anomalous reflectance spikes from bad bands in the NIR (red vertical arrow in A), and noise within the major water-absorption regions (horizontal arrows). B shows the identical pixel spectra after bands were removed. Spectral subset method that was used extrapolated "reflectance" across the regions where bands were removed (B).

removal of the bands could be avoided. The MNF noise removal successfully minimized or eliminated the anomalous spikes in many of the bad NIR-band spectra (Figure 5.4 3B), but had little effect on smoothing the band anomalies in the chlorophyll absorption feature (Figure 5.4 1B, 2B).

Because the anomalies remained in the visible region, the bands were eliminated from all data to test the effect of these bands on spurge map quality. Figure 5.2 shows example spectra from the visible region before and after the bands were removed. The sharp spikes in reflectance at 645 nm and 655 nm have been smoothed, leaving spectra that are more characteristic of normal vegetation responses within this chlorophyll absorption feature. The extrapolation of reflectance over the eliminated bands is believed to be less problematic for mapping than if the anomalous bands remained in the data. The band at 1078 nm was also removed, with reflectance extrapolated over this gap as well (Figure 5.3 B).

Four spurge classifications were run to test the effects of the band anomalies. Identical subsets from these maps are shown in Figure 5.5. The spurge was well-documented on the ground in this region, and the circled areas were known to be infested with 80-100% leafy spurge plant cover. Two algorithms were used, the MTMF and SAM. Each algorithm run twice, using imagery with and without the anomalous bands included. With the bad bands included, the dense spurge zones mapped predominantly as 35% spurge with the MTMF (Figure 5.5 1A), while the SAM algorithm mapped the same area as predominantly 100% spurge (Figure 5.5 2A). After the bands were removed, the classification with the MTMF algorithm improved, with the dense spurge zone mapping as the 80% spurge class (Figure 5.5 1B). With the SAM algorithm, however, the quality of the maps declined, with the dense spurge patches mapping as both 35% spurge (yellow) and 0% spurge (green) (Figure 5.5 2B). The effects of the band removal were inconclusive, showing both improvement and decline in map quality with band removal, which appeared to be a function of the map algorithm that was used. Because the MTMF algorithm was ultimately selected for park-wide mapping, and because results improved with the MTMF when the bands were eliminated, the anomalous bands were removed from all imagery before the final mapping.

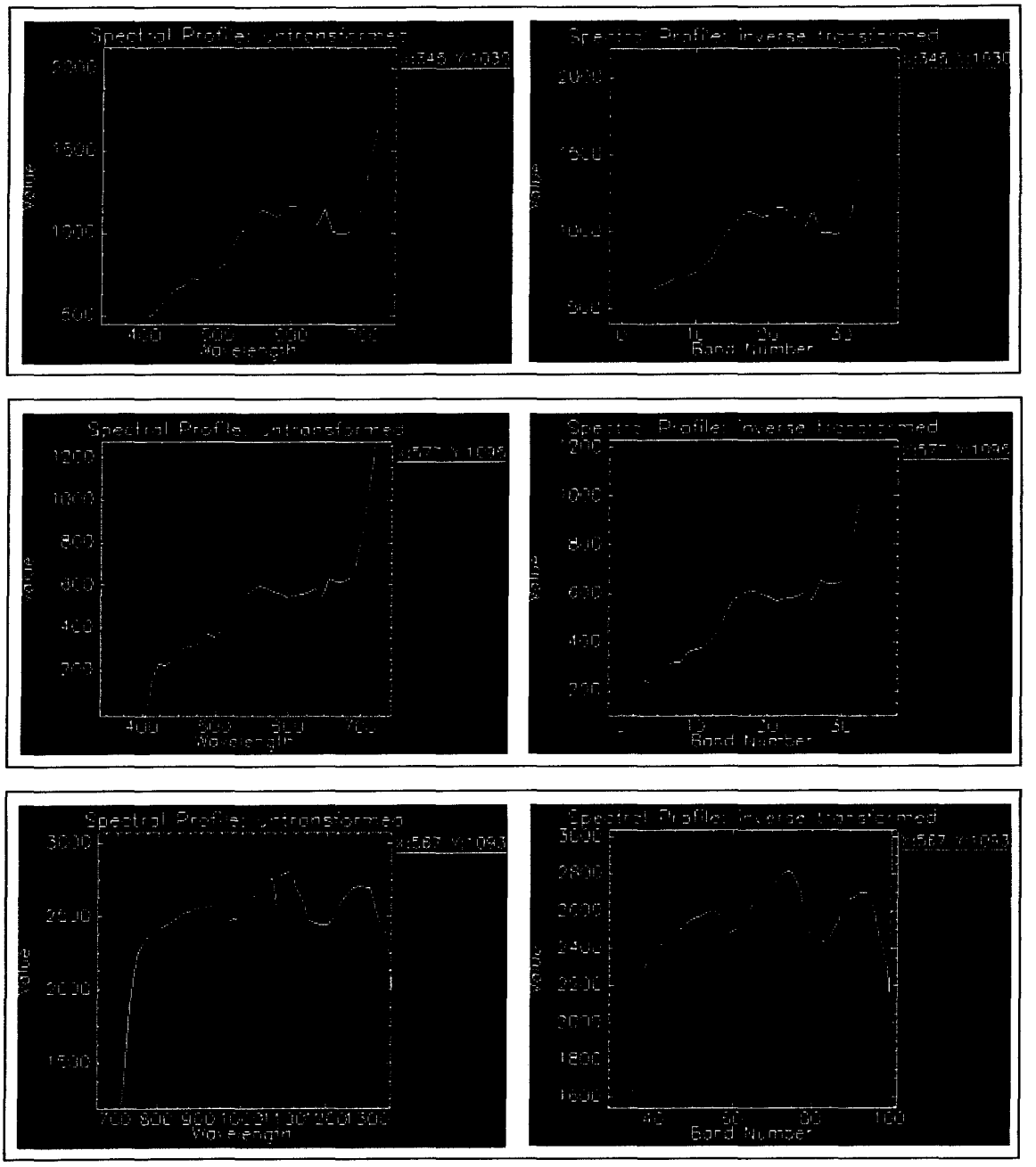

Figure 5.4. Inverse MNF transformation for removal of noise, bad bands. 1, 2, and 3 are three randomly selected single-pixel spectra. Anomalous spikes (positive and negative) are apparent in the visible region (1A and 2A, circled in red) and in the NIR (3A). Following MNF transformation, removal of noise components, and inverse transformation, spikes were eliminated from the NIR (3B), but remained in the chlorophyll absorption feature (1B and 2B). MNF noise removal and inverse transformation did not effectively eliminate all band anomalies.

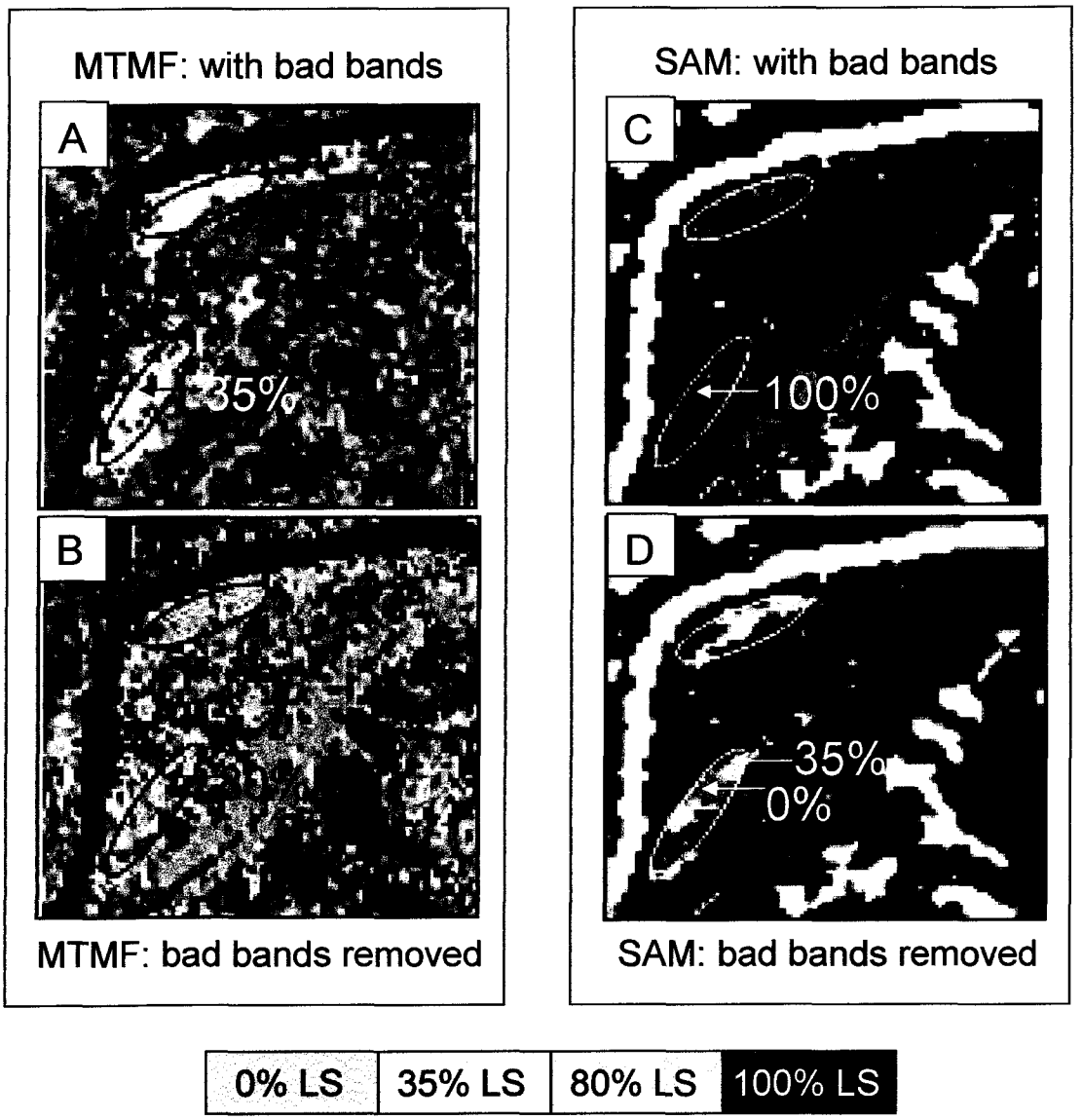

Figure 5.5. Effect of bad band removal on classifications: MTMF vs. SAM (the identical ground-derived spectral library was used for all classifications). Outlined spurge patches contained 80-100% spurge overall based on field survey. A and C show the classification results with bad bands included for the MTMF and SAM algorithms, respectively. Yellow areas circled in A mapped as 35% spurge; blue circled areas mapped as 100% leafy spurge (C). In B and D, bad bands were removed prior to mapping. Cyan areas mapped as 80% spurge with the MTMF (B); SAM algorithm classified the same areas as 35% (yellow) and 0% spurge (green) (D). The MTMF classification is more accurate with the bands removed, however, the SAM classification is more accurate without removal of the bands. Masked inert material is black in A and B, white in C and D; black areas in C and D were unclassified due to automatic application of a default threshold with the SAM algorithm.

Classifications were also run with and without the noise bands that occurred within the water absorption regions (centered at approximately 1.4 μm and 1.9 μm). Interpretable vegetation maps were produced when these bands were retained, but there were some unexpected results with certain algorithms, particularly the SAM. When this algorithm is run in ENVI, a default maximum angle of 0.10 radian is used as the threshold for including material in any given class. When this standard default angle was used for classification of imagery containing the noise bands, very little material of any kind was mapped, due to large angular differences between the ground spectral library, which contained minor noise, and the image spectra that contained only noise responses in the water absorption bands. The default angle used with SAM can be manually adjusted, and an order of magnitude increase in the maximum angle (to approximately 1.0 radian) was needed to produce a map in which a significant proportion of the image was classified.

Although it is generally not emphasized in the literature, most hyperspectral image analysts suggest that the water absorption bands be removed from the data before mapping (G. Swayze, J. Boardman, personal communication). Because of this, as well as the unusually large spectral angles, and because elimination of noise in general would likely benefit any classification, the noise bands between 1333-1482 nm and 1792-1998 nm were removed. In addition, test maps produced using the full spectral range (i.e., 0.4 μm to 2.5 μm) were superior to those produced using spectral subsets (e.g., visible, NIR, and VNIR). Of the original 224 spectral bands, 175 were used in the final analysis.

NDVI MASKING

Normalized difference vegetation index (NVDI) masking of maps was tested primarily to investigate whether isolating vegetation would improve the quality and detail of the image-derived vegetation library. By masking, the spectral complexity of the scene is decreased by eliminating inert materials with very different spectral characteristics, thereby increasing the chances of extracting different plant species and assemblages that are spectrally similar. Isolating these spectra will produce a more detailed vegetation library.

The mask was created using an NDVI image to segregate vegetation from non-vegetated materials. Several NDVI values were tested, to establish the optimal threshold value for creating a binary separation mask. A final threshold of 0.45 was selected. With this threshold, pixels containing only a partial, but significant, vegetation fraction were included in the vegetation analysis, while areas dominated by non-vegetated materials were eliminated from further processing. Small road pixels that included some vegetation signature derived from adjacent plants were included in the processing as vegetation, yet areas of inert materials that were known to be greater than one pixel were effectively eliminated with the mask.

The timing of application of a mask for vegetation may affect results. Kennedy et al. (1997) indicted that the application of a mask before or after running a cross-track correction causes the empirical cross-track correction to perform differently. They found that when certain cover types were included or excluded from the correction, the cross-track modeled response varied, and better models were obtained when specific categories of land cover were isolated and modeled separately. The mask for the THRO data was therefore applied before running the cross-track correction.

The stage at which the mask was applied relative to the MNF transformation was also of interest because the MNF bands varied visually depending on whether the image was masked before or during the MNF transformation (Figure 5.6). Transformed images were used as input to several of the mapping algorithms. In addition, MNF bands were used for the separation and collection of image endmembers, and it was unclear whether differences that were seen in the MNF images between the pre- and post-masking transformation could have an impact on the quality of the maps. It was not determined which of these was most appropriate or produced better maps; however, the clear differences in the first MNF components indicate that, minimally, the stage at which the mask is applied should be consistent for all flight lines, and for all dates that are directly compared.

CROSS-TRACK ILLUMINATION CORRECTION

The apparent reflectance of many materials, particularly plants, is known to vary with view and illumination angle, a function of sun, sensor, and target geometry (Schott, 1997).

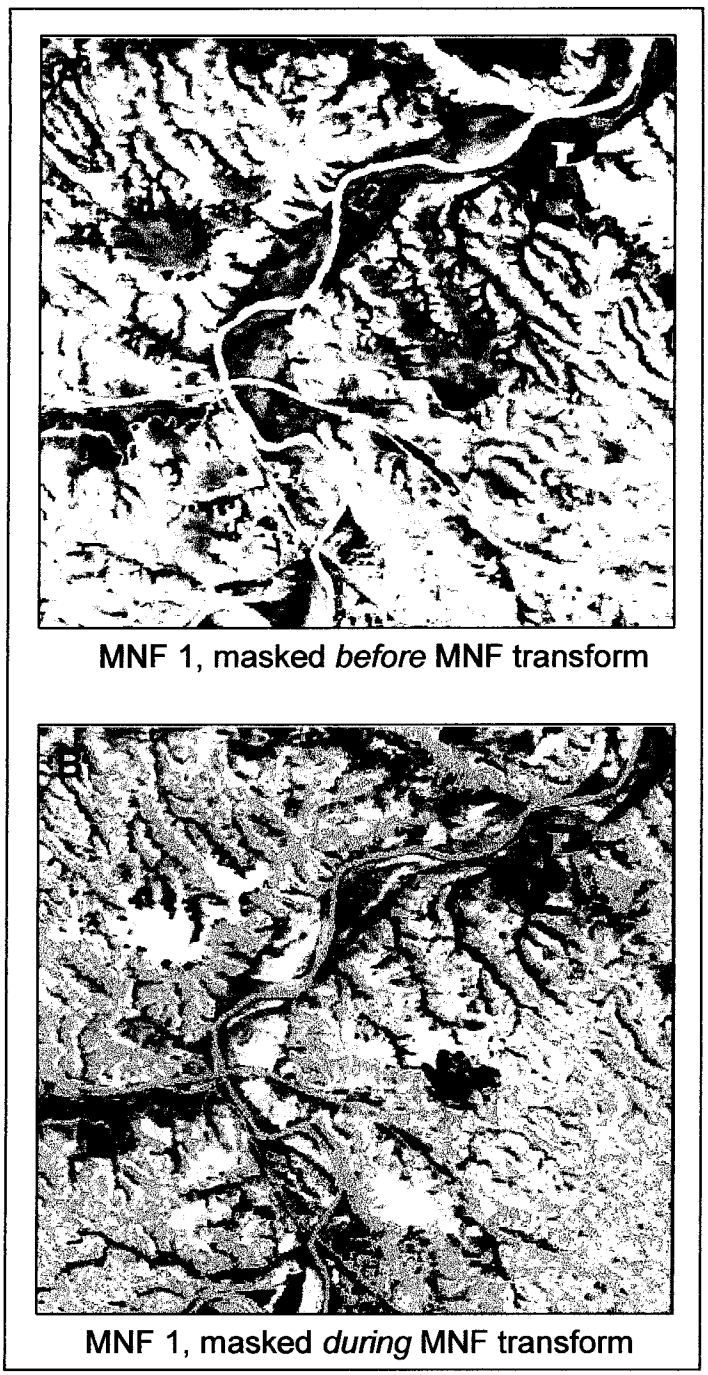

Figure 5.6. Effect of timing of masking on MNF 1, which shows the dominant source of variance in an image. In A the masked regions were treated as a "class" that was included in the MNF transformation statistics. In B (masked during transformation) the non-vegetated masked areas were not included in the MNF transformation.

Bidirectional reflectance distribution function models (BRDF) have been developed for a few plant species to characterize the reflectance over the full range of possible geometries. With known geometry and BRDF for a particular species, the apparent reflectance can theoretically be adjusted for angular differences in spectral response. These models are time consuming and difficult to derive, however, and are impractical to produce for all species or vegetation assemblages present within a scene, particularly for monitoring purposes. Kennedy et al. (1997) developed an empirical correction for variation in reflectance that is related to illumination angle and the cross-track view angle of the sensor. A similar cross-track correction can be modeled and applied using ENVI software to correct the data for the brightness variation.

The effect of a cross-track correction on the spurge maps was investigated for THRO imagery because significant variation in brightness was noted in a direction parallel to the sweep of the sensor, which was still apparent following a detailed atmospheric correction.

A pronounced brightness gradient was also evident across the scene in MNF component 1 (Figure 5.7 A). Similar to principal components analysis (PCA), the first MNF component of an image highlights the dominant source of variance in the scene. The variation in brightness from east to west for THRO MNF component 1 indicates that cross-track variation in spectral response is a dominant contributor to the overall variance in the image.

Cross-track brightness variation can have a significant impact on the map. The early test classification in Figure 5.8, for example, demonstrated the effect of variable illumination angle by the cross-track change in the dominant vegetation class. This was indicated by the change in dominant color (i.e., class) from east to west in the non-corrected image. This striping would be interpreted incorrectly as a change in the dominant vegetation class across the scene, which was known to be the same dominant species.

A first order polynomial was used to model the cross-track spectral response. The modeled apparent reflectance was then used to correct the imagery for differences in cross-track illumination. Figure 5.9 indicates the average apparent reflectance across the scene, for several sample wavelengths, along with the corresponding modeled reflectance for that same wavelength band. Several test classifications were run to compare map quality before and after the

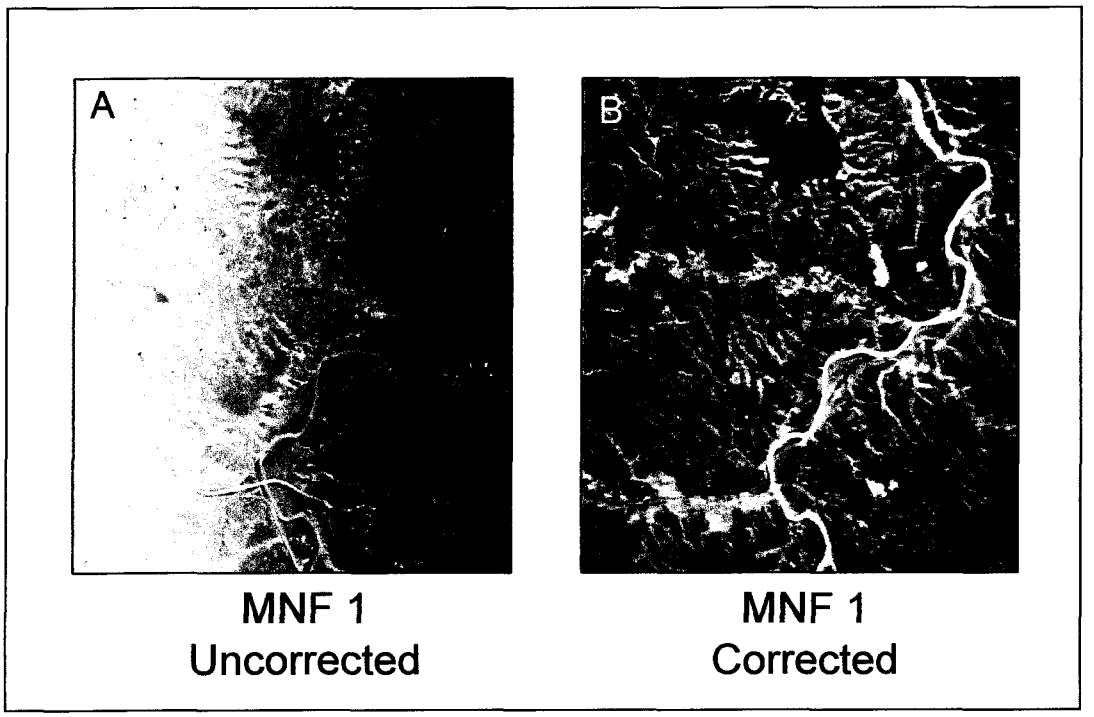

Figure 5.7. MNF 1, uncorrected and corrected, showing cross-track variation in brightness dominating variance in the uncorrected image (A). This effect was eliminated when a cross-track illumination correction was applied prior to the MNF transformation (B).

Figure 5.8. Classified map (subset) without cross-track correction showing apparent change in the dominant class (red to magenta, to green/yellow) across the scene. This is not true change in vegetation class, but an artifact of the change in scanner view angle/illumination angle. Image is approximately 10.5 km wide, from east to west.

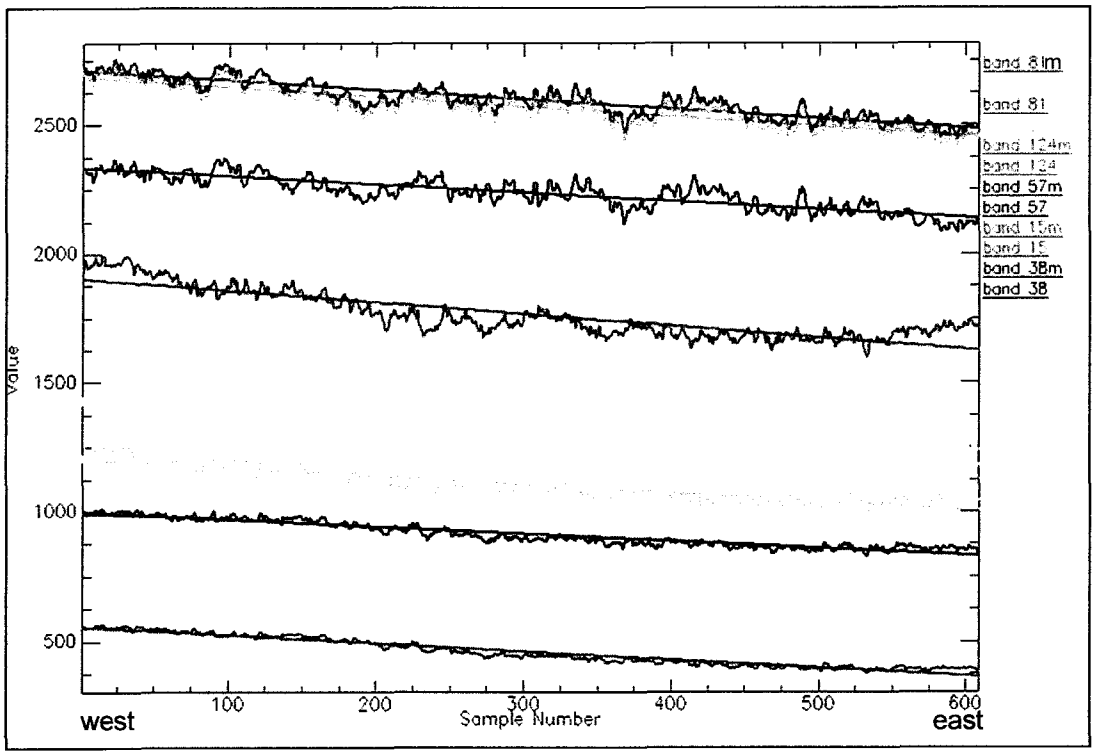

Figure 5.9. Examples of modeled vs. actual cross-track spectral response. The first order polynomial modeled responses (straight lines) are plotted with the corresponding measured response in each color pair. Each pair represents a different wavelength band. Apparent reflectance decreases from west (left side) to east across the width of the flight line. The average response for each of 609 samples or columns is plotted, across the width of the full flight line.

correction. The comparisons included the effects on MNF components and vegetation maps, vegetation maps after processing was refined, different algorithms and spectral libraries, and identical area maps.

In the cross-track corrected MNF band 1, this effect is no longer evident (Figure 5.7 B). The apparent class change across-track was also eliminated from maps following the cross-track correction.

The methods for processing were refined and improved over the course of this project (see Chapter 5, Section II); however, the effect of the variable cross-track illumination was still evident in uncorrected imagery following several refinements. In Figure 5.10, the difference in spurge classification with and without the correction is evident. The identical library was used for the maps, and green represents the leafy spurge class in all images. In Figure 5.10 C, a large area was erroneously classified as leafy spurge with the uncorrected data. The same area was correctly classified as an unusual non-native plant assemblage that was uniquely associated with prairie dog colonies in THRO when the correction was used (Figure 5.10 D). Figure 5.10 F shows an area known to be heavily infested with spurge that was correctly classified after the correction, but incorrectly mapped as other vegetation classes with the uncorrected data in Figure 5.10 E. The large documented spurge infestations shown in green in Figure 5.10 G and H were mapped with both the corrected and uncorrected data. The distribution in 5.10 H, however, matches the patches in the field more accurately. Overall, a qualitatively better map was produced from the cross-track corrected data.

Application of the cross-track correction also affected the outcome of algorithm and spectral library tests. For example, consistently un-interpretable results were obtained when the cross-track correction was *not* applied before using the ENVI SFF algorithm (Figure 5.11 B). Ten independent comparisons yielded the same poor results without the correction, while adequate maps were obtained with the correction (i.e., Figure 5.11 D). Based on the map subsets in Figure 5.12, the effects of cross-track correction vary depending on the source of the spectral library. There is a pronounced difference between the corrected and uncorrected maps when image-

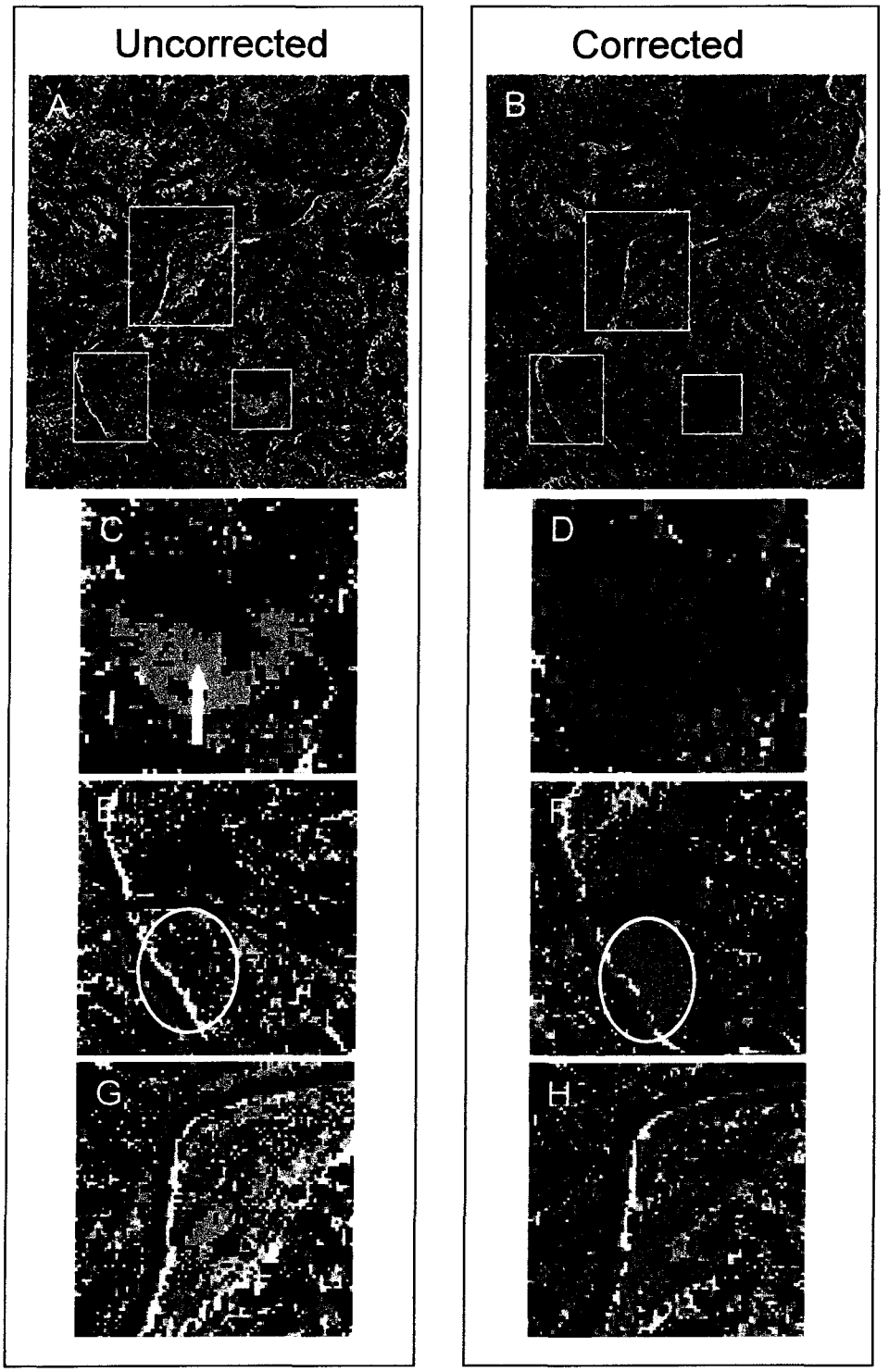

Figure 5.10. Map errors related to uncorrected imagery. Uncorrected map on left (A), corrected on right (B); three outlined areas are enlarged below the main image subset. C shows incorrect classification of spurge (green, see arrow) in area known to be devoid of spurge; same area properly classified in D after the correction. E shows spurge omission (circled areas) that are correctly mapped in F after correction (green). Spurge classification in H (green) is more correctly distributed than the uncorrected map in G, based on known field distribution. MTMF was used for both classifications.

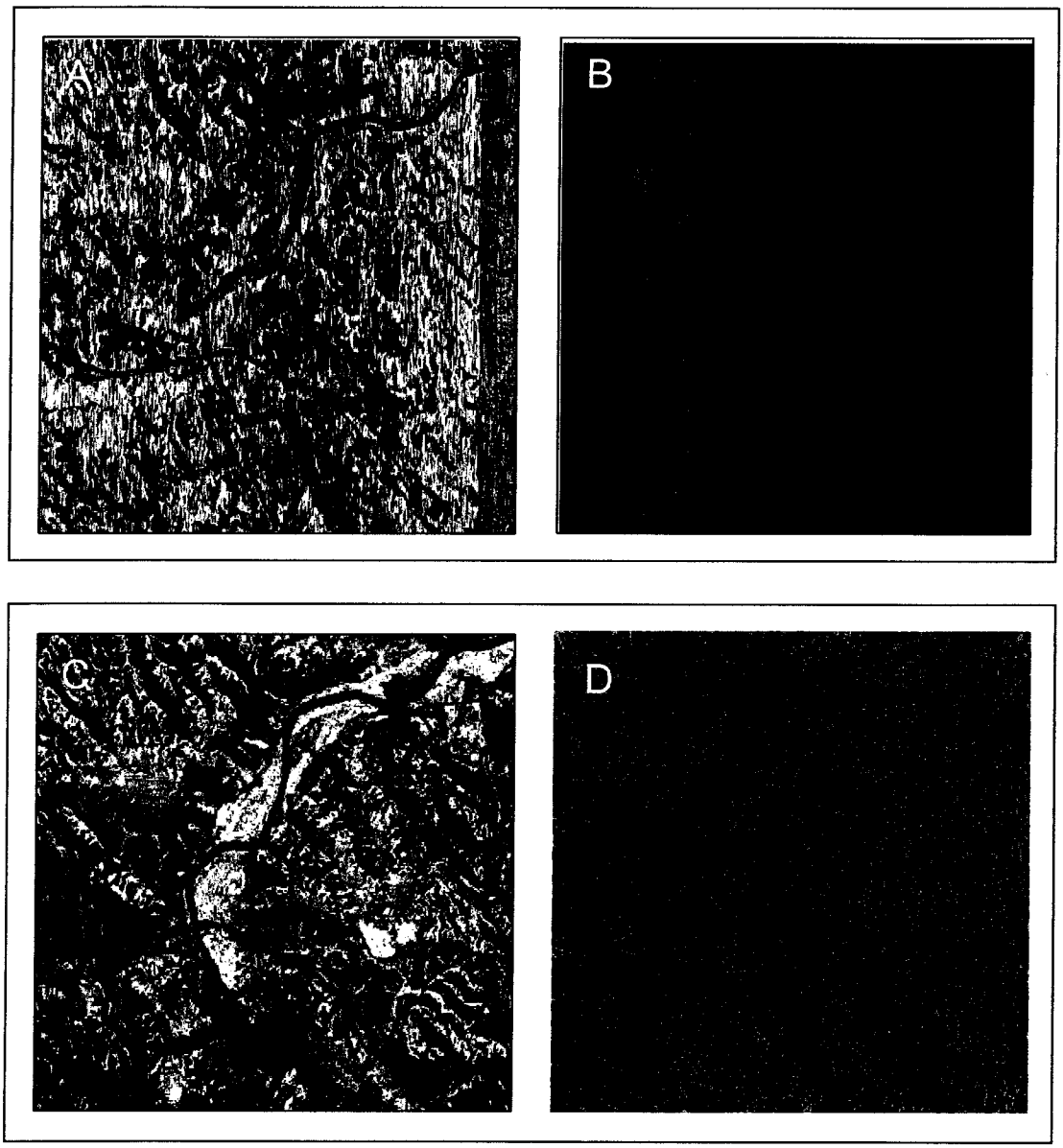

Figure 5.11. Cross-track correction effects on SFF maps. A: an example SFF "fit" image without cross track correction produces poor results, leading to an unusable, 2-class map (B). C shows the SFF "fit" image after the cross-track correction, which yields coherent results and an interpretable binary spurge map (D).

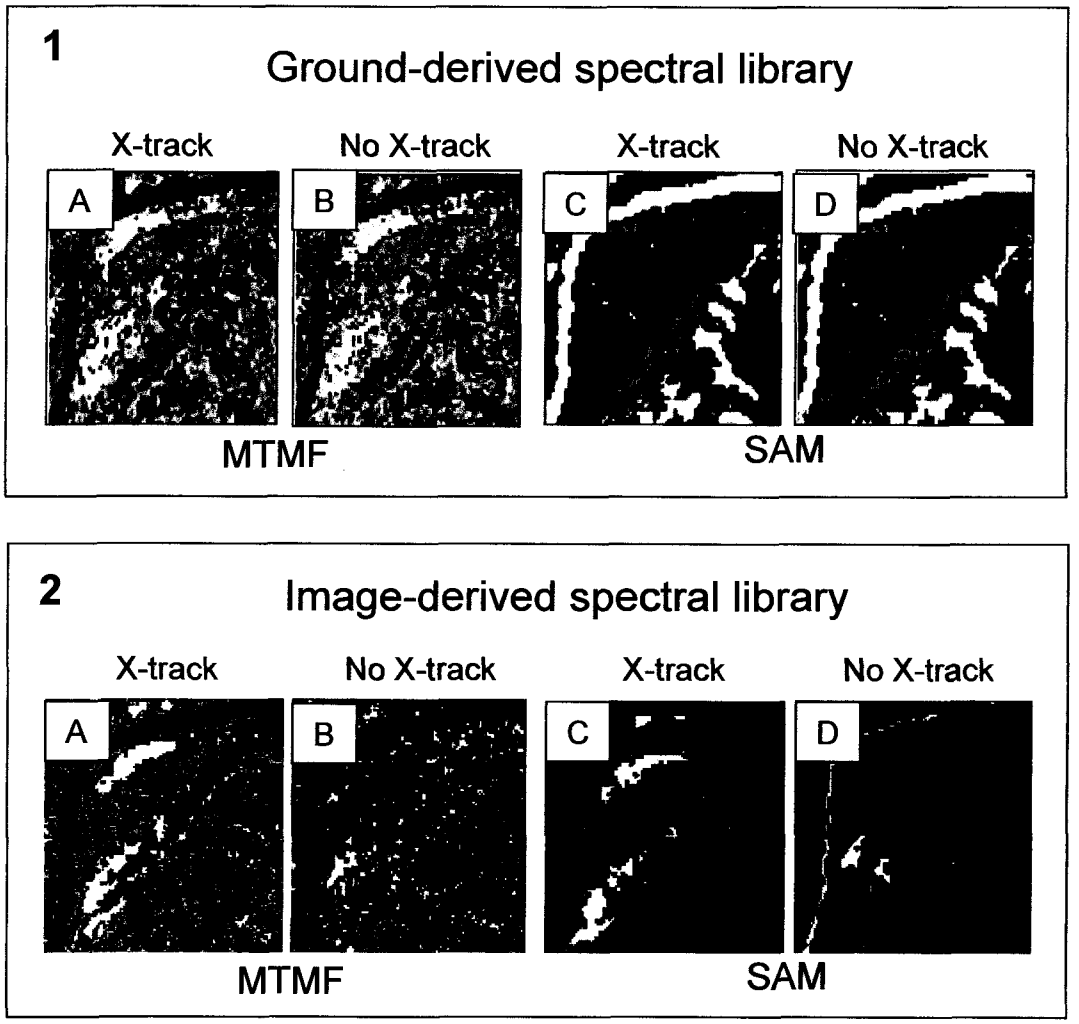

Figure 5.12. Effect of ground versus image-derived spectral library on maps, and relationship to cross-track correction and algorithm. In frame 1 all maps were produced with the field-derived library, using MTMF or SAM algorithms, with and without cross-track correction for each algorithm. The identical mapping methods were used for the classifications in frame 2, with the exception that the spectral library used for mapping was derived from the image. Two libraries were derived, from the image without a cross-track correction applied, and from the image following a cross-track correction. The leafy spurge class is yellow in maps 2A-D. Yellow indicates 35% density spurge in 1A,B; blue indicates 100% spurge in 1C and D. The identical map subset is shown in all frames. With the ground-based library, maps were nearly identical with and without the application of a cross-track correction (for a given algorithm); similar areas were mapped as spurge with both MTMF and SAM, however, different spurge density classes were assigned depending on the algorithm. With the image-derived libraries (2), the application of a cross-track correction had a more pronounced effect; cross-track corrected maps were similar regardless of the algorithm used for mapping. Non-corrected maps from the MTMF and SAM algorithms were similar as well, and large areas of dense spurge were omitted from the maps when the correction was not applied. Maps are more consistent when different algorithms are used when an image-derived library is applied, assuming that imagery is cross-track corrected before mapping.

derived endmembers were used, that is not apparent with the ground-based library (see Figure 5.12 and the following section on spectral library comparisons).

The consistency of maps produced from corrected and uncorrected data was examined by comparing the classifications of identical areas from adjacent, overlapping flight lines. Figure 5.13 B shows that the cross-track corrected data produced more comparable maps between the two flight lines than uncorrected data (Figure 5.13 A). Leafy spurge, and other vegetation classes as well, were mapped more consistently between the two flight lines when the corrected data was used. Identification of spurge, the green class in all maps, was also better with the corrected data (see yellow circled areas on Figure 5.13 A and B).

These results indicated that, in general, better results were obtained with the correction, and that a cross-track correction should be performed prior to the final area-wide mapping project.

FIELD AND IMAGE-DERIVED SPECTRAL LIBRARIES

The hyperspectral literature is dominated by processing methods that require a reference spectral library against which unknown pixels are compared and mapped. Two primary library sources are generally used, and there are conflicting opinions regarding which of these is best. The first is derived from the reflectance of known pure materials and mixtures that have been measured and characterized with laboratory and field spectrometers. The resulting spectra are saved as standard general reference files that can be used to map images, regardless of location. The second approach derives a scene-specific spectral library, where the spectra of the purest, least mixed pixels in a scene are isolated from an image and used to represent "pure" endmembers (classes). The spectra are saved to a scene-specific library against which that image is mapped. There are advantages and disadvantages to each of these two approaches to spectral library derivation (see Chapter 3), but few studies have directly compared the maps that are produced from each of these. The two spectral libraries for the THRO data were compared because it was not clear from the literature which would produce more accurate and consistent maps, or which was more appropriate specifically for leafy spurge mapping.

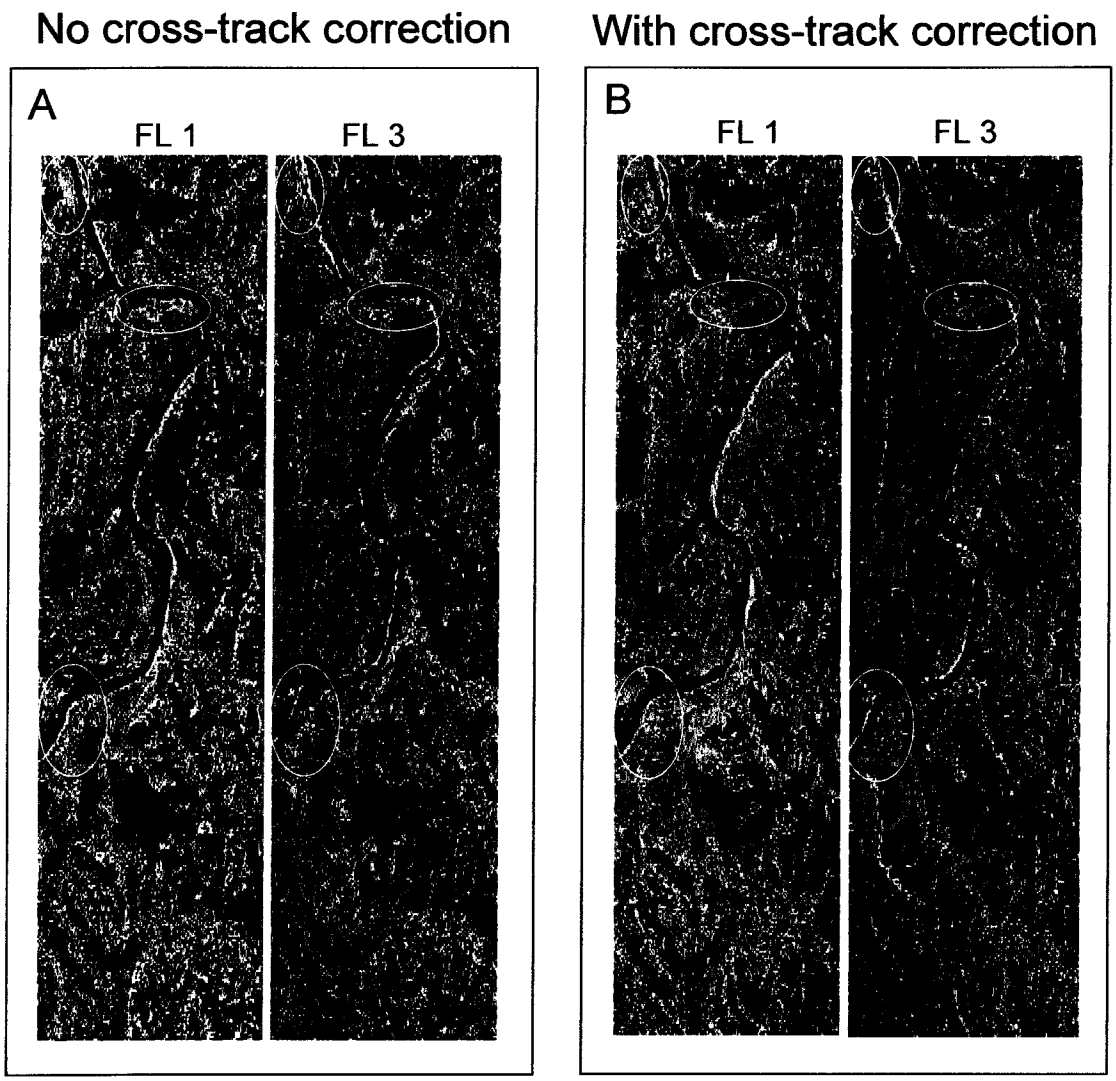

Figure 5.13. Map consistency and quality, with and without cross-track correction. In A, the same area was mapped from flight lines 1 and 3 using uncorrected data. Vegetation is not mapped as consistently as the same area after the correction was applied (B). Leafy spurge (green class in all figures) was not mapped as well or as consistently without the correction (see yellow circled areas); other vegetation classes in general appeared to be mapped more consistently between flight lines after the correction was applied (i.e., green circle).

The libraries were used either directly, or in transformed or edited formats (Figure 5.14) to produce a series of spurge maps. These included: the ground-based spectral library; assorted image-derived libraries (ranging in size from 35 to 63 endmembers); image-derived libraries that were edited for band anomalies and noise bands in water absorption regions; libraries run through MNF transformation (of both ground and image-derived); and libraries created from spectral subsets of specific absorption features that were isolated and continuum-removed (see Chapter 3 for discussion).

Figure 5.15 shows subsets of two vegetation maps that were produced from the same data, holding all processing variables constant with the exception of the spectral library. Both were cross-track corrected, MNF-transformed, band anomalies were removed, and the image was mapped with the MTMF algorithm. The leafy spurge class is blue in set 1, which was mapped with the transformed ground library. For the image-derived, transformed library used in set 2, the dense spurge class is tan. The circled area in 5.15 1A and 2A is a field-documented spurge infestation that was correctly mapped using both libraries. The circled area in Figure 5.15 1B and 2B, however, was known to include a unique assemblage of non-native forbs that was completely free of spurge. The area was mapped as spurge with the ground-based library, but was correctly mapped as other unique classes when image endmembers were used.

Figure 5.12 includes the results of another library comparison. Both ground and image libraries produced similar maps of documented spurge infestations, but only when the data were cross-track corrected before mapping. This was seen for both the MTMF and SAM algorithms. For both algorithms, the maps that were produced with and without the cross-track correction were also very similar when the ground library was used (compare 5.12 1a,1b, 2a, 2b). Without the cross-track correction, however, the maps that were produced with the image-derived library were very poor quality, as well as very different from the cross-track corrected version (Figure 5.12 3b and 4b). This suggests that the libraries may be interchangeable when imagery is cross-track corrected, but that the ground library performed better when imagery was not cross-track corrected. This also indicates that the effect of a cross-track correction on maps can vary

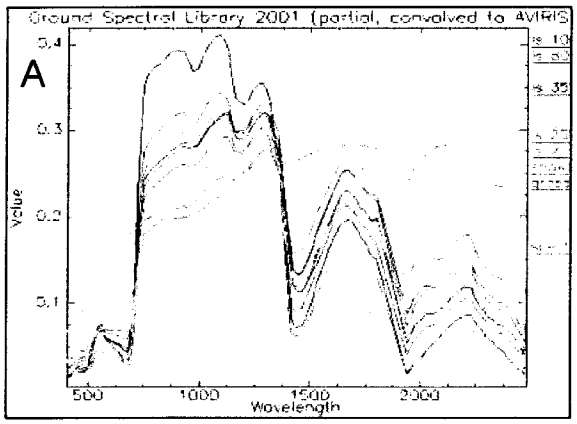

Ground spectral library

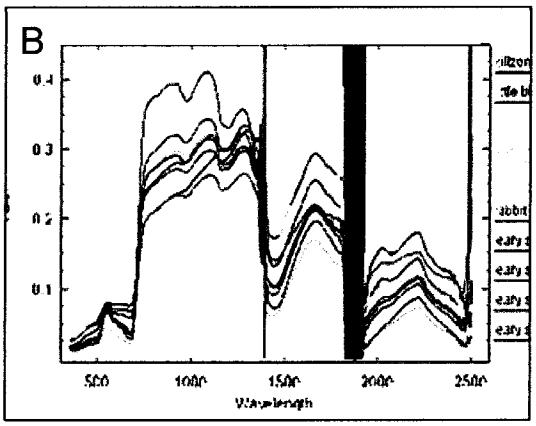

Image, full range, with bad bands

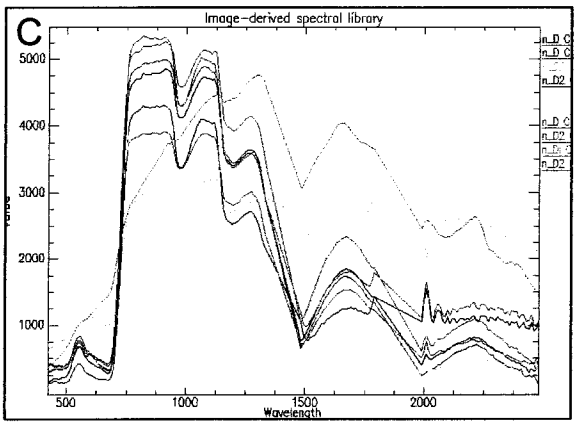

Image, full range, bad bands removed

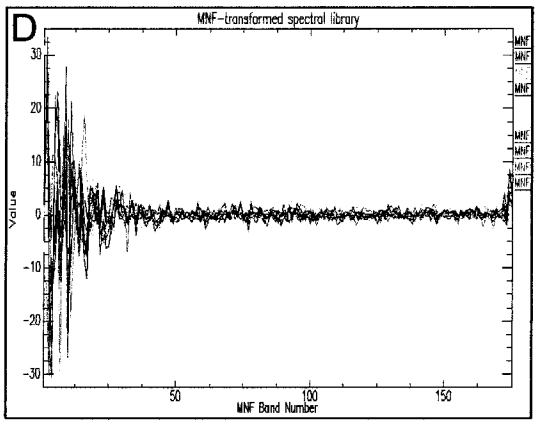

MNF-transformed

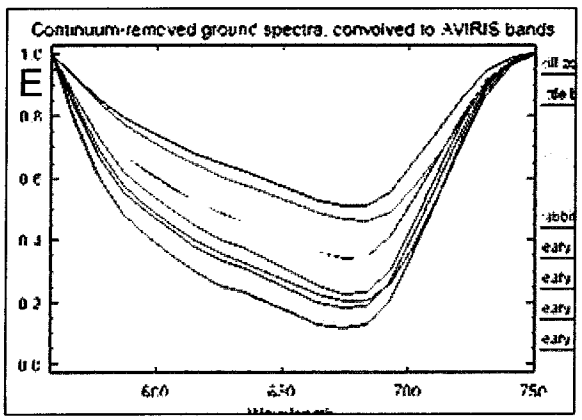

Continuum-removed subset

Figure 5.14. Spectral libraries tested for map quality: include ground-based (A); image-derived, full spectral range, all bands included (B); image-derived, full spectral range with bad bands and bands removed from water absorption regions (C); image-derived, full spectral range with MNF transformation (D); spectral subset of chlorophyll absorption feature in the visible, with continuum removed (E).

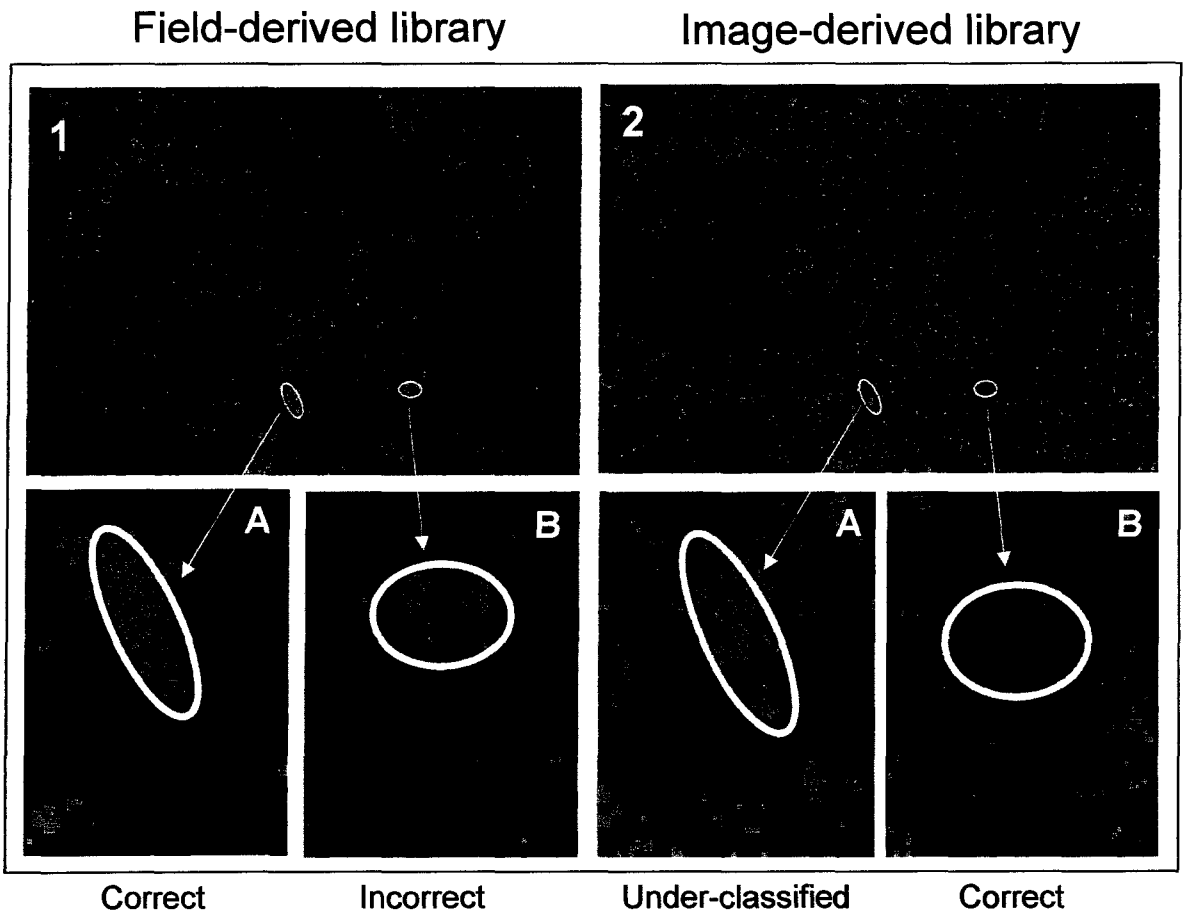

Figure 5.15. Map subsets from field and image-derived spectral libraries. All variables held constant other than the library. In 1, the leafy spurge class (green) is correctly classified within the circled area in A, but incorrectly in B, an area where no spurge was present on the ground. With the image spectral library (image 2), spurge was correctly, but incompletely mapped in A; in B, no spurge was mapped (correct) in this area where the vegetation was frequently confused with leafy spurge. Sienna areas are non-spurge vegetation; black areas are inert, masked materials.

significantly depending on the source of the spectral library, but less so when the different algorithms were used.

Although the libraries may be interchangeable under certain conditions and in specific areas of THRO, the composite maps (Figure 5.16 A and B) suggest that the image library may be preferable overall, assuming a cross-track correction is used. The arrows in A and B show patches that were incorrectly classified as spurge with the ground library (A), and correctly excluded from the spurge map when the image library was used (B). There are no known equivalent large patches that were incorrectly mapped as spurge on the image-library map (B).

When data were cross-track corrected, overall fewer problems with commission error were seen when image-derived libraries were used. With image spectra, vegetation throughout the scene can be more completely characterized, and not limited to vegetation patches that were sampled in the field. Residual, uncorrected atmospheric effects will be minimized, because the library and image will contain the same atmospheric characteristics or anomalies, and this would eliminate potential problems arising from extrapolation between field and image spectra. The image-derived endmember libraries are better suited to the analysis of mixed pixels, and were designed to be used with the unmixing algorithms in ENVI. The collection of spectra from the image is also more automated, and may reduce potential bias in the selection of specific vegetation patches in the field for a ground-based library. Image-derived endmembers appear to produce better maps overall, and were selected for mapping the full region.

ALGORITHM COMPARISONS

Many different algorithms have been used for mapping vegetation with imaging spectroscopy. Each algorithm has unique advantages and disadvantages (see Chapter 3), but very few studies have compared the quality of the maps that are produced from each of these, or indicated which is best for vegetation mapping. Because of the variation that was seen in preliminary spurge maps, and because the optimal method was unclear from the literature, several algorithms were tested to evaluate which would be the most appropriate for mapping leafy spurge. The algorithms included spectral feature fitting (SFF), spectral angle mapper

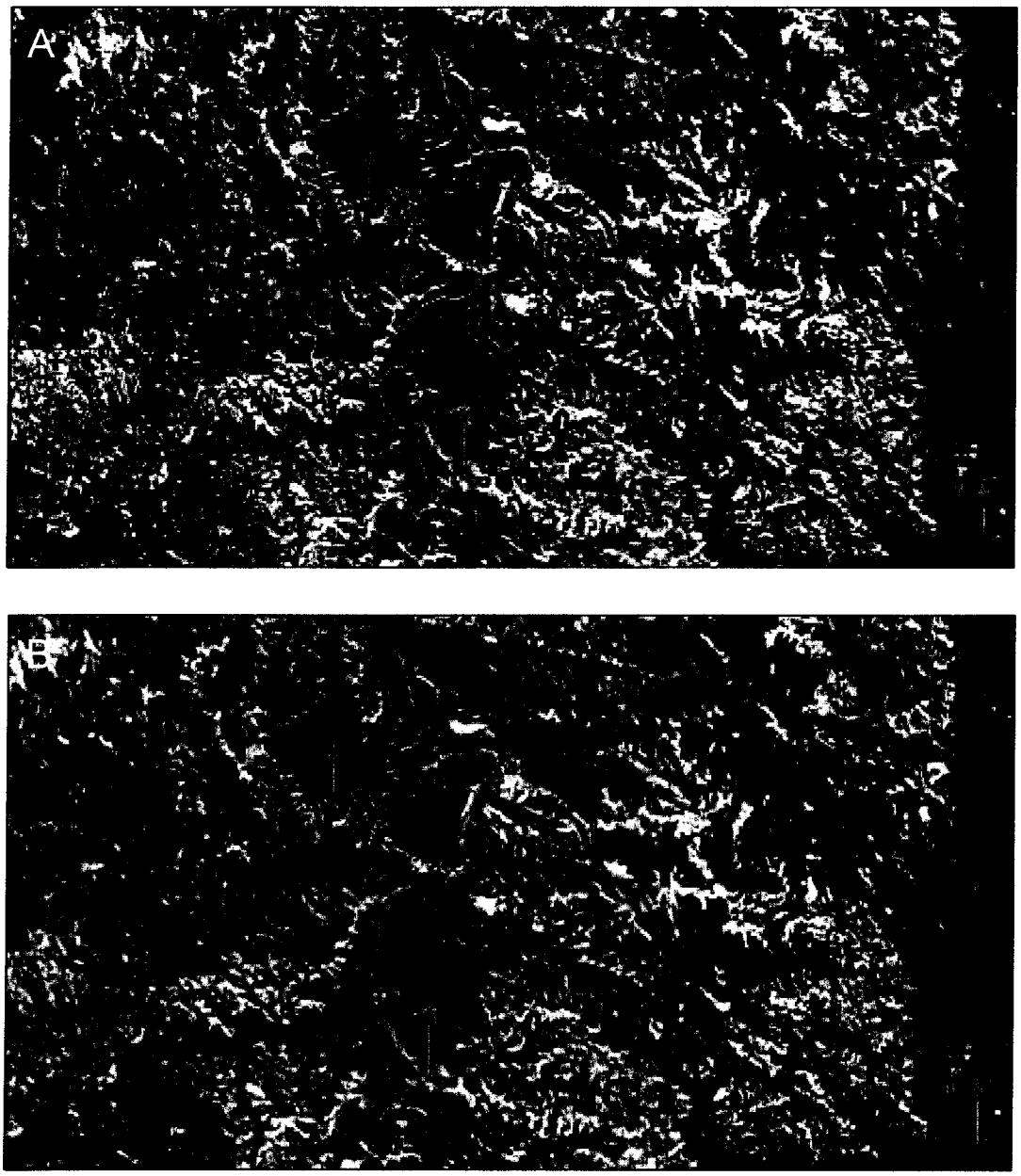

Figure 5.16. Area-wide map mosaics: ground spectra versus image-derived. Classified pixels (in red, orange, and yellow) are overlaid on a single grayscale image (band 20, 558 nm) for reference. A: leafy spurge map produced using field-derived library; B: spurge map produced from image-derived library. Arrows in A show patches that were incorrectly mapped as leafy spurge (red, orange, and yellow areas in both maps were mapped as "spurge"). These same areas were correctly excluded from the map in B. Images are approximately 35 km wide.

(SAM), linear spectral mixture analysis (SMA), matched filtering (MF), and mixture-tuned matched filtering (MTMF). In addition, SFF was run using the USGS Tetracorder algorithm.

In Figure 5.17, subsets from maps produced with the MTMF, SAM, and SFF algorithms are shown. For each classification, all band anomalies were removed, the image was cross-track corrected, and the field-based library was used. Figure 5.18 includes the results from the same set of algorithms and methods, with the exception that the image-derived library was used.

With the field-based library, the SAM and MTMF results were very similar, and all three methods mapped spurge in the areas it is known to occur based on field surveys. The SAM and MTMF mapped more of the spurge as a higher density class, however (predominantly 80-100%), while lower density spurge (20%, 25%) and grasses were mapped for portions of the same area with the SFF algorithm. These areas were dominated primarily by moderate to high density spurge (35% to 100%), and the SAM and MTMF therefore appeared to produce more accurate maps.

When the same three algorithms were compared, but mapped with the image-derived spectral library, the SAM and MTMF maps were again most similar. In Figure 5.18, dense spurge is indicated by light pink in A and B, and red in C. Much more material mapped as dense spurge with the SFF algorithm than with SAM or MTMF, which contrasts with the reduced amount of spurge that was mapped with SFF compared to the other algorithms when the field-based library was used. Commission errors were seen in the SFF map (i.e., yellow arrow in Figure 5.18 C) that were not evident with the other algorithms.

Most of the results of the comparisons outlined in Section I were irrecoverably lost before formal accuracy assessments were run, the result of a computer drive malfunction. Several classification tests were re-run to calculate and compare formal accuracy values. These included: MTMF without cross-track correction, full image library; MTMF without cross-track correction, image-derived vegetation endmembers only; SAM with cross-track correction, full image library; MTMF with correction, full image library; linear SMA with correction, full image library; Tetracorder SFF, with correction, full library. Figure 5.19 includes subsets from these maps. The overall accuracy, and producer's and user's accuracies for the leafy spurge class are

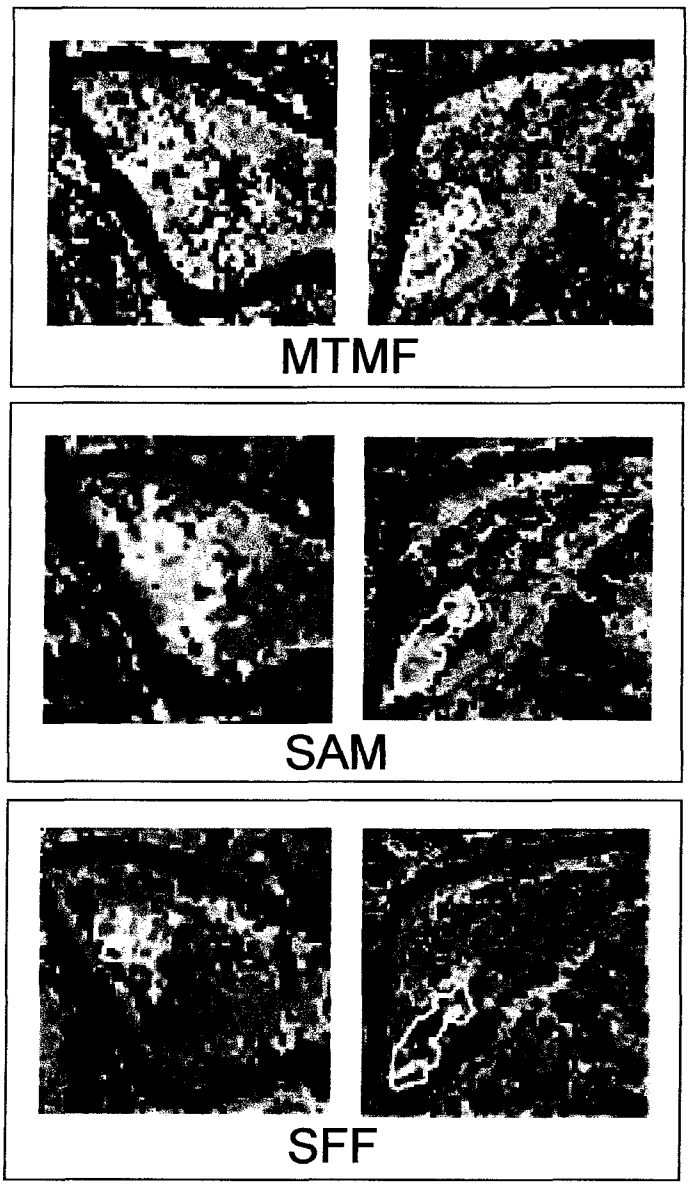

Figure 5.17. Algorithm comparisons: MTMF, SAM, SFF; field-derived spectral library. The identical library was used for all three algorithms. Other variables held constant. With this library, the algorithms have mapped identical vegetation classes somewhat differently. Dark blue: 100% spurge; cyan: 80% spurge; coral: 80-100% spurge; yellow: 35% spurge; purple: 25% spurge; red: 20% spurge; brown: snowberry; magenta and green: grasses/litter. Yellow polygons are field-defined patches dominated by dense spurge infestations. All maps were cross-track corrected, bad bands removed.

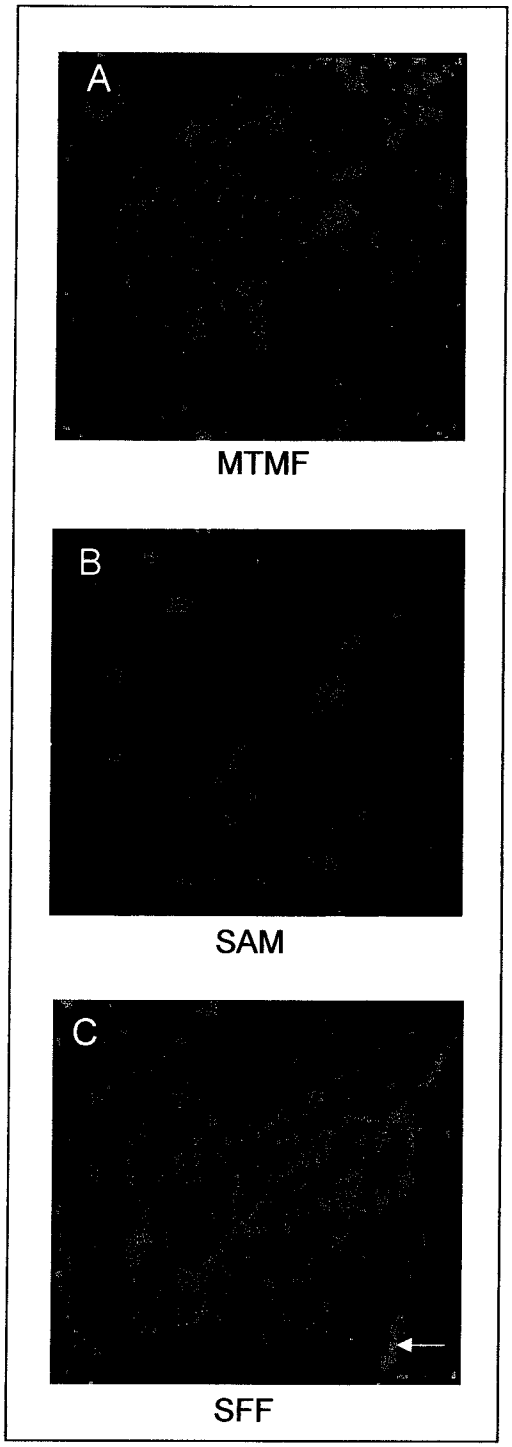

Figure 5.18. Algorithm comparisons: MTMF, SAM, SFF; image-derived spectral libraries. Dense spurge is green in each frame. Spurge is mapped with all three algorithms, but is most similar with the MTMF and SAM algorithms (A and B). Some commission error was noted in C (see yellow arrow in lower right). All images were cross-track corrected, with bad bands removed. Black areas in A and C are masked inert material; in B inert material and vegetation that was not classified due to the default classification threshold applied with the SAM algorithm.

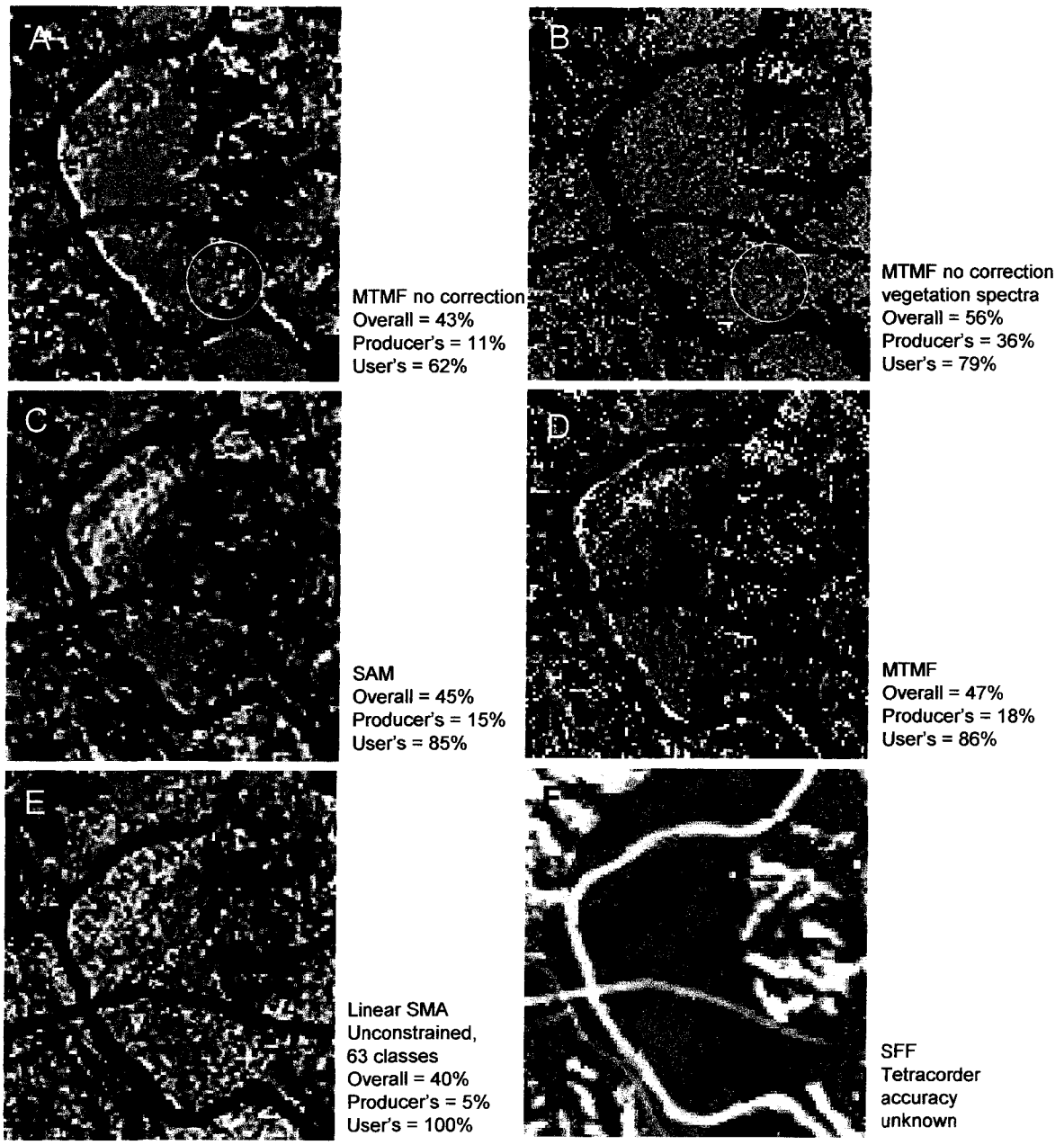

Figure 5.19. Algorithm accuracy comparisons: calculated and visual accuracy. A: MTMF without cross-track correction; B: MTMF without cross-track correction and a reduced library containing only vegetation classes; C: SAM; D: MTMF; E: linear SMA; F: SFF with Tetracorder (red is classified spurge); C through F were cross-track corrected; image-derived spectral library. The leafy spurge class is green in all maps. The area circled in yellow in A and B is known to be devoid of spurge on the ground, but has been incorrectly mapped as spurge in both.

included for all but the Tetracorder SFF map, for which the data were unavailable. Visually, the MTMF and SAM maps from cross-track corrected data are similar and have correctly mapped spurge, in general, within this map subset; however, the full SAM map indicates that spurge was over-classified within many of the deeply incised drainages leading off the higher plateaus in the park, which cannot be seen in the subset. The quality of the maps was not reflected in the calculated overall accuracy, however, which was low (45% and 47%). The highest overall accuracy was calculated for the MTMF uncorrected map, produced with vegetation endmembers, in which known spurge occurrences were mapped poorly based on visual assessment (Figure 5.19 B). Both this and the map in A contain significant commission errors for spurge. The areas circled in yellow in A and B, for example, were mapped as spurge where none was present. Both these maps indicate higher commission error (i.e., lower user's accuracy), but the magnitude of the difference between these and the SAM and MTMF user's accuracies is not as great as qualitative assessments suggest. The map from the unconstrained linear SMA was poor (Figure 5.19 E), based on visual analysis, with vegetation classes in general being poorly defined. The calculated accuracy (40%) was the lowest of the maps in Figure 5.19. Higher accuracy values were obtained with linear SMA, however, when the results were mathematically constrained, and when different numbers of endmembers were used (see Figure 5.20, and discussion in Chapter 3). In general, the calculated accuracies did not prove to be helpful in selecting the best algorithm. These values were not supported by the relative quality of the maps based on visual assessment in conjunction with detailed field surveys of selected areas within the park. The calculated and quantitative assessments produce contradictory results. Visually, the Tetracorder SFF map (Figure 5.19 F) compared favorably to the MTMF and SAM results, but this algorithm incorrectly mapped spectrally similar material as spurge, which is not seen in the subset. In addition, the production of this map required manual adjustments and weighting to adjust and improve the map, which required knowledge of the spurge distribution on the ground. The Tetracorder expert system requires more experience and training to use effectively, and it is not currently widely available. The SFF algorithm, as written in ENVI 3.4 (which was used for the early test maps), produced maps that were qualitatively inferior to SAM and MTMF maps, and

A. Constrained to 1, 41 classes
o.a. = 46%; p.a. = 13%; u.a. = 68%

B. Unconstrained, 41 classes
o.a. = 44%; p.a. = 7%; u.a. = 71%

C. Constrained to 1, 63 classes
o.a. = 48%; p.a. = 42%; u.a. = 63%

D. Unconstrained, 63 classes
o.a. = 40%; p.a. = 5%; u.a. = 100%

Figure 5.20. Linear SMA maps, constrained and unconstrained. The linear SMA algorithm produced very poor results overall, and maps were inconsistent when the number of endmember classes was varied, and when the results were mathematically constrained (see discussion in text). Overall, producer's and user's accuracies are indicated for each classification.

without a cross-track correction a coherent map could not be produced from this data with the ENVI SFF algorithm. (Update: newer versions of ENVI have added interactive options with the SFF, but leafy spurge maps were not produced using the updated SFF algorithms).

Test maps using linear SMA were also produced, and formal accuracy values were calculated. Visually, these maps were inferior to those produced with other mapping algorithms. Four iterations of the SMA were run, to test whether the presence or absence of mathematical constraints would improve the maps, or whether a larger set of endmembers could improve the quality of the maps. Figure 5.20 shows the results of these four analyses. Overall accuracy varied from 40% to 48%; producer's accuracy for spurge from 5% to 42%; and user's accuracy from 63% to 100%. The higher producer's accuracy was the result of classification of a much larger area as spurge overall, with significant commission problems, rather than a higher quality, more accurate spurge map. Visual inspection of these maps indicated that this algorithm performed poorly for spurge mapping. None of the four maps was considered useful, and the linear SMA was abandoned as a potential algorithm for park-wide mapping.

Overall, the accuracy values calculated with confusion matrices were inconclusive. The map with the highest calculated accuracy was grossly over-classified, based on a visual assessment. Maps that were qualitatively very different showed similar calculated accuracy values, and poor maps often indicated higher formal accuracy values than those that were visually better representations of known spurge infestations on the ground. The small size of the validation plots (3 m by 5 m) and poor registration between images and plots contributed to the inconsistencies between visual and calculated accuracy. The formal accuracy values could not realistically be used for selection of the "most accurate" method.

The best maps, based on qualitative evaluation, were obtained with SAM and MTMF, using image-derived spectral libraries and cross-track correction. MTMF was selected for processing the remaining flight lines because there appeared to be fewer problems with commission error overall, and because the leafy spurge maps could be refined using the infeasibility images that are produced when the algorithm is run. The MTMF is not restricted to a specific number of endmembers and can theoretically use as few endmembers as deemed

necessary for the map objective, or as many endmembers as the image contains (by using multiple iterations of the algorithm for each class). It is not restricted to the number of bands used as input (as with linear SMA). The MTMF algorithm can be used with only the class or classes of interest because symmetry is not required between an input pixel vector and a complete endmember matrix for simultaneous solution of all endmember fractions. The MTMF was designed to address mixed pixels, or fractional abundance measurements, which represent the majority of pixels in most imagery. It was considered, therefore, more appropriate than SAM, which is a whole-pixel matching method. MTMF has also been used successfully in other studies to map low abundance, rare materials and individual species (Boardman, 1998; Parker Williams and Hunt, 2002a).

SUMMARY, SECTION I

The selection of methods to use for the remaining park-wide and multi-temporal mapping was based predominantly on visual assessments of the maps. The accessibility of the software and algorithms was also a factor in method selection. Formal accuracy assessments could not be completed on most of the test maps due to an irrecoverable data loss following a computer malfunction. The accuracy values that were calculated did not support the qualitative conclusions that were based on detailed knowledge of several well-documented infestations that park managers and researchers had been tracking and monitoring for several years. The reference data that was used in the confusion matrices was marginal for validating the AVIRIS spurge maps due to the small plot size (3 m x 5 m) relative to image resolution (17 m). Using a single coordinate for plot locations in conjunction with georeferencing problems (see Chapter 6 for detail) made the formal accuracy results very sensitive to registration problems. These accuracy values were not considered in the selection of methods for park-wide mapping.

Altering the spectral libraries, preprocessing steps, and mapping algorithms clearly produced maps with very different distributions of leafy spurge and other vegetation classes. A suite of preprocessing and mapping steps was selected for mapping all remaining flight lines for 2001 and 1999 based on the comparative analysis described above. Visual comparisons of the

maps, in conjunction with field surveys and expert knowledge of park personnel on the location of spurge infestations, indicated that the best results for the single flight line and single date test images were obtained using liberal band editing, followed by NDVI-masking, cross-track illumination correction, MNF transformation, and mapping with the MTMF algorithm, using an image-derived spectral library. These steps produced satisfactory results for single flight lines and were used as the basic method that was modified and refined to improve the quality of spurge maps over multiple flight lines as well as multiple dates (see Section II).

SECTION II: Modifications and Image Analysis

Based on the comparative study described in Section 1, the following preprocessing steps were established as important for accurate mapping: cross-track illumination correction (ENVI User's Guide, 2003; Kennedy et al., 1997), and liberal editing/removal of bands, including those bands displaying anomalous spikes within the chlorophyll absorption region. The identical set of bands was removed from all flight lines to standardize mapping. An NDVI mask, applied before running the cross-track correction and MNF transformation, was critical for producing the comprehensive, image-derived spectral library that was necessary for detailed vegetation mapping. The MTMF algorithm in conjunction with an image-derived endmember library produced the most acceptable results, based on comparisons with reference data (see Section I). These maps represented a reasonable compromise between low omission and low commission error for spurge; therefore the MTMF algorithm and image-derived library were selected for all additional processing.

The methods selected above produced satisfactory results for single flight lines; however, several interactive steps in the mapping process involved discretionary decisions on the part of the image analyst that could introduce inconsistencies when mapping over time and/or space. For example, thresholds must be selected for the matched filter score and the infeasibility score (CSES, 2000) to produce hard-classified maps of dominant classes when the MTMF algorithm is

used. Threshold decisions can be subjective and may vary between image analysts, or with a single analyst over time, resulting in inconsistent covertype maps.

One objective of this study was to modify the selected processing steps (above) to: 1) decrease the influence of analyst decisions or bias; 2) reduce the need for expert knowledge or advanced training; 3) minimize the level of ground support and reference data required for actual mapping; 4) eliminate the need for conclusive *a priori* knowledge of the target endmember spectrum; and 5) increase automation and standardization for consistent map production and improved temporal analyses.

The modified MTMF that was developed here was adapted from the standard "hourglass" approach (Figure 4.4 and CSES, 2000), but included modifications and additions within the general method that are highlighted on the modified hourglass (Figure 5.21). The changes that were applied to the single flight line from each date that was used to produce a spectral library are highlighted in yellow, while the modified steps that were used for the remaining three flight lines (for each date) are highlighted in red.

Method refinement included specific changes during all three stages of processing: pre-classification, classification, and post-classification. The modifications were applied to different components of the processing during each stage. The pre-classification modifications focused on refinement and enhancement of the spectral library. During the classification, the MTMF mapping algorithm was applied in a non-traditional manner that included a significant modification to the number of input endmembers that was used when running the algorithm. Post-classification changes involved standardizing and automating the selection of thresholds to determine membership in specific classes. For clarity, the description of methods, results, and discussion for each modification are included in each respective section.

ENDMEMBER LIBRARY COLLECTION

Pre-classification modifications and refinements of the spectral library were performed. Before classification, the image-derived endmember library was refined and more extensively exploited by: 1) using a two-stage selection of endmembers to derive a more detailed spectral

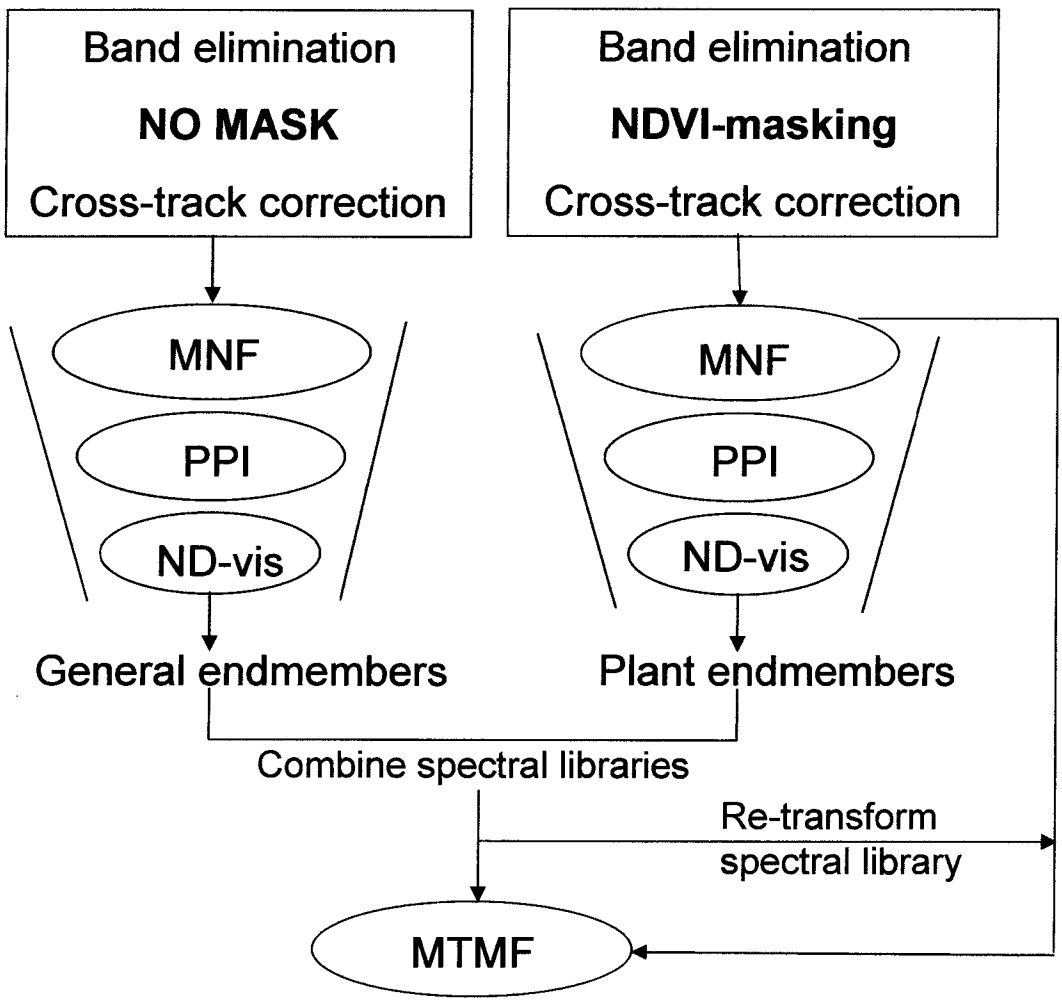

Figure 5.21. Modified hourglass processing: two-stage endmember collection from the initial flight line; the added second stage is indicated in darker yellow. Additional steps for subsequent flight lines from a single date are outlined in red. Critical pre-processing steps are indicated in the two boxes, and listed in the order applied.

library; 2) modifying the technique used to select the endmembers from the nD-Visualizer during the second selection stage; 3) selecting an exhaustive set of all possible image endmembers rather than a single target endmember; 4) in-depth editing of the spectral library; and 5) re-transformation of the spectral library using MNF statistics that were derived individually from each flight line that was being mapped. The details of these five modifications and refinements are discussed below.

NDVI MASKING

Two libraries were derived independently from the image. A two-step endmember selection process using both masked and unmasked images was used to derive a complete and detailed endmember set. This allowed accurate modeling of mixed pixels that are dominated by vegetation, but still contain non-vegetative components as a minor fraction. Selecting endmembers from a full, unmasked image will allow more accurate calculation of all general land cover components within mixed pixels, while a detailed vegetation library was obtained from the masked image.

Initially a set of general land cover endmembers was selected from the entire, non-masked scene using the unmixing and endmember selection method developed by Boardman and Kruse (Kruse et al., 1993; Boardman and Kruse, 1994; Boardman et al., 1995), and described in Chapter 4. Using the standard approach, large groups of pixels at the extremes of well-defined projections in n-dimensional space were selected as representative of the spectrally purest members of distinct classes using the nD-Visualizer tool (ENVI User's Guide, 2003) (Figure 5.22 A). The general endmember classes that were collected included shadow, plant litter, asphalt, concrete, generic vegetation, several soil and rock classes, and clear, silty, and eutrophic water classes (Figure 5.23 A). Twenty-two input MNF bands were sufficient to isolate these general land cover categories.

Early test maps indicated that vegetation endmembers were easier to isolate when spectra of non-vegetative materials were removed. For the collection of the plant endmembers, pixels that were dominated by vegetation were isolated from other land cover by applying an NDVI-based mask to the image. The threshold for the mask was set to differentiate between dominantly vegetated and non-vegetated land cover, at a value of 0.45. This value was based on empirical tests of several NDVI thresholds on this data set, which were compared to field reference data and high-altitude aerial

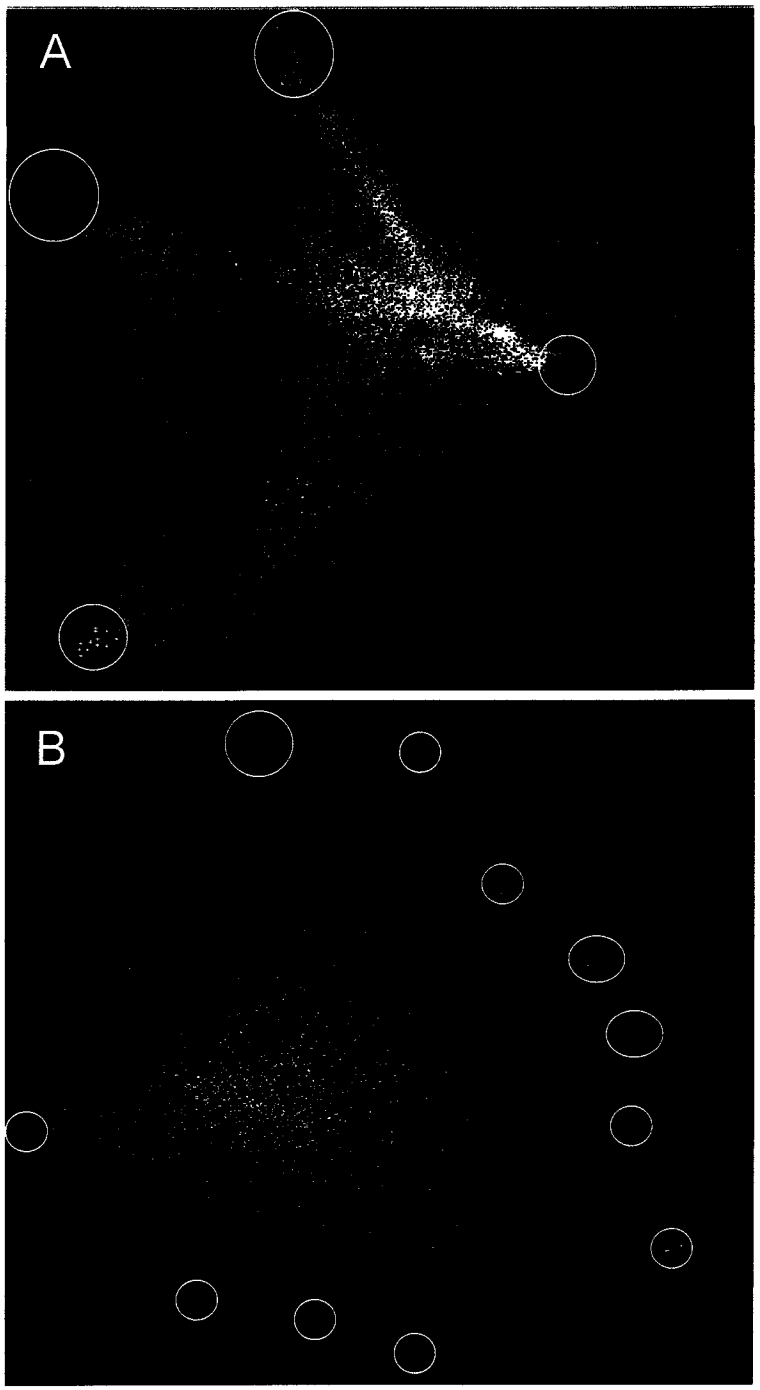

Figure 5.22. Two-step selection of endmembers from nD-Visualizer spectral scatter plots. A: general land cover class selection using large clusters of isolated extreme pixels from the full image (colored clusters circled in A); B: vegetation endmember selection from small, subtle extensions from the more homogeneous, centralized vegetation cloud, using small groups of pixels, generally 2-5 pixels per class, from masked image (circled pixels in B).

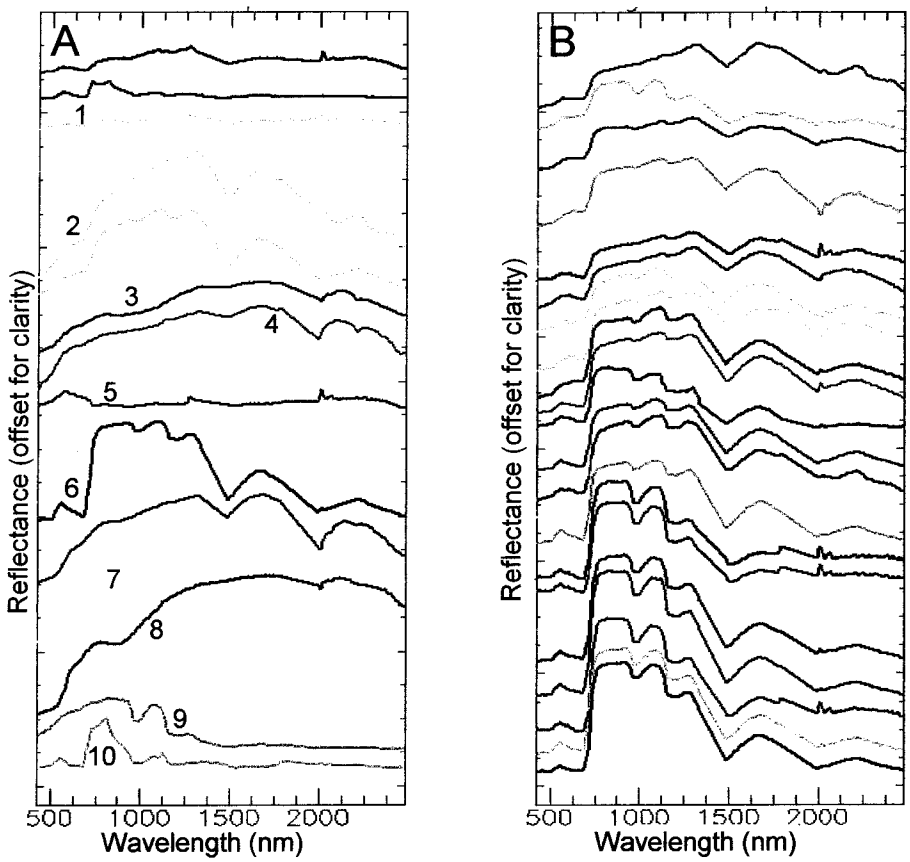

Figure 5.23. General land cover and vegetation-only image-derived spectral libraries. A: examples from the general endmember spectral library (derived from the full, non-masked image), including examples of shadow (1), senescent vegetation (2), soil and rock classes (3,4,7,8), water (5), vegetation (6), silty water (9), and eutrophic water (10). B includes sample vegetation endmember spectra (derived from the NDVI-masked image).

photography that was collected by NASA-JPL concurrently with the AVIRIS imagery collection. The threshold effectively excluded large (>> 1 pixel) soil-dominated areas, but retained portions of small roads that were adjacent to vegetated areas, that displayed some vegetation signature as a result of mixed vegetation and pavement or soil signatures. All significant vegetation within the scene was effectively included in the masked "vegetation-only" image with this threshold. All coherent MNF bands (34 to 36 depending on flight line) were input to the n-D Visualizer for selection of the plant endmembers (Figure 5.23 B).

MODIFIED STRATEGY FOR ENDMEMBER COLLECTION

Generally, when endmembers are selected using the n-dimensional visualizer tool in ENVI, aggregates of pixels are selected at the outer extremes of spectrally well-separated extensions from the central pixel cloud (ENVI User's Guide, 2003). This strategy was used to select the general land cover endmembers. Because the pixels from the masked image were dominated by vegetation, however, the pixel cloud was more homogeneous, and presented very few unique, well-defined extensions in spectral space. The spectral differences between vegetation classes were often very subtle, therefore a more liberal approach was adopted for the collection of vegetation endmembers. Only the most extreme few pixels on the ends of subtle extensions from the cluster of vegetation pixels were selected to represent the potential endmembers (Figure 5.22 B). This generally included only 2 to 5 pixels at the ends of a diffuse, small extension. The potential endmembers were not restricted to the extremes of a "complex hull" viewed in n-dimensional space, as is generally recommended (Boardman, 1993). In addition, the collapse feature in ENVI that is recommended to facilitate visualization of unselected endmembers clusters was not used. The collapse feature calculates a projection, based on either class means or covariance, which will minimize or cluster the space spanned by the classes that have already been selected. This generally allows the variation of the remaining unselected classes to be viewed more readily (ENVI User's Guide, 2003). Due to subtle differences in variance between potential plant endmembers, however, and because the masked image was dominated by vegetation pixels, it was easier to isolate the small clusters of unique vegetation without using the collapse feature. When the feature was used, plant classes

generally coalesced, and subtle differences could not be distinguished. With this approach vegetation classes were isolated in spite of very subtle spectral differences between chemically similar plant materials.

If vegetation endmembers were only collected from the full unmasked image, the collection of all possible vegetation endmembers would be hampered because it is difficult to differentiate very subtle differences in vegetation signatures when the variance of an image is dominated by the more dramatic spectral variation seen when all land cover types within the full scene are viewed simultaneously. By masking out pixels that were dominantly inert materials, and restricting the input to vegetation-dominated pixels, it was easier to find and isolate vegetation classes with subtle spectral differences.

EXHAUSTIVE ENDMEMBER COLLECTION

When the inert materials were eliminated from the pixel swarm in the nD-Visualizer window after masking, only pixels with a strong vegetation signature remained. It became apparent that there were many subtle, small clusters of pixels present that had been difficult to locate previously. The significance of these clusters was unknown, but they may have represented the effects of variable illumination or view angles, unique plant chemistry, canopy structure, unique species or plant assemblages, or various combinations of these. Because it was unknown what these small clusters represented, nor whether these would be suitable vegetation endmembers, *all* spectrally-unique clusters that could be reasonably found were selected, resulting in 61 potential vegetation endmembers.

According to linear SMA theory, the number of endmembers that can be extracted from a scene is n + 1, where n equals the number of coherent, non-noisy MNF bands that are used for mapping (Boardman and Kruse, 1994). This is often regarded as the "dimensionality" of the data (i.e., the number of unique classes). The apparent "dimensionality" varied slightly between flight lines, primarily the result of minor differences in land cover over the region. For the THRO data sets, 34 to 38 MNF bands (depending on flight line) were considered coherent enough to be used for mapping, and only these bands were input to the PPI and nD-visualizer algorithms for the selection of image endmembers. If 34 MNF bands were used, theoretically 35 endmembers

would be extracted from the image. Using the selection strategy discussed above, however, the number of potential endmember classes that were collected exceeded the theoretical maximum. If the endmember selection was restricted to 35, the first 35 endmembers would be a random selection that would vary between analysts, or over time for a single analyst. These 35 endmembers may not include all critical vegetation endmembers, including the target class. By collecting *all* possible endmembers, however, this problem is eliminated and important endmember classes will not be inadvertently omitted.

The vegetation endmember library was combined with the general land cover library derived from the non-masked images prior to mapping. The combined library was used to map only the vegetation-dominated areas from the NDVI-masked image, because the distribution and composition of the inert materials were not of interest in this study. However, by collecting a complete set of endmembers for both the vegetation and the inert materials, all components in the scene could be represented and accounted for in mixed pixels. The selection of all possible endmembers was a modification that allowed an automated threshold step to be incorporated into the MTMF classification (see Section II, "Post-classification modifications" section).

SPECTRAL LIBRARY EDITING

The quality and detail of the spectral library was critical for producing an accurate map in which commission error was minimized, while omission error remained acceptable. Careful editing of the library was required. Spectral groups were edited to remove any anomalous, non-matching spectra that were inadvertently included in an endmember group. Because very subtle spectral differences were the basis for differentiating these endmembers, the accidental inclusion of an errant spectrum could have a significant impact on the mean endmember spectrum calculated for a class. This was particularly critical when the number of pixels included in an endmember group was very small. The selected MNF spectra were inverse transformed to display as standard reflectance spectra (by wavelength) for editing purposes. If all the spectra within the group were not variants of the same spectrum, displaying slight variation in albedo, but retaining the same shape of the spectral curves, either the class was discarded or the anomalous pixel was located graphically on the nD-Visualizer screen and manually eliminated from the class. Both the vegetation and general land

cover spectra were edited for consistency. The mean spectrum for each class was calculated and added to the spectral library and redundant classes were removed to produce the final library. The final library contained 62 (for 1999) and 63 (2001) total endmembers. The identical procedure was used to derive a unique spectral library for each of the four flight lines from both dates.

All endmembers were input to the MTMF algorithm for the mapping. Two versions of the library were saved. The MNF-transformed version was used for the actual mapping of the MNF-transformed images (Figure 5.24 A), the untransformed, biophysically interpretable version was used for editing, class identification, and intra- and inter-class comparisons of spectra (Figure 5.24 B). Although 62 or 63 endmembers were input, the classified scenes were dominated by only 20-25 classes, with several classes represented by only a few pixels within all the flight lines combined (Figure 5.25).

SPECTRAL LIBRARY SELECTION FOR MAPPING MULTIPLE FLIGHT LINES

In addition to temporal consistency, an additional priority when using airborne hyperspectral imagery for regional monitoring purposes is maintaining consistent, comparable results between flight lines that were collected on a single date, when large aerial coverage is needed. Multiple flight lines can be processed either simultaneously after mosaicing all lines, or processed and mapped independently as single scenes or flight lines, with merging after classification.

Processing limitations precluded the simultaneous mapping of all four merged flight lines in this study. Pre-classification merging of flight lines was also avoided because the results from multiple classifications of identical areas on the ground were used for examining the effects of view angle on the classification of spurge (Chapter 8). For the THRO data all scenes or "cubes" within a single flight line were merged, and each full flight line was processed separately.

To individually map multiple flight lines, two options are available for the input image-derived spectral library. A single library can be derived from one flight line, which is then used to map all other flight lines. Alternatively, individual spectral libraries can be derived independently from each flight line, and used to map that respective flight line. To determine which approach was more appropriate for mapping and change detection, test maps were produced using both options. With approximately 35% sidelap between flight lines, it was possible to compare the

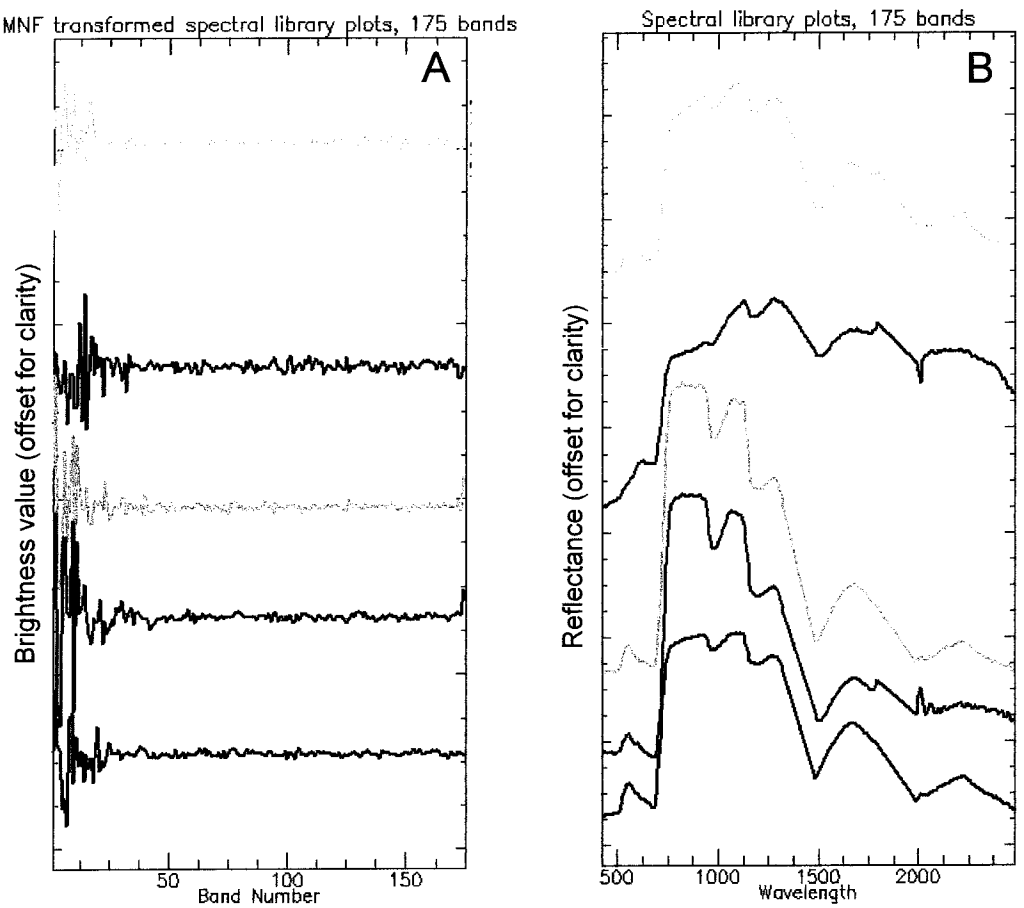

Figure 5.24. Example mean library spectra: transformed and untransformed. A: MNF-transformed spectra; B: identical spectra after inverse transformation to original format.

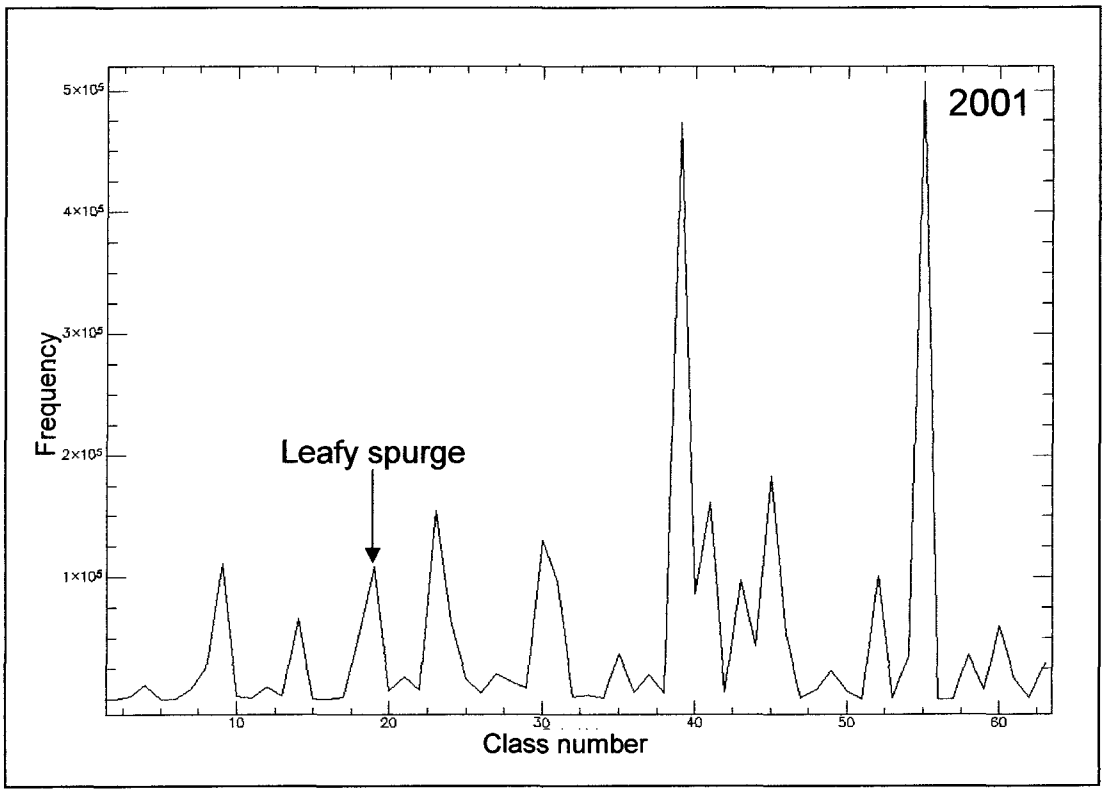

Figure 5.25. Frequency of all classes from 2001 vegetation map (MTMF rule classified result). Class 19 is spurge. 63 endmembers were used for classification, but the maps were dominated by 20-25 classes.

consistency of maps from one flight line to the next that were produced with the two spectral library options by comparing the classifications of identical areas from adjacent flight lines.

TEST 1: INDEPENDENT SPECTRAL LIBRARIES FROM EACH FLIGHT LINE. Figure 5.26 A highlights portions of maps that were created using two unique libraries (i.e., one library was derived from, and used to map flight line 1, while a second library was derived independently from, and used for mapping flight line 3). Overall land cover throughout the region was similar, therefore it was expected that the endmember classes extracted from the two flight lines would be similar. Roughly equivalent groups of pixels were mapped as distinct classes on the two flight lines, indicating that the two libraries were very similar. For example, in Figure 5.26 A, green indicates the leafy spurge class in flight line 1, while red represents spurge in flight line 3. Spatially, the classified patches of leafy spurge, as well as other vegetation classes, match relatively well between the flight lines. It was difficult to directly compare the results, however, because the libraries were not identical and the class codes and colors were unique for each flight line. Mosaicing was problematic as well. Seamless mosaics could not be produced without re-coding and re-coloring "equivalent" classes between flight lines. Classes can be correlated and recoded to match between flight lines after mapping, but this would be labor intensive when many classes have been mapped. For the THRO data set this would require matching over 60 classes per flight line, for eight separate flight lines, to a single coding system. The classes are very similar between flight lines, however, because they were derived from different flight lines they were not identical, therefore recoding to match classes from other flight lines may not be justified. Although multiple individual libraries for mapping each flight line will ensure that all cover types are represented, endmembers for specific classes that are derived independently from each flight line will vary somewhat due to natural spectral variation in materials, or due to modest differences in illumination or viewing geometry, the result of slightly different collection times from one flight line to the next. Because of this, maps of individual classes may be more variable between flight lines than if an identical library were used to map all flight lines. Another drawback of using multiple libraries is the additional time and labor required to derive separate spectral libraries from each flight line.

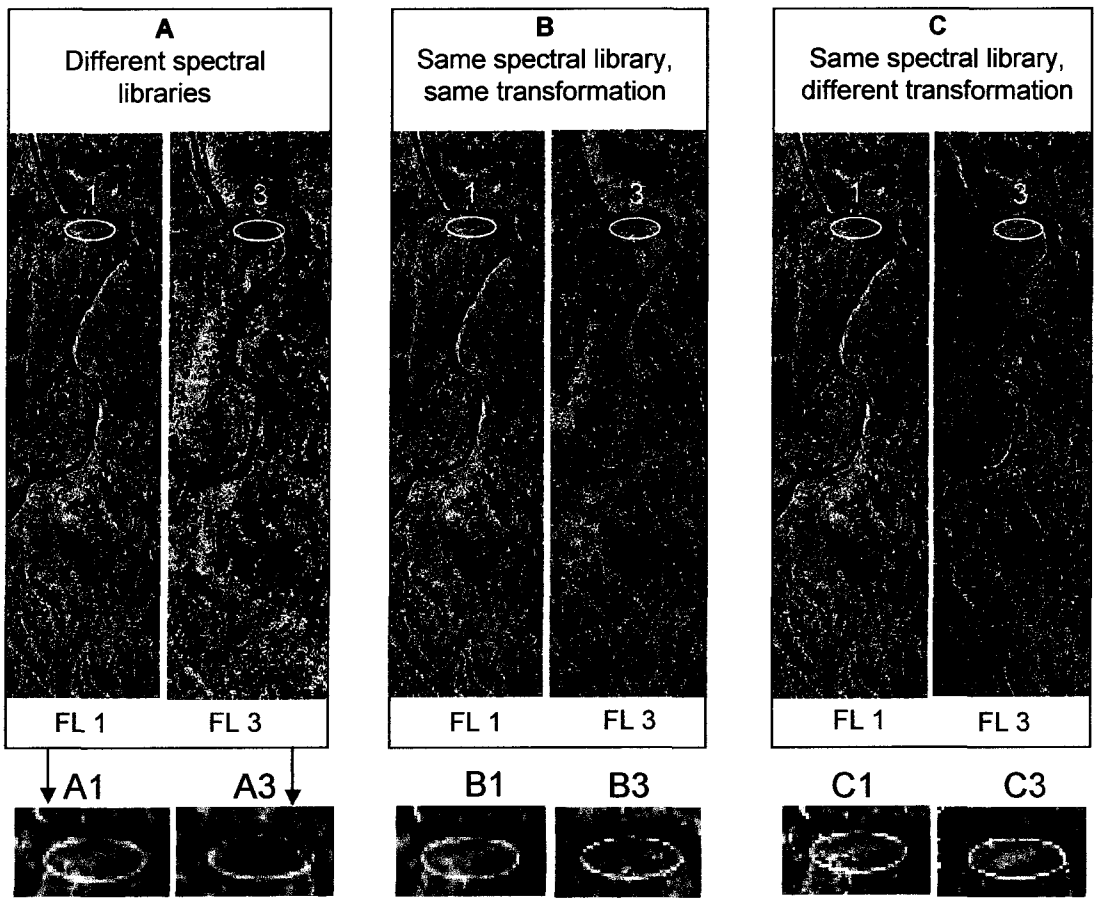

Figure 5.26. Effects of modified and different spectral libraries on identical area maps from adjacent flight lines. The area of leafy spurge circled in yellow is enlarged below each corresponding flight line. Green pixels indicate a known leafy spurge patch in A1, B1, and C1 (all are the identical classification). Spurge is well-defined in the corresponding area of flight line 3 (A3) (where different libraries were used for each flight line), and C3 (same library used, but with different transformation). Spurge is poorly classified in B3 (same library, same transformation). Comparisons are difficult between A1 and A3 due to mismatched codes between the 2 separate libraries. C indicates the most consistent, and most interpretable results between flight lines.

TEST 2: ONE LIBRARY TO MAP ALL FLIGHT LINES. Using one spectral library derived from a single flight line to map all others will ensure that an identical suite of endmembers is used for mapping an entire region, which would theoretically produce spatially consistent classifications. This approach would also eliminate the problems encountered with different coding between flight lines. A single spectral library, derived from flight line 1, was applied directly to map all four flight lines from 2001. Figure 5.26 B shows the maps of an identical area mapped from both flight lines 1 and 3. Because the identical library was used to map both flight lines, the green endmember class should indicate leafy spurge in both images. Field-verified infestations of spurge are correctly mapped on flight line 1, but incorrectly on flight line 3 (see Figure 5.26, B1 vs. B3). It is difficult to identify a single spectral class that accurately represents leafy spurge in the classified image from flight line 3. The remaining vegetation classes also do not correspond well between the two flight lines.

MNF transformed imagery and spectral libraries were used in the above comparisons. The imagery from each flight line was run through a separate transformation, which could account for the poor quality maps when the library transformed with flight line 1 MNF statistics was used on the remaining fightlines. The single flight line library may be more successful when neither the image nor library is transformed. Hyperspectral maps are typically less accurate, however, if the data is not transformed because the mapping algorithms were designed for optimal performance when used with MNF-transformed data.

TEST 3: ONE LIBRARY FOR ALL FLIGHT LINES, WITH INDIVIDUAL MNF TRANSFORMATIONS FOR EACH FLIGHT LINE. Because neither spectral library source that was tested produced optimal results for mapping multiple, MNF-transformed flight lines, an alternative approach was tested. Each of the four flight lines for a given date was processed independently using a spectral library derived from flight line 1, however, rather than applying the library directly, it was first transformed independently for each flight line using the transformation statistics files that were calculated during the MNF transformation of the imagery from each flight line.

This method was tested after it was noted that the MNF images from different flight lines

varied even though the land cover classes were generally similar throughout the region. Local, within-flight line variation in cover, as well as the relative proportions of a given cover type, and differences in illumination geometry resulted in different contributions to the maximum variance in each equivalent MNF band, from each flight line. When the MNF images of identical areas from different flight lines were compared, several equivalently numbered MNF images were similar, while others differed markedly (Figure 5.27). Because each flight line was transformed independently, the variance statistics calculated for that particular area and transformation were unique. It was not appropriate, therefore, to map all flight lines using an endmember library that had been transformed with the MNF statistics that were unique to a specific flight line (as in Test 2).

With this method, good visual correspondence between classes was obtained from one flight line to the next (see Figure 5.26, C1 and C3). Because the endmember library was derived from a single flight line, the classes were identical in terms of the number of classes, the coding, and labeling between flight lines. This eliminated the substantial post-classification processing that would be required if separate libraries had been used. Inter-flight line analyses of classifications and spectral characteristics were facilitated. Seamless mosaics could be produced because all classes were identical and coding was consistent between flight lines. Processing and analyses were streamlined by eliminating the need to extract spectral libraries from each flight line, or to adjust codes following classification. The re-transformation of the spectral library was a critical step for consistent mapping between flight lines, over large areas.

Disadvantage of single, re-transformed library. A potential drawback with the above method was noted. If a unique or rare land cover class was not represented in the flight line from which the library was derived, this class would not be represented in the endmember library. That material would be mapped to an alternative spectrally similar material, leading to classification errors. This problem was seen in some agricultural fields in which a significant number of pixels were initially incorrectly mapped as leafy spurge (Figure 5.28 A and C). Flight line 1, from which the library was derived, was dominated by wildlands, and agricultural fields were absent, therefore, crop endmembers were not extracted for the library. Many of these

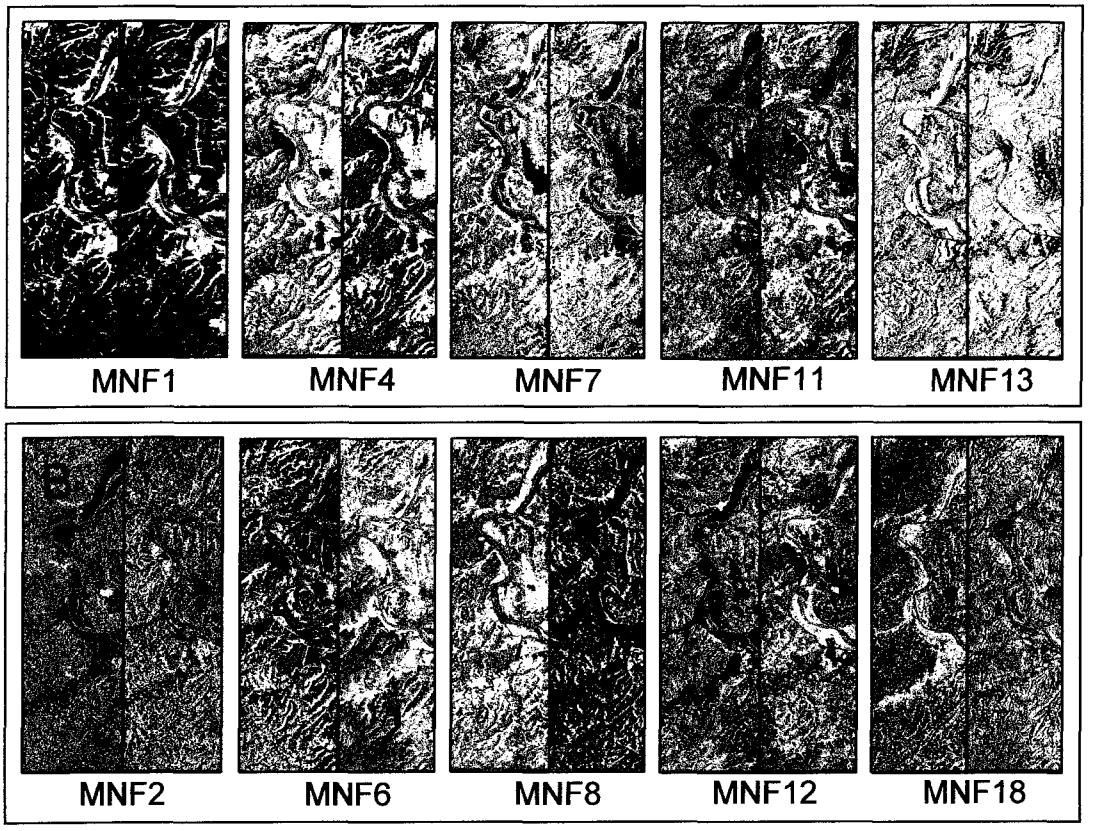

Figure 5.27. MNF comparisons of identical areas between flight lines. In each MNF pair, the left image is from flight line 1, the right image from flight line 3. Set A shows that some transformed images are similar between flight lines, while set B MNFs vary from one flight line to the next for the equivalent component.

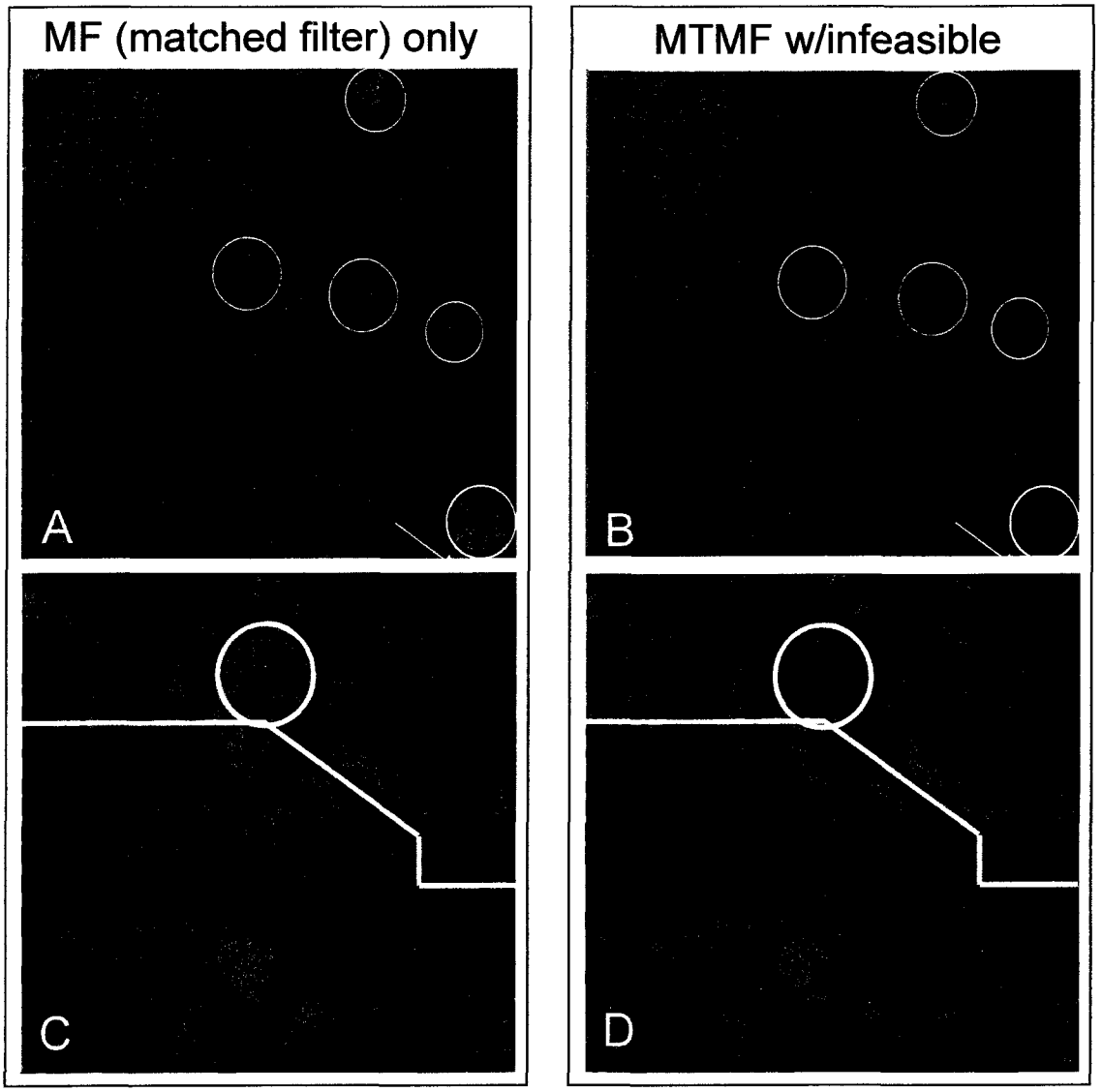

Figure 5.28. Elimination of crops incorrectly classified as leafy spurge after MTMF infeasible refinement applied. Green areas mapped as leafy spurge, brown is non-spurge vegetation, black is non-vegetated (masked). A and C are MF-score images; B and D are images of the same areas after the infeasible refinement was applied (MTMF). Areas circled in yellow are agricultural fields that have been erroneously classified as spurge in A and C; the same areas are correctly omitted from the leafy spurge maps in B and D. Yellow line (C, D) marks the northern boundary of THRO, and a division between wild land and agricultural land use.

patches that were erroneously classified as spurge were ultimately eliminated from the leafy spurge maps, however, when the infeasible image refinement was applied (Figure 5.28 B and D).

When pixels are eliminated from a class following the infeasible refinement it suggests that an appropriate endmember for the class was not represented in the spectral library. If this problem is encountered, the non-represented classes can be targeted and re-mapped by isolating the appropriate endmember class from another flight line where the class is represented, and then adding this endmember to the original library. Alternatively, spectra can be collected from pixels within the eliminated patch, averaged to produce a mean spectrum, and then added as an endmember to the original library to correct the problem. A correction is only a concern, however, if the map errors involve confusion with a critical target class (for example, crops mapped as leafy spurge), or if it is necessary to obtain a fully classified map.

Although crops were erroneously mapped as leafy spurge, because most of the agricultural patches were removed from the leafy spurge class after applying the infeasibility correction, it was not necessary to modify the spectral library and re-map the THRO data.

Re-transformed library applied to multiple dates. The re-transformed single spectral library extracted from flight line 1, 2001 was unsuccessfully tested for mapping the 1999 flight lines. The 2001 library could not be used directly with 1999 data due to a 2.5 to 3 nm shift in bandcenters between 1999 and 2001, the result of modifications and upgrades of the AVIRIS sensor between the two years. The offset bands prevented the transformation of the 2001 spectral library using the MNF statistics file from 1999 images. The 1999 spectra were resampled, therefore, to match the bandwidths of the 2001 data. This produced distortions of the resampled 1999 spectra, however, and the maps produced from the resampled data were poor. Known areas of leafy spurge were incorrectly mapped with the resampled spectra. An image library was therefore created for each date. Because the method used to select endmembers extracted all classes that could be reasonably found, it was assumed that the endmember libraries from 1999 and 2001 contained similar endmember spectra that represented the same land cover classes. The two libraries were selected and edited independently, without reference to the alternate-date library. The final counts of 62 and 63 endmembers for the 2 years

suggested that similar classes had been extracted. The order in which the endmembers were selected for each library was random, therefore class codes were not consistent between dates. The spectral analyst tool (ENVI User's Guide, 2003) was used to identify the highest probability matches between endmember classes from the two dates (Table 5.1). The 2001 library was used as the reference against which the 1999 endmember library was matched. The spectral analyst was run with the MF, SAM, and binary encoding algorithms. In some cases, the highest probability class (i.e., best match) varied depending on the algorithm that was used. Because the MF (MTMF) algorithm was used for the spurge mapping project, the highest probability match based on the MF algorithm was considered the best predictor of equivalent classes between the two spectral libraries. Land cover classes were not labeled before classification, and the equivalent endmembers from each date were not compared *a priori.* Following classification the leafy spurge endmember class was identified on each map, and the equivalent classes suggested by the spectral analyst tool corresponded visually on the 1999 and 2001 maps as well. The spectra of the spurge endmembers from 1999 and 2001 (Figure 5.29) are similar, but did not correspond precisely.

If bandwidths were identical between dates it is possible that a single library (with the appropriate MNF transformations) could be successfully and accurately applied to multi-date imagery. This could not be tested with this data set. This would assume that no significant changes in the land cover that was represented in the initial library had occurred, in which case deriving a new library for each date may be more appropriate.

CLASSIFICATION MODIFICATION

A critical modification of the mapping stage involved running the MTMF algorithm using a hybrid approach between linear SMA and the MTMF. Specifically, the process was modified with respect to the input endmember spectral library. The MTMF algorithm was designed to run with a single target endmember, and it solves only for a single selected target, while all other materials are treated as background (Boardman, 1998). The method used here, however, applied the logic of standard linear spectral mixture analysis (SMA) in which a "full" set of image-derived endmembers

	SAM		SFF		BIN ENCOD		OVERALL HIGH SCORE	
"Unknown"	High Score	01 Class	High Score	01 Class	High Score	01 Class	High Score	01 Class
99 1	0.903	25	0.121	12	0.944	12	1.998	12
99 3	0.87	23	0.362	23	0.966	4	2.186	23
99 6	0.894	24	0.325	41	0.983	37	2.16	41
99 9	0.9	33	0.438	14	0.944	33	2.288	14
99 10	0.91	33	0.461	43	0.989	33	2.305	33
99 11	0.9	9,2nd	0.586	28	0.989	9,2nd	2.372	9,2nd
99 14	0.746	44	0	no match	0.914	44	1.661	44
99 15	0.868	30	0.273	4	0.983	4	2.112	4
99 16	0.888	24,2nd	0.277	41	0.983	24,2nd	2.115	24,2nd
99 17	0.868	30	0.291	4	0.977	30	2.078	30
99 19	0.895	37	0.24	41	0.989	39	2.06	41
99 20	0.659	44	0	no match	0.989	44	1.648	44
99 22	0.88	34	0.516	13	0.977	43	2.26	13
99 23	0.87	28	0.664	34	0.891	28	2.396	34
99 25	0.897	39	0.342	24	0.983	24	2.212	24
99 26	0.91	3	0.51	3	0.983	3	2.403	3
99 27	0.904	41	0.388	25	0.944	12	2.26	25
99 30	0.891	41	0.269	41	0.989	12	2.143	41
99 33	0.888	40	0.411	30	0.983	30	2.191	30
99 37	0.853	31	0.363	39	0.977	30	2.113	40
99 45	0.888	41	0.241	12	0.994	12	2.099	12
99 46	0.879	24,2nd	0.342	25	0.994	12	2.185	25
99 6,2nd	0.872	37	0.195	41	0.983	37	2.014	24,2nd
99 37,2nd	0.869	30	0.276	4	0.977	4	2.111	4
99 46,2nd	0.875	19	0.277	4	0.989	13	2.071	19

Table 5.1. Highest probability matches between 2001 and 1999 spectral library endmember classes. The highest probability value and the associated 2001 class number from 2001 are indicated for each class from 1999 after running the ENVI spectral analyst using SAM, SFF, and Binary Encoding algorithms to determine the highest probability match between endmember classes from the 2 years. The 2001 library was used as the "reference" library against which "unknown" 1999 endmember classes were matched.

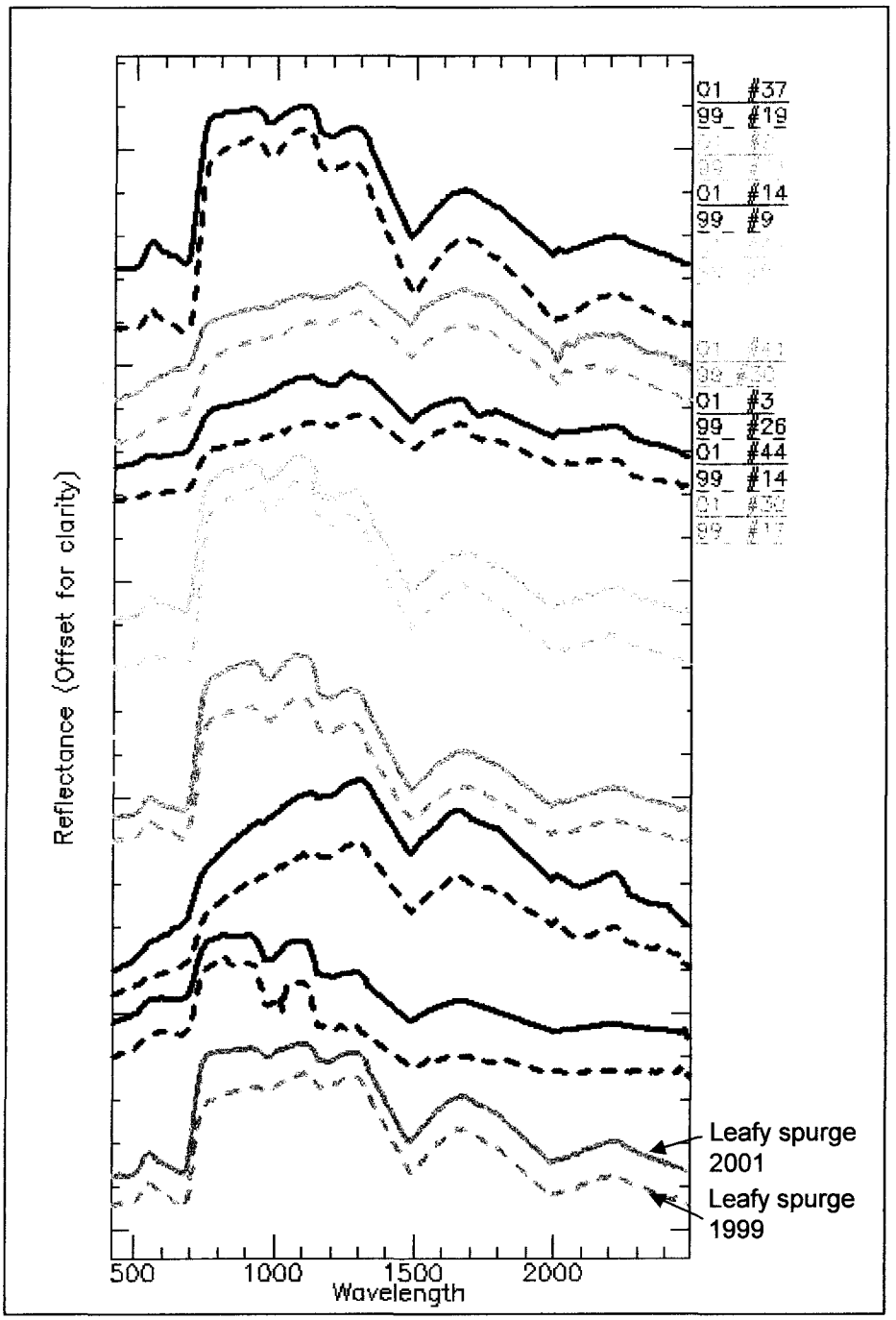

Figure 5.29. Comparison of selected, equivalent vegetation spectra from 1999 and 2001 spectral libraries, based on ENVI spectral analyst best-match scores. The equivalent endmember spectra are plotted in identical color pairs; 1999 are dashed, 2001 solid. Leafy spurge endmembers are labeled (bottom pair). In general, the red-edge shoulder is more well-defined in 2001, and NIR reflectance is higher for 2001 spectra. The chlorophyll absorption feature in the visible region is deeper for some of the 1999 spectra relative to the equivalent 2001 endmember. The 2001 endmember library was used as the "reference" to which "unknown" 1999 endmembers were compared. Legend indicates year (99 or 01) and the arbitrarily assigned class numbers.

was used simultaneously as input to the mapping algorithm to produce a complete vegetation map. Rather than running the SMA for the actual mapping, however, the MTMF algorithm was used.

The approach differed from the linear SMA in some respects, however. The number of endmembers input to the algorithm, for example, was not constrained to n +1, where n represents the number of input bands from an MNF-transformed image. Dimensionality is generally regarded as the number of coherent, non-noise MNF bands plus one (Boardman and Kruse, 1994). This limit on endmembers is imposed with SMA because this algorithm uses a matrix inversion of the individual pixel vectors and the endmember library matrix to simultaneously solve for the fraction of all endmembers within each pixel. The SMA algorithm, therefore, requires an endmember vector for all classes to calculate the fractional abundances (Adams et al., 1993).

Based on the homogeneity of spectral plots at high MNF values (Figure 5.30 B), as well as the absence of spatial patterns in the imagery with increasing MNF number (Figure 4.5), only the first 34 to 36 MNF bands (depending on flight line) were considered coherent enough to use for mapping the THRO data set. Sixty-three endmembers, however, were used for the classification with the MTMF algorithm. Because this algorithm solves for one endmember, with all other materials treated as background, the program ran iteratively, solving independently for each of the 63 endmember classes. There appeared to be many more potential endmembers than the theoretical maximum number based on the apparent data dimensionality. If only the first 35 to 37 of the 63 endmembers was used, many of the endmember spectra would have been omitted, and the target endmember could have been inadvertently excluded. If the SMA algorithm had been used, nearly half of the potential endmembers would have been discarded. If the number of classes were restricted, this would impose an unnatural constraint on a highly complex and variable landscape that will vary by region, sensor and data quality, and landscape components.

Although it is generally considered an advantage of the MTMF that it requires only one to a few target endmembers to map specific materials, running the MTMF algorithm with all possible endmembers was a critical modification for the establishment of a consistent mapping protocol. With the traditional approach that uses a single endmember, the target endmember spectrum

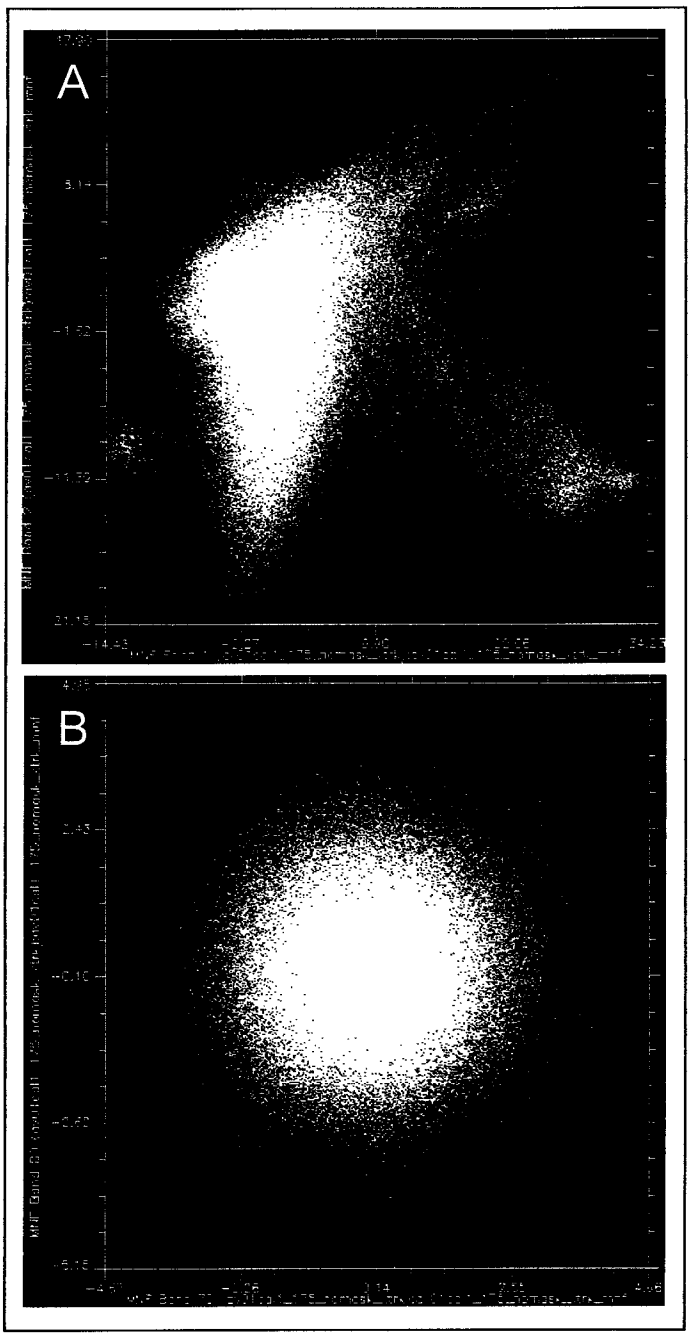

Figure 5.30. Two-dimensional scatter plots of MNF bands. Low MNF bands (1 and 2) are plotted in A; high numbered MNF bands (70 and 80) are shown in B. In A, the distinct, unique clumps of pixels plotted in "MNF spectral space" indicate different materials contributing to variance in the two MNF bands. The homogeneous MNF spectral plot in B indicates that the two MNF bands contain little unique information, and are dominated by noise.

must be unequivocally identified before mapping. This can be difficult for plant species or assemblages, particularly when a large number of similar endmembers have been extracted from an image. Figure 5.31, for example, shows the similarity between different image-derived vegetation endmembers. This accentuates the subtleties in the spectra that were being differentiated when extracting the endmember library, as well as the difficulty of selecting *a priori* one out of several similar endmembers as the appropriate spectrum for the leafy spurge class. This new method is an improvement because selection and identification of endmembers are not required to complete the map. With the alternative approach, because *all* possible endmember classes were input to the algorithm, the identification of endmember classes was not required, and no *a priori* decision regarding the most appropriate single target endmember spectrum was required by the analyst. Because all possible endmembers were selected, it is more likely that the target was included as well. Better maps of the dominant vegetation throughout the scene can be produced as well because all possible endmembers will be represented and compared to each unknown pixel spectrum in the image.

POST-CLASSIFICATION MODIFICATIONS: ELIMINATION OF THRESHOLDS

The output of the MTMF algorithm is both a matched filter (MF) score image and an infeasibility image for each endmember. For the THRO data set, 126 images were produced, two for each of the 63 endmember classes. The matched filter image output provides a "goodness of match" measurement between the endmember spectrum for the target class and all the unknown pixel spectra in the image. The higher the MF score, the better the match for that class. The infeasibility value represents, for a particular MF score, how likely or "feasible" it is that the pixel is actually in the class, based on an adjustable standard deviation scale that becomes more restricted as the MF score increases (CSES, 2000). The infeasible value is used to refine maps that include false positives, which are indicated by high infeasibility values coupled with high MF scores. Pixels with high MF *and* low infeasibility scores for a particular class represent the most suitable pixels for accurate representation of that class on the map (RSI, 2002).

In the traditional application of the MTMF algorithm, maps are produced by manually

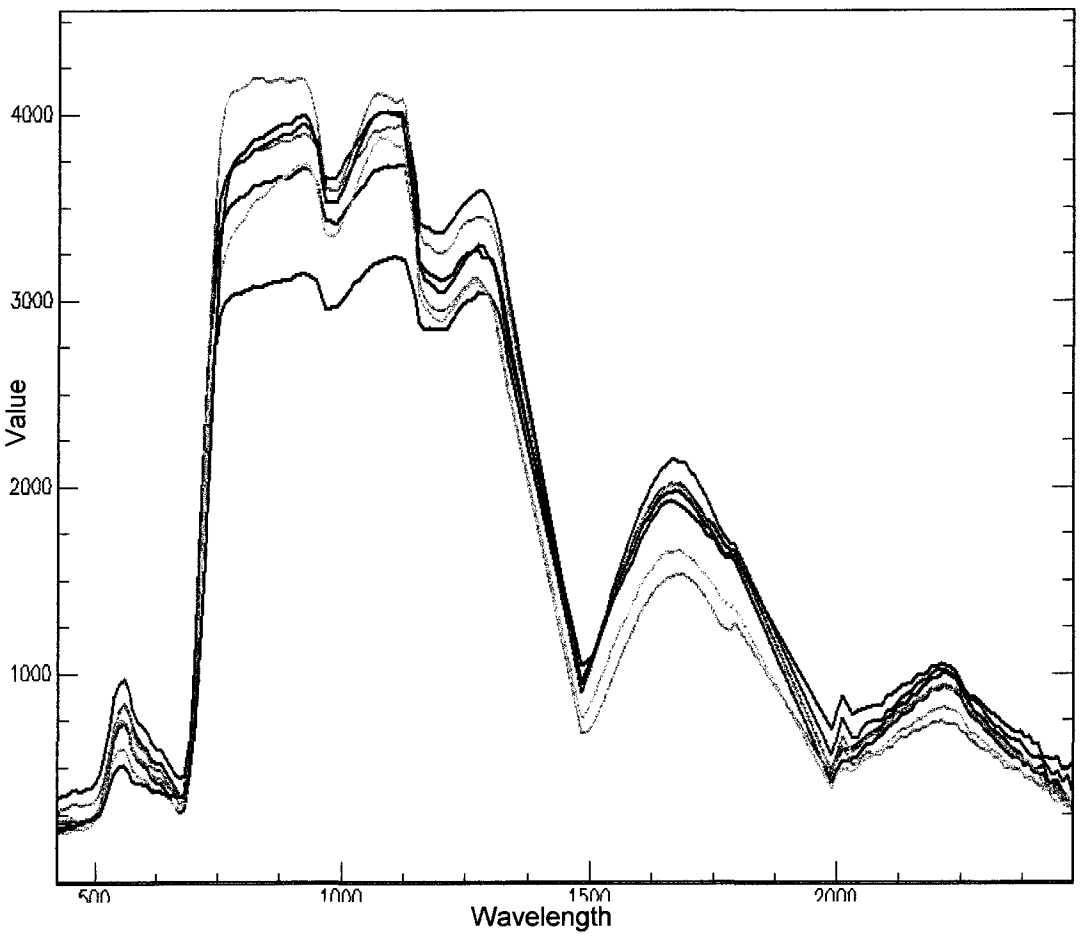

Figure 5.31. Visual similarity between sampled image-derived vegetation endmember spectra. The black spectrum is the leafy spurge endmember; other endmembers were not identified (similarity metrics were not calculated between the different endmembers).

selecting hard thresholds for a target class from a plot of the MF score versus the infeasibility score for that class (RSI, 2002). These are selected by defining a region of interest (ROI) on the plot that includes high MF and low infeasibility pixels. This interactive approach is subjective, however, and the ROIs and thresholds can be inconsistent between analysts and over time. The final target map can be somewhat arbitrary due to hand delineation of ROIs on a plot, where minor adjustments of the ROI can produce very different thematic maps. Thresholds that are established this way are often manually adjusted if a map shows significant omission or commission errors for the target class. This method of threshold selection and adjustment requires interactive decisions and substantial knowledge regarding the distribution of the target material on the ground.

Acceptable maps of leafy spurge were produced from the THRO data using the standard manual threshold selection described above, but only after adjusting the ROI cluster several times (Figure 5.32 A, B, C, D). Each adjustment required visual inspection of the resulting map, followed by continued re-selection and re-adjustment of the ROI until the pixels that were mapped as leafy spurge matched the known occurrence of spurge on the ground (Figure 5.32 C). These adjustments were only possible because the leafy spurge distribution on the ground in this area was well documented and the threshold could be adjusted until the map fit the known distribution. Requiring reference data to produce accurate maps negates the utility of remotely-collected data. When good reference data are unavailable, the threshold, and therefore the distribution of the target material on the map, will necessarily be based on the analyst's best judgment and may be incorrect.

An additional difficulty with the standard manual/graphical threshold selection became apparent during mapping of full, mosaiced flight lines and multiple flight lines. The graphics display plot in ENVI, from which the MF and infeasible ROI thresholds are selected, is only accessible from the "image" window in ENVI, which can only display a subset of an entire flight line. As a result, only the MF and infeasible values for pixels that are within the currently displayed image window are included in the graphics plot, and the thresholds selected from the plot are only applied to those pixels. Thresholds can be established over an entire scene, flight

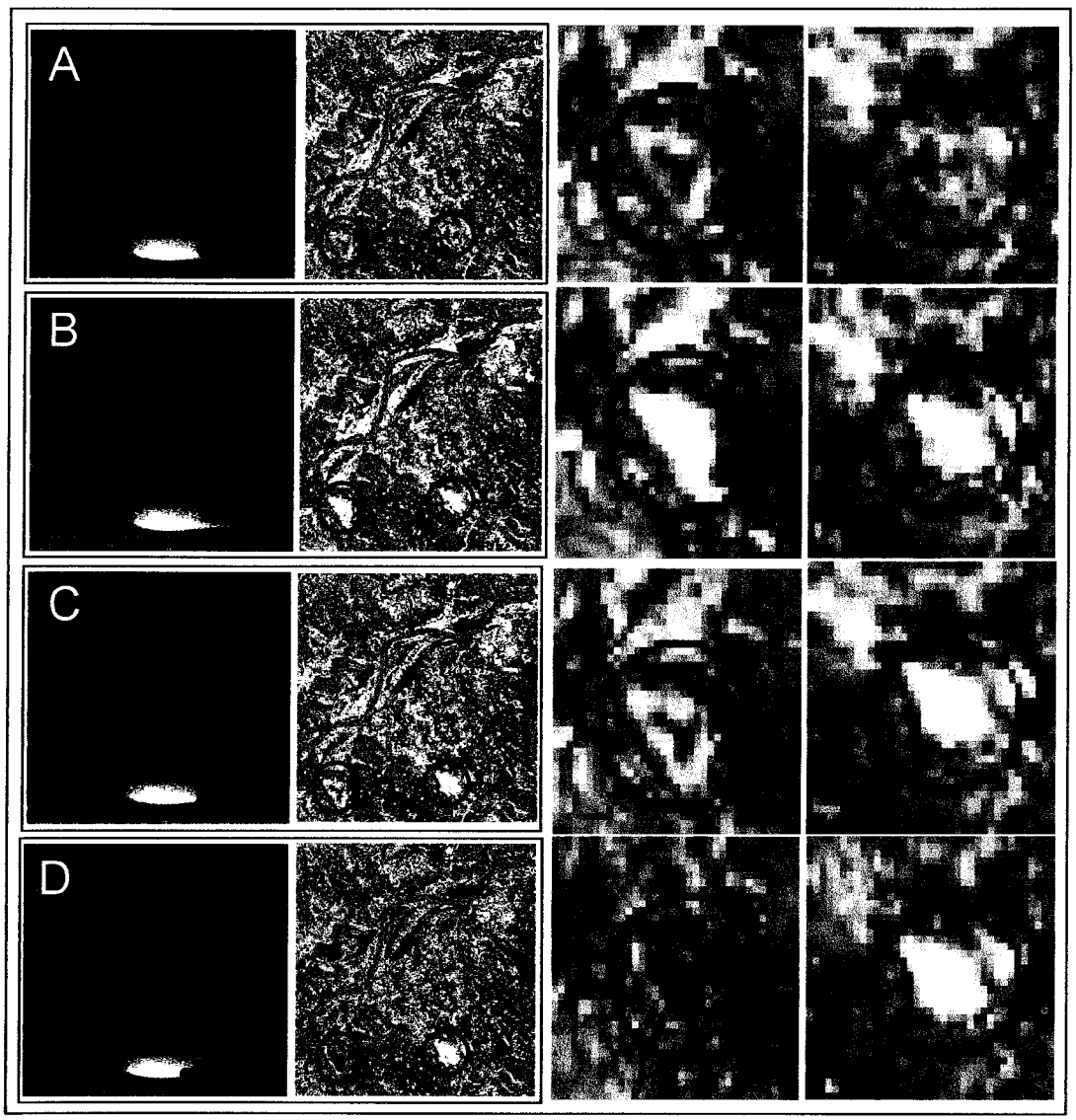

Figure 5.32. User-defined graphical selection of thresholds for mapping leafy spurge. Red pixels are those that have been labeled leafy spurge, based on the corresponding scatter plot ROI to the left. The area circled in black contains a known dense infestation of spurge; the red circled area is known to be free of leafy spurge. In A, C, and D the ROIs have correctly included MF/infeasible values to map the spurge (see black circles); the A and B ROIs have also incorrectly included values within the leafy spurge mapping threshold for other types of vegetation as well and therefore required adjustment (see red circles). C and D are close to the known occurrence of leafy spurge in the field, but D is over-classified (black circle); while C is slightly under-classified (black circle). Ground reference data was required to adjust the ROIs until the map fits the correct distribution.

line, or multiple flight lines by viewing, manually selecting, and saving the most appropriate threshold ROI for the currently-displayed portion of the image, then changing the displayed area and repeating the procedure until the entire area has been viewed and processed. This will result in inconsistencies and variation in thresholds from one section of the image to another, however. This is also time-consuming and cumbersome when the ROIs must be selected for many scenes or flight lines. Alternatively, the thresholds could be graphically selected from one subset of the flight line, with the value then applied to the remainder of the image. It may not be appropriate, however, to apply thresholds based on a single image subset to an entire region. For example, with a single threshold, if the score for a class was above the set threshold, pixels would map as that class regardless of whether or not the class was the *dominant* component of the pixel. Conversely, a material may be the most abundant within a pixel, but it would not be included on a map if the fraction fell below the single set threshold. A single, image-wide threshold will not always produce a map that represents the dominant material in each pixel.

NEW AUTOMATED THRESHOLD PROCEDURES

A new approach was used to establish MF and infeasible thresholds for the THRO data in order to eliminate subjective and variable boundary decisions by the analyst. MF and infeasible thresholds were established independently and automatically in a two-step process. This included: 1) using the ENVI "rule classifier" to establish the MF threshold; and 2) select the infeasibility threshold by applying a standardized threshold value of +1 standard deviation above the mean infeasibility value from the leafy spurge infeasible image.

STEP 1: MF THRESHOLD. With the post-classification "rule classifier" (ENVI User's Guide, 2003), a fully classified, thematic map similar to the output from traditional multi-spectral classifiers (Lillesand and Kiefer, 2000) was produced by allowing all 63 MF images to compete for the best single-class assignment. This was based on the highest MF score from all classes, where the class of the dominant, highest fraction material was assigned on a per-pixel basis. With this method the threshold was automatically adjusted to the highest value for each pixel rather than requiring that the analyst select a single threshold to determine whether a pixel should be included in a hard-classified map. Manual adjustment of the threshold based on intimate

knowledge of the ground was not required. This technique yielded a full vegetation map based on the highest of the 63 endmember MF scores for all vegetation dominated pixels in the scene.

STEP 2: INFEASIBILITY THRESHOLD. Because the goal of this study was to map leafy spurge, this was the only class that was fine-tuned with its corresponding infeasibility image. The pixels that mapped as spurge were isolated from the full vegetation map before the infeasible refinement by using a combination of re-coding, masking, and band math.

Empirical tests of several different threshold values indicated that one standard deviation above the mean value of all pixels from the leafy spurge infeasibility image was an appropriate boundary to use for refining the leafy spurge classification. Infeasible image values are listed in terms of "noise sigma unit" values (ENVI User's Guide, 2003). The mean infeasible values for leafy spurge from all flight lines ranged from approximately four to six noise sigma units. The +1 standard deviation threshold ranged from approximately eight to ten noise sigma units, depending on the flight line. This cutoff placed the threshold at an optimal location for eliminating most known false positives, while still correctly mapping documented areas of leafy spurge, including known low density patches. No obvious, documented patches of leafy spurge were eliminated with this new threshold method, although isolated pixels or patches of leafy spurge could have been removed that were not readily apparent. Reference information was insufficient to determine this, however. A range of values close to one standard deviation above the mean produced acceptable results, but the +1 sigma value was selected as the standard threshold because it can be calculated and applied without requiring interpretive decisions from the image analyst. With this method the thresholds will be comparable and standardized over time. The 1-sigma threshold improved the leafy spurge classification in all eight flight lines from the two dates that were mapped in this study by eliminating obvious false positives. It was, therefore, adopted as the method for defining the infeasibility image threshold to use for refining leafy spurge maps. This was an appropriate boundary for the leafy spurge class for all flight lines classified in this study, however, this threshold selection strategy was not tested on other vegetation classes. It is unknown, therefore, whether it represents a good general threshold method or whether it is valid only for specific vegetation classes, in this case leafy spurge. The 1-sigma threshold was used to refine maps in which leafy spurge was the dominant component of a

pixel (the "primary" map), as well as those in which it was a subordinate fraction (the "secondary" spurge map) (for discussion of primary and secondary maps see: Section II, Post-classification, Map production).

IMPROVEMENTS WITH NEW METHOD

The 2-step, automated threshold approach described above addresses some of the problems associated with the currently used manual selection of thresholds. A map of the dominant material in each pixel was produced without requiring intimate knowledge of the ground to manually adjust the threshold. The MF threshold was automatically adjusted on a pixel-by-pixel basis because the highest value MF score for each individual pixel was selected, regardless of the absolute value. More detailed information can be presented when the threshold can be individually adjusted to the maximum score, and therefore the dominant material, for each pixel. At the same time, information on sub-pixel abundance for specific target classes is preserved, regardless of whether or not these represent the dominant fraction of a pixel. By using band math to combine the binary, presence/absence map with the MF score image for a target class, the fractional abundances can be retained. Loss of sub-pixel information is generally a drawback of hard-classified, thematic maps that are produced with arbitrary thresholds (Aspinall, 2002).

If more than one class will be mapped, a threshold would need to be manually selected for each individual class if the graphical method was used. With the new method, by using the post-classification rule classifier, the MF threshold selection is automated and completed simultaneously for all classes by selecting the highest MF score from all 63 classes to assign a class as the dominant component of the pixel.

An additional advantage of the method developed here over the manual graphical approach is that the entire scene or flight line can be processed at one time. This avoids the difficulties of selecting matched filter and infeasibility thresholds only for those pixels within the image window field of view, which can be cumbersome and create inconsistencies from one subset to the next when mapping large regions.

The methods that were developed in this study for establishing thresholds address the problems with the arbitrary nature of the traditional threshold method. By using the rule classifier

and the +1 sigma for establishing thresholds, subjective decisions were eliminated, which should improve map consistency. Because the selection of thresholds was standardized from one image to the next, between flight lines as well as between dates, the consistency of temporal and spatial comparisons was improved. Temporal differences in dominant land cover will not be confused by apparent change that is the result of inconsistencies in selected thresholds or manual adjustments by image analysts.

The maps produced with the hybrid, modified MTMF method successfully defined known patches of leafy spurge, while at the same time spectrally similar vegetation that had been easily confused with leafy spurge using other classification strategies was effectively excluded (Figure 5.33). The black and red circled areas in this figure correspond to those in Figure 5.32, and show a similar distribution to the map in Figure 5.32 C, the most correct classification that was obtained by repeated manual adjustment of ROI thresholds. The automated, modified mapping method, however, produced a good classification without requiring decisions, interpretation, or manual adjustments to produce a map with the best fit to known ground locations.

POST-CLASSIFICATION PROCESSING AND MAP PRODUCTION

ENDMEMBER TARGET IDENTIFICATION

Once the mapping was completed, comparison with reference data was used to identify the leafy spurge endmember class and to validate the spurge maps. The endmember associated with the target class, leafy spurge, was readily identified by using a GIS overlay of vegetation polygons on the classified image. Comparison with the 30 m^2 grids in which all contained vegetation was characterized, as well as verification by resident park managers were used to substantiate the identification of spurge. In addition, spectral reflectance data collected over known vegetation types in the field were visually compared to the image-derived endmembers to support the identification of the endmember class for leafy spurge. Additional vegetation classes were not identified as they were not the subject of this study, and there was insufficient reference data to validate the maps of other types of vegetation with anything more than a crude visual comparison to an older, coarser-scale photo-interpreted vegetation map.

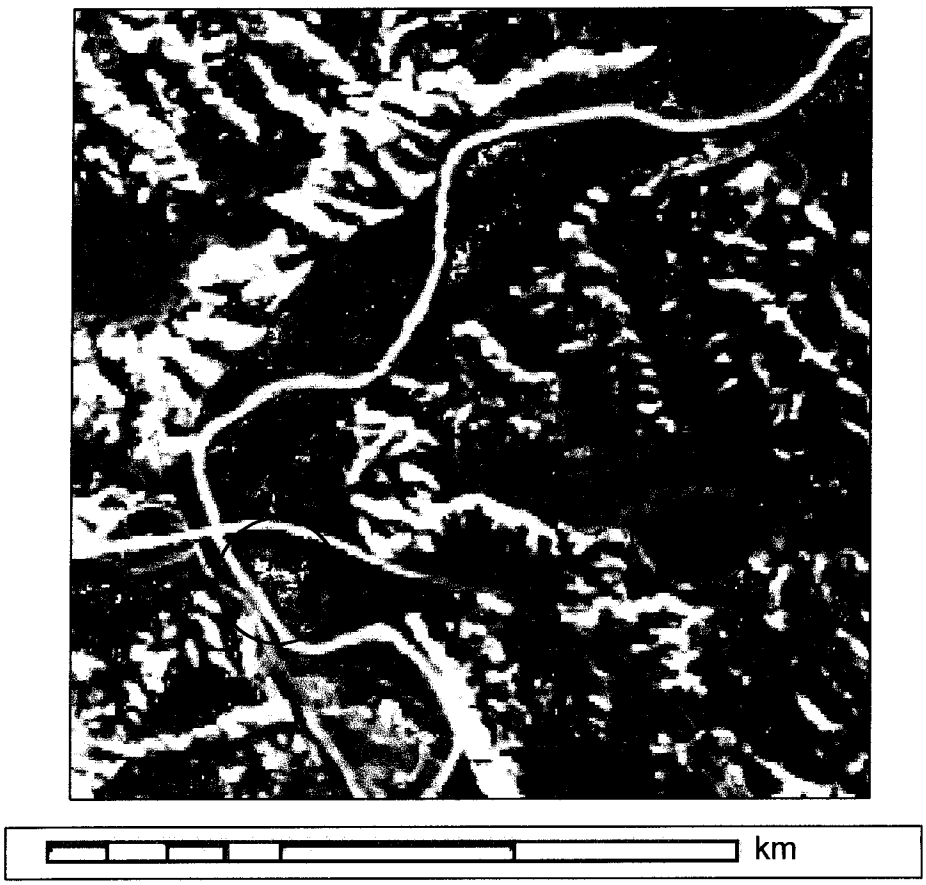

Figure 5.33. Hybrid modified MTMF map subset. 63-endmember map. Circled area A is correctly identified as spurge, no spurge is mapped in B, an area that was frequently misclassified as spurge in other maps.

MAP PRODUCTION

Each of the eight flight lines was independently mapped, using the modified methods described in Section II. The following four area-wide maps were produced for both 1999 and 2001:

1) Binary, presence/absence maps of leafy spurge (indicating where spurge was/was not the dominant, most abundant class within a pixel);

2) Relative abundance, or fraction, maps of leafy spurge (where spurge was the *dominant* class within a pixel), the "primary" fraction map;

3) Relative abundance maps of leafy spurge (where spurge was a *subordinate* class within a pixel), the "secondary" fraction map;

4) Combined primary and secondary fraction maps;

5) Full vegetation maps indicating the dominant or highest fraction vegetation class for each pixel (excluding the masked areas that were dominated by non-vegetative land cover).

Change maps were produced as well and are discussed in Chapter 7.

BINARY MAPS. The binary presence/absence maps of leafy spurge were produced by masking and isolating all pixels that mapped leafy spurge as the dominant component of a pixel based on the spurge MF score. This map was then fine-tuned using the threshold based on the leafy spurge infeasible image. Using re-coding and band math, the leafy spurge infeasible values were transferred to the pixels that mapped as leafy spurge as the dominant fraction. From these infeasible scores for "spurge" pixels, a binary map was created that segregated "spurge" pixels falling above or below the +1 sigma threshold. Further re-coding and masking were used to remove the infeasible pixels (i.e., those greater than 1 sigma above the mean) from the leafy spurge classification. A binary map of the infeasible-refined, leafy spurge-dominant areas was reconstructed using band math, with the final classes representing spurge, "other" vegetation, and the areas that were dominated by inert materials that were not classified and remained masked. Individual binary maps were produced for both 1999 and 2001 (i.e., Figure 5.34).

ABUNDANCE MAP (PRIMARY, LEAFY SPURGE DOMINANT). The binary, presence/absence map described above was used in conjunction with the leafy spurge MF score

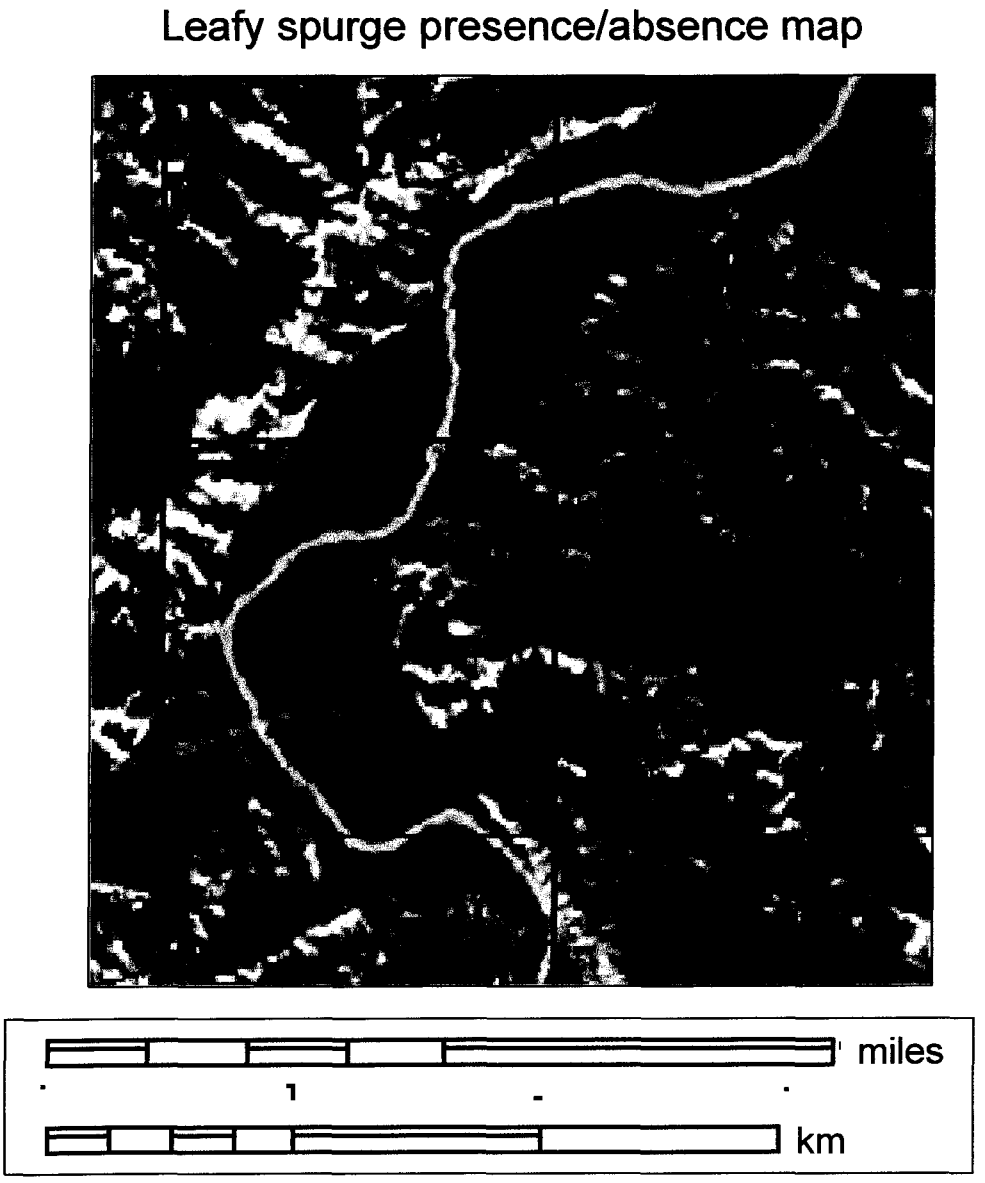

Figure 5.34. 2001 leafy spurge binary (presence/absence) map. Red indicates pixels that mapped leafy spurge as the dominant component of a pixel. Above map is a subset of the regional map.

image to produce a map of the relative fraction of leafy spurge within spurge-dominated pixels. All pixels except those classified as leafy spurge-dominant were masked, with masked areas recoded to 0, and leafy spurge to 1. Band math was used to assign the relative fraction to the leafy spurge class by multiplying the recoded leafy spurge map and the MF score image for leafy spurge. This allowed the leafy spurge MF scores to be assigned only to areas where leafy spurge mapped as the dominant fraction of a pixel. The MF score is assumed to represent a surrogate measurement of abundance (Boardman et al., 1995) and may be used as a rough estimate of the average density of a material. The final map of relative abundance for leafy spurge was produced by density slicing the leafy spurge MF scores into five equal-interval density-slice classes. This divided the fraction map into categories that loosely characterized the relative density of leafy spurge within individual leafy spurge-classified pixels. This procedure yields maps indicating the relative abundance only in pixels in which leafy spurge represents the dominant fraction (Figure 5.35).

ABUNDANCE MAP (SECONDARY, LEAFY SPURGE SUBORDINATE). The maps described above underestimate the occurrence of leafy spurge, because they do not include spurge that is a subordinate, yet still significant component of a pixel. To address this problem a secondary leafy spurge map was created using the identical MF density slice ranges that were used on the primary spurge map, but using only the pixels that did *not* map leafy spurge as the dominant class. These pixels were isolated by recoding, masking, and excluding the pixels that classified leafy spurge as the dominant vegetation. For the remaining pixels dominated by other vegetation classes, band math was used to attach the leafy spurge infeasible scores in order to eliminate any false positive pixels above the +1 sigma threshold for leafy spurge. All remaining pixels were recoded to one and multiplied by the MF score image to produce a relative abundance map of leafy spurge for pixels in which the weed was not the dominant land cover class. The leafy spurge-classified pixels and the additional vegetation pixels that had been eliminated with the infeasible refinement were recoded to zero. The same density slice ranges were used to assign the relative abundance categories for leafy spurge to pixels in the secondary map (Figure 5.36 B), with different color codes used for the secondary maps. In Figure 5.37, the

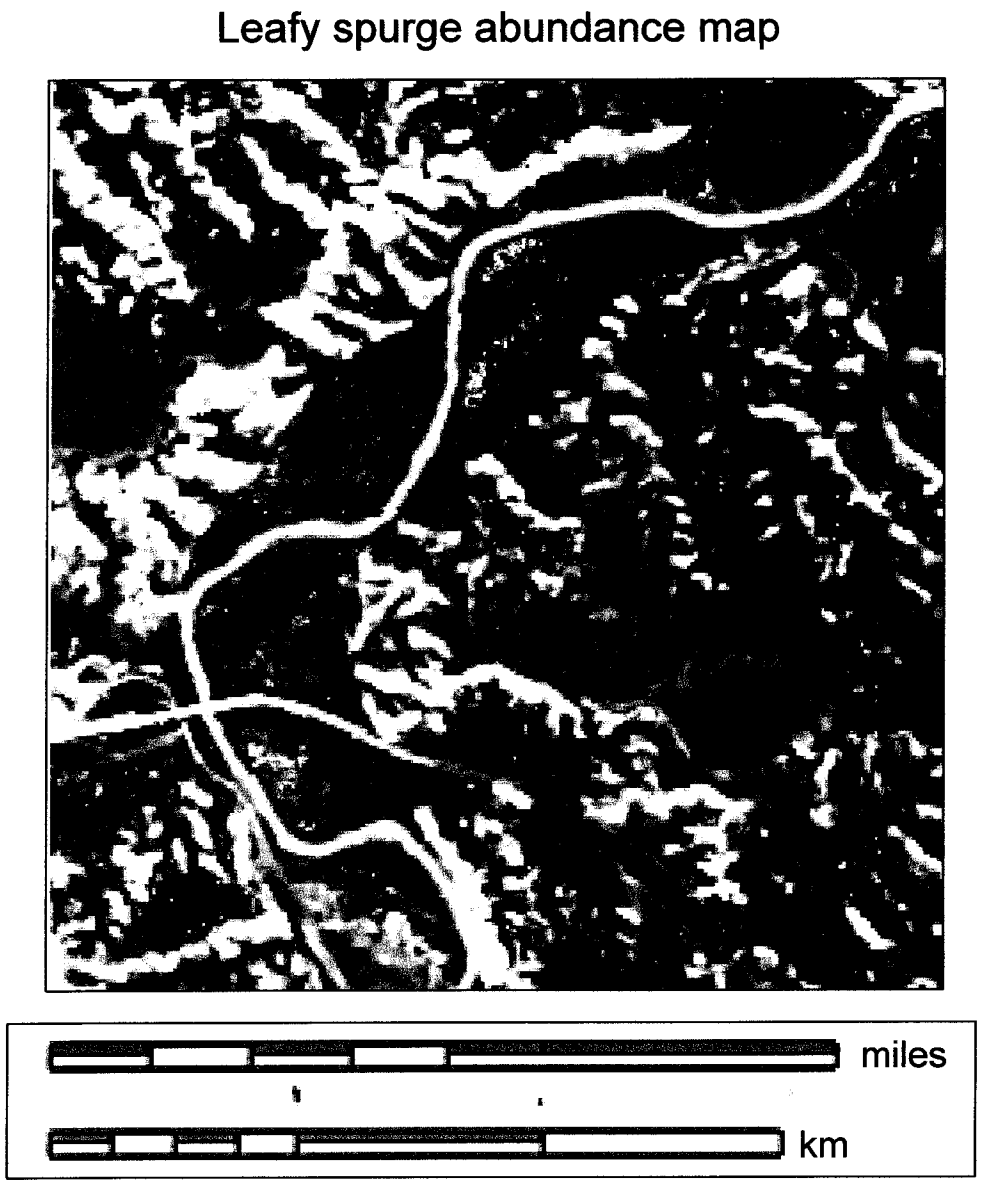

Figure 5.35. 2001 leafy spurge relative abundance map subset; derived from the spurge-dominant, binary map (Figure 5.34). Red indicates highest fraction, followed by orange, yellow, green, and cyan as the lowest fraction. Map above is a subset of the regional map.

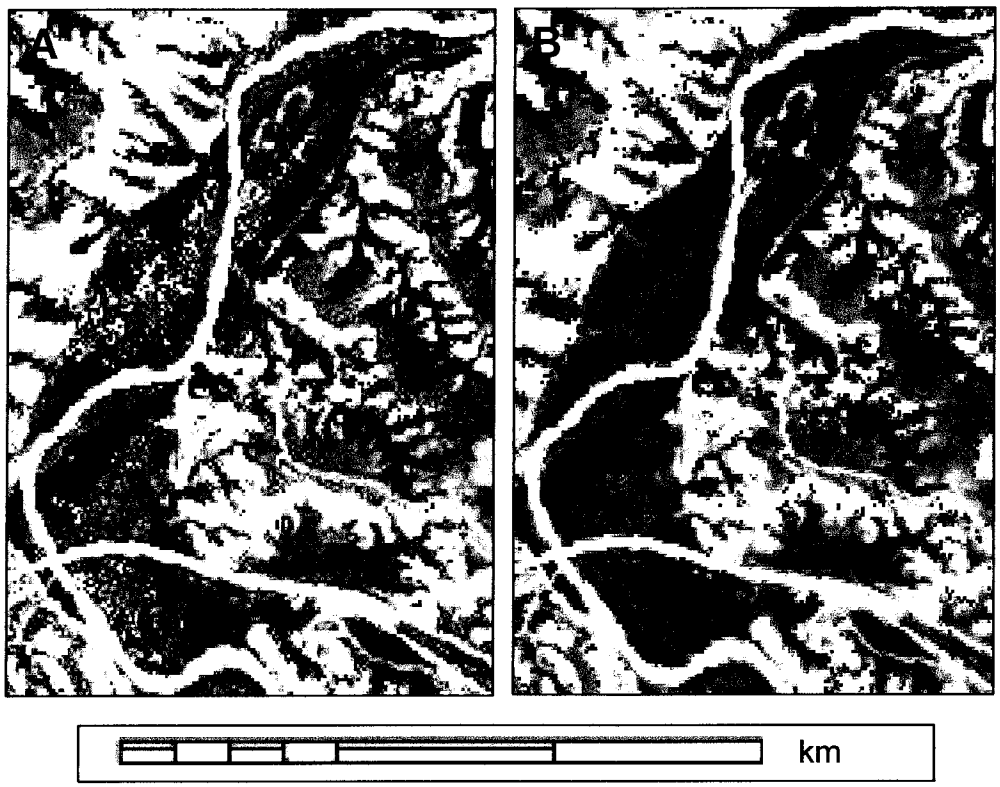

Figure 5.36. 1999 primary and secondary map subsets. A: primary (spurge dominant) map; B: secondary (spurge non-dominant) map. Density sliced classes indicated by dark green (lowest fraction spurge), green, yellow, orange, red (highest fraction) in A; dark magenta (lowest spurge fraction) through light magenta (highest spurge fraction) in the secondary map (B).

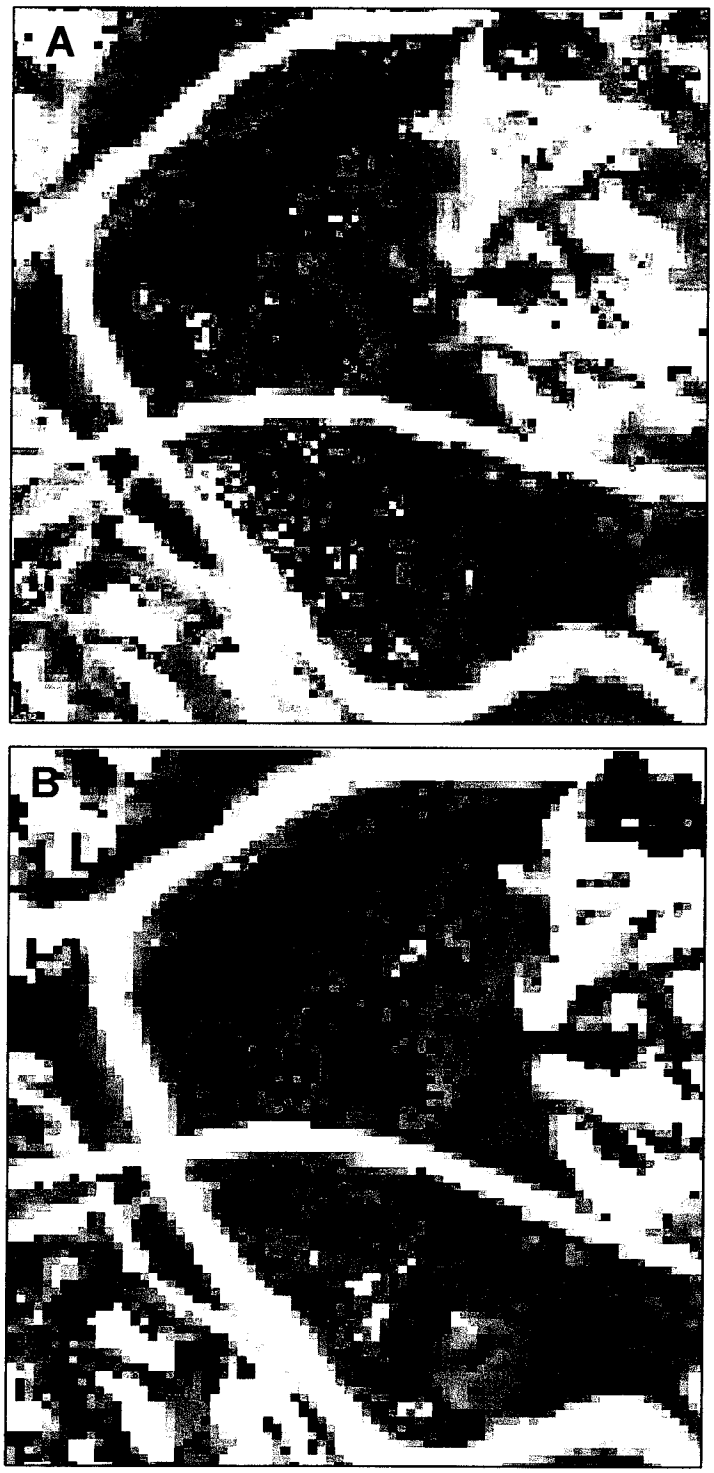

Figure 5.37. Combined primary and secondary maps from 1999 and 2001. A: 1999 primary and secondary leafy spurge maps combined; B: 2001 primary and secondary maps. Primary spurge maps in green (lowest fraction), yellow, orange, and red (highest fraction); secondary spurge maps in shades of magenta (lighter indicates higher fraction).

primary and secondary maps were combined to indicate areas in which any spurge was mapped, regardless of whether spurge was the dominant fraction.

The areas circled in yellow on Figure 5.38 indicate pixels that did not map as leafy spurge dominant in 1999, but *were* classified as leafy spurge dominant in 2001. In 1999, these areas contained continuous patches of leafy spurge, which occurred as low fraction, non-dominant components of these pixels, which were apparent only on the secondary (non-dominant) map. The location of these extensive or continuous, low-density spurge patches may prove useful for predicting areas that may be prone to future heavy infestations.

The lower abundance pixels on the secondary maps could be interpreted as either: 1) homogeneous, low-density mixtures of spurge and other materials occurring throughout a pixel; or 2) small (<< 17 m) homogeneous patches of leafy spurge intermixed with other dominant material within one pixel. Although it is not possible to distinguish between these, the lower abundance pixels will nevertheless be of interest to managers that are concerned with locating nascent patches of leafy spurge to facilitate early intervention, in addition to tracking the success of controls that have been applied in the area. Early intervention, within the first 2 years of establishment, is considered critical for effective control of leafy spurge (Lajeunesse et al., 1997).

RAPID, AUTOMATED VEGETATION MAPS. An advantage of the modified method that was used for mapping leafy spurge in this study is that an area-wide vegetation map was produced as an intermediate product of the processing (Figure 5.39 B for 1999 and 5.39 C for 2001). These maps compared favorably to a published vegetation map (see Figure 5.39 A) that was produced from 1:10,000 scale aerial photography flown in 1993 (Anderson et al., 1994; Anderson et al., 1996). Species and/or assemblages that are relatively stable over time (i.e., cottonwood stands, prairie-dog vegetation assemblage) compare reasonably well between the photo-interpreted and AVIRIS-based maps. In general, the AVIRIS maps are more detailed and they subdivide some of the more generalized plant associations from the photo-interpreted map into smaller associations and/or individual species (e.g., circled areas in Figure 5.39). There is good general correspondence between these, although the AVIRIS maps are more detailed. The AVIRIS maps were not filtered

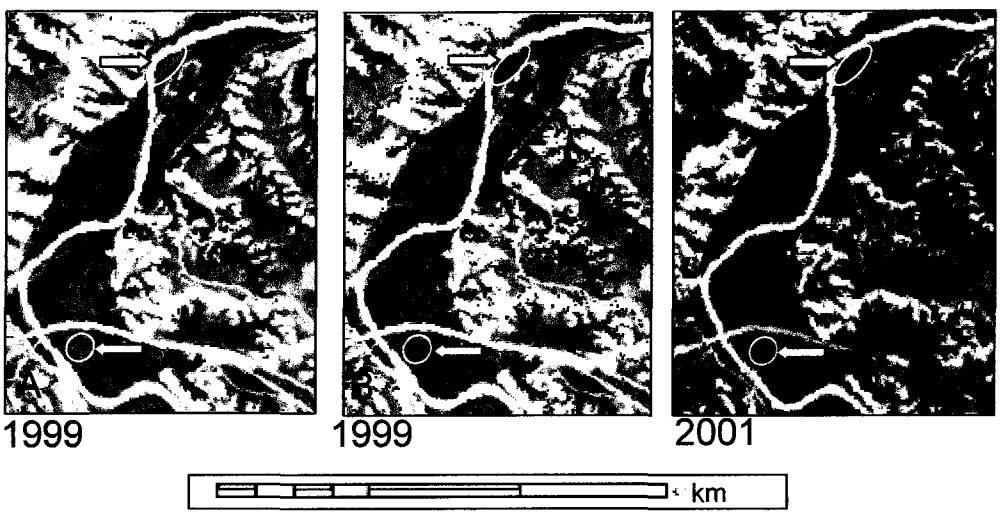

Figure 5.38. 1999 secondary spurge infestations become primary infestations by 2001. A and C: binary (presence/absence) maps of leafy spurge, 1999 and 2001; B: density sliced map of leafy spurge as a subordinate fraction of pixels (lightest magenta represents the highest fraction, deep magenta the lowest fractional abundances). Circled areas show that spurge was present as a non-dominant component in 1999, but the infestation was more pronounced in 2001, where these areas now indicate large patches in which spurge is the dominant vegetation within the area. The secondary (non-dominant) spurge maps may be useful for predicting locations susceptible to expansion of the weed.

Photo-interpreted1993

AVIRIS 1999

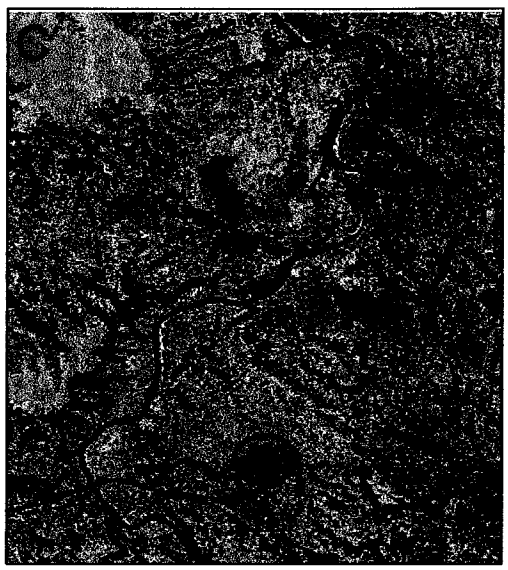

AVIRIS 2001

Figure 5.39. AVIRIS and photo-interpreted vegetation maps, showing advance and decline in leafy spurge (light green) between 1993 and 2001. 1993 photo-interpreted vegetation map (A) and AVIRIS-derived vegetation maps (B and C) compare favorably, although AVIRIS maps provide additional separation between some species/assemblages (i.e., area circled in red is labeled a single class in A, but two distinct classes in B and C). Advance (by 1999) and decline (by 2001) of spurge infestation can be seen by the extent of the light green spurge class in the three maps. Black in the AVIRIS maps indicates non-vegetated land cover that was masked.

after classification because the patchy distribution and isolated pixels of spurge were an advantage for detailed characterization of the distribution of the weed that is required for effective control.

Hyperspectral imagery processed with the modified MTMF may prove to be a reasonable alternative to manual photo-interpretation for the production of area-wide vegetation maps, and may provide additional detail that is generally absent from traditional photo-interpreted maps. Once the processing protocol was established, the AVIRIS maps were produced relatively quickly. With a well-defined protocol and some training, imaging spectroscopy could prove to be an efficient tool for regional monitoring programs. Data collection is expensive, however, and it can be difficult to routinely obtain high quality imagery.

SUMMARY

Initial test maps of leafy spurge produced from identical data varied depending on the procedures that were used to create them, indicating that the appropriate methods and algorithms should be selected carefully. To establish which procedures produced the most accurate maps several processing methods were compared.

Maps produced from field and image-derived spectral libraries were compared. In addition, the results of several algorithms (including linear SMA, SFF, SAM, MF, and MTMF) were compared. Maps created with and without NDVI masking, with and without liberal band editing, and with and without cross-track illumination correction were also compared.

Accuracy values were computed with error matrices where possible, but the results were inconclusive, and in some cases contradicted the visual assessments of the quality of the maps. This was assumed to be the result of the combination of georeferencing problems and marginal (poor, inappropriate) reference data. The plots were located on the map using points that represented the centroid of the plot. The small plot size was not appropriate for validation of AVIRIS-resolution imagery (17 m), and the point centroids were sensitive to registration problems. Visual assessments were used to select the best processing steps to use for the remaining flight lines.

Preprocessing steps that enhanced the quality of leafy spurge maps included: 1) application of a cross-track illumination correction; 2) removal/editing of extraneous noise bands and band

anomalies; and 3) application of an NDVI mask to isolate vegetation. The most accurate maps were obtained when the endmember library was derived from the image. The MTMF algorithm performed well, and the associated infeasibility images allowed the classification to be fine-tuned, therefore this algorithm was selected for all further processing.

The basic mapping method was modified and fine-tuned using only commercially available software and algorithms, to decrease the interactive processing that was required and to increase the consistency of maps, both spatially and temporally. The critical modifications included: 1) separate extraction of general and vegetation libraries from unmasked and masked images, using a two-step endmember collection with a modified selection strategy used to isolate classes;

2) selection of all possible endmembers from the imagery, with no restriction or limit imposed by a theoretical maximum number;

3) detailed editing of endmember spectra and the final spectral libraries;

4) MNF retransformation of a single spectral library prior to mapping each flight line;

5) mapping with the MTMF algorithm using a hybrid approach that included all possible endmembers used as input to the algorithm rather than a single target endmember;

6) using a post-classification rule classifier to establish the MF threshold automatically and eliminate interactive, manual, and often subjective selection of the subjective decisions on MF threshold used for mapping;

7) applying a +1 sigma above the mean score from the infeasibility image to standardize the infeasible threshold selection for refinement of classification.

Several maps were produced from both the 1999 and 2001 data. These included:

1) binary (presence/absence), spurge dominant (primary map);

2) density-sliced, spurge dominant (primary map);

3) density-sliced, spurge non-dominant (secondary map);

4) area-wide, full vegetation maps; and

5) a change map created from the spurge-dominant (primary) maps from 1999 and 2001 (see Chapter 7).

This comparative analysis of mapping methods indicated that individually and/or collectively, adjustments in seemingly minor processing steps can impact the outcome, variability, and consistency of maps that are produced with imaging spectroscopy.

By comparing, selecting, and refining processing, a number of improvements were made that resulted in increased automation and greater consistency in imaging spectroscopy maps. Advantages of the improved mapping methods are summarized below.

The selected methods and modifications outlined in this chapter capitalized on the optimal characteristics of the MTMF and linear SMA algorithms, while minimizing the drawbacks of each method. For example, restrictions on the number of endmembers were eliminated, and a simultaneous solution for all endmember fractions was not required. The unique infeasibility images produced with the MTMF algorithm allowed the maps to be refined for greater accuracy. As with the linear SMA, theoretically all endmembers are derived and fractional abundances of all classes are calculated to produce a fully classified map, and no decisions on thresholds are required.

With no restriction on the number of endmembers with the modified MTMF, subtly different classes were collected for more successful, thorough species mapping. Because all endmembers were collected, the target endmember would not be inadvertently omitted. No *a priori* identification of the specific endmember target from many similar, unknown endmembers was required, as is the case with the standard MTMF application when a single endmember is used. It can be difficult to select the "most" correct image-derived endmembers before mapping is completed. This eliminated another interactive decision and possible source of error or variability at this processing stage. By using image-derived endmembers, classes are not restricted to only those that could be characterized by ground-based spectral measurements, as when a field-based spectral library is used for classification. In the field it is difficult to collect representative field spectra of all possible endmembers over large regions.

Because all MF scores "compete" for class assignment with the rule classifier, the threshold was automatically adjusted as needed on a pixel-by-pixel basis. The best score class from all

possible classes is simultaneously assigned, rather than requiring that each target class be individually mapped.

Sub-pixel abundance measurements are retained in the MF score images for each class and can be used to produce both "primary" and "secondary" fraction maps. The target map can be extracted from the full vegetation map and then coded by fractional abundance to produce the primary (spurge-dominant) map. The same MF score image can be used to produce secondary maps of fractional abundance for specific targets when the target is a subordinate, but still a significant fraction of a pixel, by focusing on only those pixels in which spurge was not mapped as the dominant class.

In addition to individual maps of a specific target, complete area-wide vegetation maps of the dominant material in each pixel can be produced rapidly and automatically, with greater detail than obtained with standard photo-interpreted vegetation mapping strategies. Mapping relative abundance could be easily extended to other vegetation classes, given sufficient ground data to positively identify the other classes that were mapped.

Because the spectral library was extracted from a single flight line, all class coding was identical, and comparisons, mosaicing, and analyses between flight lines were facilitated. The transformation with the MNF statistics from specific flight lines produced standardized and comparable classified maps between flight lines, over a large area. Spatial and temporal consistency of the maps was improved.

In addition, threshold variation between image subsets that results from the graphic threshold selection from isolated blocks of the full image was eliminated. The thresholds were determined automatically, using standardized criteria and methods. Arbitrary decisions with respect to threshold placement were minimized, allowing images to be processed with less expertise or training, a bonus for monitoring and management applications. By standardizing and automating thresholds, maps from different dates were more comparable, and change maps more consistent, because the thresholds were applied using consistent criteria over time, and change maps produced from them were more accurate, or minimally more consistent, because variability in processing and decision-making were eliminated.

The interactive steps used in the standard processing protocol require reference data to properly adjust the thresholds to produce accurate maps. By eliminating the need to interactively determine thresholds, reference information was only required for map validation, rather than for interactive, manual adjustment and production of the maps. In addition, reference data were not required for training or guiding the selection of specific target endmembers, and because the processing uses software and algorithms that are commercially available, no unique (in-house) programs or modifications of programs/software were required.

By reducing interactive steps, eliminating variables where possible, and minimizing the required analyst input, maps will be more comparable, consistent, repeatable, and standardized, and less sensitive to the analyst's interpretation. With the modified method, maps were as good as or better than any produced using interactive adjustments, and they were completed more rapidly because several interactive steps were eliminated.

The combined effects of the modifications at various stages in processing lead to greater consistency overall, particularly when used for temporal monitoring. By increasing standardization and consistency of individual maps, change maps produced from them will more accurately represent real land cover changes, rather than apparent change that is actually an artifact of processing differences. By explicitly defining a procedure to use for mapping, eliminating interactive decisions, and by increasing automation, processing hyperspectral is facilitated and can be completed with less training. This may lead to increased use by land managers who would benefit from using this technology for temporal and spatial monitoring of leafy spurge and other materials.

CHAPTER 6

ACCURACY ASSESSMENT

INTRODUCTION

Long-term monitoring of landscape characteristics with remote sensing requires accurate and consistent results over time. In the past, projects using hyperspectral data have emphasized experimentation and proof of concept (Green et al., 1998). Applied studies were uncommon, and these sensors were rarely used to facilitate practical management decisions. In addition, few of these early analyses focused on the consistency and accuracy of results, and formal accuracy assessments were absent from much of the early imaging spectroscopy literature. Difficulties with the registration of airborne hyperspectral scanner data can create problems with accuracy assessment, which can be further complicated when maps are detailed and fragmented. Recently, accuracy assessments have been seen with greater frequency, and have typically used the standard confusion matrices and point-based reference data that were developed for multi-spectral land cover validation (Congalton and Green, 1999). Others have adopted accuracy assessment methods that capitalize on the ability of imaging spectroscopy to map continuous variables. Regression analysis, for example, has been used to evaluate the correspondence between hyperspectral image estimates and field estimates of leafy spurge density within specified diameter plots and subplots (Parker Williams and Hunt, 2002a). Species-specific polygons have been defined in the field to use in both qualitative and quantitative assessments (Dudek et al, 2004; Dudek et al, 2005; Glenn et al, 2005). In other cases the method used for accuracy assessment was not clearly defined. To use imaging spectroscopy systems effectively for temporal monitoring, an appropriate method for assessing the accuracy of the maps must be established that would allow the quality *and* consistency of maps that are used in change analysis to be monitored.

There is a large body of literature regarding the advantages and disadvantages of various approaches to accuracy assessment for thematic maps generated by classifying remotely sensed images (Foody, 2002; Foody, 2004; Congalton and Green, 1999; Hollister et al, 2004). These generally pertain to classified multi-spectral data. The direct applicability of these methods to hyperspectral land cover maps has not been evaluated, and potential problems that are encountered during quantitative validation of hyperspectral classifications (including registration and fragmentation of classified maps, and validating partial class membership) have not been addressed.

Point-based error matrices are often used to assess the accuracy of maps produced from remote imagery without regard to the assumptions underlying the accuracy method, or whether the method and/or the point-based reference data are appropriate for the map and its intended application. Error in the reference data is possible, yet it is generally assumed that the source of error is the map produced from the remote data. Foody (2002) suggests that blanket application of the confusion matrix should be avoided unless the underlying assumptions have been addressed (i.e., pure pixels, perfect registration).

This study applied both standard error matrices as well as regression analyses to evaluate whether accuracy assessment strategies that were developed for validation of multi-spectral classifications are appropriate for maps produced from imaging spectroscopy, given the unique objectives of many hyperspectral projects and the detailed maps that can be obtained with these types of data.

Accuracy methods were evaluated: 1) because of the significant discrepancy that was seen between the visual assessments of the spurge maps, which suggested high accuracy, and early quantitative accuracy measurements that yielded surprisingly low accuracy values; 2) because limited information was available regarding the appropriate methods to use for validating hyperspectral maps; and 3) because formal accuracy values were necessary to provide a baseline for comparing the accuracy of maps produced with different processing methods.

Several factors were examined that were suspected of contributing to low accuracy values, and the apparent discrepancy between quantitative and qualitative assessments.

Registration errors between reference data and imagery, for example, were believed to be influencing quantitative accuracy values. In addition, the available reference data were not collected specifically for validating remote sensing maps produced from AVIRIS data, and may not be suitable for these accuracy assessments, particularly considering the patchy, fragmented distribution of spurge on the maps, and the discrepancy between the size of the field plots and the resolution of the AVIRIS data. The method used to produce the maps may have affected the accuracy as well. Alternatively, it may not be possible to accurately map leafy spurge with AVIRIS data. Any one of these factors could negatively affect accuracy values, and the impact of several of these factors simultaneously may cause dramatic accuracy problems. Several assessments were run to determine which of the above factors, if any, was responsible for the low values and the discrepancies that were seen, and which approach to accuracy assessment was most appropriate for the THRO hyperspectral maps.

Accuracy comparisons were also used to assess the consistency of maps that were produced with the modified mapping method that was developed to improve consistency and quality of multi-temporal maps, and maps produced from multiple flight lines (Chapter 5). The sensitivity of standard accuracy assessments to subtle, yet significant, differences in maps that resulted from different processing methods was also evaluated.

THRO ACCURACY ASSESSMENT

Two primary types of accuracy assessment were used on the THRO leafy spurge maps. These included standard confusion matrices and regression analyses.

The confusion matrices used coincident classified pixels and point-based, sampled reference data to create basic accuracy measurements for the primary, spurge-dominant maps from 1999 and 2001. This followed the current standard method that is used for validating hard-classified, multi-spectral remote sensing maps.

Standard confusion matrices were also used in several comparative tests to evaluate: 1) the effects of different mapping strategies on accuracy; 2) different sources and types of reference data; 3) the consistency of the spurge maps; and 4) the influence of registration

problems and fragmentation of maps on accuracy. Some of the assessments were run on classified images modified by buffering, filtering, or re-registration.

Regression was used to evaluate the correlation between field-measured density of leafy spurge and image-derived fractional abundance measurements of spurge. These relationships were evaluated at a pixel-level scale, as well as at a coarser, patch-level to determine the appropriate scale for this type of analysis.

Unless otherwise noted, the accuracy results discussed in this chapter are presented for the primary, leafy spurge-dominant maps from 1999 and 2001 that were produced using the modified, hybrid MTMF method described in Chapter 5.

REFERENCE DATA SOURCES

Three primary sources of reference data were used for the accuracy assessment. These included: 1) the centroid point locations from randomly-located 3 x 5 m plots in which the vegetation had been characterized in detail; 2) vegetation polygons of varying size that were delineated by continuous collection of GPS points while walking the perimeter of homogeneous patches of vegetation, dominated either by a single species or mixed assemblage; and 3) a 32 m x 32 m grid network covering only areas that contained leafy spurge, with all vegetation characterized within each grid cell.

Two secondary sources of reference data were used to support the primary accuracy assessments. These included a photo-interpreted leafy spurge map based on 1993 aerial photography, and an additional set of reference plots, located by centroid coordinates, that was collected during the summer of 2003.

REFERENCE DATA COLLECTION

The primary reference data were obtained either nearly simultaneously with the collection of the imagery or within the same growing season, and in all cases it was collected independent of image classification. The plots and polygons were not acquired with validation of remote sensing maps as the main objective. The grid network, however, was collected for the validation of leafy spurge maps that were produced from Hyperion data for a related study (Harrison, 2001).

Grid sampling was designed for validation of the 30 m-resolution Hyperion imagery, rather than 17 m AVIRIS data.

Plot point collection. These points represent the coordinates for the centroid of 3 m x 5 m vegetation plots that were collected for an unrelated leafy spurge monitoring project (Larson and Grace, 2004). Stratified random sampling was used to locate geographic coordinates for the centroid, around which the plot was constructed. This sampling procedure was used to ensure that a sufficient number of plots of spurge present and spurge absent were represented. All vegetation within the plots was characterized using stem counts and estimates of percent plant cover for all species occurring within the plot boundaries. Where leafy spurge occurred within the plot, the estimated density of spurge ramet cover within the plot was recorded as well. Each vegetation plot was represented by a single point location. The reference point was labeled positive for leafy spurge if the plot contained any spurge, regardless of the density of spurge within the plot. In 1999, 549 total plots were collected, which included 447 spurge-infested plots and 102 non-infested plots. In 2001, 207 leafy spurge and 153 non-infested plots were collected. These points were converted to shapefiles that represented either spurge present or spurge absent. This information was provided by THRO park personnel to use as an independent reference source for validating the leafy spurge classifications. Vegetation polygons were not collected in 1999, therefore these plots were the only primary reference data that were available to test the accuracy of the 1999 maps.

Polygon collection. The perimeter of spurge and other vegetation polygons were defined on the ground to provide geographic reference for the field spectra that were collected within the area defined by the polygons. These spectra were collected to create a library for mapping leafy spurge using low altitude CASI imagery (the Compact Airborne Spectrographic Imager) for a related leafy spurge mapping project conducted by the USGS Spectroscopy Laboratory (Kokaly et al., 2001c). Concurrent with collection of the field spectra, the outer boundaries of the targeted vegetation patches were defined by walking the perimeter of the patches while continuously collecting coordinates using a GARMIN GPSMAP 76 Global Positioning System (GPS) receiver to define the size and shape as well as location of each patch.

Positional error between the recorded and actual positions was estimated (on the receiver) at 18 m or less. The vegetation polygons were delineated in the field within 2 weeks of the 2001 AVIRIS overflight. The percent cover estimates of leafy spurge, as well as other land cover components, including additional vegetation types, soil, and litter in polygons with less than 100% leafy spurge, were characterized for each patch. Ten spurge patches were selected to represent a range of densities occurring throughout the region, and varied from approximately 25% to effectively 100% leafy spurge, where "100%" represented very dense spurge monocultures with a minor component of shadow within the canopy. Twelve polygons enclosing homogeneous patches of other types of vegetation or vegetation assemblages that are characteristic of the region were collected as well. The polygons were collected before mapping, and independent of the mapping results. Patch sizes varied from approximately one pixel (17 m^2 or approximately 0.03 ha) to 143 pixels (covering approximately 4.09 ha).

Grid collection. During the summer of 2001, a field crew was hired to measure and locate approximately 675 grids (32 x 32 m) over areas infested with spurge. In each cell, the percent cover for spurge and all other vegetation within the grid was documented. These data were only collected during the 2001 field season.

The grid network was collected with a fundamentally different approach than that used for the polygon collection. The network was measured and delineated in the field. If a cell contained any leafy spurge, all vegetation within that cell was characterized by percent cover; however, the spatial distribution of the vegetation within that cell was not recorded. A cell labeled "50% spurge", for example, could indicate that half the cell was infested with a patch of 100% density spurge. Alternatively, this could indicate that 100% of the cell was infested with a 50% density spurge patch (or many other combinations of density and percent cover). This is in contrast to the polygon reference data in which distinct, relatively *homogeneous* patches of spurge, other species, or homogeneous mixtures were delineated and characterized, regardless of the size or shape of the patch.

Secondary reference sources. Two secondary reference data sources were used to support the primary accuracy assessments. Vegetation maps that were produced from 1993

aerial photographs as part of the USGS vegetation mapping program were used for visual support of the formal accuracy assessments. Because of the 6 and 8 year gap between collection of the aerial photography and the AVIRIS imagery the photo-interpreted maps were not used in a quantitative assessment of the accuracy of vegetation maps produced from AVIRIS data. In addition, accuracy based on centroids from plots collected in 2003 that indicated presence/absence of spurge were used for comparison to the accuracy derived with the 2001 points. These were specifically collected for validation of the leafy spurge maps, but 2 and 4 years following the collection of the imagery.

The points, polygons, and grids were converted to coverages and shapefiles to overlay directly on the classified imagery to be used in both quantitative and qualitative accuracy assessments (Figure 6.1). The accuracy assessments and tests that are discussed in this chapter are outlined in Figure 6.2.

CONFUSION MATRICES

BASIC ACCURACY ASSESSMENT

Methods. Standard confusion matrices were used for accuracy assessment of the primary leafy spurge classifications for both 1999 and 2001. The centroid coordinates of the field plots from both 1999 and 2001 were used to produce point shapefiles using ArcView software. These shapefiles were imported to ENVI, saved as ENVI-format vector files, then converted to raster-based, single-pixel regions of interest (ROIs), and coded for leafy spurge present or absent. These ROIs were used as reference "points" to compute the accuracy of the classified images using a standard confusion matrix. Because vegetation classes other than leafy spurge were not identified on the maps, only two vegetation classes were used in the confusion matrix: leafy spurge present, and non-leafy spurge vegetation. Overall, user's, and producer's accuracies, as well as omission and commission errors for both classes were computed using ENVI software for the 1999 and 2001 leafy spurge maps.

Results. Tables 6.1 through 6.9 include the results from the error matrices that were obtained for the basic assessments as well as the alternative test assessments. The initial

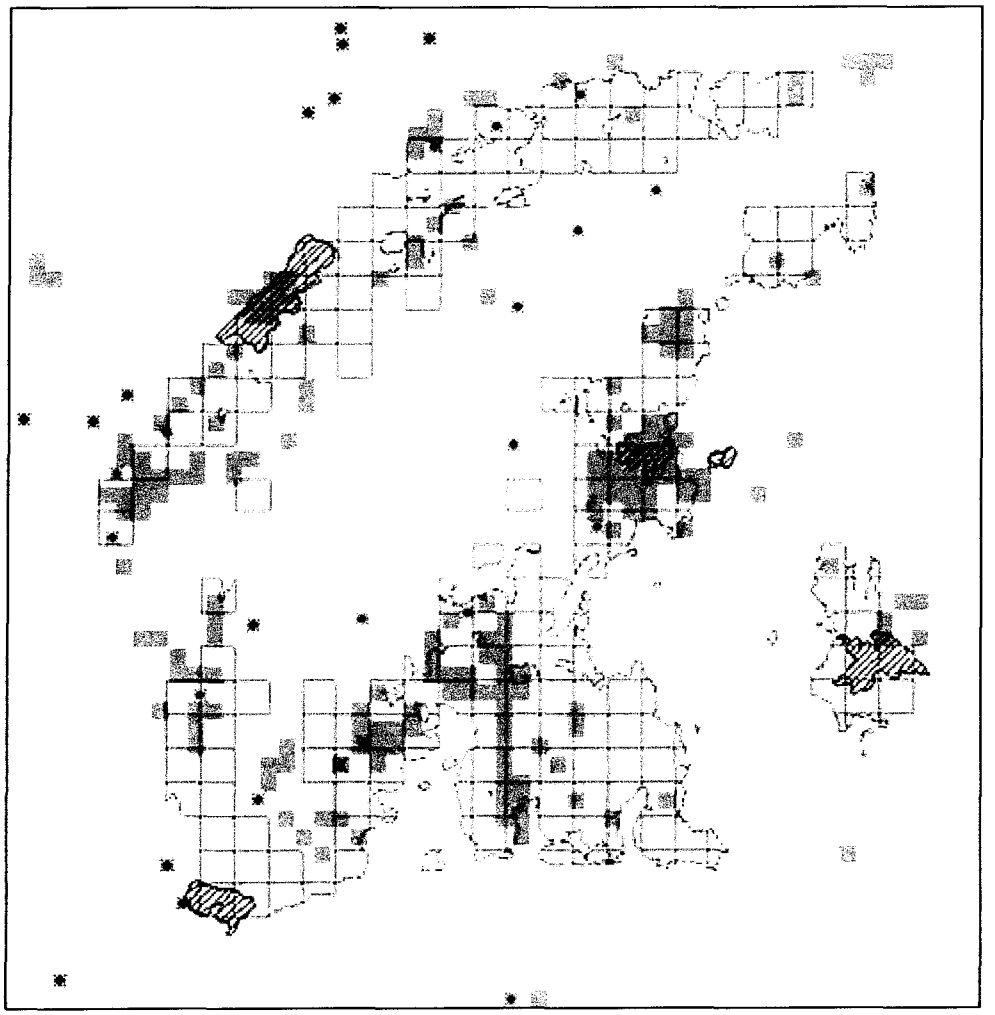

Figure 6.1. Examples of the three reference data sets used to assess accuracy of THRO classifications: 30 m^2 grids (sienna); polygons (black); and plot centroids, with leafy spurge points in red, and non-spurge vegetation in blue; classified leafy spurge from the primary, spurge-dominant map is shown in green. The irregular black-hatched polygons are homogeneous-density leafy spurge patches that were defined in the field.

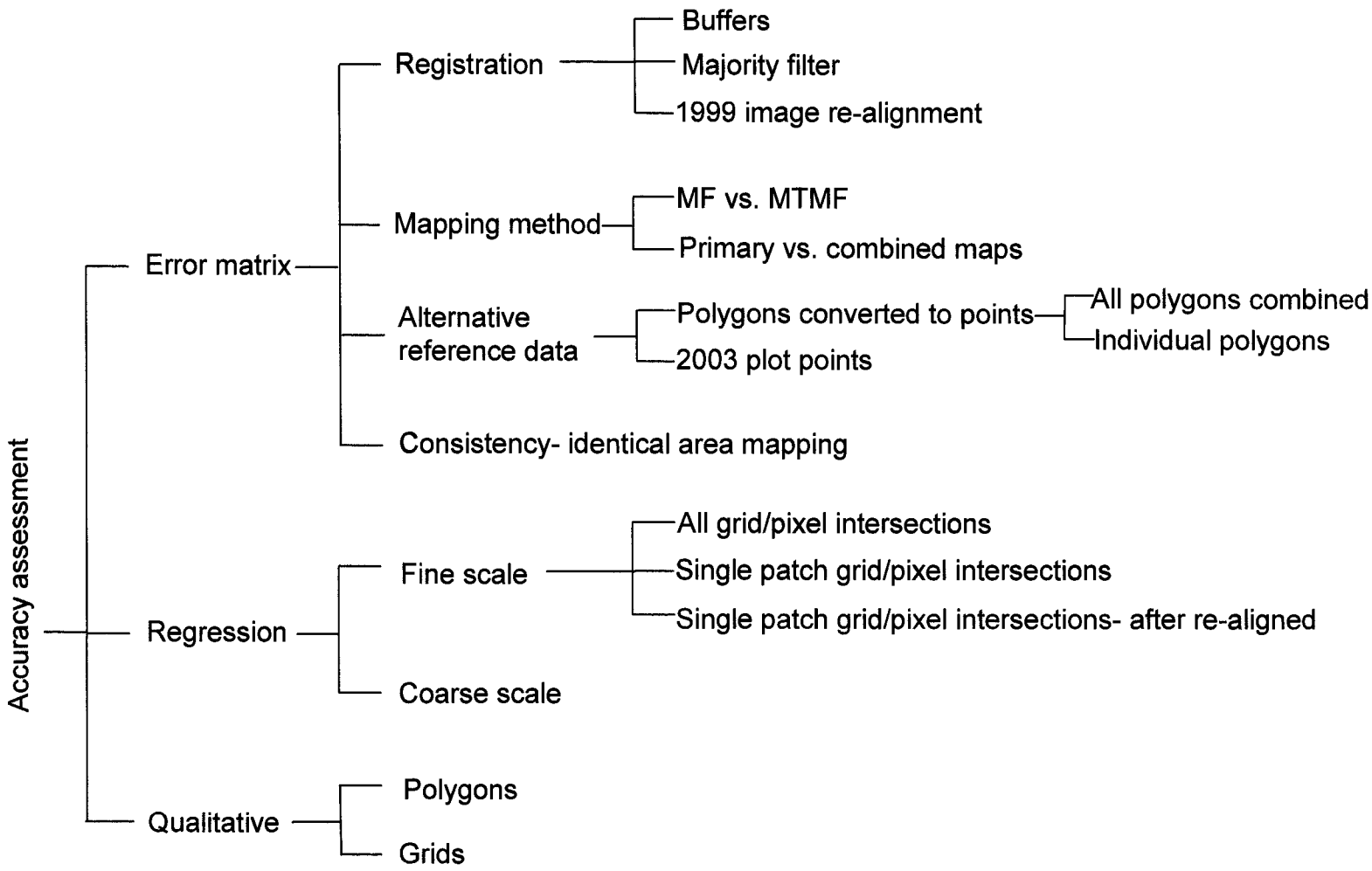

Figure 6.2. Accuracy assessments and tests run on THRO leafy spurge maps produced from 1999 and 2001 AVIRIS imagery.

accuracy values derived using the confusion matrix with reference points were low for the two-class map of leafy spurge and non-spurge vegetation (Table 6.1). Overall accuracies of 40% and 47% were obtained for 1999 and 2001 maps, respectively, before applying the infeasible refinement. Following the infeasible refinement, the 1999 accuracy dropped slightly to 39%, while the 2001 accuracy was effectively identical to the non-refined value of 47%. Commission error was low (0% for MTMF maps from 1999; 14% in 2001). User's accuracy, therefore, was very high (100% in 1999, and 86% for 2001). The producer's accuracy, a measure of omission of leafy spurge from the classified maps, was very low however (26% for 1999; and 18% in 2001).

Discussion. These values were surprisingly low, and at face value suggest that imaging spectroscopy is not effective for leafy spurge mapping; however, visual assessment of overlaid field polygons indicated that the classifications realistically portrayed known leafy spurge infestations in both 1999 and 2001. The results were particularly disappointing because of the low omission error for spurge. This was considered more critical than low commission (i.e., it was more important to include as much spurge as possible, at the expense of over-classifying and erroneously including other vegetation as spurge on the map). From a management perspective, areas of leafy spurge missing from the map would not be located and treated, and could accelerate expansion of the weed.

ACCURACY TESTS TO EVALUATE QUANTITATIVE/QUALITATIVE DISCREPANCIES

Due to the apparent discrepancies between the low calculated (quantitative) accuracies and the perception of favorable qualitative results, additional accuracy tests were run to evaluate the potential effects of registration, sources of references data, and changes in mapping method on quantitative accuracy. The results of several accuracy assessments run under different conditions and/or with different reference sources are presented below.

In all cases, the identical set of reference points was used for calculating each error matrix, except where the specific intention was to compare different sources of reference data. For each test, the methods, results, and discussion are presented together within the same section for clarity.

LEAFY SPURGE CLASS ACCURACY/ERROR: comparison of matched filter (MF) results with infeasible-refined MF results											
REFERENCE SOURCE	DATE	MAPPING METHOD	TOTAL # REFERENCE	TOTAL LS REFERENCE	PRODUCER'S ACCURACY		USER'S ACCURACY		OVERALL ACCURACY		KAPPA COEF
					#	%	#	%	#	%	
PLOTS	1999	MF	549	447	126/447	28.2%	126/126	100.0%	221/549	40.3%	0.12
		MTMF	549	447	118/447	26.4%	118/118	100.0%	213/549	38.9%	0.111
PLOTS	2001	MF	360	207	40/207	19.32%	40/47	85.1%	170/360	47.2%	0.089
		MTMF	360	207	38/207	18.36%	38/44	86.4%	169/360	46.9%	0.086

Table 6.1. Basic accuracy for 1999 and 2001 with MF and MTMF mapping results indicated; reference source: 3 x 5 m plot centroids. Overall accuracies are 7-8% lower in 1999 than 2001. MTMF overall accuracies are either essentially identical (for 2001) or approximately 3% lower (1999) than the MF results.

Registration, general. It was suspected that registration errors affected accuracy values that were calculated with point-based reference data. The magnitude of the spatial shifts between imagery and reference data varied and was unpredictable within a single image, but was estimated at 5 or more pixels in some areas. This registration error, coupled with the fragmented distribution and small patches of spurge could significantly alter accuracy values calculated with a point-based error matrix.

To evaluate potential registration effects, accuracy was calculated: 1) following adjustments of registration (specifically, the 1999 map was re-registered to the 2001 imagery); 2) after application of a majority filter; and 3) with buffers applied around classified areas to accommodate spatial shifts between reference and mapped data.

Re-registration, 1999 to 2001. Based on the initial basic accuracy assessments, the 1999 map showed lower overall accuracy than the 2001 map (by 8%, see Table 6.1). Because the alignment between the two images was inconsistent after the two data sets were independently georectified, the 1999 image was re-registered to the 2001 imagery to determine whether the lower 1999 accuracies could be related to differences in registration between the two dates. It was hypothesized that if the 1999 image registration corresponded more closely with the 2001 image, then the 1999 accuracies would improve, based on the assumption that the higher accuracy of the 2001 map was more "correct".

Methods. Approximately 400 ground control points were collected from RGB (red, green, blue) composites of the two dates using a covariance-based, automated tie point selection program (Kennedy and Cohen, 2002). Two hundred of these points were used in a standard image-to-image registration that was performed to tie the 1999 classified map to the 2001 ground control points and image. After the re-registration of the 1999 spurge map, the accuracy was re-calculated and compared to the original 1999 accuracy assessment, using identical reference points.

Results. Following the re-registration the alignment improved between the two dates in some areas, while others were unaffected, and in some portions of the image the registration offsets between the two dates *increased* following the re-registration. In addition, the overall

accuracy of the re-registered 1999 image *decreased* approximately 3 percentage points from the original 1999 values for both the MF and MTMF maps (Table 6.2). Both producer's and user's accuracies decreased as well, by either one or two percentage points, depending on the mapping method.

Discussion. The lack of improvement could reflect the different reference data sets used for the two dates, although theoretically with high quality, representative reference data, accuracy would not differ because of the reference data itself. An alternative explanation for the lower values in 1999 could be the unique endmember libraries that were independently derived and used for mapping the imagery from each date. The different libraries were necessary due to the 3 nm shift in the locations of band centers between the two dates. Also, improvements in the AVIRIS sensor between 1999 and 2001, including the adjustment of the band positions, could explain the improved accuracy results in 2001. In addition to the band shifts, the signal-to-noise ratio (SNR) was increased (Eastwood et al., 2000). Increased SNR allows a more refined analysis because more subtle spectral differences can be detected due to decreased masking of true signal when the noise signal is reduced. Because the spatial correspondence was inconsistent, and because the overall accuracy decreased with re-registration, the 1999 image re-registered to 2001 was not used for further analysis or change detection.

Majority filter. A majority filter was used as an alternative strategy to accommodate inaccurate registration between reference data and imagery, and to test whether accuracy of the spurge map could be significantly improved if poor registration was accommodated by generalizing the map. This is a standard method used with multi-spectral maps to generalize maps for enhanced visual appeal and to increase accuracy values.

Methods. A 3 x 3 majority filter was applied to the full thematic vegetation map to smooth and generalize the classification. The map was converted to the two-class, spurge/non-spurge vegetation map prior to running the accuracy assessment. The accuracy assessment was run on the filtered map using the same method and reference data that were used for the initial, basic accuracy assessment. The filter was also applied directly to the binary spurge/non-spurge maps, and the accuracy re-calculated.

LEAFY SPURGE ACCURACY RESULTS										
REFERENCE SOURCE	DATE	MAPPING METHOD	TOTAL # REFERENCE PIXELS (LS)	PRODUCER'S ACCURACY		USER'S ACCURACY		OVERALL ACCURACY		KAPPA COEFFICIENT
				#	%	#	%	#	%	
PLOTS	1999 (REREFERENCED to 2001)	MF	447	122/447	27.3%	122/124	98.4%	207/549	37.7%	0.091
		MTMF	447	110/447	24.6%	110/111	99.1%	196/549	35.7%	0.082

Table 6.2. Accuracy results for 1999 spurge maps before and after the map was re-registered to the higher accuracy, 2001 map. Overall accuracy values did not improve following the re-registration, but decreased by 3%.

Results. While the overall accuracy was one percentage point lower after applying the filter to the full vegetation map, the kappa coefficient was slightly, but not significantly, higher (by 0.005), and producer's and user's accuracy both increased three percentage points for the spurge class compared to the unfiltered map (Table 6.3). For the non-spurge class, however, producer's accuracy was lower by seven percentage points, which accounted for the lower overall accuracy after the filter was applied. The non-spurge user's accuracy did not change after filtering. When the filter was applied directly to the binary vegetation map rather than the full vegetation map, the overall accuracy was three percentage points lower than the non-filtered map.

Discussion. Applying the filter directly to the binary present/absent map decreased the overall accuracy of the map. This was likely because the non-spurge vegetation class dominated the two-class image, and more spurge was removed by the filter and assigned to the dominant non-spurge class when the filter was applied directly to the two-class map (Table 6.3 B). In the best case, where the filter was applied to the 63-class map, filtering improved accuracy results for the spurge class slightly, primarily by filling in between the larger, irregular spurge patches; however, many smaller isolated patches of spurge were also eliminated when the filter was applied. Overall, the improvement with the filter was minor for the spurge class. The elimination of smaller patches of spurge was considered problematic because these may indicate new spurge outbreaks that should be targeted and treated early for the most economical and effective weed control. This was an unacceptable effect of the filtering, and because the spurge class accuracy did not improve dramatically, and the overall accuracy decreased, the filter was not applied during the production of the final, park-wide spurge maps.

Buffering. An additional method was used on the 2001 spurge map to test the potential effect of poor registration on accuracy, and to accommodate the spatial offset that was suspected between the plot reference points and the imagery. Buffers were used to accommodate the range in offset that was estimated throughout the image, up to five pixels. An example of the offset is seen in Figure 6.3 in which a vector overlay of the plots (points) on the classified image shows several spurge reference plots falling one to three pixels from the edge of the Little

A LEAFY SPURGE CLASS: FULL VEGETATION MAP

	Producer's accuracy	User's accuracy	Kappa	Overall accuracy
Non-filtered	19	85	0.089	47
Filtered	22	88	0.094	46

NON-SPURGE CLASS

	Producer's accuracy	User's accuracy	Kappa	Overall accuracy
Non-filtered	85	44	0.089	47
Filtered	78	44	0.094	46

B LEAFY SPURGE CLASS: BINARY MAP

	Producer's accuracy	User's accuracy	Kappa	Overall
Filtered	11.0-14.0	92.0-93.0	0.05-0.06	44

Table 6.3. Filtered, non-filtered accuracy. A: includes results for the majority filter applied to the full vegetation thematic map (converted to binary prior to the accuracy assessment); B: results for direct applications of the filter to the binary, present/absent map (leafy spurge class only is shown).

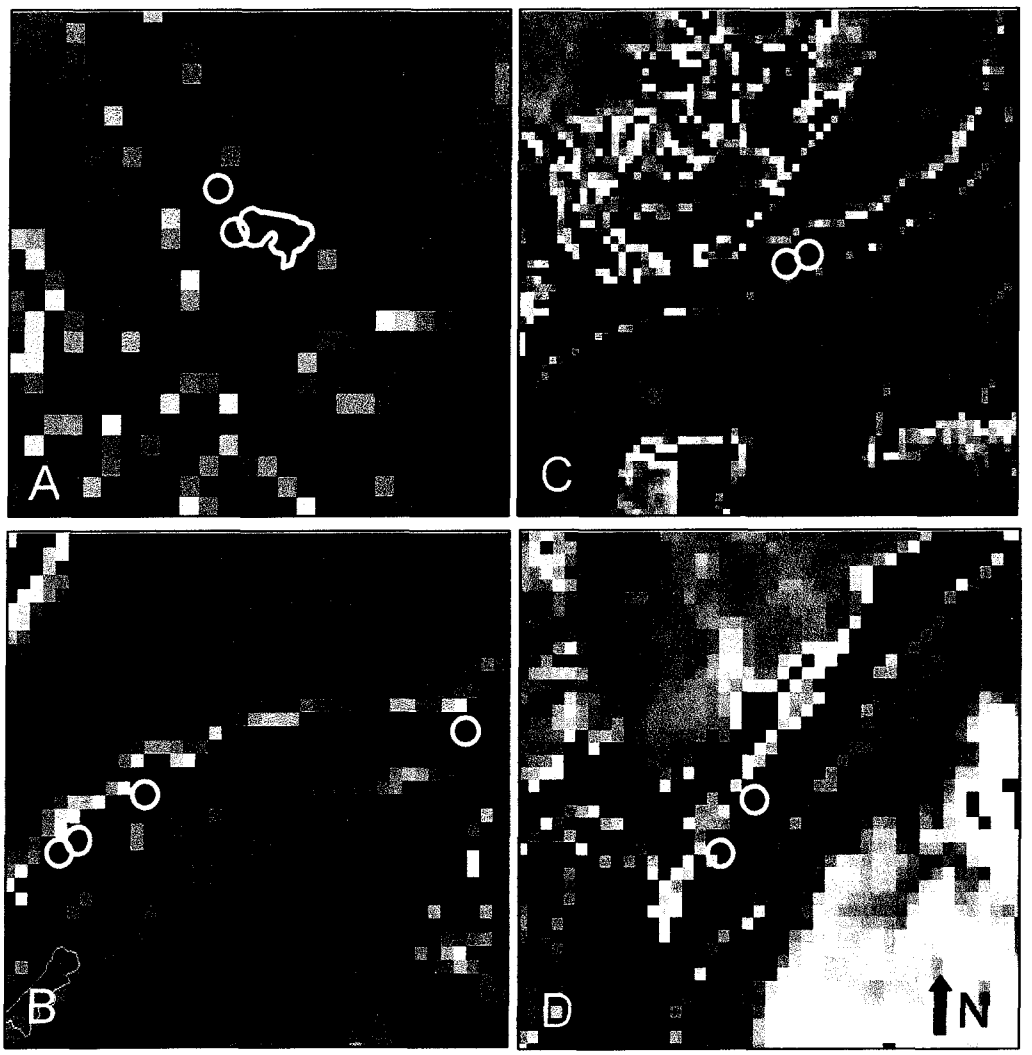

Figure 6.3. Reference/classified registration offset. Spurge reference points, indicated by small green crosses; several incorrectly located points are circled in yellow; yellow irregular patch in A is a spurge reference polygon; black areas are masked river and rock exposures. Several points plot *in* the Little Missouri River, 1 to 3 pixels from the masked edge, indicating the minimum estimated shift between imagery and reference data in these areas.

Missouri River, *within* the river. This indicates a minimum shift of one to three pixels in this area. If the quality of the registration was acceptable, then the non-changing, inert land cover classes should be well aligned between the 1999 and 2001 images as well. Figure 6.4, however, shows offsets between inert materials (the white areas on the maps) between 1999 and 2001. The offset is indicated by the overlay of the identical 1999 classification on gray-scale bands from both 1999 and 2001. The masked or inert materials are shifted by up to five pixels between the two dates, depending on location, based on the relative position of the classified areas from the two dates. The potential effect of registration error is demonstrated in Figure 6.5, which shows the theoretical change in accuracy values that could be seen when one- and two-pixel wide buffers were added around a single classified pixel, with the given hypothetical spurge and non-spurge reference points.

Methods. Pixels classified as leafy spurge were buffered with one to five pixels. These were applied isotropically around the classified pixels because the direction and magnitude of the apparent offsets between reference data and classified pixels were not systematic or predictable throughout the image. The buffers effectively coarsened the spatial resolution of the classified pixels from 17 m^2 to 51, 85, 119, 153, and 187 m^2 (with one-pixel through five-pixel wide buffers added, respectively).

Accuracies were re-calculated after applying each of the buffers, using the identical reference points for each assessment. The reference points were overlaid on the leafy spurge map. If the area classified as spurge and/or the surrounding buffered region contained leafy spurge field plots, the classification was considered correct for those plots, while any non-spurge vegetation reference points occurring within the buffered region were considered incorrect, and a commission error for the spurge class (and vice versa for field plots falling outside the buffered regions).

Results. The accuracy results for the non-buffered classification and the five buffered classifications are presented in Table 6.4, and the accuracy and error trends for the leafy spurge and non-spurge classes with increasing buffer size are shown graphically in Figures 6.6 and 6.7, respectively, to compare the differences in trends for the spurge and non-spurge classes. The

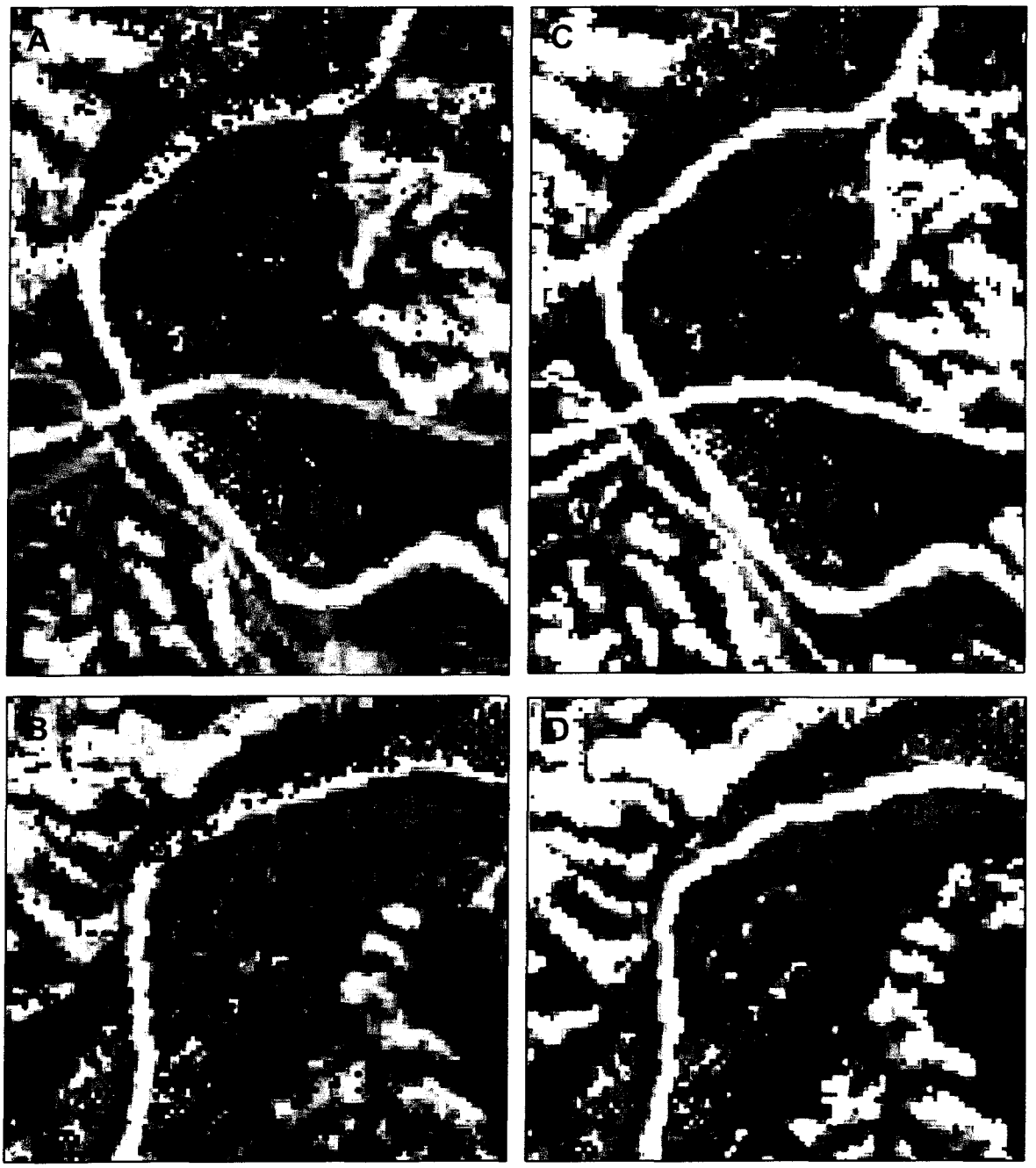

Figure 6.4. 1999 spurge fraction maps overlaid on 1999 and 2001 single band images to show registration offset between 1999 and 2001 imagery. 1999 level-sliced leafy spurge dominant pixels (red, orange, yellow, green); level-sliced non-dominant leafy spurge pixels shown in shades of magenta; in A and B the 1999 classification was overlaid on band 20 from 2001; in C and D the 1999 classification is overlaid on band 20 from 1999. A and B show the registration offset between 1999 and 2001, based on classified vegetation falling in the middle of Little Missouri River, the linear white feature (see arrows in A and B). The classification is aligned correctly in C and D. The shift averaged between 3 to 5 pixels, depending on location.

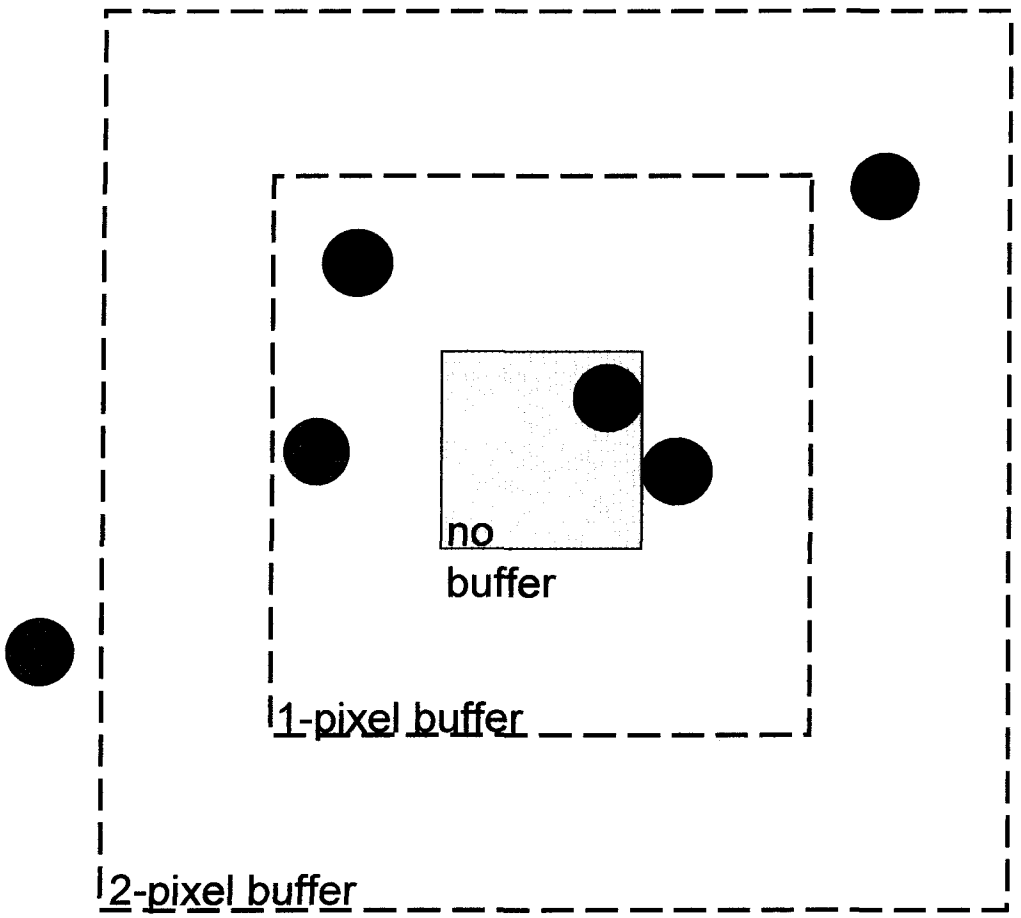

Figure 6.5. Theoretical affects of buffers on accuracy: smallest center blue square represents a single spurge-classified pixel, dotted lines represent 1- and 2-pixel width buffers; red are leafy spurge reference plot centroids; blue are non-spurge plot centroids. For the leafy spurge class, with no buffer, producer's accuracy is 25% (only 1 leafy spurge reference pixel was correctly classified as spurge), user's accuracy is 100%. With a 1-pixel buffer, producer's accuracy increased to 75% (3 of 4 spurge reference points coincide with the spurge-classified area); user's decreased to 75% (1 of the 4 spurge-classified reference points was not spurge and was incorrectly included). With a 2-pixel buffer producer's accuracy is 100% (all spurge reference points correctly classified as spurge); user's is 80% (of the 5 reference points classified as spurge, 1 was "other" vegetation that was incorrectly classified as spurge). Direction of shift varies throughout image, so buffer is applied equally in all directions surrounding classified pixels.

BUFFERED ACCURACY RESULTS: LEAFY SPURGE CLASS													
REFERENCE SOURCE AND BUFFER SIZE	DATE	MAPPING METHOD	TOTAL # REFERENCE PIXELS (LS)	PRODUCER'S ACCURACY		USER'S ACCURACY		OMISSION ERROR		COMISSION ERROR		OVERALL ACCURACY	
				#	%	#	%	#	%	#	%	#	%
PLOTS +0	2001	MTMF	207	38/207	18.4%	38/44	86.4%	169/207	81.6%	6/44	13.6%	169/360	46.9%
PLOTS +1	2001	MTMF	207	108/207	52.2%	108/130	83.1%	99/207	47..8%	22/130	16.9%	239/360	66.4%
PLOTS +2	2001	MTMF	207	138/207	66.7%	138/184	75.0%	69/207	33.3%	46/184	25.0%	245/360	68.1%
PLOTS +3	2001	MTMF	207	168/207	81.2%	168/237	70.9%	39/207	18.8%	69/237	29.1%	252/360	70.0%
PLOTS +4	2001	MTMF	207	184/207	88.9%	284/270	68.1%	23/207	11.1%	86/270	31.9%	251/360	69.7%
PLOTS +5	2001	MTMF	207	191/207	92.3%	191/293	65.2%	16/207	7.7%	102/293	34.8%	242/360	67.2%

BUFFERED ACCURACY RESULTS: N0N-LEAFY SPURGE VEGETATION CLASS													
REFERENCE SOURCE AND BUFFER SIZE	DATE	MAPPING METHOD	TOTAL # REFERENCE (Non-Sp)	PRODUCER'S ACCURACY		USER'S ACCURACY		OMISSION ERROR		COMISSION ERROR		OVERALL ACCURACY	
				#	%	#	%	#	%	#	%	#	%
PLOTS +0	2001	MTMF	153	131/153	85.6%	131/296	44.3%	22/153	14.4%	165/296	55.7%	169/360	46.9%
PLOTS +1	2001	MTMF	153	131/153	85.6%	131/230	57.0%	22/153	14.4%	99/230	40.0%	239/360	66.4%
PLOTS +2	2001	MTMF	153	107/153	69.9%	107/176	60.8%	46/153	30.1%	69/176	39.2%	245/360	68.1%
PLOTS +3	2001	MTMF	153	84/153	54.9%	84/123	68.3%	69/153	45.1%	39/123	31.7%	252/360	70.0%
PLOTS +4	2001	MTMF	153	67/153	43.8%	67/90	74.4%	86/153	56.2%	23/90	25.5%	251/360	69.7%
PLOTS +5	2001	MTMF	153	51/153	33.3%	51/67	76.1%	102/153	66.7%	16/67	23.9%	242/360	67.2%

Table 6.4. Change in accuracy with the addition of buffers from 1 through 5 pixels wide.

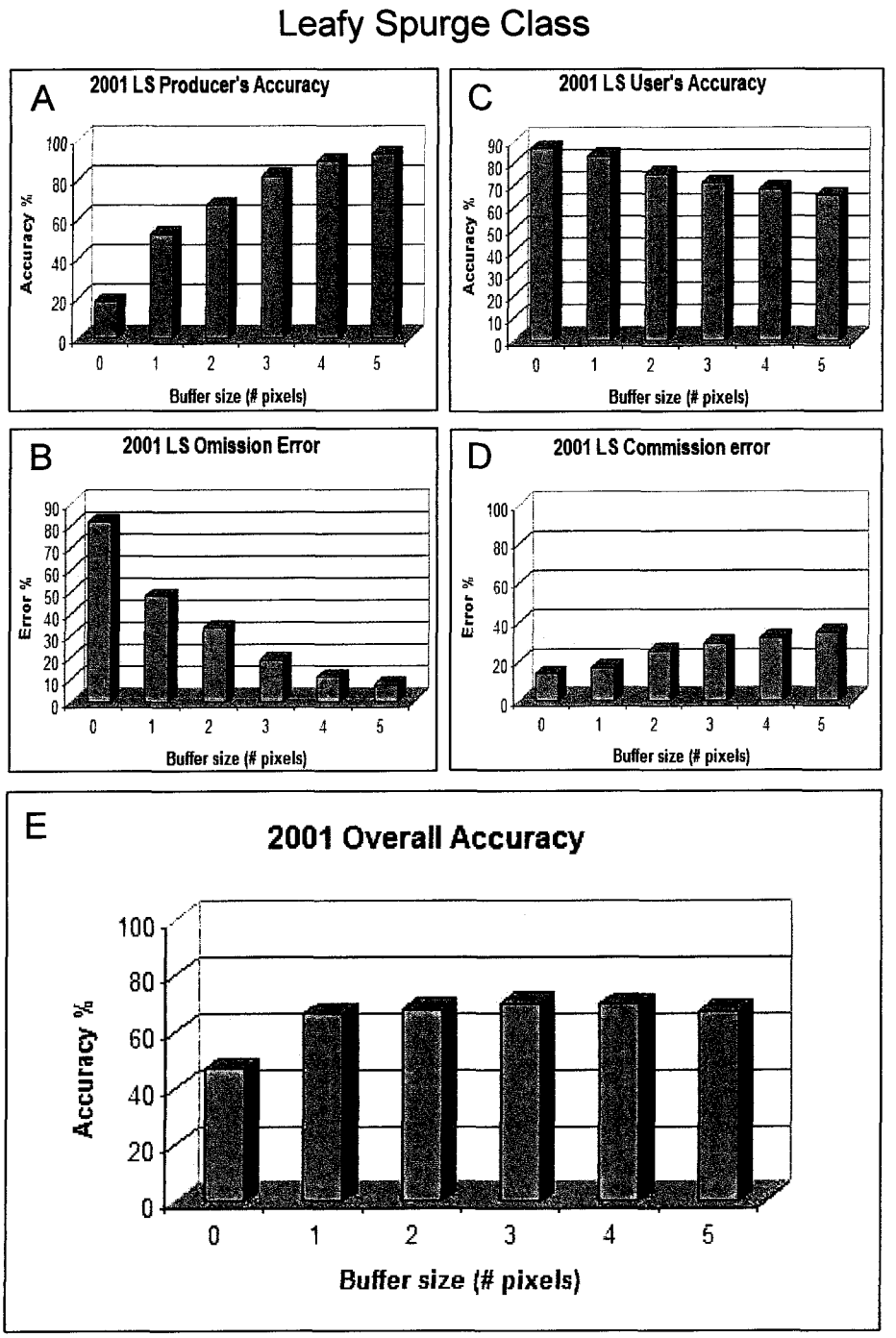

Figure 6.6. Change in accuracy and error for the leafy spurge class with increasingly larger buffers. There is a noticeable increase in producer's accuracy evident in A (and decrease in omission error, B) with increasing buffer size, while the corresponding change in user's accuracy in C (and commission error, D) is considerably less. The highest overall accuracy is with the 3-pixel buffer (E).

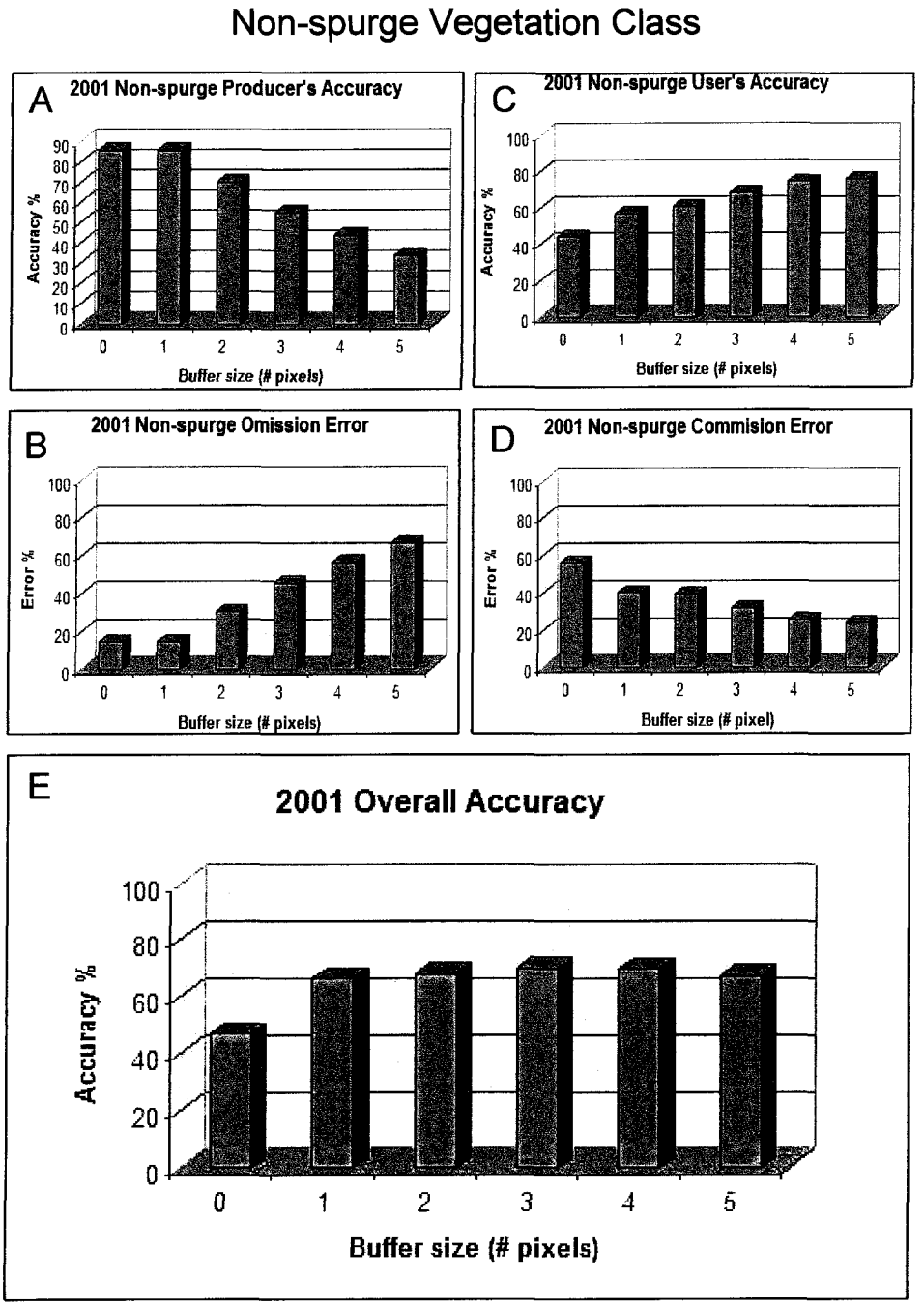

Figure 6.7. Change in accuracy and error for non-spurge vegetation class with increasingly larger buffers. The relative changes in producer's (A) and user's (C) accuracies (omission (B) and commission errors (D) are similar, i.e., as one increases, there is an approximately corresponding size decrease in the other, suggesting that the changes are related to increasing the area only, rather than poor registration.

highest overall accuracy for the 2001 data was obtained with the three-pixel buffer (Figures 6.6 E and 6.7 E). In this case, the overall accuracy increased from 47% with no buffer to a high of 70% with the three-pixel buffer. When the five-pixel buffer was applied, the overall accuracy decreased again to 66%. The greatest increment in overall accuracy occurred after the one-pixel wide buffer was applied to the classification. Overall accuracy increased from 47% to 66%, an increase of 19 percentage points with the addition of this single pixel-width buffer.

The producer's accuracy increased from 18% with no buffer to 92% when the five-pixel buffer was applied, a difference of 74 percentage points. The corresponding user's accuracy decreased 21 percentage points, from 86% to 65%. The greatest increment in producer's accuracy with a single increment in buffer size was seen after the one-pixel buffer was added: an increase of 33 percentage points, while the corresponding user's accuracy decreased only three percentage points.

Producer's accuracy for the non-spurge class was essentially identical for the non-buffered map after a one-pixel buffer was added, then decreased at a fairly constant rate with each subsequent buffer (Figure 6.7 A). The one-pixel buffer had the least effect on non-spurge producer's accuracy. User's accuracy for the non-spurge class, however, showed the most significant jump with a one-pixel buffer, then gradual decline and leveling off with the four- and five-pixel wide buffers.

Discussion. More significant than overall accuracy was the increase in *producer's* accuracy for spurge that was obtained with increasingly larger buffers (Figure 6.6 A). Producer's accuracy (and omission error) for the leafy spurge class is the measure of greatest concern to managers that are monitoring leafy spurge infestations. From a management perspective, it is more problematic to omit actual patches of leafy spurge from the map than to erroneously include other vegetation in the leafy spurge class on a map (i.e., it is critical to locate all infestations, at the expense of over-classifying some additional vegetation as spurge). If the increased producer's accuracy were *only* the result of classifying an expanded portion of the image as spurge, at the expense of the non-spurge vegetation class, the increase in producer's and decrease user's accuracies should be similar in magnitude. The order of magnitude difference in

the change between producer's and user's accuracies (33 versus 3 percentage points) with the addition of a one-pixel wide buffer suggests that many spurge reference points may have been omitted from the original classification that were in close proximity to classified areas, with possible misalignment due to registration errors, while at the same time, relatively few non-spurge reference points were included when the spurge-classified area was expanded by buffering.

To determine an optimum buffer size, the overall, producer's, and user's accuracies were compared for all buffered results. With the one-pixel buffer there was a significant improvement in producer's accuracy for spurge (see Figure 6.6 A versus 6.6 B), but little effect on the producer's accuracy of the non-spurge class (Figure 6.7 A, 6.7 B). There was little change in user's accuracy for the spurge class with the single pixel buffer, indicating that very minor additional non-spurge vegetation was incorrectly added to the map when the area mapped as spurge was expanded with the buffer (Figure 6.6 C). The largest increment in user's accuracy for the non-spurge class was also obtained with the one-pixel buffer, an indication that much of the spurge that had been incorrectly classified as non-spurge without the buffer was correctly excluded from the non-spurge class with the one-pixel buffer, leading to the higher user's accuracy for the non-spurge class. Stated another way, the largest decrease in commission error for the non-spurge class was with the one-pixel buffer (see Figure 6.7 C and D). With the addition of a two-pixel buffer, a more pronounced decrease in accuracy was seen for the non-spurge class (Figure 6.7 A). At the same time, accuracy also increased for spurge, though the *rate* of the improvement was lower than with the one-pixel buffer (Figure 6.6 A). The highest overall accuracy was calculated with the three-pixel buffer, which suggests that this may be the most appropriate size for a buffer, as it represents the best compromise between increased producer's and decreased user's accuracies for the two classes (Figure 6.6 E and Figure 6.7 E). Producer's accuracy for the spurge class increased dramatically with the five-pixel buffer (from 18% to 92%), an increase of 74 percentage points over the non-buffered results. The corresponding decrease in user's accuracy with the five-pixel buffer, from 86% to 65% (21 percentage points), was more moderate. For the non-spurge class, the decrease in producer's accuracy with zero to five-pixel wide buffers was 52 percentage points, while the corresponding

increase in user's accuracy was 32 percentage points. For the non-spurge class the magnitude of the relative increase and decrease were within a more similar range.

The marked differences in accuracy trends that were seen between the spurge and non-spurge classes with buffering suggest that it is unlikely that these are entirely the result of random differences due to simple increase in area labeled leafy spurge, at the expense of the non-spurge vegetation. The dramatic increase in producer's accuracy with buffering may be related to offsets in registration between the reference points and imagery. The buffer results support that the classification accuracy is higher than suggested by the initial, non-buffered, point-based accuracy assessments. Some increased accuracy is genuine improvement. In other cases, the improvement is the result of random processes (i.e., producer's accuracy may increase simply because a larger proportion of the image was "classified" as spurge with increased buffer size).

An ideal map for invasive species monitoring would display very low omission error, as well as low commission error for the weed class, although moderate commission error for the target class would be acceptable. The results from the five-pixel buffer indicate low omission error (8%) and moderate commission error (35%) for spurge, suggesting that the maps are approaching an ideal condition when boundaries are buffered to accommodate georeferencing problems, assuming that the spatial relaxation or coarsening represented by the buffering is acceptable. Because it shows the highest overall accuracy, however, the three-pixel buffer may be a good compromise between the increased producer's and decreased user's accuracies that were seen with increased buffer size.

Summary discussion of registration. The contribution to total error from classification versus location errors could not be quantitatively evaluated due to insufficient and/or inappropriate reference information, and the inability of the standard confusion matrix to distinguish between these. Location problems, however, are believed to be significant. In conjunction with "geographically restricted" point-based reference data, location errors are produced if registration is shifted at all (Carmel et al., 2001). Small patches are sensitive to the same registration and accuracy issues that are encountered when mapping edge pixels and heterogeneous landscapes in multi-spectral classifications.

Registration errors were considered a major factor influencing accuracy values. Because leafy spurge often occurs in small or fragmented patches, the accuracy of the maps was particularly sensitive to registration shifts when traditional point-based assessment methods were used. Spatial shifts between the map and reference data were often as large as or greater than the size of the entire classified patch, resulting in greater frequency of errors, and lower accuracy values for small patches.

Managers tasked with controlling noxious weeds are interested in determining how these infestations are changing over time, and which control measures have been most effective. Spatial analyses, and change detection in particular, can be seriously affected by poor registration (Chrisman, 1989). Because the magnitude of location errors was in some cases greater than the scale at which the different controls were applied in the park, the spatial analysis of the effectiveness of different treatments, based on change in fractional abundance, was abandoned. Fine scale, localized analysis of change and response to treatments will require the development of significantly better methods for registering the imagery.

MAPPING METHOD

MF versus MTMF. Although the main accuracy assessments focused on the infeasible-refined, MTMF maps, the accuracy was also calculated for the non-refined maps that were produced from the MF algorithm alone to test whether the standard confusion matrices and reference data were sensitive enough to differentiate between the accuracy of these two maps. Visual comparisons indicated that the MTMF successfully eliminated several large agricultural patches that were incorrectly identified as spurge with the MF. With the MTMF mapping method, results can be refined with infeasibility scores to produce, theoretically, more accurate maps (Research Systems, 2002).

Method. The standard two-class confusion matrices and the primary field plot (point) reference set were used to calculate accuracy both before (MF results) and after (MTMF results) the standardized infeasible threshold was applied to the classified image (see Chapter 5).

Results. Table 6.1 summarizes the producer's and user's accuracies for non-buffered spurge maps, as well as overall accuracies for the MF and MTMF mapping methods from both

1999 and 2001. For the 1999 maps, the overall accuracy with the MTMF (and infeasible refinement) *decreased* slightly (approximately one percentage point) relative to the MF results; the overall accuracies for the MF and MTMF were essentially identical for the 2001 data at 47%. Producer's accuracy for the 1999 spurge map decreased two percentage points, while user's accuracy remained stable at 100% with the MTMF refinement. The producer's accuracy for 2001 decreased one percentage point, while users accuracy increased by approximately one percentage point for the MTMF results.

Discussion. Theoretically, the results obtained with the MTMF refinement should be more accurate; however the accuracy results above suggest that the infeasible fine-tuning created more erroneous maps, or minimally, maps that were no better than those that were not refined. Qualitatively, however, the infeasible refinement improved classification problems that were noted in the non-refined (MF) maps. In the non-refined maps, large patches of spectrally similar, non-spurge vegetation within agricultural fields were erroneously mapped as spurge (circled areas in Figure 5.28 A and 5.28 C). These were eliminated after the MTMF refinement (Figure 5.28 B and 5.28D). Within only a single patch that was erroneously classified as spurge with the MF, approximately 1000 pixels were correctly removed from the spurge classification following the infeasible refinement (see arrows in Figure 5.28, A versus B). Several of these large, incorrectly classified patches occurred throughout the scene on the MF map, but were eliminated after the MTMF refinement. These improvements in the spurge map were *not* reflected in the calculated overall accuracy, or the user's accuracy for spurge. Conversely, no obvious known patches of leafy spurge were erroneously omitted after the infeasible refinement was applied. The conflicting results between the visual and quantitative assessments are difficult to explain, but suggest that the point reference data do not appear to be sensitive enough or complete enough to reflect the actual differences between the two maps.

Primary map versus combination primary/secondary map. The basic accuracy assessment for all *primary* leafy spurge maps indicated high omission for spurge. The modified method described in Chapter 5 that was used to produce the primary maps will under-estimate the weed because spurge was only included on the map when it represented the highest fraction

material within a given pixel. Spurge that occurred as a minor fraction of a pixel would be excluded from the map. The omission error would be anomalously high under these conditions, resulting in lower overall accuracy.

Methods. To determine whether the high omission error could be reduced without creating new, significant commission errors, the primary map was combined with the secondary map (see Chapter 5) to include additional minor spurge infestations. The accuracy was calculated for the combined primary/secondary map without buffering, and again after applying a three-pixel wide buffer around classified spurge. The identical set of primary reference points and the two-class confusion matrix were used for the re-calculated accuracy.

Results. The accuracies of the primary, and the primary/secondary combined maps from 1999 are presented in Table 6.5. Without buffering, the overall accuracy of the combined (primary and secondary) leafy spurge map improved to 72% (up from 39% for the primary 1999 map). Leafy spurge user's accuracy decreased moderately, from 100% to 90%, while the producer's accuracy increased from 26% to 74%. When the three-pixel buffer was applied to accommodate poor registration, 81% overall accuracy was obtained. Spurge producer's accuracy climbed to 98%, and user's accuracy fell to 82%. In the combined map, both buffered and non-buffered, the producer's and user's accuracies for the non-spurge class were low, however (65% and 36% without buffering, and 8% and 50% with the three-pixel buffer). Although the producer's and user's accuracies of the non-spurge class were low with the three-pixel buffer, this did not substantially affect the overall accuracy because non-spurge reference data represented less than 20% of the total number of reference points collected in 1999 (i.e., although much of the non-spurge was erroneously classified as spurge, this was not reflected in the overall accuracy).

Discussion. Although omission error for spurge improved considerably (down to 26% from 74%), it remained high enough to suggest that a significant amount of leafy spurge was still omitted from the combined map. This indicated that other factors affected the producer's accuracy (and omission error) in addition to the expected under-estimation of spurge from the

A

LEAFY SPURGE CLASS: ACCURACY/ERROR FOR DOMINANT ONLY VS. DOMINANT/NON-DOMINANT LS MAPS COMBINED (from 1999)									
	COMM #	COMM %	OMISS #	OMISS %	PROD AC #	PROD AC %	USER AC #	USER AC %	OVERALL AC
LS Primary	0/118	0%	329/447	73.60%	118/447	26.40%	118/118	100%	231/549 38.9%
LS Combined	37/365	10.00%	117/445	26%	328/445	74.00%	328/365	90.00%	393/547 72%

B

LEAFY SPURGE CLASS: ACCURACY/ERROR FOR DOMINANT ONLY VS. DOMINANT/NON-DOMINANT LS MAPS COMBINED (from 1999)									
	COMM #	COMM %	OMISS #	OMISS %	PROD AC #	PROD AC %	USER AC #	USER AC %	OVERALL AC
LS Combo +3 buf	94/531	18.00%	8/445	2%	437/445	98.00%	437/531	82.00%	445/547 81%

Table 6.5. Difference in accuracy for primary map (spurge-dominant only) and combined primary and secondary map from 1999. Non-buffered accuracy results are presented in A; results with a 3-pixel wide buffer applied are shown in B for the combined, primary/secondary map.

modified MTMF method. Registration was believed to be a factor, and the improvement in producer's accuracy (to 98%) with a three-pixel buffer supports this hypothesis.

The improvement in omission error without the buffer was significant, however, and suggests that the combination maps may be the best representation of all spurge infestations, low through high density. A drawback of the combined map, however, is the re-introduction of user-defined thresholds that were required to produce the secondary maps. This would re-introduce problems with consistent map production and comparisons over time unless a standardized method is established for defining the low MF score threshold for including material as "spurge" on the secondary map. In addition, a visual evaluation of the combined maps from 2001 indicates some over-classification of spurge (Figure 6.8). Nevertheless, providing both the primary and secondary maps will reduce the high omission error that persisted when the modified mapping method was used (Chapter 5), while still supplying the primary map to indicate the most prominent or densest infestations. In conjunction with the secondary map that included the lower density infestations, the combined map will allow land managers to make more informed decisions regarding where and how to focus control efforts and resources.

ALTERNATIVE REFERENCE SOURCES

The 3 m x 5 m plot centroids that were used for the previous assessments were collected for an unrelated leafy spurge study and were not intended to be used specifically for validation of remote sensing classifications. These points were not ideal for validating maps produced with 17 m resolution imagery.

Primary reference points were collected using stratified random sampling, and were sufficiently high in number for a valid accuracy assessment. The plot size was small (3 m x 5 m), however, relative to the spatial resolution of the AVIRIS imagery (17 m x 17 m). A plot with 100% leafy spurge cover, for example, might fill only a small portion of a single AVIRIS pixel. Plots were labeled positive for spurge if the plot contained any spurge at all. Because these "spurge" reference points could represent areas with very low density and/or very small patches they could fall below the detection limit of the AVIRIS sensor for this species, which could contribute to the apparent high omission rate seen with the basic accuracy assessment. In addition, some of the

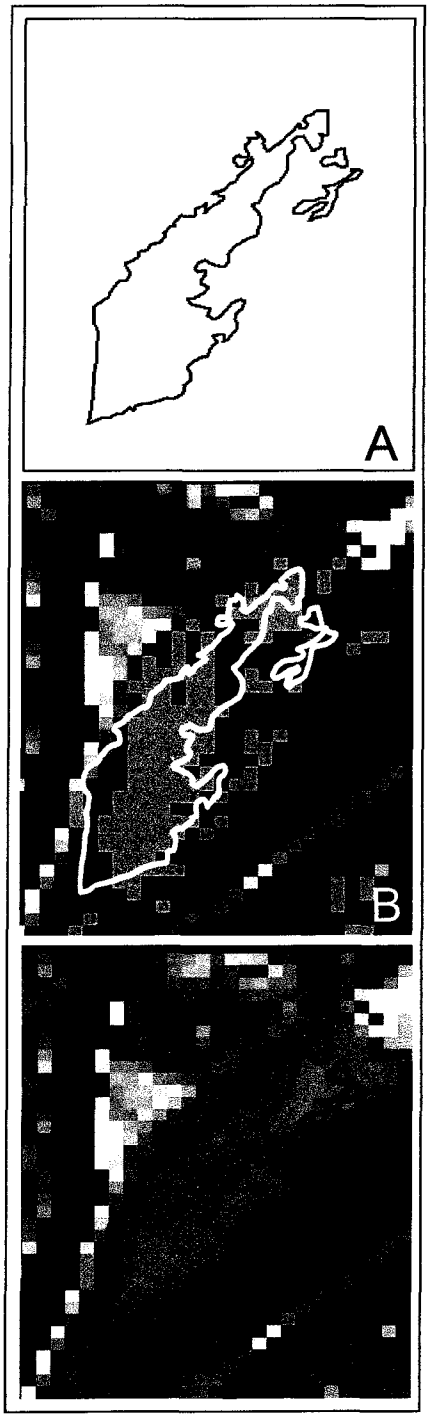

Figure 6.8. Primary, and primary/secondary combined maps with overlaid reference polygons. Primary shown in yellow in A, primary and secondary are green and magenta, respectively, in B, and combined map is green in C. Acreage of primary map and overlaid polygon are approximately equal (A); however, the combination map has over-classified spurge as mapped spurge extent is significantly greater than the associated field polygon (C). Classified spurge and spurge polygons are overlaid on band 20 (558 nm) image in B and C.

field plots were located beneath tree canopy, and the under-story vegetation within these plots may not have been detected by the sensor. The unmixing techniques that were used for mapping would need to be extremely sensitive to detect very low density infestations for these reference points to be an appropriate validation source for the spurge maps. This would also require excellent registration between the imagery and reference data; however, the registration was questionable for the THRO data sets. In addition, because the plot data was converted to points (the geographic coordinates of the plot centroid), this reference set was particularly sensitive to registration problems.

The plot reference points were useful nonetheless to establish a baseline accuracy against which other accuracy comparisons could be made, including the effect of different sources of reference data. To evaluate whether accuracy was significantly different with alternative sources of reference data and to determine the best source from the available reference data for validating hyperspectral spurge maps, the basic accuracy results from the 1999 and 2001 spurge maps were compared to accuracy values derived using: 1) "points" derived from the field polygons that were collected in 2001; and 2) point-based plot information collected in 2003. These alternate reference sources were used to determine whether the apparent discrepancy between qualitative and quantitative accuracy was related to inappropriate or poor-quality reference data.

Alternative reference sources: polygons converted to raster images. *Methods.* Individual pixels occurring within overlaid reference polygons were converted to individual reference points to use in the error matrix. To produce these points from the field polygons, the boundaries of vegetation polygons were used to generate coverages and shapefiles in ArcINFO. These were imported into ENVI, converted to ENVI-format vector files, and then converted to 17 m grids. Individual regions of interest (ROIs) were created for each grid from within the boundary of the original spurge polygon. Each ROI was then used as a reference location for spurge in an error matrix for the accuracy assessment. The conversion of polygons to raster ROIs produced 217 leafy spurge and 44 non-spurge vegetation reference "points" against which the spurge-classified pixels were compared. The number of pixels that were classified as non-

spurge vegetation that fell within the spurge polygon boundaries was tabulated as well, to calculate omission error for the leafy spurge class.

Two accuracy analyses were completed using the polygon "points". In the first, the points from all reference polygons were combined into one set that was used in an error matrix to calculate a single producer's accuracy value for all spurge, as well as a single value for all non-spurge polygons combined. A second set of accuracy assessments was calculated with the same polygon-to-points method, however, an independent assessment was run for *each* individual polygon "point" set. These producer's accuracy values were used in a regression analysis to determine the relationship between patch size (from both the field polygon and the corresponding classified patches) and producer's accuracy, as well as the relationship between patch density and producer's accuracy. The relationship between patch density and size was evaluated also. Spatial correlation and non-ideal sampling methods are likely problematic with the above methods, but were not specifically addressed in this study.

Results: Polygons to raster "points", single assessment with all polygons combined. The accuracy values obtained for the 2001 classification with the single assessment using all polygon points combined were substantially higher than those obtained using the field plot centroids (Table 6.6). The overall accuracy increased from 47% when the plot centroids were used, to 64% with the polygon points. The producer's accuracy for the spurge class was 56%, up from 18% with the field plot centroid reference data. There were no cases in which classified spurge occurred within non-spurge reference polygons, therefore the commission error (with respect to the leafy spurge class only) was 0% for the non-spurge class.

Discussion: Polygons to raster "points", single assessment with all polygons combined. The difference in overall accuracy of 17 percentage points between the conventional random points and the polygon raster "points" indicates that the source of reference data and the method used to apply it in an assessment can significantly alter the apparent accuracy of a classification. Which source and method was most appropriate for this data was unclear, however. The size of the field polygons was more appropriate for the scale of the THRO AVIRIS imagery than the centroid points from small field plots. In addition, the polygons enclosed relatively homogeneous

LEAFY SPURGE CLASS ACCURACY/ERROR: comparison of plot results with polygon results										
REFERENCE SOURCE	DATE	MAPPING METHOD	TOTAL # REFERENCE	TOTAL LS REFERENCE	PRODUCER'S ACCURACY	USER'S ACCURACY	OMISSION ERROR	COMISSION ERROR	OVERALL ACCURACY	KAPPA COEF
					# %	# %	# %	# %	# %	
PLOTS	2001	MF	360	207	40/207 19.32%	40/47 85.1%	167/207 80.7%	7/47 14.9%	170/360 47.2%	0.089
POLYGONS	2001	MF	261	217	130/217 59.9%	130/130 100%	87/217 40.1%	0/130 0.0%	174/261 66.7%	0.337
PLOTS	2001	MTMF	360	207	38/207 18.36%	38/44 86.4%	169/207 81.6%	6/44 13.6%	169/360 46.9%	0.086
POLYGONS	2001	MTMF	261	217	122/217 56.2%	122/122 100%	95/217 43.8%	0/122 0.0%	166/261 63.6%	0.304

Table 6.6. Comparison of accuracy results with alternate reference sources: points from 3x5 m plot centroids vs. points from field polygons

patches of vegetation or vegetation mixtures, while the field plots were randomly located points around which the plot was constructed, and, while all vegetation within the plots was documented, the distribution was not necessarily homogeneous throughout the plot. The combination of scale and homogeneity of the polygons removed some of the complexity that was encountered when the small, heterogeneous plots were used to validate classifications based on 17 m-resolution imagery. The number of polygons was low, however (10 spurge and 12 non-spurge), and the size of the individual polygons varied. The reliability of the results would improve if additional polygons were available, and if a well-designed sampling procedure were used for selecting the polygons. Imprecise registration between polygons and classified patches was also problematic, similar to the registration problems encountered with the plot centroids.

An additional drawback of the polygon points was that only the accuracy of the classified vegetation that occurred *within* the boundary of the sampled reference polygon could be assessed (i.e., no formal reference data were collected outside the polygon boundaries). Figure 6.9 indicates the pixels that were considered correct, incorrect, and unknown (therefore "not used") for the spurge class. Areas outside the boundaries of a specific spurge polygon were often, but not always another vegetation type, and included: non-spurge vegetation or mixtures, spurge of a different density, or soil, rock, litter, wood, or mixtures of these materials. As a result, only a partial error matrix could be calculated because only producer's accuracy (and omission error) for the spurge class could be determined based on the corresponding field polygon. This precluded calculation of commission error for leafy spurge with the polygon points. Figure 6.10 shows the relationship between each spurge field polygon and the corresponding image-mapped spurge.

For the non-spurge reference polygons, the number of spurge pixels within the non-spurge polygons was also tabulated. The non-leafy spurge polygons were used to evaluate only the portion of the commission error for the non-spurge class that was contributed by leafy spurge (i.e., any areas where leafy spurge was erroneously classified as another vegetation class, based on the occurrence of classified spurge within non-spurge reference polygons). The non-spurge polygons defined homogeneous patches of several different species that were located in the field;

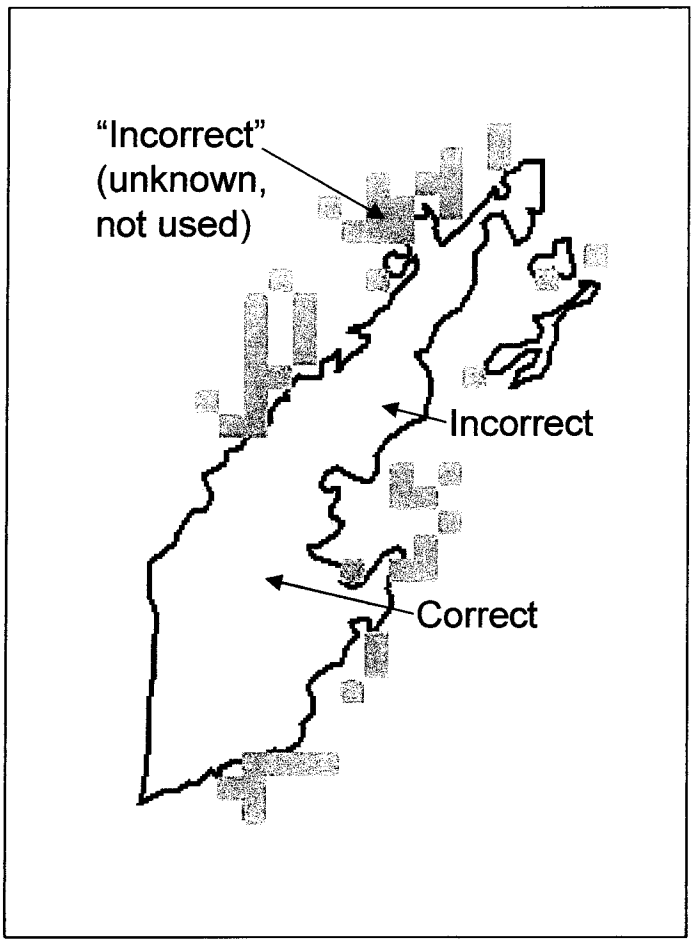

Figure 6.9. Pixels within boundaries of overlaid polygons were converted to "points" for accuracy assessment. Yellow pixels indicate intersection between classified and reference polygon; white pixels within the polygon boundary were incorrectly omitted from the classification; green pixels were classified as spurge but occurred outside the perimeter of the polygon; these could not be used to calculate commission error because vegetation outside the polygon was not characterized in the field, and may have contained spurge of a different density class, a different vegetation class or mixture, or other non-vegetative material, therefore the actual identity of vegetation within classified pixels outside the perimeter of the polygons could not be determined.

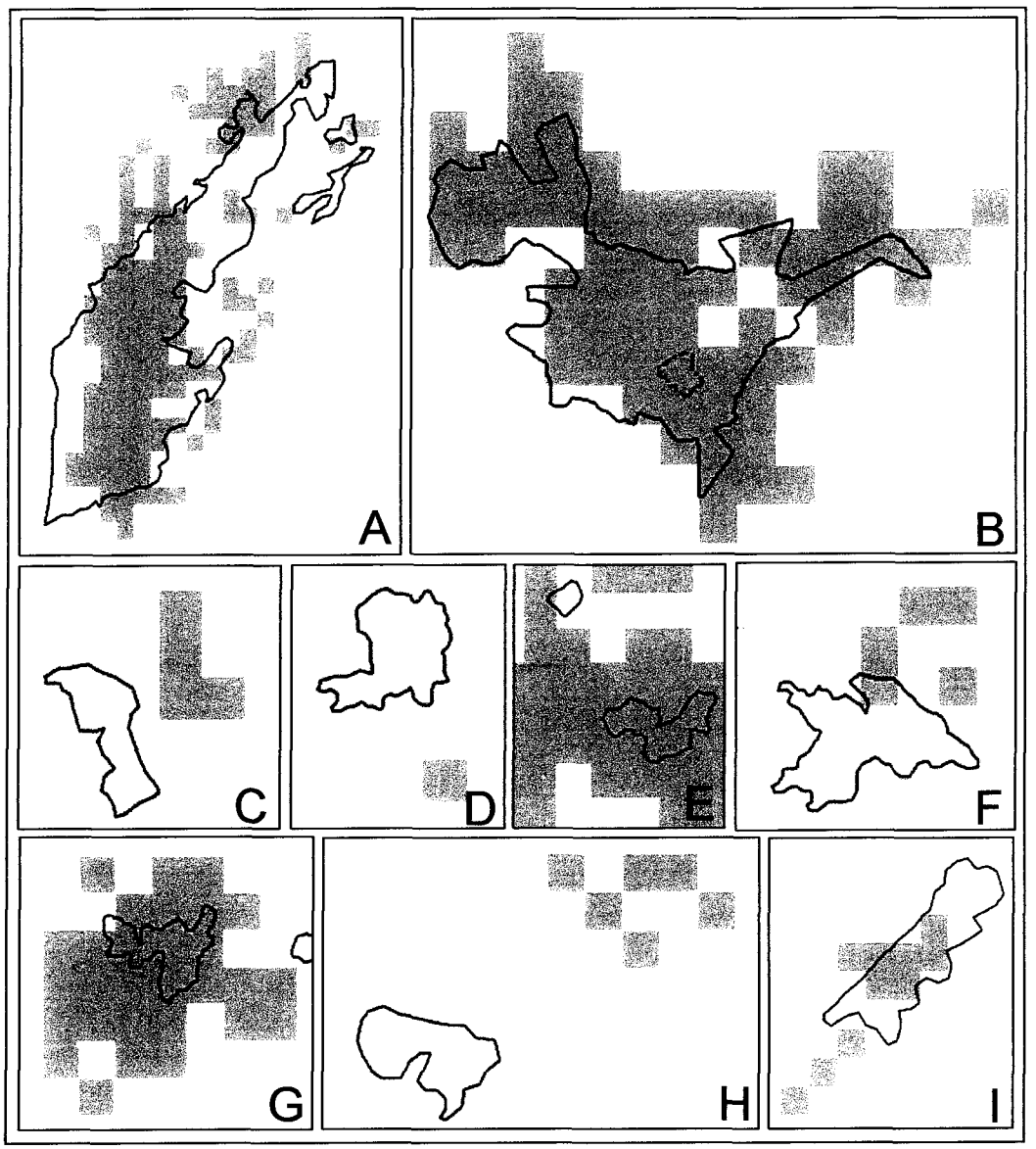

Figure 6.10. Leafy spurge reference polygons, outlined in black, overlaid on subsets from the 2001 leafy spurge map (spurge-classified pixels in green; areas classified as non-spurge vegetation are white). Scale is variable; single pixel represents 17m² in each frame. Correspondence between reference and classified data is variable (i.e., B vs. H). Polygons used for error matrix-based accuracy assessments gave significantly different results for individual polygons, (i.e., spurge producer's accuracy is 100% for the large polygon in E; 0% for H). Size and shape of classified patches and corresponding polygons indicate that maps are more accurate than formal assessments suggest, assuming allowance is made for spatial shifts between reference data and imagery.

however, the non-spurge vegetation on the classified map was not identified to species, but clumped into a general, non-spurge class. As a result, the producer's accuracy (and omission error) for the non-spurge polygons could not be calculated beyond whether correctly classified as "non-spurge". Non-spurge polygons overlaid on the spurge map indicated that no classified spurge occurred within, or in the vicinity of, the non-spurge polygons.

Results: Polygons to raster "points": individual polygon accuracy analyses. Table 6.7 includes the producer's accuracy for the individual leafy spurge polygons, as well as size and spurge density of each polygon. When producer's accuracy values were calculated individually for each spurge polygon, the results varied widely (from 0% to 94%).

Discussion: Polygons to raster "points": individual polygon accuracy analyses. The wide range in producer's accuracy is likely due to a combination of registration problems and the size and density of the polygons. This was suggested by the results of a regression of size on producer's accuracy (Figure 6.11) that indicated a weak positive correlation ($r^2 = 0.275$) between classified patch size and producer's accuracy, but no correlation between the size of the field polygon and accuracy ($r^2 = 0.039$). Patch densities and producer's accuracy were more strongly correlated ($r^2 = 0.551$, Figure 6.12). Figure 6.13 shows example field photographs, with mean spurge plant density for the patch and relative size indicated along with corresponding producer's accuracy of the patch.

If registration error were the dominant factor affecting reduced accuracy, a greater effect (i.e., lower accuracy) would be expected for smaller polygons. This appeared to be the case based on the values in Table 6.7, but was not strongly indicated by the regressions of classified and polygon patch sizes on producer's accuracy. If classification error dominated, a correlation between density and accuracy would be expected, and a modest positive correlation was indicated. Density and size are not independent of one another, however. Figure 6.14 shows the results of the regression of classified patch size on density ($r^2 = 0.468$) and polygon size on density ($r^2 = 0.272$), indicating low to moderate correlation between size and density. Because of this it is difficult to isolate the relative effects of registration and classification errors based on the correlations between size vs. producer's accuracy and density vs. producer's accuracy.

Polygon name	LS density	Area: field poly	Area: classified	Producer's accuracy
section 27 north	95%	36 pix; 1.028 ha	63 pix; 1.799 ha	83%
campground	up to 95%; patchy	143 pix; 4.084 ha	140 pix; 3.999 ha	59%
sunglass	50-95%; 85% overall	4 pix; 0.1142 ha	30 pix; 0.8568 ha	94%
no man's: large	up to 80%; 40% overall; patchy	4 pix; 0.1142 ha	21 pix; 0.5998 ha	15%
river, north hwy	55%; patchy	15 pix; 0.4284 ha	10 pix; 0.2856 ha	37%
canyon mouth	35%; patchy	9 pix; 0.2470 ha	5 pix; 0.1428 ha	11%
section 27 south	35%	5 pix; 0.1428 ha	4 pix; 0.1142 ha	0%
5 m circle	30%	1 pix; 0.0286 ha	1pix; 0.0286 ha	0%
no man's: small	30%	4 pix; 0.1142 ha	1pix; 0.0286 ha	0%
river by fence	25%	7 pix; 0.1999 ha	6 pix; 0.1714 ha	0%

Table 6.7. Accuracy values for individual polygons (polygon-to-points reference set).

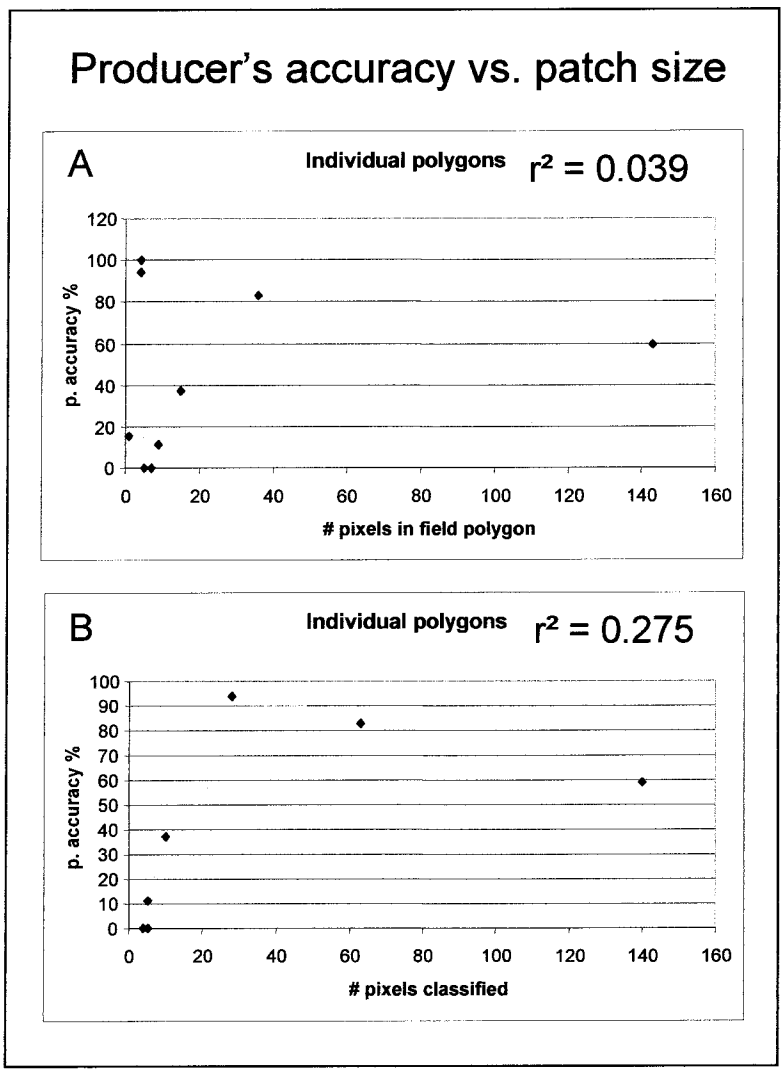

Figure 6.11. Correlation between accuracy and patch size (field polygons and classified spurge patches). Producer's accuracy shows no correlation to the size of the field polygons (A); there is a low positive correlation between producer's accuracy and the size of the classified patches (B).

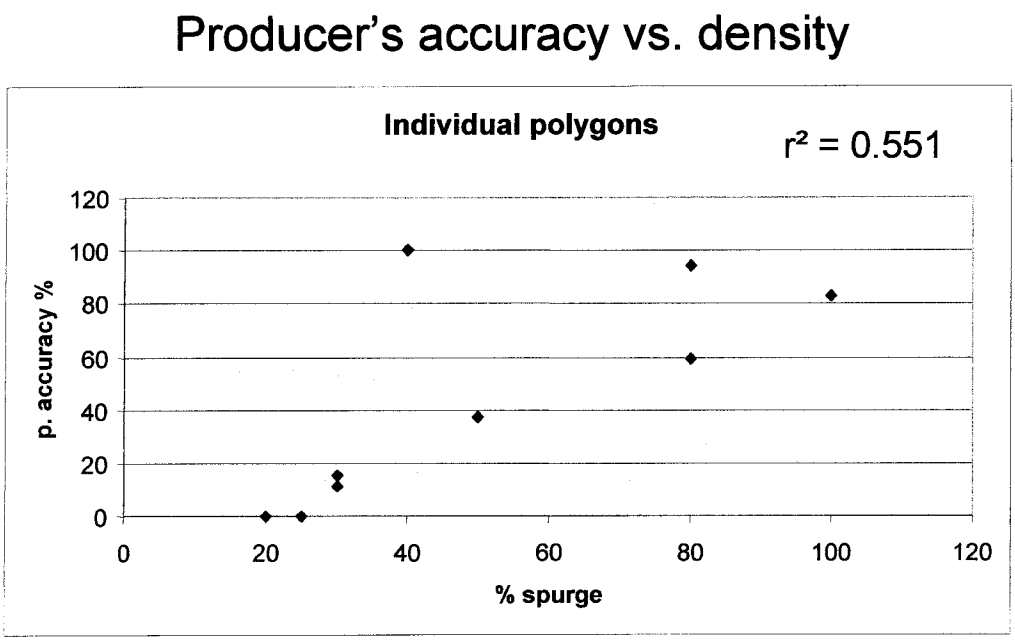

Figure 6.12. Correlation between field-measured % spurge (plant) density and producer's accuracy; overall accuracy could not be produced for the polygons. Moderate correlation is seen between density and producer's accuracy, with $r^2 = 0.551$.

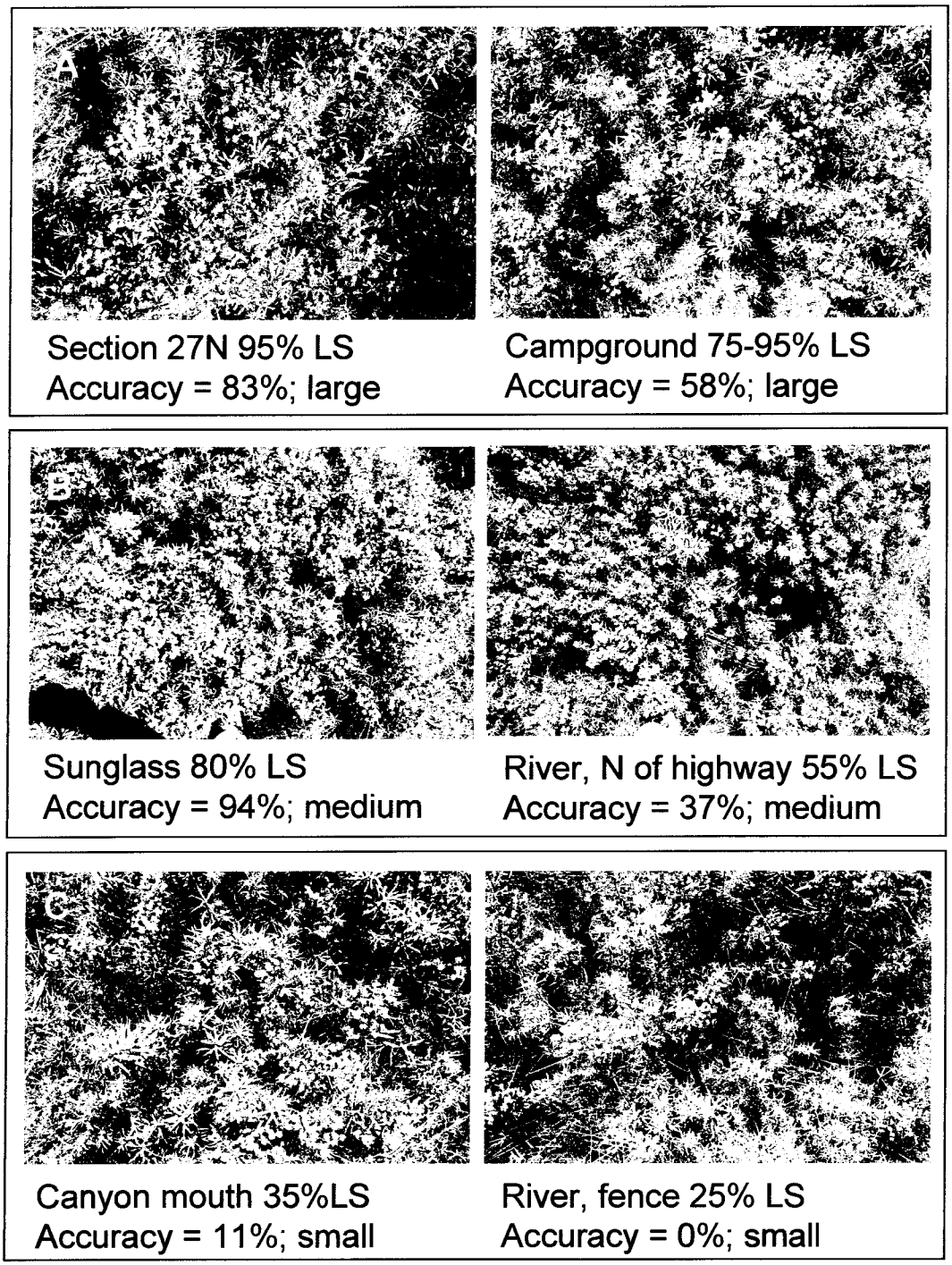

Figure 6.13. Polygon density and size vs. accuracy. Classification accuracy is roughly correlated with patch density and size: high density, large polygons (>30 pixels) in A, moderate density, intermediate-size polygons (10-30 pixels) in B, low density, small (<10 pixels) in C. Accuracy generally decreased with decreased density and size. Producer's accuracies only are reported.

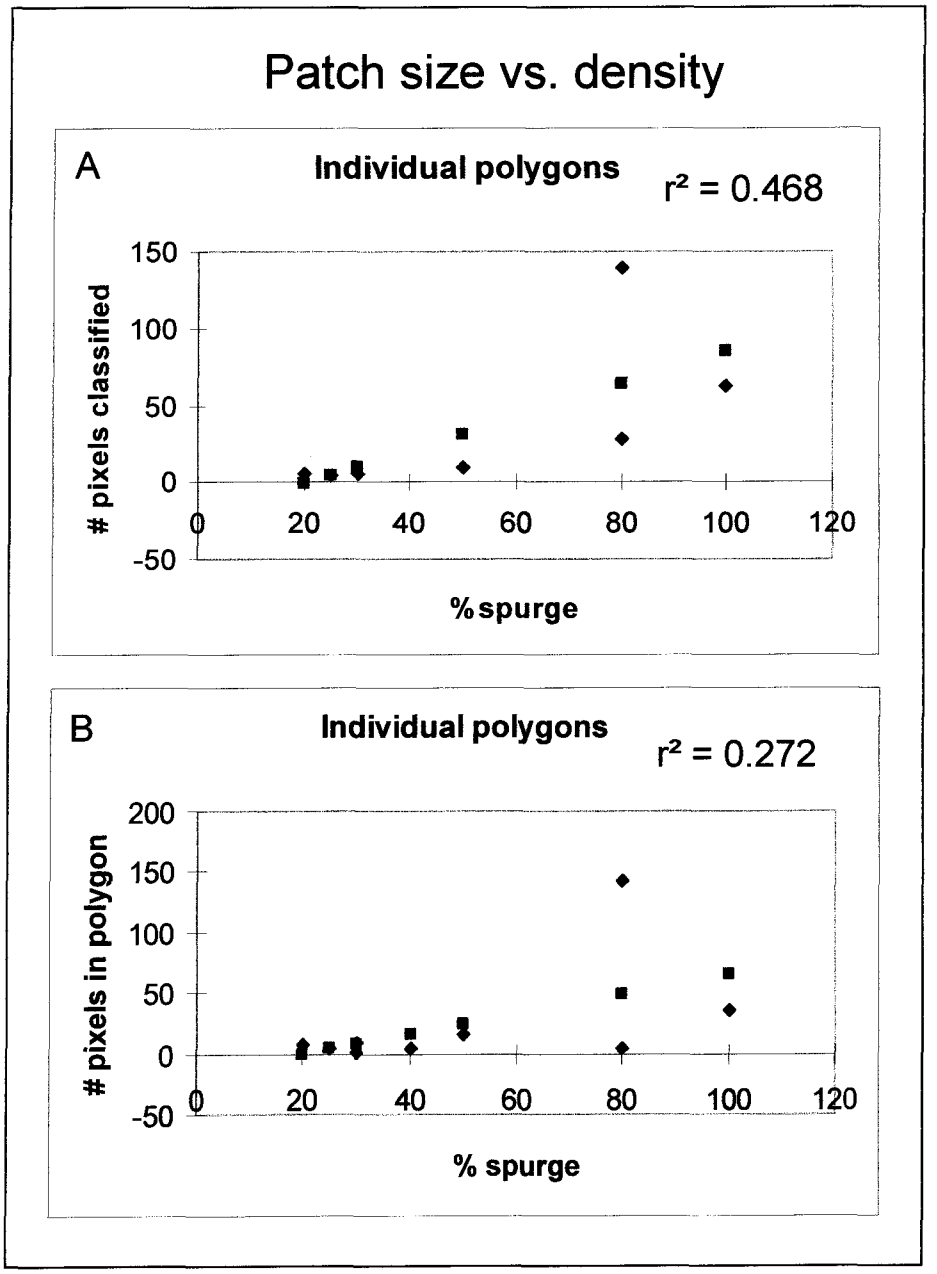

Figure 6.14. Correlation between patch size and field-measured density. Moderate correlation is indicated between classified patch size and density (A); low correlation is indicated between polygon size and spurge density (B).

The calculated producer's accuracies were generally lower as the size and density of patches decreased. These relationships could be used as a rough guide to selecting the most appropriate size for polygon reference data. Ideally, however, all densities should be represented in the reference set.

2003 alternate reference points. *Methods.* Accuracy of the 2001 spurge map was calculated using a set of reference points for spurge/no spurge that was collected in 2003. This reference data was used in the two-class error matrix to compare accuracy values obtained with the point reference data collected in 2001 and 2003 in order to test whether a data set collected specifically for validation of the remote imagery, with a better spatial sampling design, produced higher accuracy values. The accuracy assessments were run on the identical map, with the reference data the only variable between the two assessments.

Results. Using the reference points collected in 2003 to validate 2001 maps yielded low accuracy results. Overall and producer's accuracies were very low (19% and 17% respectively). User's accuracy for the spurge class, however, was 99%. Table 6.8 indicates the accuracies and errors for both vegetation classes that were obtained with the 2001 and 2003 reference points. The producer's accuracies from both 2001 and 2003 data are nearly identical for the spurge class (17% and 18%), and the user's accuracies differ by 13 percentage points (86% vs. 99%); however, the overall accuracy was considerably lower when the 2003 reference set was used (19% vs. 47% with 2001 data, a difference of 28 percentage points).

Discussion. The very low producer's accuracy obtained using both the 2001 and 2003 reference data suggests that a significant proportion of the leafy spurge was not included on the map. High user's accuracy, however, indicates that only a very small fraction of the non-spurge reference points were erroneously classified as spurge. The substantial difference in overall accuracy obtained with the two reference sets reflects the impact of a much higher commission error (98%) for the non-leafy spurge class with the 2003 points, versus 56% with 2001 points. This is the result of the unequal distribution of reference points that were collected for the two classes in 2003. In 2003, 798 spurge points were collected, but only 14 non-spurge, while in 2001, 201 spurge and 153 non-spurge points were collected. Direct comparison between the two

2001 Accuracy with 2001 reference points

		COMM #	COMM %	OMISS #	OMISS %	PROD ACCUR #	PROD ACCUR %	USER ACCUR #	USER ACCUR %	OVERALL ACCUR %
	NL	165/296	55.7	22/153	14.4	131/153	85.6	131/296	44.3	196/360
	L	6/44_	13.6	169/207	81.6	38/207	18.4	38/44	86.4	46.9%

2001 Accuracy with 2003 reference points

		COMM #	COMM %	OMISS #	OMISS %	PROD ACCUR #	PROD ACCUR %	USER ACCUR #	USER ACCUR %	OVERALL ACCUR %
	NL	661/674	98.1	ONE/14	7.14	13 /14	92.9	13/674	1.93	150/812
	L	1/138	0.72	661/798	82.8	137/798	17.2	137/138	99.27	18.5%

Table 6.8. Alternate reference points: accuracy of the 2001 THRO spurge map using original plot centroids collected in 2001 vs. plot centroids from 2003. L = leafy spurge class; NL = non-spurge vegetation class. Larger plots in 2003 were more appropriate for validation of high altitude AVIRIS data.

reference sets is difficult because of this skewed distribution of points between dates. The sampling strategy for the 2003 points was better in terms of the size of the patches represented by each point or centroid, however, the under-sampled non-spurge class biased the outcome of the accuracy assessment. The 2003 data were also collected 2 years after the imagery, and were less reliable for validating 2001 vegetation classifications due to changes within a dynamic ecosystem, particularly considering the extensive spurge control efforts in the area, in addition to natural variation over time.

Because of the divergent sampling methods that were used to collect the different reference data, *direct* comparison of the quality of one data set to another was difficult because the differences reflected the combined effects of reference source *and* sampling strategy. The three reference data sets that were compared each had advantages and disadvantages for validating the spurge maps, and none of these was considered optimal for validating the THRO maps. Each provides somewhat different, but complementary and useful information: polygons provide reference for specific spurge density classes; the points were collected with statistically valid sampling methods, including stratification and random location; while the grids provided close to a complete representation of spurge of all density classes for the areas in which they were collected.

These comparisons highlight the variable accuracy that can be obtained and the difficulty with interpretation that was encountered with the spurge maps produced in this study. The results underscore the need for a systematic, consistent approach to the collection of reference information and the validation of vegetation maps produced from imaging spectroscopy.

CONSISTENCY OF MAPS PRODUCED FROM MULTIPLE IMAGES COLLECTED OVER IDENTICAL AREAS ON THE GROUND

The consistency of mapping methods and the comparability of maps over time and space is critical for accurate temporal monitoring. To test the quality and consistency of the maps produced with the modified MTMF method (Chapter 5), the accuracy of maps that were independently produced using data collected over identical areas on the ground, but from different overlapping flight lines, was compared. This allowed the same area to be mapped using

different data sets; however, because the data was collected on the same date, at nearly the same time, many sources of variance (i.e., temporal, phenological, or environmental variation) were eliminated. This allowed the consistency of the maps to be directly compared. If the mapping method is consistent, the maps and the corresponding accuracy values should be identical or nearly so.

The same standard confusion matrices described previously were used to evaluate the consistency of maps that were produced with the modified methods presented in Chapter 5. Two regions from the 2001 AVIRIS data collection were associated with a sufficient number of reference points to formally calculate accuracy. Two intersecting subsets from each area were created from the thematic vegetation maps, which then were converted to the binary presence/absence format prior to calculating the accuracy. Accuracy assessments were run on each subset, using the identical set of reference points for each subset in a pair.

The results of accuracy assessments for the identical regions mapped from different flight lines are outlined in Table 6.9. For the overlap between flight lines 1 and 3 (see Figure 6.15 A), overall accuracies were 54% and 52%, respectively, a difference of two percentage points. The same difference (55% and 57%) was seen between overlapping areas of flight lines 3 and 4 (Figure 6.15 B). Producer's accuracy (and omission error) varied by four percentage points between flight lines 1 and 3, and by two percentage points between the identical areas of 3 and 4. Commission error was identical between flight lines 1 and 3 at 0%, but differed by 19 percentage points between 3 and 4 (0% vs. 19%).

With the exception of the higher commission error for the leafy spurge class from flight line 3 east, all other accuracy values for spurge compared favorably between the flight lines, differing by zero to four percentage points. Although the accuracy values were low, they were *stable* from one flight line to the next. Because the overall accuracies were consistent, they indicate that the processing strategies that were developed in this study (see Chapter 5) should be consistent, reproducible, and appropriate for applied monitoring and change analysis. In addition, these values were generally consistent even though the extremes of view angle

AREA 1	Leafy spurge				Non-spurge		
	fl 1 east	fl 3 west	**dif**		fl 1 east	fl 3 west	**dif**
omission error %	77	81	**4**		0	0	**0**
producer's accuracy %	23	19	**4**		100	100	**0**
comission error %	0	0	**0**		53	54	**1**
user's accuracy %	100	100	**0**		47	46	**1**
	fl 1 east	fl 3 west	**dif**				
overall accuracy %	54	52	**2**				

AREA 2	Leafy spurge				Non-spurge		
	fl 3 east	fl 4 west	**dif**		fl 3 east	fl 4 west	**dif**
omission error %	61	63	**2**		16	0	**16**
producer's accuracy %	39	37	**2**		84	100	**16**
comission error %	19	0	**19**		56	57	**1**
user's accuracy %	81	100	**19**		44	43	**1**
	fl 3 east	fl 4 west	**dif**				
overall accuracy %	55	57	**2**				

Table 6.9. Accuracy results from identical areas mapped from different flightlines. A: the overlap between the eastern edge of flightline 1 and the western edge of flightline 3. B: overlapping region of flightlines 3 and 4. Accuracy and error values are generally similar for the identical areas for both cases.

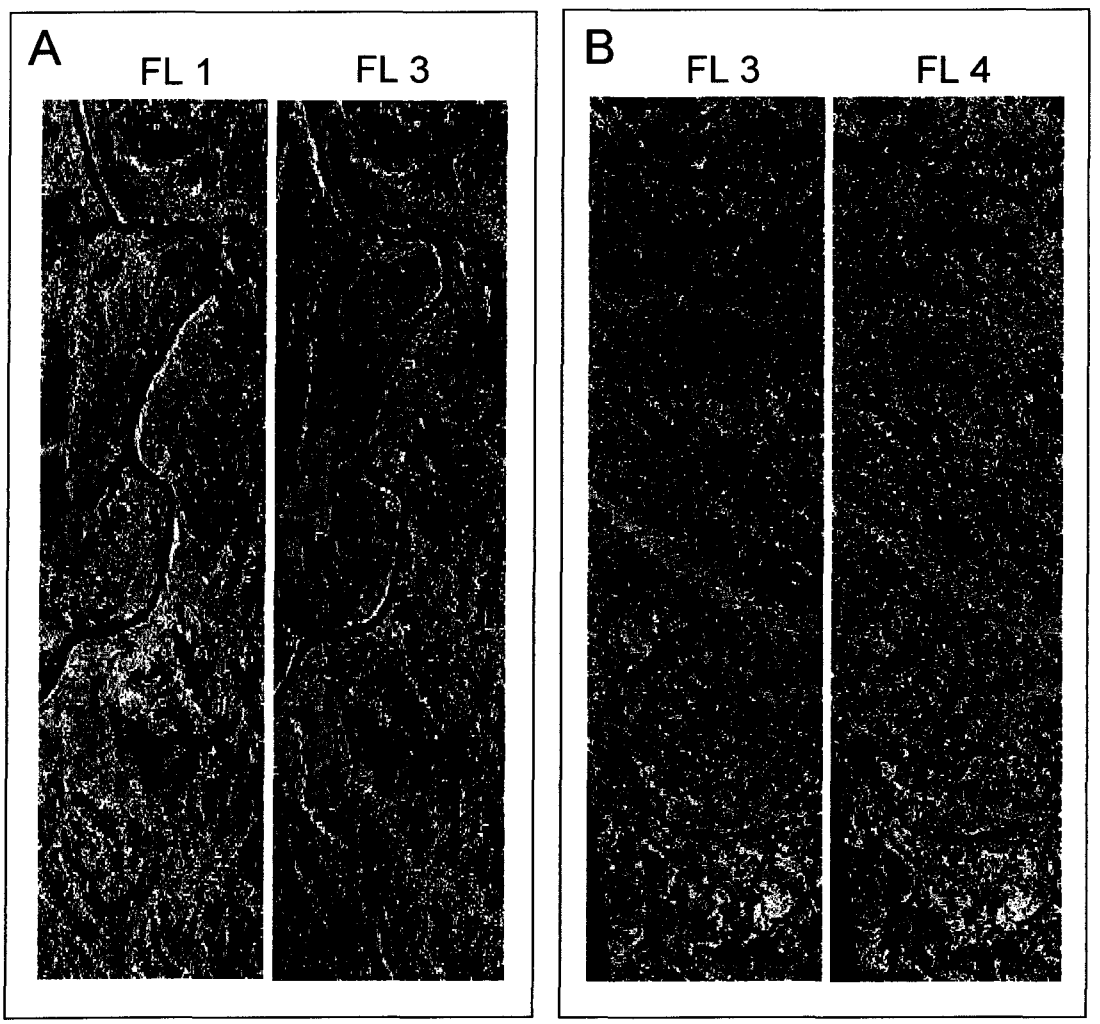

Figure 6.15. Identical area maps from multiple flight lines, 2001. Subsets from classified maps of identical areas were mapped independently using data from adjacent, overlapping flight lines. A: area 1 overlap between flight line 1 east and flight line 3 west; B: area 2 overlap between flight line 3 east and flight line 4 west. In general, the maps appear to be consistent between flight lines.

geometry between flight lines were compared, where classification differences related to geometry would be at a maximum. A visual comparison of the thematic map pairs in Figure 6.15 also indicates that the mapping procedure is consistent. Overall, the consistency of these results demonstrates an improvement over earlier hyperspectral test maps that showed pronounced differences in mapped spurge depending on the processing method that was used (see Chapter 5, Part I).

The accuracy of all land cover classes was also computed for flight line 3 using the identical area map from flight line 1 as a reference image. When unclassified background and masked (non-vegetated areas) were excluded from the error matrix, an overall accuracy of 19% was calculated. Producer's accuracy for the leafy spurge class was 20%, and user's accuracy 24%. The highest producer's accuracy obtained for any class was 29%, and the highest user's accuracy for any class was 38%. Registration differences between the two flight lines, differences in the IFOV for "corresponding" pixels from the two flight lines (related to platform/sensor position as well as sensor viewing angle), and spectral differences related to viewing angle (see Chapter 8) may have contributed to both spatial and classification errors between the two flight lines. Post-classification filtering may reduce the effects of spatial error on overall accuracy and lead to higher accuracy values with this method, but was not completed.

REGRESSION

Standard multi-spectral accuracy assessments are designed to validate only the correct presence or absence of classes on thematic land cover maps. In addition to presence/absence, it was possible to extract the approximate abundance of materials from the THRO images by using the MTMF unmixing method for mapping. This additional information is valuable for detailed descriptions of cover or abundance which allows monitoring of change *within* classes, particularly when no change in the class is indicated on a thematic, presence/absence map. This extra information could facilitate earlier prediction of land cover change or identification of within-class trends that are not possible with hard-classified presence/absence maps. With earlier intervention, new infestations can be more successfully controlled, and problem areas within

established patches can be identified and targeted for focused control efforts. The change in fraction over time will be an important component of spatial analyses of the response of the weed to different control techniques and to determine the most effective method(s) for eradicating or controlling the weed.

The MF scores produced from the MTMF unmixing algorithm represent the approximate fraction of a pixel occupied by materials; therefore the leafy spurge MF scores from classified pixels could be correlated with the density estimates from the field using regression analysis. The field density measurements were either estimates of the mean density of spurge for each "homogeneous" polygon (representing a homogeneous non-linear mixture of spurge and other materials), or the percentage of each 32 m^2 grid that was occupied by spurge. The grid percentage could represent the percentage of the area of a grid covered by a 100% spurge patch (a linear mixing problem), or a non-linear, homogeneous mixture of spurge and other materials, or some combination of these. The MTMF algorithm is a non-linear unmixing method that can solve for spurge fraction from both linear and non-linear mixtures. The regression was run on the assumption that the spectra of "equivalent" non-linear and linear mixtures of spurge were sufficiently similar to yield equivalent MF (fraction) values.

The correlation was tested at a coarse, patch-level scale using the polygon reference data, and at a finer, pixel-level using the grid reference set to determine if a correlation was evident, and if so, at what scale this could be detected.

PATCH LEVEL REGRESSION

Methods. For the patch-level correlation, the density for each polygon was compared to the mean MF value for all classified pixels within the patch associated with each polygon. Three mean MF values were calculated for each patch due to the poor alignment between the classified patches and field polygons. These mean values included: 1) all pixels falling within the boundaries of an overlaid field polygon (this included spurge-classified as well as unclassified pixels; see Figure 6.16, Case 1); 2) the mean MF score for the entire leafy spurge classified patch that was associated with each spurge reference polygon; in this case some pixels fell outside the

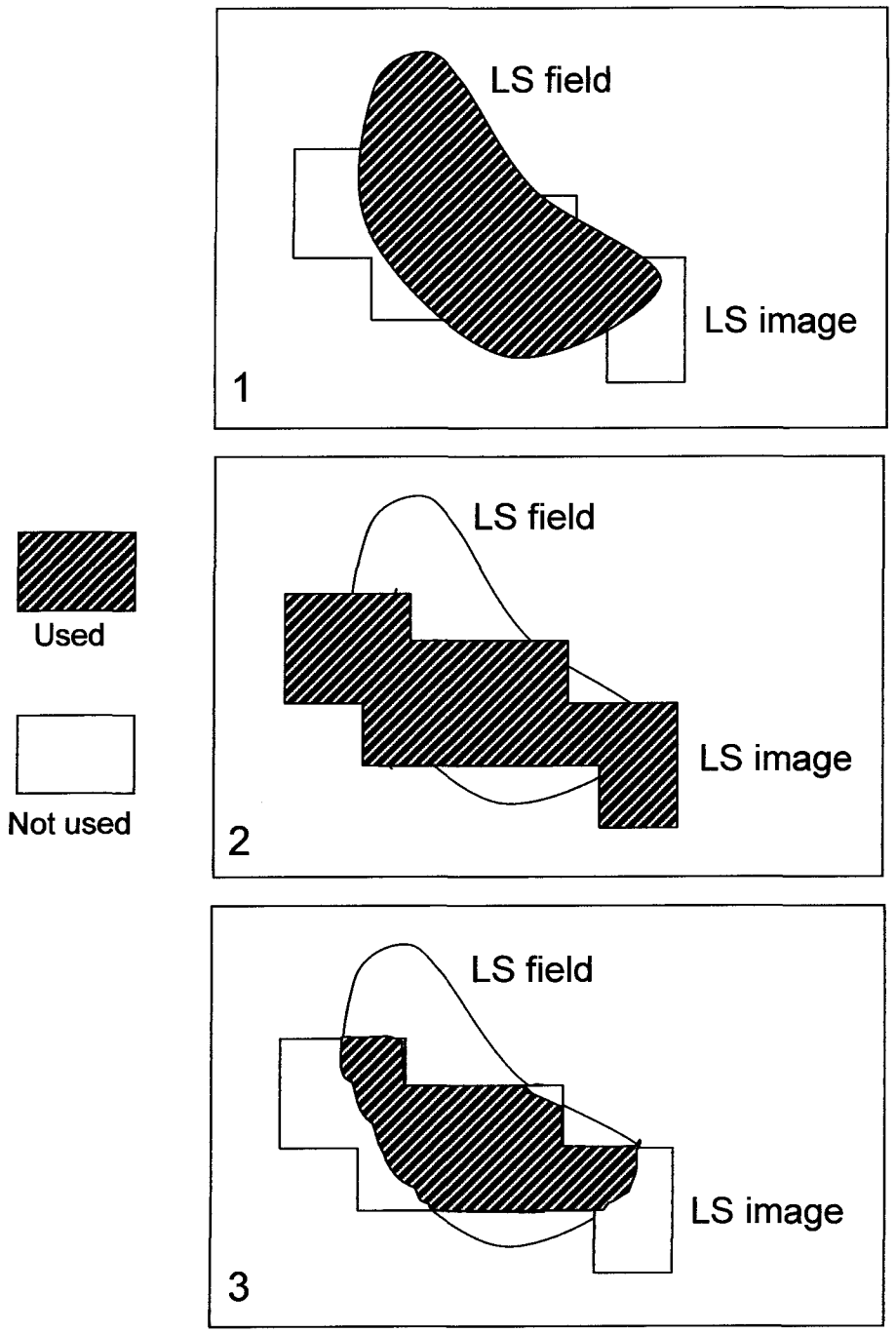

Figure 6.16. Diagram showing portion of image used in calculation of mean MF score for cases 1, 2, and 3 image/polygon coarse-scale regression.

boundaries of the overlaid polygon (Figure 6.16, Case 2); and 3) spurge classified pixels only, that occurred within the boundary of the vector overlay (i.e., the intersection between field polygons and classified spurge, Figure 6.16, Case 3). These are referred to below as Case 1, Case 2, and Case 3, respectively. The regression also included the non-spurge field polygons, using the mean MF score from the spurge matched-filter image, and the field density for spurge (all 0%). Three regressions were run, one for each of the above cases. For Case 1, all 22 polygons were used, which included the 12 non-spurge vegetation patches. Because Case 2 evaluated the correlation for only the spurge-classified pixels, the analysis was restricted to the 10 spurge polygons. In the third case, only seven of the spurge-classified patches intersected the corresponding field polygon, therefore the regression was restricted to these seven patches. The remaining three spurge patches occurred outside, but in close proximity to the polygon boundaries, and therefore were not used in the Case 3 regression.

Results. The r^2 values indicated moderate to good positive correlation for the three cases (Figure 6.17), with Case 1 = 0.725, Case 2 = 0.558, and Case 3 = 0.707. It is difficult to directly compare the results of the three regressions, however, due to the different number of patches used for each case. To allow a direct comparison of the three cases, the seven polygons that were used in the most restricted Case 3 (the intersection) were used to re-run the regressions for Cases 1 and 2, but restricting the input to these seven patches. After re-running the regressions, the correlation for Cases 1 and 2 decreased. Case 3, the intersection, showed the highest correlation ($r^2 = 0.707$), while r^2 for Case 1 (all pixels within a polygon) dropped to 0.626, and for Case 2 (all classified pixels), $r^2 = 0.449$ (Figure 6.18).

Discussion. Assuming that the reference and classified patches were spatially shifted from one another, the best correlation would be expected between either the *full* classified patch mean, (including pixels falling both inside and outside the polygon boundaries) and mean density from the field polygon, or the mean of the intersection and polygon density; however, of the three cases examined the highest correlation ($r^2 = 0.725$) was obtained for Case 1 (all pixels within the boundary of the overlaid polygon). For Case 3, the intersection, $r^2 = 0.707$, and $r^2 = 0.558$ for Case 2, the full classified patch. A lower correlation had been expected for Case 1 because both

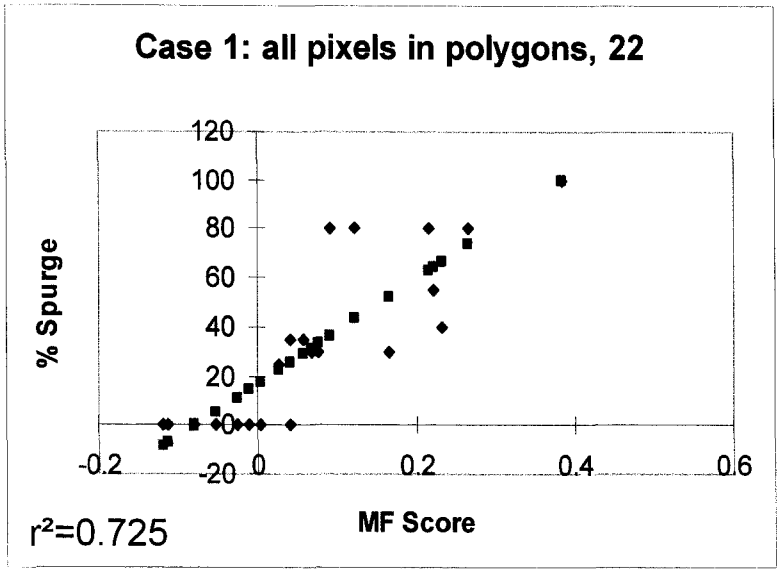

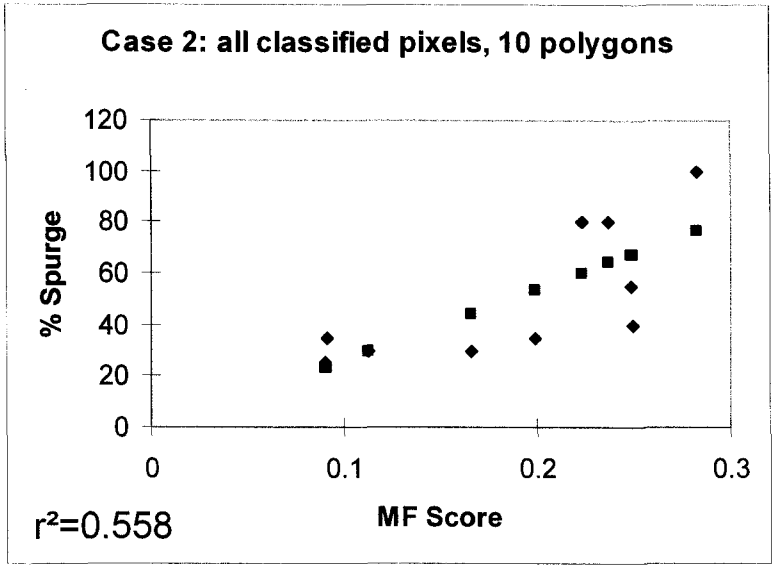

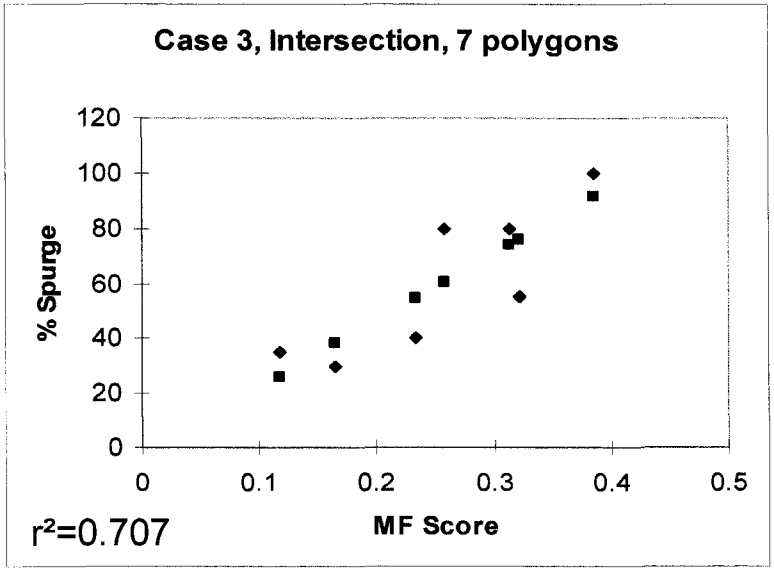

Figure 6.17. Coarse-scale regression comparisons: Case 1 includes mean MF score for all pixels within the boundary of the field polygon; Case 2 mean MF from all pixels in the full classified patch; Case 3 only mean MF score from intersection between polygons and spurge-classified pixels.

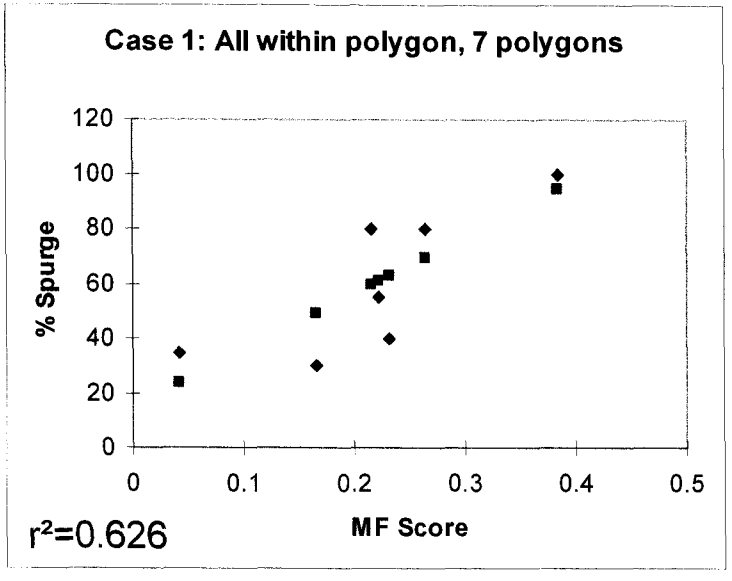

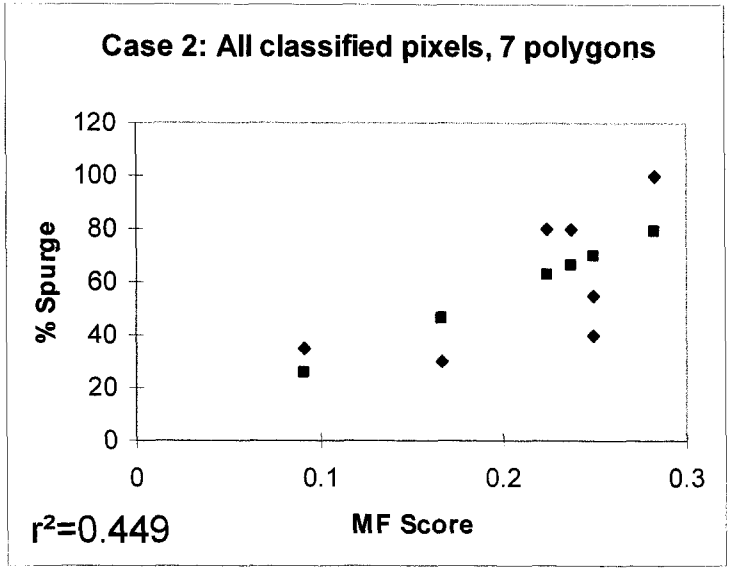

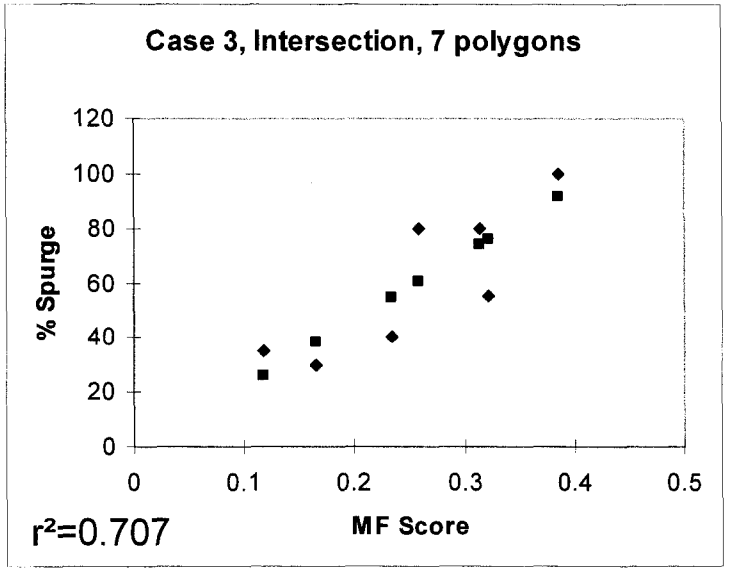

Figure 6.18. Coarse-scale regression comparisons; identical 7 polygons used in each case. Best correlation is seen between the patch density and the corresponding MF scores from the intersecting spurge classified pixels (Case 3).

spurge-classified and non-spurge classified pixels were included in the mean MF calculation. The MF scores for the non-spurge pixels were expected to be lower than for pixels that actually were classified as spurge. This would result in a lower mean MF, and presumably a lower correlation with the polygon density measurements. The better correlation between the mean MF score from the full polygon and % spurge (Case 1) could be accounted for by the larger number of polygons that were used in the analysis.

After the regressions were re-run using the identical set of reference polygons, Case 3, the intersection, showed the highest correlation, followed by all pixels associated with a polygon (Case 1), then all classified pixels (Case 2). These results argue against a pure registration shift, as the pixels with the best visual correspondence to the polygons (i.e., all pixels within a classified patch, Case 2) that were believed to just be shifted from the polygons show lower correlation than the combined classified and unclassified from within the polygons (Case 1). The intersecting pixels (Case 3) would be expected to show high correlation if a modest registration shift was present, and these show the highest correlation when the regressions for the identical seven polygons were compared.

PIXEL/GRID SCALE REGRESSION

Methods. A grid-based regression was run, using the percent spurge and corresponding MF scores from all intersecting grids and spurge-classified pixels (Figure 6.19). To establish a link between grids and pixels to automate the regression, ENVI, Arcview and ArcINFO software were used to generate a point coverage for the spurge-classified pixels, that was buffered and intersected with the grid coverages, and linked to original classified spurge coverage containing the MF scores. A regression was run on the MF scores and percent spurge from the grids, using the 257 intersections that were established.

The 32 m x 32 m grid field data provided approximate spatial information on the location of spurge, although precise density estimates were difficult to correlate to individual classified pixels because the vegetation within the grids was not homogeneous, and the size and orientation of the AVIRIS pixels and field grids did not correspond and the quality of the

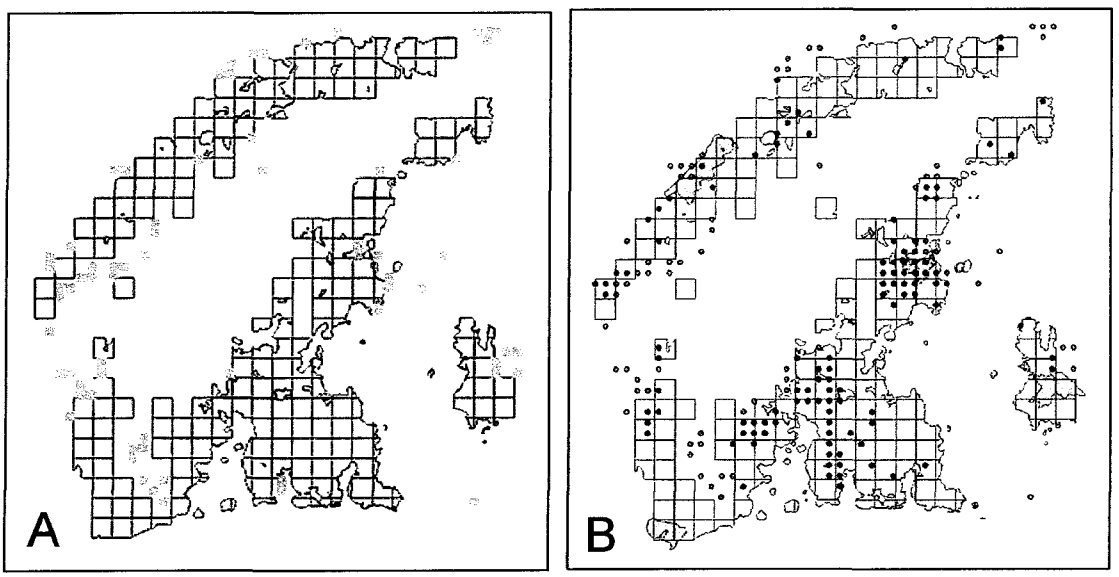

Figure 6.19. A. Field grids (30m²) overlaid on leafy spurge primary map; intersecting pixels shown in yellow; non-intersecting in green. Classified pixels were converted to points (in B) to determine the correlation between MF scores for individual pixels and the corresponding grids. Red points are the converted yellow pixels that intersect spurge-containing grids (aqua), and were used in the regression; blue points (converted from green pixels) did not intersect the grids and were not included in the analysis.

registration between individual pixels and corresponding grids was unclear. Nevertheless, the MF scores for spurge-classified pixels that intersected the grids, and the spurge density estimates from the corresponding grids were regressed against one another to determine whether any correlation could be seen at this finer scale.

Two additional fine scale regressions were run on a single, 2.5 ha (~ 6.1 acre) test patch that corresponded well in size and shape to a grid patch, but was spatially offset (Figure 6.20 C). The regressions were done before and after the grid patch was roughly re-registered to the classified patch to test whether individual pixel-to-grid correlations were significantly different after re-registration, and to see whether better spatial alignment would improve the correlation between field-measured densities and MF scores.

Results. The fine-scale regression using *all* intersecting grids and classified pixels showed no correlation, with $r^2 = 0.01$ (Figure 6.21). For the single patch regression, again no correlation was evident, with an $r^2 = 0.03$. An image-to-image registration was performed on a small subset of the data from the immediate area surrounding the test patch. The grids were re-aligned with the corresponding classified area using the tie points that were generated during the re-registration. Figure 6.22 shows the grid and classified patches before and after re-registration. The spatial correspondence between the two improved, but remained poorly aligned (Figure 6.22 B).

Following the re-alignment of the patch, $r^2 = 0.07$, again indicating no correlation and no dramatic difference in the results before and after re-registration. A different number was used in each analysis, therefore direct comparison of the results was difficult; however, there was no obvious improvement after the re-registration.

Discussion. The results of these fine-scale regression analyses indicate pixel-to-pixel (or pixel-to-grid) correlation between image MF scores and grid-level spurge density measurements could not be seen. These results suggest either: 1) no correlation exists between MF score and % leafy spurge; *or* 2) that it is not possible to analyze the correlation between field-based measurements and the fractional abundance of individual pixels at this scale. Because of pixel-to-pixel and grid-to-grid variation in density and MF scores within a patch, good correlation

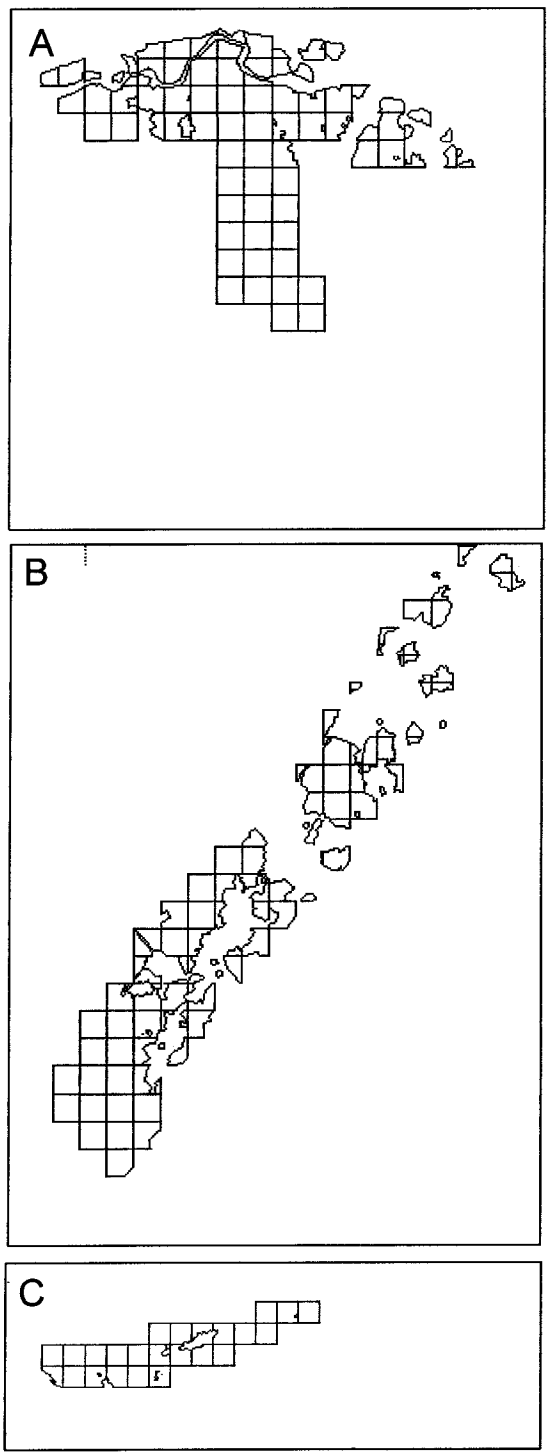

Figure 6.20. Grid network overlaid on spurge classification. Direction and magnitude of shift between spurge field grids (black) and classified spurge (yellow) varied throughout the image. Top of page is north in each figure. Grids are shifted NW in A; NE in B; and W in C, where the magnitude is greatest with a 7-8 pixel shift indicated.

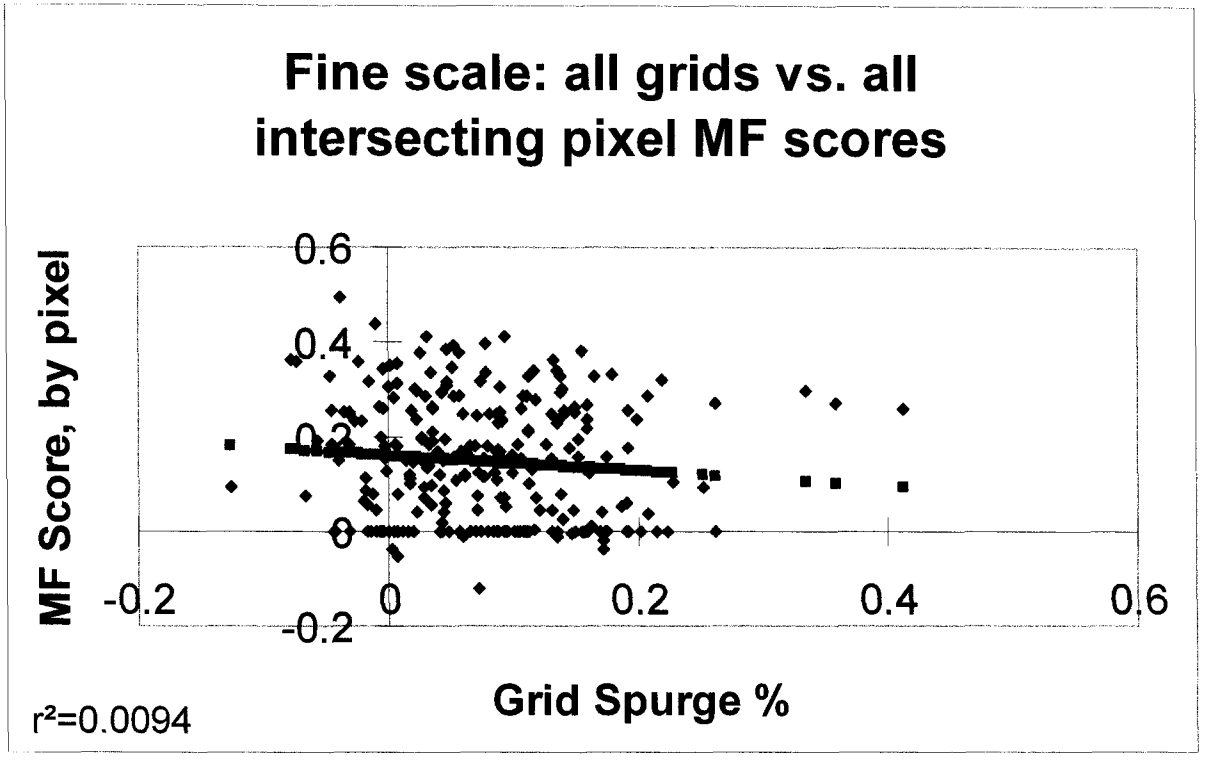

Figure 6.21. Fine-scale regression, all grids versus MF scores for individual intersecting pixels; no correlation is seen between the field and classified data at this scale.

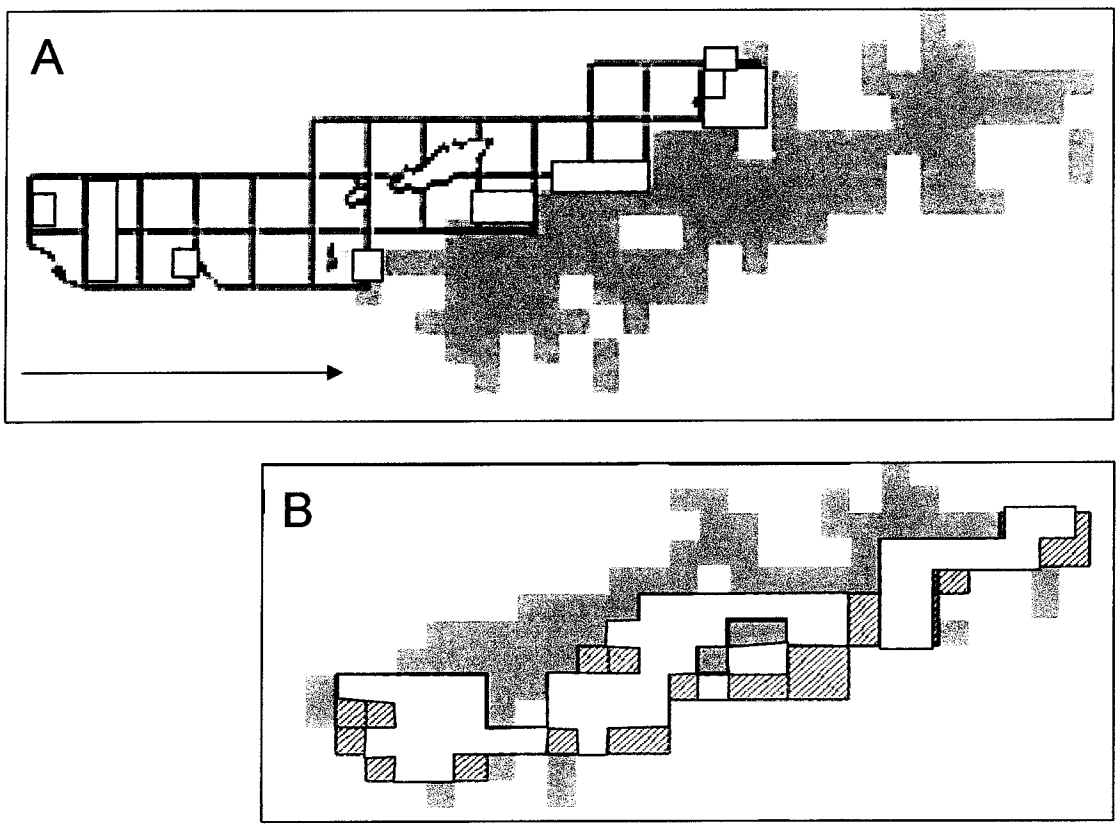

Figure 6.22. Intersection between classified pixels and reference grids for a single test patch of spurge before (A) and after grid was re-registered to classified image (B); yellow indicates the intersecting areas (approximate) between grid and classified patches that were used in the regressions; black hatched areas are non-intersecting grids; green are non-intersecting classified pixels. MF scores of intersecting pixels regressed on % leafy spurge for the corresponding grid (fine-scale regression). After re-registration, alignment improved, but remained poor. No correlation was apparent following the re-registration ($r^2 = 0.07$) Arrow in A indicates approximated magnitude of the shift after re-registration.

will be unlikely at this scale unless perfect alignment can be obtained. Currently this is not possible with the georectification methods that are available for airborne scanner data.

GENERAL DISCUSSION, REGRESSION

At the coarser scale, the moderate to good positive correlation between fractional abundance (MF) scores and percent spurge shows that the regression approach can be used successfully for gauging the quality of a classification, specifically whether abundance measurements are accurately represented. This is an advantage of the regression over confusion matrices, which are restricted to gauging the accuracy of thematic presence/absence maps, with no method to evaluate variation in abundance within a class. Until registration can be improved substantially, regression as an accuracy measurement is unlikely to be successful at the pixel level.

The ability to assess the accuracy of fraction maps is important because detailed monitoring of change in abundance over time would be possible in addition to standard thematic class change. Abundance measurements could be linked to the severity of infestations, providing added detail on weed distribution that would be useful for planning and allocating resources for control operations. More sophisticated spatial analyses could be completed as well. These subtle differences (i.e., no change in the actual land cover class, but changes within a class) are important in general for accurate landscape characterization (Foody, 2002). This type of change cannot be addressed with standard post-classification change detection based on multi-temporal thematic maps.

SUMMARY DISCUSSION OF ACCURACY ASSESSMENTS

Several accuracy assessments were run on the THRO leafy spurge maps to address inconsistencies that were seen between early quantitative and qualitative assessments of the maps. The effects of registration, reference data, and mapping methods on accuracy were evaluated. These tests included:

1. Application of standard accuracy assessments, as well as accuracy tests for registration effects (including a majority filter, re-registration, and buffering).

2. Assessing the effect of different reference data on accuracy (polygon pixels converted to points, and 2003 plot centroids).
3. Determining the sensitivity of the standard accuracy assessment method and reference data to detecting differences between mapping strategies.
4. Testing the accuracy of the combined primary and secondary map to evaluate whether problems with omission error that were seen in the primary map could be improved.
5. Comparing the accuracy of identical areas that were produced independently from different flight lines to test the consistency of the modified hybrid MTMF mapping method.
6. Using field vector overlays to visually assess the spatial relationships between field and classified data that could not be examined with standard point-based accuracy assessments.
7. Quantifying the strength of relationships between field-measured density and image-derived spurge fractions using regression analyses at both pixel-level and patch-level scales.

Table 6.10 includes a summary of the leafy spurge accuracies for all analyses based on the standard confusion matrices, as well as the results of the regression analyses of the THRO maps.

The basic accuracy values from standard point-based confusion matrices were low for both 1999 and 2001, and at face value suggest that imaging spectroscopy is ineffective for mapping leafy spurge. Although *user's* accuracy for spurge was high (100% and 86%), producer's accuracy, an indication of the degree of omission of spurge from the classification, was very low (26% and 18%). The overall accuracy was low for both 1999 and 2001 (39% and 47%) (Table 6.10 A and B).

In spite of the low overall and producer's accuracies, the commission error for the leafy spurge class was reduced considerably in these maps compared to early test maps in which spurge had been grossly over-classified (see Chapter 5). At the same time, several known low-density leafy spurge patches that were not mapped in these same early classifications *were* correctly mapped using the modified method developed in this study.

	Year	Map method	ref source	Accur asses	Buffere	Overall acc % or r^2	Prod acc LS %	User acc LS %
A	1999	MTMF	dl plots 99	error matrix	n	39	26	100
B	2001	MTMF	dl plots 01	error matrix	n	47	18	86
C	1999	MF	dl plots 99	error matrix	n	40	28	100
D	2001	MF	dl plots 01	error matrix	n	47	19	85
E	2001	MTMF w/maj.filter	dl plots 01	error matrix	n	46	22	88
F	2001	MTMF	2003 plots	error matrix	n	19	17	99
G	2001	MTMF w/buffer	dl plots 01	error matrix	y 1-5	66-70	53-92	83-65
H	2001	MTMF w/buffer	2003 plots	error matrix	y 1-5	39-82	39-83	99-98
I	1999	MTMF prim/sec combo	dl plots 99	error matrix	n	72	74	90
J	1999	MTMF prim/sec +3buf	dl plots 99	error matrix	y +3	81	98	82
K	2001 ident areas	MTMF	dl plots 01	error matrix	n	1/3 54,52 ; 3/4 55,57	1/3 23,19 ; 3/4 39,37	1/3 100,100 ; 3/4 81,100
L	2001 ident areas	MTMF	dl plots 01	error matrix	y +1	1/3 68,67 ; 3/4 65,71	1/3 51,49 ; 3/4 59,65	1/3 93,93 ; 3/4 81,88
M	2001 ident areas	MTMF	fl1 image	error matrix		fl3 19	fl3 20	fl3 24
N	2001	MTMF	polys p/a	error matrix	n	64	56	
O	2001	MTMF	indiv polys	error matrix	n	na	11 to 94	na
P	2001	MF	combo polys	error matrix	y 1-5	67	60	100
Q	1999 re-reg to 2001	MTMF	dl plots	error matrix	n	36	25	99
R	1999 re-reg to 2001	MF	dl plots	error matrix	n	38	27	98
S	2001	MTMF	polys	gis overlay	n	na		
T	2001	MTMF	grids	gis overlay	n	na		
U	2001	MTMF	grids all combin-fine	regression	n	r^2= 0.009		
V	2001	MTMF	grids gr to pix-fine	regression	n	r^2= 0.034		
W	2001 re-reg to grids	MTMF	grids gr to pix re-reg	regression	n	r^2= 0.066		
X	2001	MTMF	polys-coarse	regression	n	r^2= 0.449-0.725		

Table 6.10. Summary of mapping method, reference source, assessment method, and leafy spurge accuracy values or r^2 for all accuracy assessments that were used to evaluate the THRO leafy spurge classifications.

Majority filtering, re-registration, and buffering were used to examine the possible effects of poor registration on accuracy values. With both the majority filter and re-registration the change in accuracy was minor (Table 6.10 E versus B and Q, R versus A). The overall accuracy for the re-registered 1999 image showed a modest decrease (from the original 39% to 36% after re-registration). Although the alignment between portions of the 1999 image and the 2001 image improved, it deteriorated in others, resulting in lower accuracy for the re-registered image. The re-registration was therefore not considered an effective method for improving poor registration or accuracy values. A slight (one percentage point) increase in overall accuracy was seen after the majority filter was applied, but this was not considered a major improvement.

A one-pixel wide buffer resulted in a notable increase (19 percentage points) in overall accuracy (see Table 6.10 G versus B, and Table 6.4). Producer's accuracy also increased dramatically (34 percentage points), while user's accuracy remained fairly constant, with a decrease of three percentage points. With the largest, five-pixel buffer, the change in overall accuracy relative to the non-buffered classification was 20 percentage points, while producer's accuracy increased 74 percentage points. User's accuracy decreased 21 percentage points, a much smaller difference than was seen for the producer's accuracy. The dramatic decrease in omission error, with only moderate increase in commission error suggests that the buffering is valid and that registration error had a negative effect on accuracy values. Although registration is believed to negatively affect accuracy, accepting the values that were derived with the buffers assumes that it is valid to soften the class boundaries by buffering the classified pixels.

When different reference sources were used in the error matrices (2001 centroids, 2003 centroids, and polygons converted to "points"), the overall accuracy for the identical map (e.g., 2001 imagery and MTMF method) varied widely (from 19% to 64%) (Table 6.10 B, F, and N). Producer's accuracies were low to moderate, and variable (17% to 56%), while user's accuracies ranged from 86% to 100%. Because these values were inconsistent when different sources of reference data were used on the *identical* maps, the accuracy results were considered inconclusive. Each reference set had advantages and disadvantages, but none was considered optimal for validation of the THRO spurge maps. Problems were predominantly related to

sampling strategy and included: insufficient number, non-random location, skewed distribution of classes, incomplete samples, inappropriate plot size or varied polygon size, poor location (i.e., under tree canopy), absence of spatial context or extent; and collection date.

Accuracies of maps produced with the MF and MTMF methods were compared to determine whether the standard assessment with error matrices and the available reference data could differentiate between the maps. The infeasible refinement of the MTMF, in theory, produces higher quality maps, and should improve accuracy as well. For the 1999 and 2001 THRO maps, with the MTMF method the calculated accuracy either remained essentially the same as the MF results (both 47% in 2001), or *decreased* slightly (from 40% with MF to 39% with the MTMF in 1999) (see Table 6.10 B versus D, and A versus C). Visual inspection, however, indicted that the MTMF maps were an improvement. Several large patches of vegetation within agricultural fields that had been erroneously classified as spurge were successfully eliminated after the infeasible refinement. This was a significant improvement that was *not* reflected in the calculated accuracy value. The point-based reference data were not sensitive enough and/or the reference data were insufficient to quantitatively reflect this improvement in the MTMF-refined map. Overall, the magnitude of the accuracy differences was insignificant. The removal of incorrectly classified material that was discovered based on the qualitative evaluation was a notable improvement, however.

A disadvantage of the method that was used to produce the primary maps was the exclusion of non-dominant pixels in which spurge was the dominant fraction of the pixel. Additional spurge that was present as a subordinate, yet still significant fraction of a pixel was excluded from these maps, leading to higher omission error and corresponding lower producer's accuracy for the leafy spurge class. Low density spurge infestations were the most likely to be excluded from the primary maps. The basic accuracy results from the primary maps did indicate low producer's accuracy (high omission error). When the secondary map was combined with the primary spurge map from 1999, however, producer's accuracy was increased substantially (from 26% to 74%, see Table 6.10 A versus I). Overall accuracy increased from 39% for the primary map to 74% when the two maps were combined. When a three-pixel buffer was added to

accommodate poor registration, 81% overall accuracy was calculated and omission of spurge was reduced further (omission error only 2%) (Table 6.10 J); however, the commission error was also higher in this map (18%). The producer's and user's accuracies of the non-spurge class were low with the three-pixel buffer, but did not substantially affect the overall accuracy because non-spurge represented less than 20% of the total number of reference points collected in 1999.

Overall, omitting some of the leafy spurge could have much more detrimental outcome, from a management perspective, than erroneously mapping other vegetation as spurge. Unmapped spurge would not be treated and could proliferate and become well-established, making it very difficult to control. Substantially increased commission error, however, can be equally undesirable or counterproductive. A grossly over-classified map would be too generalized to be effective for economically tracking, treating, and monitoring infestations. Providing both the individual primary and secondary maps was considered the best option. The primary map would be useful for locating the most severe infestations (where leafy spurge is the dominant material), for focused, intensive control efforts. The secondary map would be useful for locating new, smaller outbreaks, for monitoring the progress of control efforts in previously treated areas, and may prove to be useful for predicting areas that are prone to proliferation of spurge (see Chapter 5, Figures 5.36 – 5.38 and discussion).

Because the focus of this study was to test the suitability of imaging spectroscopy for applied temporal monitoring of a particular species, the reliability and *consistency* of the results over time and space were critical concerns. Comparisons of the accuracies of identical areas from data collected on the same date, but from different flight lines offered a unique opportunity to test the consistency of the method that was developed to produce the maps (see Chapter 5). The accuracies were generally consistent in the two coincident areas that were studied (Table 6.10 K). For Area 1 (flight lines 1 and 3), overall accuracies were 54% and 52%, producer's accuracies were 23% and 19%, while user's accuracies were 100% for both flight lines. For Area 2 (flight lines 3 and 4), overall values were similar at 55% and 57%; producer's accuracies were 39% and 37%, however, user's accuracy varied by 19 percentage points (81% vs. 100%). The consistency of the map accuracy was considered more important for applied temporal analysis of

the THRO data than the absolute magnitude of the calculated accuracy, which was affected by registration problems and inadequate reference data. The consistency of the formal accuracy assessments, supported by visual comparison of the maps, indicates that the maps are consistent between flight lines. The method outlined in Chapter 5 for processing imaging spectroscopy produced consistent results that are suitable for temporal monitoring of spurge.

An assessment of the accuracy of fractional abundance measurements was possible by regressing field density estimates against fractional abundance measurements that were derived from the image. When values were compared at a patch-level, good correlation was seen (r^2 of 0.725). This suggests that the maps are accurate and reliable. The regression analysis complements the accuracy information obtained with confusion matrices by providing a tool to evaluate the accuracy of partial class membership derived from imagery. Because mixed pixels dominate remotely-sensed imagery, the regression is an important component of accuracy measurement for hyperspectral maps. Fractional abundance, and the change in fraction, will be important metrics for characterizing a landscape thoroughly, particularly as registration methods improve.

DISCUSSION/CONCLUSIONS

The two approaches used for accuracy assessment of the leafy spurge maps had unique advantages and disadvantages. With point-based error matrices the outcome was very sensitive to registration error. This approach was designed to use with thematic maps, therefore partial class membership cannot be addressed with the confusion matrix. An assumption underlying the use of confusion matrices is the presence of pure, discrete pixels, a rare condition in reality. Pure pixels are also assumed when applying the kappa statistic, and because mixed pixels are the norm, the kappa statistic may not be appropriate for remote sensing maps (Foody, 2002). Error matrices, however, are very effective for describing both accuracy and error simultaneously for many land cover classes. The confusion matrices provided a baseline for comparing relative differences in accuracy: 1) from different methods and refinements; 2) with filtering and buffering

of maps; 3) between identical areas mapped from adjacent flight lines; and 4) between primary and secondary maps.

For the coarse-scale regression analysis, sampling was problematic. Only 22 non-randomly selected polygons were collected for the analysis, and fewer still were available when the regression was restricted to intersecting spurge polygons and classified patches. With the fine-scale regression analysis, poor registration was also problematic. Mixed pixels and fractional abundance measurements could be evaluated with the regression analysis, however. Regression is useful when the focus of the mapping effort and accuracy analysis is a single class; however, unless other representative vegetation surrounding the polygon is characterized in the field, there is not an effective method to determine true commission error. When classified areas fell outside the perimeter of the spurge reference patches that were used for the regression in this study, there was no formal reference data regarding land cover outside the patch.

In spite of the variable quantitative accuracy results obtained from confusion matrices, visual inspection of reference polygon and grid vectors overlaid on the classified map indicated that the size and shape of many of the classified and field patches matched reasonably well, although they were often shifted spatially and poorly aligned. Because of the difficulties with the traditional approaches to accuracy assessment in this study, including poor registration and inappropriate or incomplete reference data, the polygon and vector coverages provided a useful supplement for characterizing the quality of the maps.

The goal of many hyperspectral analyses is to provide very detailed maps that differentiate spectrally similar materials. Because of the high spectral resolution more classes can be differentiated, resulting in greater map detail than has been possible with coarser-resolution, multi-spectral imagery. In mapping invasive species, for example, detailed maps indicating patchy and isolated distribution of vegetation are critical for management decisions that require the optimal distribution of resources for controlling infestations. This detail, however, results in maps with increased sensitivity to location errors, and therefore, lower accuracy values than a more generalized map with fewer thematic classes. The implication is that the "quality" of the hyperspectral map is lower (based strictly on calculated accuracy), when the maps may, in

fact, provide a more realistic representation of land cover. Maps produced from multi-spectral imagery obtained over high frequency, heterogeneous, and complex landscapes are known to be associated with lower formal accuracy values than more homogeneous, filtered, or generalized land cover maps (Loveland et al, 1999; Scepan, 1999). When random points are generated for accuracy assessment, it is recommended that points that fall on or near hard-classified boundaries be discarded to avoid the confusion and lower accuracy that are associated with the "fuzzy" boundaries in transition zones between covertypes or mixed land cover classes. These areas are susceptible to both classification errors, due to spectral mixing, and registration errors resulting from proximity to class boundaries. Much of the leafy spurge that was mapped with AVIRIS data occurred in isolated, small, or fragmented patches that could be characterized as edge or transitional pixels based on the proximity to the boundary of classified areas. Discarding reference points that were associated with these small patches would bias the reference set and accuracy calculations toward larger, and often denser patches. This problem is exacerbated for airborne scanner data because it is especially difficult to rectify accurately over an entire scene. This study suggests that problems with registration could seriously impact the accuracy of detailed spurge maps when using point-based reference data.

Typically, error in a map can be traced to radiometric and atmospheric effects, poor registration to the ground, or classification error (Carmel et al., 2001). For the THRO maps, atmospheric effects are unlikely to be a substantial source of error because of the rigorous atmospheric calibrations that were completed for all imagery. Radiometric effects between dates could account for some differences, because of modifications and upgrades to the AVIRIS sensor between 1999 and 2001, (2001 map accuracies were several percent higher than 1999); however, this was not considered a major factor affecting accuracy of the spurge maps. A wide accuracy range was obtained for maps produced from identical data, and in some cases for the identical map. The greatest differences in accuracy of identical maps were seen with the buffering that was used to accommodate registration error, and between the alternative reference sources. Registration and reference data are assumed to be significant factors contributing to low accuracy for THRO spurge maps.

With accuracy assessments it is generally assumed that the reference data are accurate, and low accuracy is generally interpreted as "failure of remote sensing" to provide useful information for mapping land cover (Foody, 2002). The map is assumed to be the least accurate component in an assessment, therefore the error is typically assumed to be in the map, which is not always the case. Low accuracy may instead indicate problems with the accuracy assessment. The three major problems that are confronted when using confusion matrices include: sample design, ground data accuracy, and registration (Foody, 2002). All three were problematic in the THRO validations. The reference data itself may have been affected by registration problems. Improperly collected reference data may contain greater error than the classified map that they are being used to evaluate (Foody, 2002). The labeling or description of the reference data can be subjective as well. Sampling methods may compromise the value of the reference data. For example, a mismatch between the size of the reference sample and the resolution of the imagery may limit the utility of the reference data. The random points that were used with confusion matrices were the centroids from 3 m x 5 m plots, which were not optimal for validating 17 m AVIRIS imagery, and could result in "errors" that are related to inappropriate reference data rather than map errors.

The accuracy variation of the THRO maps was not just the result of poor registration and reference data, however. The modified method, though consistent, will routinely underestimate the extent of spurge because only pixels in which spurge is dominant are mapped as spurge. This results in omission error for spurge and unrealistically low producer's accuracy.

Whether the low accuracy suggested by the basic confusion matrices is primarily the result of location or classification errors, or is related to poor quality reference data or the mapping method could not be absolutely determined for this study. Varied results were obtained depending on the reference source and assessment techniques that were used, and dramatic improvements in accuracy were seen when the buffers were applied, and when the combined primary and secondary maps were assessed. It was difficult to isolate the affects of registration, reference data, and mapping method, however. These are the main areas that need to be improved to obtain a more realistic assessment of accuracy. Reference data collection should be

carefully designed and acquired, and the techniques used to evaluate accuracy should be carefully selected. An optimal approach to reference data collection would include the advantages of each of the individual reference sets used in this study, combined within a single reference set. For example, the statistical sampling of random points coupled with the spatial information of homogeneous polygons and/or large area plots. Nested polygons, with appropriate dimensions for the image resolution, could be used to define different density classes for the species of interest, as well as associated vegetation. A combination of nested polygons for the species of interest coupled with random point sampling within a specified area surrounding the polygon cluster would be useful (Figure 6.23). With more careful and complete field characterization, current quantitative accuracy analyses could be more effectively and confidently applied to hyperspectral maps. To date, a single ideal standardized method is not available to suit the accuracy assessment requirements of all studies (Foody, 2002).

It was unresolved which of the divergent accuracy values from the accuracy tests presented above was correct, and "real" accuracy was undetermined; however, regardless of which of these accuracy values is correct, if the method adopted in this study is used, then it is possible, minimally, to make consistent comparisons between dates and flight lines for ongoing monitoring purposes.

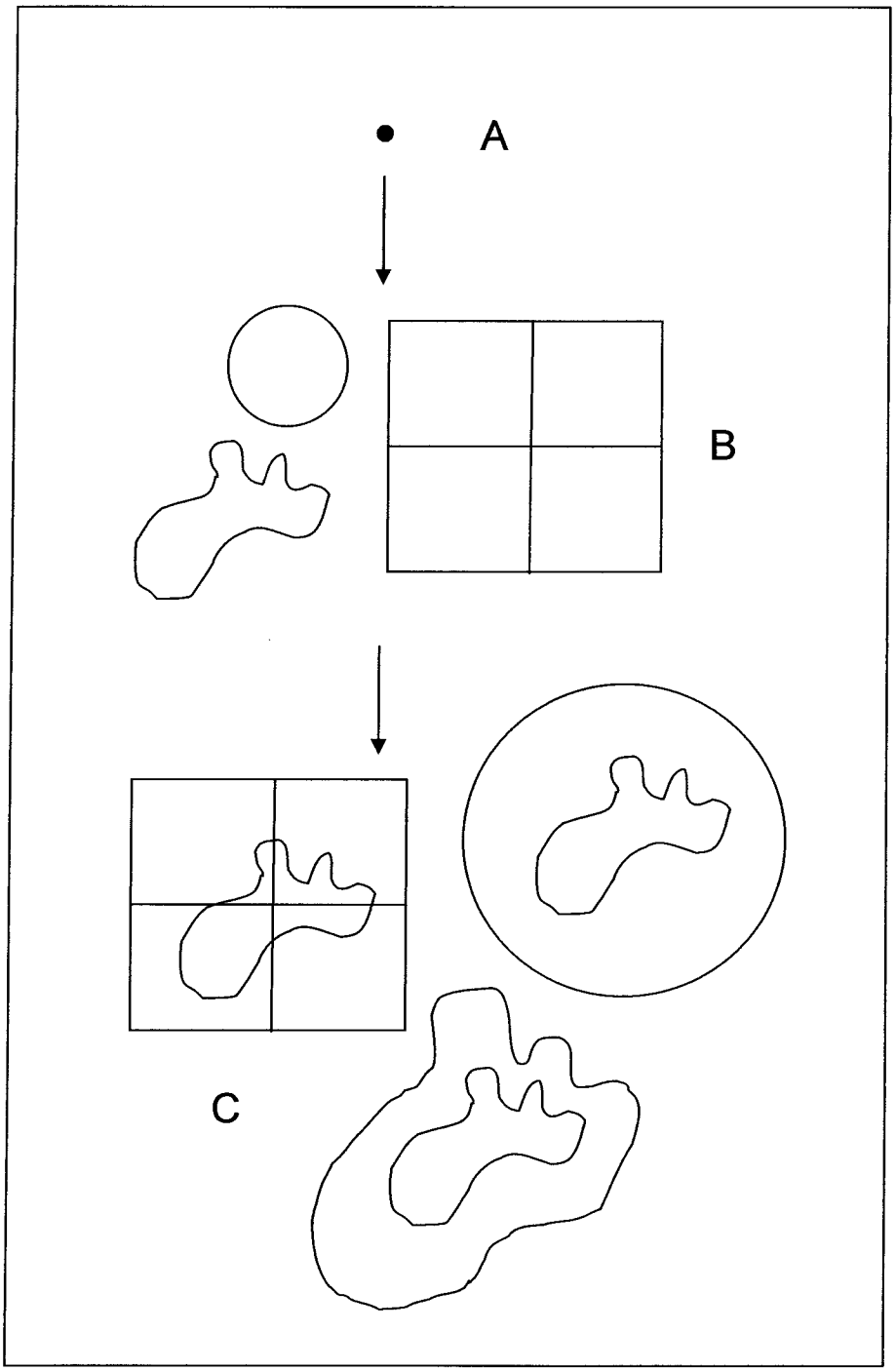

Figure 6.23. Possible alternative sampling schemes for hyperspectral map validation. A: standard point location; B: spatial component added with standardized plots, or polygons enclosing homogeneous patches; C: Polygons for detailed definition of spatial properties of homogeneous patches coupled with buffered or standardized plots to validate adjacent vegetation, using stratified random sampling to locate plots and polygons. (A and B used in this study).

CHAPTER 7: CHANGE DETECTION

INTRODUCTION

Monitoring change is a common application of remote sensing, and will become more important in the future, as it is predicted that environmental change will accelerate in the years to come (Lunetta, 1998). It will become even more important to identify the onset of critical ecological changes early enough to intervene and minimize potentially negative effects of either natural or anthropogenic stress factors on vulnerable ecosystems (Lunetta, 1998).

Traditional methods for change detection using multi-spectral imagery fall into two general categories: simultaneous processing of imagery from multiple dates; and post-classification comparisons of independently processed, single-date images (Jensen, 1996). Simultaneous methods include composite analysis, image differencing or ratioing, vegetation index differencing, principal components analysis (PCA), change vector analysis, correlation analysis, and spectral mixture analysis (Lunetta, 1998; Yuan et al., 1998; Cohen and Fiorella, 1998; Roberts et al., 1998). Post-classification change detection involves the separate classification of imagery from individual dates to produce thematic maps, which are then compared with GIS techniques (Lunetta, 1998).

Each approach has both advantages and disadvantages. Post-classification change, for example, does not require data normalization between dates (Lunetta, 1998; Coppin et al., 2004). This method is also relatively simple to implement and interpret. A change map can be created without requiring the selection of a threshold to define areas of change/no change, as is required with image differencing. Post-classification methods, however, require time and additional costs because separate maps for each date must be created prior to assessing change. In addition,

problems with classification consistency and error propagation can impact the success of post-classification change (Carmel et al., 2001). For example, post-classification change maps are especially affected by registration errors between dates (Wang and Ellis, 2005; Townsend et al., 1992). Processing inconsistencies over time or between analysts can lead to classification errors that will be compounded in a post-classification analysis.

*Simultaneous processing methods for change detection are more time efficient than post-*classification change (Carmel et al., 2001) and are not impacted by the multiplicative error propagation that is seen with post-classification processing (Lunetta, 1998). Simultaneous methods, however, often use data reduction techniques (e.g., tasseled cap, ratioing, or NDVI) that may eliminate useful data, and when applied to hyperspectral imagery, may negate the advantage of using the high spectral resolution data. The interpretation of images produced from multi-date PCA or differencing is challenging, and establishing optimal thresholds for defining the boundary between areas of change/no change can be difficult with the image differencing method (Yuan et al., 1998). In addition, data normalization is required between dates.

Comparative studies of change techniques using multi-temporal, multi-spectral data (e.g., Landsat) over biologically complex areas have yielded inconsistent results with respect to the relative performance of these different methods (Lunetta et al., 2002). No comparison of change detection methods or determination of the optimal method to use for hyperspectral change detection was found in the literature. With few exceptions imaging spectroscopy has rarely been used for land cover change detection. Glenn et al. (2005) mapped untreated spurge patches over two consecutive summers to show that no change in spurge distribution occurred during that time. Other multi-temporal studies have generally focused on changes in biophysical characteristics over time (water content, leaf area, etc.) that are related to phenological changes within a single season, and these characteristics can typically be derived from a small set of general endmembers [i.e., shade, soil, green vegetation (GV), and non-photosynthetic vegetation (NPV)] (Ustin et al., 1992; 1998b; Roberts et al., 1997; Merton and Silver, 2000; Perry et al., 2000; Sabol et al., 1995; Sabol and Roberts, 1993; Vanderbilt et al., 1998; Wessman et al., 1993; Yuhas et al., 1993). The paucity of land cover change detection studies using imaging

spectroscopy may reflect the historical use of this technology for proof of concept or research questions rather than management-oriented, applied projects. In addition, there are unique challenges encountered when using hyperspectral data in multi-temporal analyses, including sensitivity to registration and processing methods.

Registration and viewing geometry can create problems with precise alignment of multi-temporal images. With the exception of the "proof of concept" Hyperion sensor, carried on the EO-I satellite platform (http://eo1.usgs.gov/hyperion.php), hyperspectral sensors are generally flown on airborne platforms that are affected by stability problems so that georeferencing imagery is difficult and the alignment of multi-temporal hyperspectral data for post-classification change detection is an added challenge. Detailed, fragmented species maps for individual dates can be produced with imaging spectroscopy. The change maps that are derived from these will be particularly affected by poor image-to-image alignment, similar to the notable affect of location shifts between reference data and small fragmented patches for calculating the accuracy of a single-date map (see Chapter 6).

A deterrent to the effective use of imaging spectroscopy for post-classification temporal change and monitoring is the inconsistent processing methods that are used to produce maps from the individual dates, the result of interactive processing steps that can dramatically change results (see discussion in Chapter 5). Apparent change can be confused with differences between multi-temporal images that are simply the result of processing methods (Dudek et al., 2004).

Change maps will be affected by varying atmospheric conditions between dates. Because hyperspectral results are particularly sensitive to atmospheric fluctuations, reliable change with imaging spectroscopy also requires careful, model-based atmospheric corrections, applied in conjunction with refinements based on spectral measurements from the field. Any errors in these corrections over time will also affect the quality of change maps. These corrections are time consuming and expensive, but critical in order to obtain valid change results.

The results of simultaneous change detection methods obtained using multispectral imagery can be difficult to interpret (Lunetta et al., 2002). The order of magnitude increase in the

dimensionality of hyperspectral data creates added complications with interpretation of these types of data. For example, distinguishing between change classes and land cover classes with 60 potential endmembers and all possible combinations of change would be difficult. The few studies that have used hyperspectral imagery for change detection typically used post-classification processing (i.e., Glenn et al., 2005).

If these inconsistencies can be minimized or eliminated, hyperspectral imagery could become a very powerful tool for large-scale (local to regional) ecological monitoring of landscapes where tracking change in vegetation assemblages or species is critical for interpretation. Recent ecological applications of single-date hyperspectral imagery have included invasive species studies, post-fire recovery analysis, fire fuels mapping, vegetation stress, etc. (see Chapter 2 and contained references). Adding a temporal component to these investigations will be invaluable for monitoring and investigating landscape dynamics at a fine scale, over small areas. A primary goal of this study was to evaluate temporal patterns in expansion and recession of leafy spurge over a 2-year period in THRO, to aid monitoring and management of the weed, and in particular, to improve the likelihood of early intervention. It was also hoped that these patterns could be used to assess the effect of different treatments that have been tested to control the weed. This study represents one of the first regional, multi-temporal hyperspectral analyses to be used for guiding land management decisions.

METHODS

It was unknown which change detection method would be most successful for leafy spurge temporal changes with this data set, therefore, both simultaneous processing and post-classification methods were investigated. Many of the processing algorithms in ENVI, including MNF transformation, require identical bandwidths to simultaneously process multi-date imagery, however. Direct simultaneous processing of the 1999 and 2001 data was precluded due to non-aligned band sampling between the two dates. This was due to modifications of the AVIRIS sensor between 1999 and 2001 that included shifting band positions by approximately 2.5-3.0 nm. The 1999 bands were re-sampled to 2001 to adjust bandwidths for simultaneous processing

of both data sets. This produced distortions in the 1999 spectra, however, that were significant enough to produce substandard map results. An interpretable map could not be produced with the re-sampled 1999 imagery, and it was assumed, therefore, that the results of any simultaneous processing of 1999 and 2001 data would also be un-interpretable. As a result, the change analysis was restricted to post-classification methods. Simultaneous methods could be pursued, however, if multi-temporal AVIRIS data were collected and compared for years in which the bandwidths were identical.

Two types of post-classification change maps were produced. The first depicts change between the hard-classified leafy spurge class between 1999 and 2001 (using the "binary" present/absent maps). The second map represents the difference in the leafy spurge matched filter images between 1999 and 2001. Because the matched filter DN is considered a good approximation of the fraction of a material within a pixel (i.e., relative abundance) it was hypothesized that this map would provide additional insight into the nature of the change in leafy spurge distribution by providing detail regarding the magnitude of the change, or whether the spurge fraction fluctuated between 1999 and 2001, even when no class change was indicated on the binary change map. This additional information on subtle land cover change (both within and between classes) could be valuable for an analysis of different spurge control measures.

BINARY CHANGE MAPS

The primary, binary maps of leafy spurge that were derived independently for 1999 and 2001 contained two vegetation classes, spurge present and spurge absent, and the masked, non-vegetated areas. "Spurge present" indicated only pixels in which spurge was the dominant fraction on the primary map. "Spurge-absent" indicated vegetation pixels that either did not contain spurge or spurge was present as a minor fraction. The change map was created by subtracting the 1999 map from 2001, with the results restricted to areas that mapped spurge in one or both years. This general change map displayed three categories of change: expansion (or change to leafy spurge); a stable, persistent class (no change in spurge); and elimination of spurge as the dominant component of a pixel (change from leafy spurge between 1999 and 2001). This thematic change map was restricted to pixels in which spurge mapped as the

dominant component in order to distinguish change in areas that mapped as spurge dominant in one year, and spurge as a non-dominant component at another time. This change would not be apparent if binary maps indicating the presence of any spurge within a pixel were used to construct the thematic change map.

Before differencing, the two binary maps were uniquely recoded for pixels that classified leafy spurge as the dominant component of a pixel, as well as for non-leafy spurge vegetation, and inert non-vegetated materials. Leafy spurge was coded 3 on the1999 map, and 30 for 2001; non-spurge vegetation was coded 2 for 1999 and 20 for 2001, and the non-vegetated regions were changed to 1 (1999) or 10 (2001). This coding strategy allowed the identification of which of the three classes was present in the original (1999) and final (2001) maps, in addition to the primary change category (i.e., change to, change from, or no change in spurge). In Table 7.1, for example, 27 (30 - 3) indicates that leafy spurge dominated a pixel in both 1999(3) and 2001(30), and no change occurred over the 2 years. Seventeen (20 – 3) represents areas that were dominated by spurge in 1999(3), while non-spurge vegetation dominated the same area in 2001(20), a change from spurge between 1999 and 2001.

On the binary change map (Figure 7.1) and in Table 7.1, the elimination of leafy spurge between 1999 and 2001 is indicated in blue; pixels that classified as leafy spurge dominant both years (i.e., no change in spurge distribution) are represented in green; and pixels in which leafy spurge mapped as the dominant component in 2001 but not 1999, indicating new infestations, expansion, or increased density of the weed between 1999 and 2001, are shown in red. Only the blue, green, and red change codes in the table were included on the change map. These represent the changes that involved spurge in either one or both years. The resulting map was restricted to changes and trends in the leafy spurge-dominant pixels only. The change image indicated either a decrease, increase, or no change in the distribution of leafy spurge as the dominant fraction of a pixel between 1999 and 2001.

The numerical codes were required to subtract the maps, but an additional code was assigned to the classes for clarity. Spurge was identified as "S"; non-spurge vegetation with "N";

and other, non-vegetated material with "O". The 2001/1999 letter codes were included in Table 7.1 adjacent to the corresponding numerical difference code.

30,3= spurge (S) 20,2= non-spurge vegetation (N) 10,1= other non-veg material (O)

2001 – 1999	01/99	2001 – 1999	01/99	2001 – 1999	01/99
30 - ***3*** =		20 - ***3*** = 17	N/S	10 - ***3*** = 7	O/S
30 - 2 = 28	S/N	20 - 2 = 18	N/N	10 - 2 = 8	O/N
30 - 1 = 29	S/O	20 - 1 = 19	N/O	10 - 1 = 9	O/O

Table 7.1. Codes for leafy spurge change map. The numbers in bold (3 and 30) indicate spurge pixels in either 1999 or 2001. Difference values indicate the type of land cover change between 1999 and 2001; blue (7, 17) indicates eliminated spurge between 1999 and 2001; green (27) represents areas of no change in spurge; red (28, 29) are areas of spurge expansion. These are identical to the color codes used on the spurge change map (Figure 7.1).

MATCHED FILTER ABUNDANCE CHANGE MAP

A second change map was created based on the differences between the matched filter images of the leafy spurge class from 1999 and 2001. Initially, fraction values for all non-masked, vegetation pixels from 1999 were subtracted from 2001 to establish the change in fraction for spurge. The results were level sliced into equal range categories to highlight the magnitude of the change. This yielded confusing results, however, because the magnitude of the temporal differences in leafy spurge fraction could be identical for both very low MF scores (i.e., pixels that would not map as spurge) and high-fraction pixels with strong, but slightly different spurge signatures and fractions between the two dates. Binary masks were created to isolate only pixels that mapped as spurge. These masks were created for both the 1999 and 2001 leafy spurge classified maps, and combined into a single mask that included all pixels that mapped as leafy spurge dominant in 1999 and/or 2001. The masks were applied to the fraction difference image to isolate and highlight the change in fractional abundance for pixels that mapped leafy spurge as the dominant vegetation.

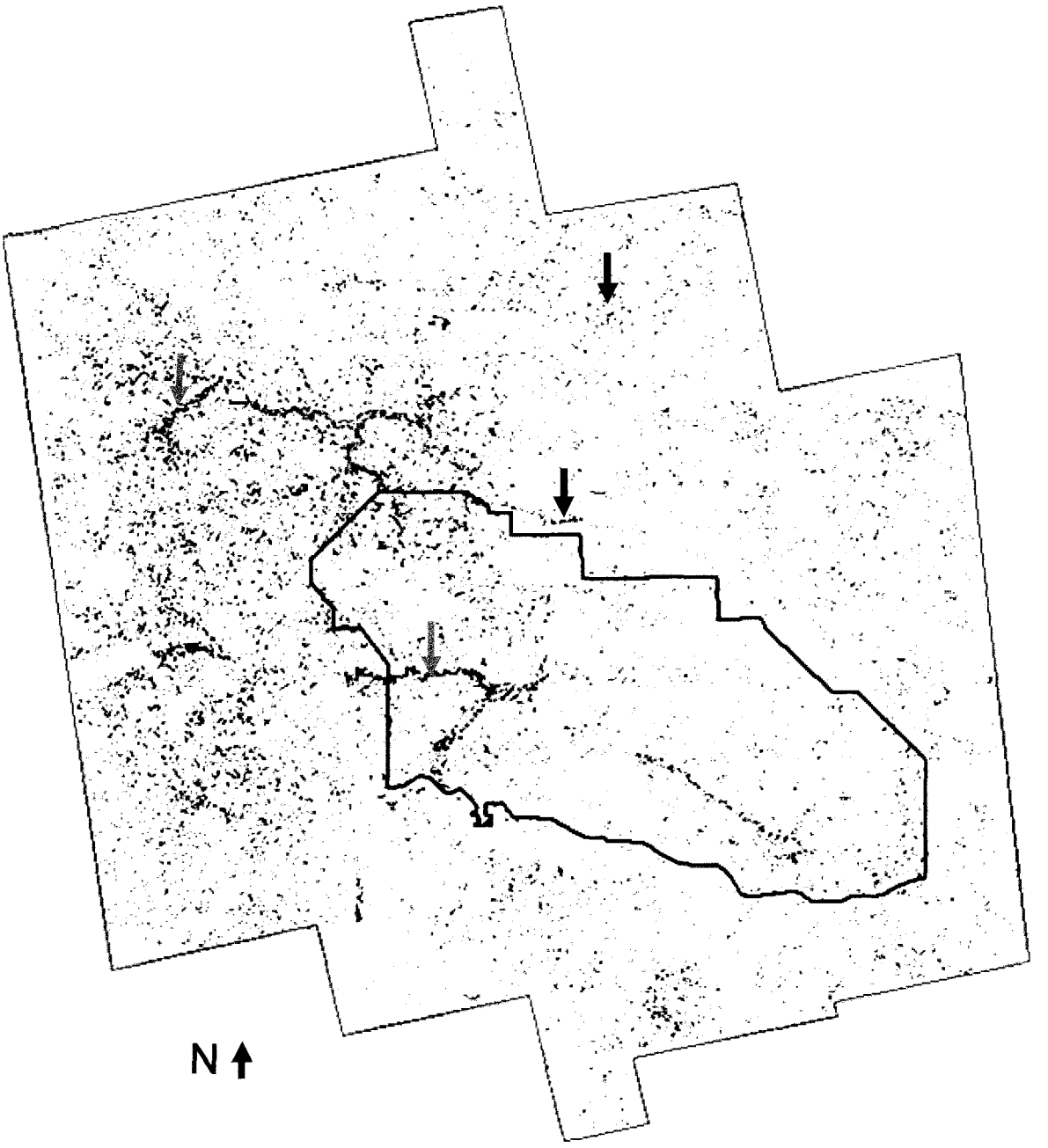

Figure 7.1. Regional change map: 1999 to 2001. Blue indicates areas classified as spurge-dominant in 1999 changing to other vegetation dominant by 2001 (i.e., reduction of spurge). Green shows pixels classified as spurge both years (no change). Red areas were classified as spurge in 2001, but not in 1999, indicating expansion of spurge between 1999 and 2001. The concentrated blue in the western third indicates significant reduction of spurge in this area between 1999 and 2001, a response to concerted control efforts in this area. Only the coincident area between the coverage of the 1999 and 2001 AVIRIS imagery was included in the change map. See text for discussion of areas highlighted with arrows.

RESULTS

BINARY CHANGE MAP

Several temporal trends in leafy spurge distribution, on both regional and local scales, were evident from the spatial patterns in the binary change map.

Regional trends. By 2001 there was a notable decrease in leafy spurge in the western third of the park, and in the grasslands west of the Little Missouri River, particularly within draws and drainages that had been heavily infested in 1999 (Figure 7.1, blue arrows). In this same region, however, there was an apparent increase in small, isolated, occurrences scattered throughout the higher elevation plateaus. This was particularly evident east of the Little Missouri River, to the north and northeast of the south unit of the park, again indicated by isolated, scattered pixels and small patches throughout the area (northeast portion of Figure 7.1). Several concentrated new infestations were evident as well, for example along Government Creek just north of the park boundary (Figure 7.1, red arrows). The green arrows in Figure 7.1 highlight persistent infestations that were concentrated in riparian areas.

The regional spatial trends in spurge infestation from 1999 to 2001 are evident in Figure 7.2, where the number of pixels classified as leafy spurge in each of the four flight lines was plotted, from west to east, for both 1999 and 2001. In 1999, the total area infested with spurge declined considerably from west to east, while in 2001 the spurge is more evenly distributed throughout the region. In the area covered by the westernmost flight lines, the spurge infestation had declined significantly by 2001 in the area where control efforts had been concentrated, whereas an expansion of the weed occurred in the eastern region over this same 2-year period, an area that had not been extensively monitored. Table 7.2 denotes the total area that classified as leafy spurge dominant each year, both within the boundary of the South Unit of THRO, as well as outside the park. An overall decline in the severity of spurge infestations throughout the region between 1999 and 2001 is indicated. The decrease within the park was estimated at 36%, and 41% in the surrounding region between 1999 and 2001. This corresponds to a decline from 6.4% of the total vegetation cover within the park to 4.1% of the total by 2001, and 6.1% down to 3.6% of the total vegetation cover outside the park boundary. These values are supported by the

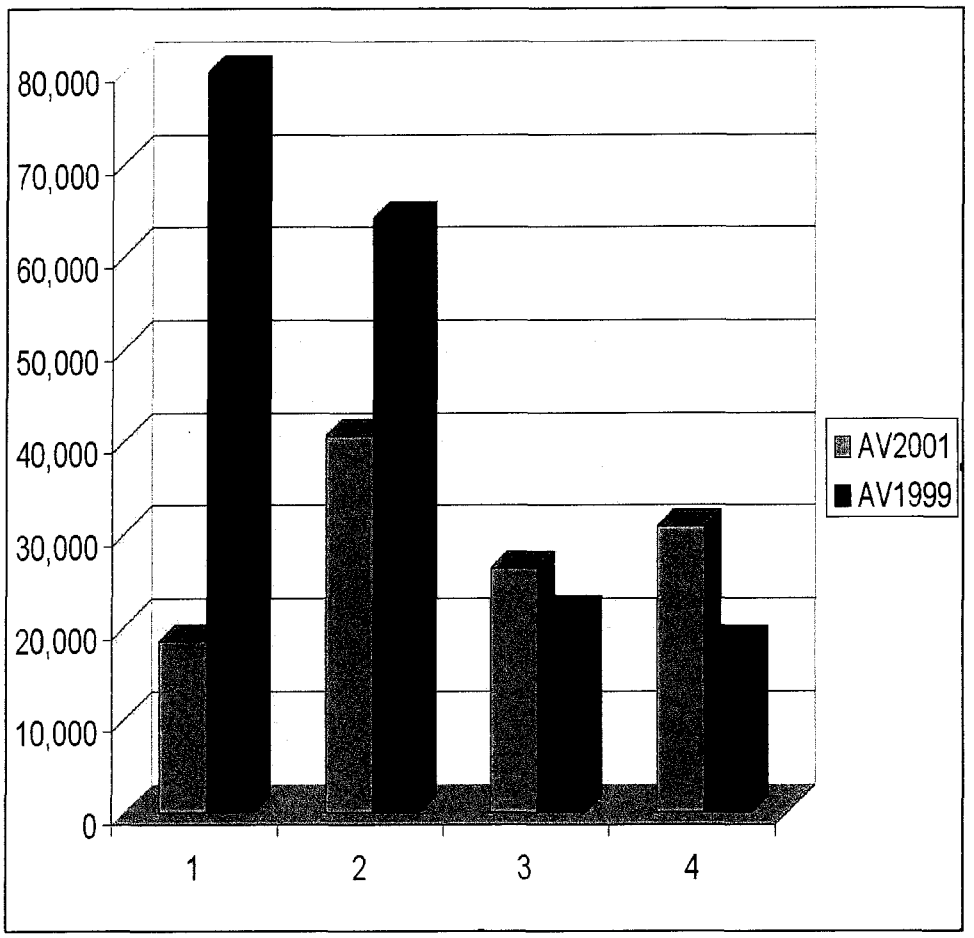

Figure 7.2. Change in spatial distribution and frequency of classified leafy spurge between 1999 and 2001: 1999, maroon; 2001, blue. Flight lines are consecutively numbered beginning with 1 on the west, and 4 the easternmost flight line. Reduction in the west and expansion in the eastern regions by 2001 is indicated.

	Inside park		Outside park	
	Leafy spurge (hectares)	Leafy spurge (% of total vegetation)	Leafy spurge (hectares)	Leafy spurge (% of total vegetation)
1999	834	6.4%	3369	6.1%
2001	520	4.1%	1859	3.6%
change	36% decrease		41% decrease	

Table 7. 2. Change in leafy spurge infested area: 1999 vs. 2001. Total area and the percentage of total area infested within the South Unit of THRO are and in the surrounding range/grasslands is indicated, along with the percent decrease between 1999 and 2001.

estimates of land managers in the region (S. Hager, personal communication, 2003). Although the overall change in total infested area cannot differentiate between a natural decline or response to control measures, nor indicate whether this was a gradual or abrupt process, it nevertheless indicates that leafy spurge populations decreased significantly in the region between 1999 and 2001.

Local trends. More localized temporal spurge patterns were seen as well. For example, Figure 7.3 D indicates that the Knudsen Creek drainage was very heavily infested in 1999, but the map suggests that by 2001 spurge was virtually eliminated (indicated by blue). This change was substantiated by field personnel. Further west within this same drainage, the western boundary of THRO divides an area within the park where dense leafy spurge has been eradicated (indicated by the blue area in Figure 7.3 D), while west of the boundary, the map suggests that untreated leafy spurge has persisted (green area, see arrow in Figure 7.3 D). Significant expansion and merging of spurge patches between 1999 and 2001 within the Government Creek riparian environment is indicated by the dominant red and isolated green pixels in Figure 7.3 C. This expansion was also verified by THRO personnel. Several large, persistent patches of spurge (e.g., dense green area in Figure 7.3 B) were indicated on the change map, which occurred in regions that were difficult to access and were not field checked in either 1999 or 2001. Figure 7.3 A-1 suggests that a number of isolated spurge patches adjacent to the river in an area that had been treated were eliminated by 2001, while a new zone of isolated, patchy infestations is indicated upslope, on the eastern side of the river (Figure 7.3 A-2). To the west of the river, minor expansion along the primary floodplain is suggested (Figure7.3 A-3), as well as within secondary drainages (Figure 7.3 A-4). In Figure 7.3 G, a new infestation surrounded by an area of no change in spurge, in turn surrounded by eliminated spurge is suggested by the central red core, rimmed with green, and then blue. This pattern could be interpreted as an overall migration and coalescence of an infestation into a more centralized patch over the 2 years. Although flea beetles were released in this area, spurge infestation had expanded by 2001 (S. Hager, personal communication). Figure 7.3 E shows a portion of the Little Missouri River floodplain where spurge has persisted, been eliminated, and newly

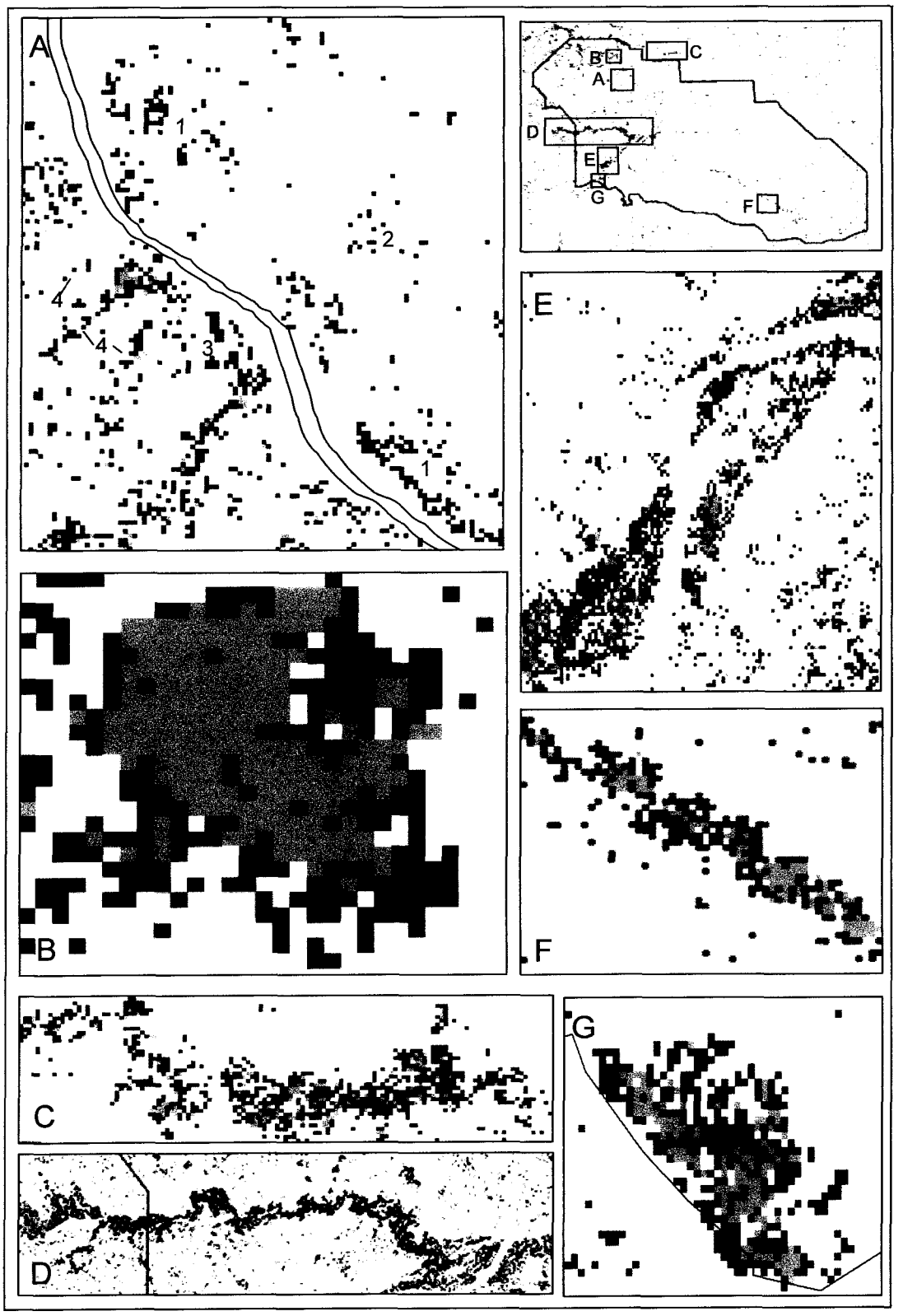

Figure 7.3. Localized change in leafy spurge. Top right frame indicates boundary of the South Unit and locations of the enlarged areas in A through G. Decline in spurge between 1999 and 2001 is shown in blue; persistent spurge (no change) in green; new infestations by 2001 shown in red. See text for discussion of individual frames.

established all within a local area. These changes were well documented on the ground in this area that has had been plagued with chronic, persistent spurge infestations. These infestations have been heavily treated with variable success. In Figure 7.3 F the elongated, parallel strips suggesting a decrease (blue), no change in spurge (green), and then increase in spurge (red) over a small area could be interpreted as a localized migration of the infestation to the northeast over time.

MATCHED FILTER ABUNDANCE CHANGE MAP

Subtracting the 1999 MF values from those of 2001 yielded both positive and negative fractions, suggesting both increased and decreased spurge fractions within mixed pixels between 1999 and 2001. Values closest to zero indicated minimal change in the fractional abundance of leafy spurge over the 2 years, while negative values indicated higher abundance in 1999 relative to 2001 (therefore a decline in spurge fraction by 2001); positive values suggest expansion of leafy spurge, indicated by higher fraction in 2001 than 1999. In Figure 7.4 A, the difference scores for all vegetation-dominated pixels are indicated. Figure 7.4 B is the same difference image, shown after masking out the areas that were not classified as leafy spurge in either 1999 or 2001. The most significant reduction in fraction is indicated by red, followed by orange, and yellow. Cyan and blue highlight the greatest increase in spurge fraction. Many of the high magnitude differences in fraction are only evident in the unmasked change image, in pixels that were not mapped as spurge in either year. These represent either a significant change in fraction that was nevertheless insufficient to dominate a pixel, or these may have been false positives for spurge that were removed from the primary spurge map during the infeasibility refinement (see Chapter 5). Smaller magnitude changes in fraction are shown in maroon (low positive) and dark green (low negative values). These represent fraction differences of 0.20 or less, indicating small but measurable variation over time.

The MF maps for spurge were not refined before creating the fraction change map, and included both feasible and infeasible "spurge" pixels. In general, this did not dramatically affect the map due to the small number of pixels that were excluded after the refinement; however,

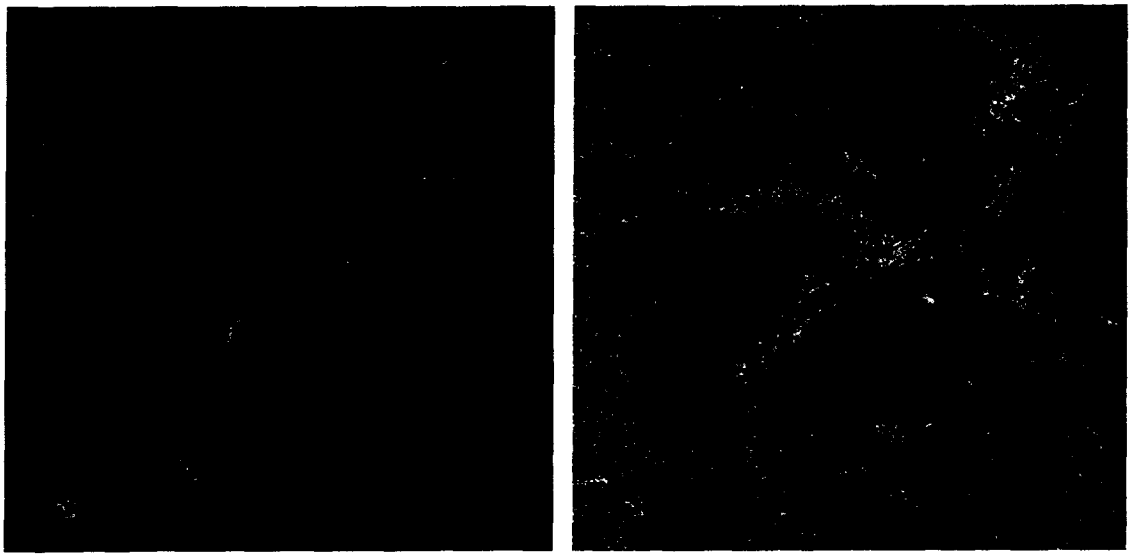

A. 1999/2001 combined mask B. No mask

Increase (listed highest to lowest):	Decrease (listed highest to lowest):
Blue	Red
	Orange
Magenta (light)	
Magenta (dark)	Green

Figure 7.4. Change in spurge fractional abundance, 1999 to 2001. In A, areas that did not classify as spurge dominant in either 1999 or 2001 are masked (black); unmasked fraction change map in B. Large increase in spurge fraction between 1999 and 2001 is indicated in blue and cyan; large decrease in spurge fraction by 2001 shown in red, orange, and yellow. See text for additional discussion.

some localized areas containing infeasible spurge in one or both years may be incorrectly included on the map of change in spurge fraction using this approach.

DISCUSSION

BINARY CHANGE MAP

Several regional temporal trends in leafy spurge distribution can be inferred based on the binary change map. For example, widespread new outbreaks of spurge to the north-northeast of THRO, as well as throughout the eastern two-thirds of the park are indicated by a dominance of scattered, small red patches in the area, and suggest that control efforts should be shifted to include these infested areas.

The dominant areas of decreased spurge (indicated in blue) in the western third of the park and national grasslands to the west indicate that concerted control efforts in this region have been successful. Infestations have been expanding to the east, however, where little effort has been expended on weed management.

Locally, an extremely heavy infestation in Knudsen Creek was successfully eliminated following intensive control efforts in the area (Figure 7.3 D). While the majority of the spurge along this riparian corridor within the park was eliminated, untreated stretches west of the park boundary shows areas of dense, persistent spurge (dense green patch), indicating that the weed has persisted along the creek in the areas where controls were not applied.

The expansion of spurge into the Government Creek riparian zone north of the park may also be related to absence of controls (Figure 7.3 C). This area is located on private land, outside the jurisdiction of federal management personnel, where no known controls had been applied before the collection of imagery in 1999 and 2001.

Several large patches of spurge on the change map indicate persistent infestations that should be targeted for localized, aggressive treatment (for example, the dense green zones in Figure 7.3, frames A, B, D, F, and G).

A considerable effort was expended by managers of THRO to establish a flea beetle (*Aphthona* spp.) population for biological control of leafy spurge within the floodplain of the Little

Missouri River in the park (Andrascik, 1994a, b). Figure 7.3 E shows that these controls were very effective in some areas (blue pixels); however, continual monitoring is required in these heavily infested and vulnerable areas because other patches have persisted (green), expanded (green and red), or large new infestations have become established (red). Areas that develop extensive, dense new infestations in spite of bio-control efforts within monitored zones often require more aggressive chemical treatment.

Some of the localized change indicated on the binary change map is misleading, and should be interpreted cautiously. For example, the apparent migration of spurge that is suggested in Figure 7.3 F is more likely due to registration shifts between dates, the result of poor image-to-image registration between the 1999 and 2001 imagery in the area. The infestation is believed to be a static, persistent zone of leafy spurge. Initially, this area was believed to be free of spurge, and the map was considered incorrect (S. Hager, personal communication, 2002). A ground survey found that the area was densely infested, however, and an aerial spraying campaign was initiated over this infestation, based in large part on these AVIRIS maps.

MATCHED-FILTER ABUNDANCE CHANGE MAP

Theoretically, a map of the change in fractional abundance over time should allow more detailed analysis of subtle spectral changes between dates. For example, within the "no change" class based on thematic maps, the land cover fraction could be identical over time, or there may be a trend toward higher or lower leafy spurge density (or fraction), based on the difference between the matched filter scores. These changes in fraction will not be detected in a thematic change map that only indicates change in presence or absence of spurge as the dominant component of a pixel.

Low magnitude differences in fraction, shown in maroon and dark green (Figure 7.4), are more difficult to interpret than the high magnitude, obvious changes. For example, these lower values may be within the range of natural species or phenological variation, or within the change noise, and therefore not a clear change in fraction. Alternatively, these could represent real, but subtle variation in the fractional abundance of spurge between 1999 and 2001. Reference data was insufficient to distinguish between these options, however.

Some areas that indicated a significant change in fraction corresponded with the temporal change in the leafy spurge thematic class that was indicated on the binary change map. For example, the significant decline in leafy spurge within the Knudsen Creek drainage was also indicated by the fractional change map (Figures 7.3 D and 7.4); however, the greatest changes occurred outside the areas that were classified as spurge dominant, as indicated on the binary change map.

Other zones of apparent change in spurge fraction could be misinterpreted, however. For example, the cyan and blue regions highlighted in Figure 7.4 A suggest a substantial increase in the fraction of leafy spurge between 1999 and 2001. Field checks indicated that these areas contained no leafy spurge in 2001, but instead, a unique assemblage of exotic species that had been frequently confused with leafy spurge in early test maps. With the classified spurge mask applied, this area was eliminated from the fraction change map because it was not mapped as spurge-dominant either year. This supports the decision to apply the infeasible mask, even though some useful trends in spurge fraction within pixels classified as non-spurge vegetation could be eliminated.

The binary change map in Figure 7.1 shows many well-defined areas of change, yet on the masked fractional abundance map many of these areas would not be interpreted as zones of significant change in spurge fraction (i.e., these areas are dominantly within the low-magnitude increase level-slice category, shown in maroon in Figure 7.4). In spite of inconsistencies or confusion in the results from the fraction change map, it nevertheless provides additional data that contributes to change interpretation by providing information that is not apparent from the binary change map alone. In particular these maps provide information on changes in pixels that likely contained spurge, but not as the dominant component of a pixel. On the binary change maps no information is provided on fraction change within these pixels, only on the change in the material that dominated (i.e., the largest fraction) a pixel in a given year.

The fraction change map is considered a reliable measure of change between whatever pixels were aligned between dates; however, because of registration difficulties, it is likely not the identical areas on the ground that are being compared from one date to the next. The maroon

and dark green codes simply indicate that little difference in the leafy spurge fraction was calculated between 1999 and 2001, yet nothing is indicated regarding the initial relative size of the fraction (i.e., the individual spurge fractions could have been very high or very low). A dense infestation with little change could map with the same MF difference value as a very light infestation (i.e., a change from 90% to 80% will map the same as a change from 15% to 5%). Conversely, a change in fraction from 40% to 5% will appear as a dramatic change on the fraction difference map, but the individual fractions may still be lower at both 40% and 5% than another dominant species, and therefore, never map as spurge dominant, even though a significant change in the fractional abundance of spurge occurred between the 2 years. This phenomenon could explain the "high change" areas (red, orange, and yellow) in Knudsen Creek where a significant change in fractional abundance was indicated, but these areas were never classified as leafy spurge dominant.

The fractional abundance change map provides additional, but somewhat different information than the thematic leafy spurge change map, and is best interpreted in conjunction with the binary change map, as well as the individual spurge maps from 1999 and 2001. The density sliced primary (spurge dominant) and secondary (non-dominant spurge) maps supply information regarding density, the dominance of leafy spurge, and classification status. The binary change map provides information on regional and some local patterns of change in spurge, where it is a dominant (and therefore presumably dense or significant) component of a pixel. Pixel-to-pixel changes, however, are not reliable. The fraction change map provides information on relative differences over time, but nothing on the magnitude or value of the score (and therefore no information on the density of spurge). The synthesis and interpretation of the information provided by these unique change maps becomes complex. The fractional abundance change maps have the potential to be most useful in terms of evaluating possible subtle responses to different weed treatments (by providing the magnitude of the fraction change), but this will be difficult to unravel and analyze until registration problems can be resolved and reliable pixel-to-pixel alignment can be routinely accomplished.

PHENOLOGY

For the change analysis, it was assumed that the phenological stages were comparable between the two dates. The 2001 imagery was collected on June 21, within 2 weeks of the anniversary date of the 1999 collection (July 6). Although collection on the exact anniversary date was not possible, both data sets were obtained within the window of peak inflorescence that facilitates the location and identification of the spurge with remote imagery. The assumption regarding comparable phenology may be incorrect, however, because significant phenological variation can still be encountered in some species, when calendar anniversary dates are used rather than the "environmental year", or precisely matched phenological stage (Webber, 2001). Growing degree days (GDD) and accumulated precipitation (AP) are the primary factors affecting growth stage, but it is also affected by humidity, wind, and the rate and type of precipitation (Webber, 2001; Lillesand and Keifer, 2000). This information was not compiled for this project, and GDD and AP were not available for analysis.

Field surveys in 2001 and 2002 indicated that the phenological stage of the spurge varied through the region on a single date, depending on local environmental conditions (from pre-flowering stages to seed setting and approaching the post-flowering dormant period). Because of this, it was not possible to restrict the images to a single phenological stage throughout the region. The spectra from different stages within a single-date image could not be directly compared to evaluate possible seasonal phenological changes in spectra due to other confounding factors. These included soil type and exposure, spurge density, variation in intermixed species and plant litter, and differences in slope, aspect, and elevation. No information was available on the phenological variation in spectra within a single infested patch throughout a season. Ideally, isolated patches should be monitored throughout a season to track spectral changes that occur with plant development.

CHANGE ACCURACY

The true accuracy for the individual date spurge maps was not determined unequivocally (see Chapter 6), and the proportion of error contributed by location versus classification is unknown. Location errors within this data set are believed to be significant, and likely are

negatively affecting individual date accuracies (see Chapter 6). Location errors between dates can seriously impact any spatial analyses that use these maps, especially change detection (Chrisman, 1989), and when location and classification errors are combined, there can be an interactive effect on overall error which will be compounded even further in a post-classification change map (Carmel et al., 2001). Standard post-classification change detection methods are known to be very sensitive to registration problems (Jensen, 1996). Exact pixel-to-pixel correspondence between dates was unrealistic. Even if the image-to-image registration could be perfected (on a pixel-by-pixel basis), the ground instantaneous field of view (GIFOV) for any given pixel will not be identical over time when an airborne platform is used for multi-temporal, hyperspectral data collection.

The impact of poor registration is most pronounced for small patches. Figure 7.5 shows diagrammatically the effect of a single pixel offset between multi-date images on the interpretation of change for two hypothetical spurge patches. Both polygons theoretically represent areas of no change that are simply offset between dates. This would be interpreted as an area from which spurge was eliminated, adjacent to a new infestation for the small patch (i.e., a migration) (Figure 7.5 B). In Figure 7.5 A the same relative shift would be interpreted as a small area eliminated, a small new infestation, but predominantly a patch that has not changed over time. The first interpretation would be 0% correct, while the second interpretation is 80% correct (i.e., 80% of the area is interpreted as "no change"). For the binary change map, spatial relationships need to be considered to arrive at the correct interpretation, with particular caution exercised around small, fragmented "change" zones. In spite of this, certain trends can be assumed in some cases, for example, the occurrence of many scattered new leafy spurge pixels in the absence of an equivalent number of eliminated pixels suggests that many new small patches have emerged.

Ideally, registration error for multi-date analysis should not be greater than 0.5 pixel (Lunetta, 1998). Although alignment varied throughout the images, local offsets up to five pixels were estimated between dates (see Figures 6.3 and 6.4). This is well above the suggested maximum for successful change analysis. Where the infestation or change in infestation spans a large area, it is possible to interpret overall temporal change patterns or trends in spite of

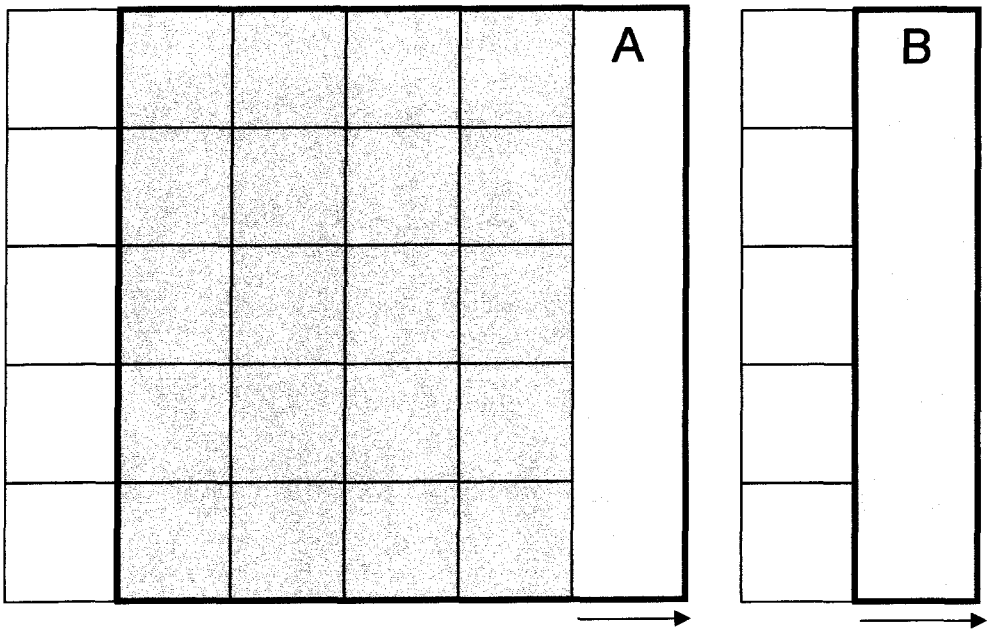

Figure 7.5. Theoretical effect of a 1-pixel offset between multi-temporal classified maps on interpretation of change. Green represents spurge in year 1, red is area classified as spurge in year 2. A would be interpreted predominantly as an area of no change, B could be interpreted as a migration of a patch over time. Due to registration problems between the 1999 and 2001 THRO maps, A and B would likely represent persistent patches of spurge over time, offset by misalignment..

registration problems. For small areas and isolated spurge pixels, however, it is difficult to interpret change accurately.

Different sets of field plots were used for calculating error matrices for the 1999 and 2001 maps. Because these were not coincident geographically over time (i.e., no change reference set was available), formal accuracy of the change map could not be determined using the standard change error matrix (Congalton and Green, 1999). A rough estimate could be calculated, however, based on individual date accuracies. The accuracy of the change is roughly equal to the product of the individual date accuracies (Yuan et al, 1998). Using the straight, point-based accuracy values for 1999 and 2001 (see Chapter 6), the estimated accuracy of the change map would be 18% (39% x 47%).

Although precise spatial relationships and accuracy of the change maps can be difficult to interpret due to imperfect alignment of images between dates, the area-wide estimate of change in total infested area over the 2 years should not be affected significantly by shifts in registration. Erroneous areas of expansion due to a shift away from an area with a stable persistent infestation would be approximately offset by a corresponding apparent reduction in spurge. In areas where spurge was mapped only in 1 year, the aerial extent will be correct, even when the geographic location is not. The image-wide percent change will be "accurate" (within the accuracy constraints imposed by the individual maps); however, localized spatial change patterns will often be incorrect.

FRACTIONAL ABUNDANCE CHANGE MAP

In addition to discriminating the change in dominant, thematic classes, imaging spectroscopy was used to discriminate subtle changes in fractional abundance of a "class" over time. These are not believed to provide accurate measurements on a pixel-by-pixel basis, but rather general trends within localized areas. With these maps, subtle changes in the density of a class were detected, even when the thematic class remained constant over time. While a fraction change map was created, the inability to perform precise image-to image registration throughout the images hampered efforts to analyze fractional change at the pixel level. Pixel-level change in abundance was difficult to interpret, as the largest fraction changes between 1999 and 2001 (for

spurge) often were not within areas that classified as spurge in either year (Figure 7.4). No reference data was available in any of these areas to establish the reason for the large difference in spurge fraction in areas that were not classified as spurge either year.

Maps of change in fraction would be particularly valuable for monitoring the effects of different types of biocontrol, or success of controls within different environments. These effects can be subtle and may require several seasons before dramatic, obvious differences can be seen. Because treatments were applied at a finer scale than the estimated registration error, these quantitative relationships cannot be analyzed without improved registration. In addition, calculated accuracies for individual dates were questionable, and the errors in individual date maps would be compounded over time in a with change detection, therefore the spatial analysis of the effectiveness of different treatments based on fractional abundance was abandoned.

The generalized binary change map does not include change information for pixels in which spurge was present, but in a smaller fraction than another material. For example, areas that appear to be new infestations in 2001 may have already been infested in 1999, but if the density was lower than another material in the pixel, it would not be mapped as spurge. Similarly, "eliminated" spurge may not be actually eliminated but rather reduced to a non-dominant fraction, which would also not be mapped as spurge, and areas without spurge either year may be undergoing a change in spurge abundance that would not be captured with the binary change map. Because of this, the secondary (non-dominant) spurge maps from 1999 and 2001 could also be used to produce a "secondary" binary change map for a more complete characterization of the spurge over time, in addition to fraction change maps.

SUMMARY

In spite of registration issues, the map of change in leafy spurge between 1999 and 2001 shows the general change in patterns of spurge that mapped as the dominant fraction of a pixel. While the binary change map summarizes regional patterns of change, some localized trends could be seen in the map as well, although the trends needed to be analyzed cautiously to avoid misinterpretation due to poor image alignment.

Overall estimates of the change in acreage of spurge as the dominant material in a pixel will be valid quantitatively, even though the individual maps are often spatially shifted. Erroneous patches of apparent expansion, the result of registration shifts between images, will be offset by a roughly corresponding area of erroneous elimination, (i.e., the errors related strictly to registration will cancel one another in the calculation of overall acreage change).

A qualitative review of the binary change map suggests that the regional trends, as well as some local trends, are generally accurate. The change maps indicate temporal patterns that are useful for planning management strategies both regionally and locally. The maps indicate some areas that have, in general, been successfully controlled with biological agents, as well as some that may require more aggressive biological or chemical treatments where spurge is advancing rapidly, and appears to be resistant to the controls that have been used. Several infested zones within THRO have been extensively monitored by park personnel and researchers who verified the accuracy of the general trends that were indicated by analysis of the multi-date AVIRIS imagery (G. Anderson, personal communication, 2003). Managers were sufficiently confident in the change map to consider additional monitoring and potential control efforts in the northeastern region, where small, dispersed, widespread infestations were indicated on the change map. This was an area that had not been mapped recently, and had not been considered problematic with respect to spurge infestations. In addition, an area that had been considered free of spurge was targeted for aerial spraying, to control a large, dense infestation that mapped as a persistent spurge patch on the change map, and was subsequently verified in the field. A detailed analysis of the effects of different treatments could not be completed, however, because the registration error was coarser spatially than the scale at which the treatments were applied.

Imaging spectroscopy has significant potential for applications-driven, temporal monitoring. For this to be used successfully, however, requires: 1) processing techniques that produce consistent results over time, whether processing single or multi-date imagery, or for change detection products based on these; and 2) precise registration of airborne scanner data. The processing method that was presented in Chapter 5 is a significant step toward standardizing multi-temporal, hyperspectral analysis. The problems with apparent change resulting from

processing differences were believed to be significantly reduced, while subtle differences in plant materials could still be detected. By producing consistent, repeatable results, comparable over time, it is possible to derive true change, rather than the composite effects of processing *and* actual land cover change.

A significant difficulty with this application, however, is that the detailed information on fractional abundance of materials that can be extracted with imaging spectroscopy cannot be fully exploited due to poor spatial correspondence between dates. Registration problems are believed to be the most significant impediment to detailed, pixel-level change assessment in this study. Accessible georectification and registration methods should be developed and distributed specifically for airborne imaging spectroscopy. With the advent of a high quality, satellite-borne hyperspectral sensor, registration difficulties will theoretically be minimized. In the short term, an alternative may be to use image-to-image registration of small subsets over critical problem areas, or areas of particular interest. More detailed, large-scale analyses of change are required to perform meaningful comparisons between the different treatments on a regional scale. This is a significant concern of land managers in regions that are plagued by extensive infestations of leafy spurge.

CHAPTER 8

VIEW ANGLE EFFECTS ON SPATIAL CONSISTENCY

INTRODUCTION

Bidirectional effects on apparent reflectance of surface materials are well known and are especially pronounced for vegetation (Schott, 1997). BRDF (bidirectional reflectance distribution function) models have been created for some species to characterize apparent reflectance variation for all possible combinations of view and illumination angle (Ranson et al., 1985a; 1985b). Variation in target brightness with change in view/illumination geometry for single wavelength bands have been examined in some BRDF studies, while others have included the full spectral range covered by the sensor (Demirican et al., 2000; Qi et al., 1995). These models can theoretically be used to correct apparent reflectance for the effects of varying sun/sensor/target geometry. Typically bidirectional studies have explored the effects of viewing geometry on derived structural and biophysical parameters, for example fractional cover, leaf area index (LAI), and fraction of absorbed photosynthetically active radiation (*f*APAR) (Asner et al., 1998; Chopping et al., 2003; Pinty et al., 1990). In general, these studies model and/or measure the reflectance of known materials, often using field-based (canopy/leaf level) goniometer measurements. Few studies, however, have quantified or correlated geometry-related changes in remote spectral response to changes in class distribution on vegetation maps (exceptions include Pellikka, 1996 and Kennedy et al., 1997). Directional effects on vegetation classification are often ignored because it is impractical to create a full BRDF model for every species or assemblage within a scene, particularly when the purpose of the mapping is temporal monitoring of land cover.

Precise temporal change maps that are produced from hyperspectral data will require a method to compensate for any bidirectional effects that are significant enough to result in different

class assignments for identical areas on the ground when viewed from different angles. The method that was developed and described in Chapter 5 successfully removed several of the interactive processing steps and threshold decisions that affect temporal and spatial consistency of maps between multiple flight lines collected on a single date and over time. A critical step for improving consistency both within and between flight lines for the THRO data was an empirical correction for variation in cross-track illumination based on a first order polynomial model of the cross-track illumination component of BRDF (see Chapter 5). This successfully corrected the effect of brightness variation across the sensor track, which was a significant component of the bidirectional reflectance variation in the data. The initial visual comparison of vegetation maps of identical areas produced from adjacent flight lines indicated good correspondence for most vegetation classes (see Figure 6.15), suggesting that the correction successfully minimized directional effects on classification.

When the maps were examined in greater detail, however, subtle differences in the maps were evident. The variation between the corresponding mapped areas was most apparent along the edges of flight lines, where differences in sensor view angles between flight lines were greatest. To determine the relationship between sensor view angle and the map inconsistencies, cross-track change in land cover class distribution across flight lines and between identical areas mapped from overlapping flight lines were analyzed in greater depth.

METHODS

The four overlapping flight lines from 2001 provided three different coincident areas that were evaluated for map consistency using the following procedures. The frequency of *all* land cover classes from flight lines 1 and 3 was compared for the intersecting areas between the flight lines. In addition, the variation in frequency of classified spurge was evaluated across track for two full flight lines from 2001, and for the three overlapping regions of the four adjacent flight lines. The spectral characteristics of pixels that consistently mapped as spurge across track throughout the overlapping areas of adjacent flight lines (i.e., classified spurge on both flight lines) were compared to the spurge pixels that were re-assigned to another class with increased

viewing angle (i.e., pixels mapped as spurge with low angle views, but other vegetation at high angles). Additional leafy spurge maps were created after second and third order polynomial cross-track corrections were applied to the data to evaluate changes in maps that were related to the cross-track correction model that was used. Accuracy values were calculated for the new maps. The cross-track frequency of classified spurge from the second order map was plotted and compared to the first order corrected map. Mean spectra were calculated and compared for the region of flight line 1 that overlapped with the adjacent flight line, and for a high angle subset from flight line 1 after first, second, and third order corrections were applied.

FREQUENCY: ALL CLASSES

The frequency of all land cover classes was calculated over the coincident areas between adjacent flight lines 1 and 3. Classified pixels were converted to regions of interest (ROIs) from which the number of pixels in each class was calculated for the coincident area of each flight line. Vegetation maps of the coincident regions from flight lines 1 and 3 were divided into western, central, and eastern thirds (Figure 8.1) to separate the coincident area maps into high/low angle pairs from the two flight lines to isolate these regions for calculation of land cover class frequencies when the data was collected from high versus low view angles.

FREQUENCY: LEAFY SPURGE

For the leafy spurge class the cross-track frequency across the full scene was calculated for flight lines 1 and 3 in greater detail by calculating the frequency for map subsets three samples (pixels) wide, running the length of the flight line (approximately 2400 lines for flight line 1 and 2200 lines for flight line 3). This produced roughly 200 subsets per flight line for which spurge class frequency was calculated. The total number of leafy spurge pixels in each subset was calculated using the ENVI ROI (region of interest) tool, then plotted by subset number, from west to east, across the entire scene for both flight lines 1 and 3 to evaluate trends in spurge frequency that corresponded to changing view angle. Leafy spurge frequency was also plotted for the coincident areas of flight lines 2 and 1, 1 and 3, and 3 and 4 from the three overlapping regions of the 2001 maps using similar 3-sample-wide subsets (ranging from 50 to 70 sets depending on the flight line pair).

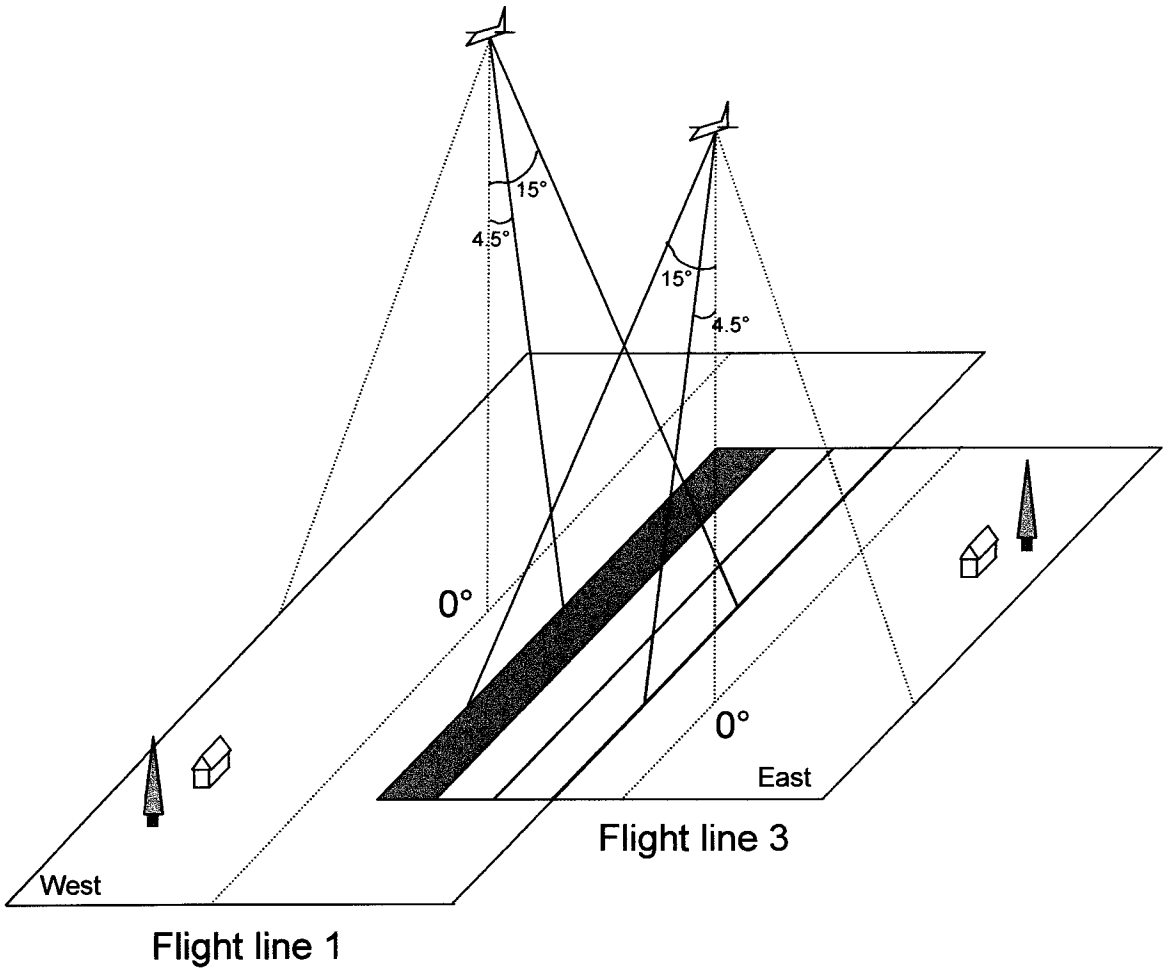

Figure 8.1. Angular relationships and coincident coverage between overlapping, adjacent flight lines. A low angle (4.5°) area from flight line 1 corresponds to the same area viewed at a high angle (15°) from flight line 3 (see magenta region), and vice versa (green region). Within the overlapping blue region, the view angles are approximately equal, but in opposite directions, for the two flight lines. The colored areas represent the three subsets of the coincident area that were isolated for frequency calculations and spectral comparisons of high/low view angle pairs. Diagram is not to scale.

COINCIDENT AREA MAPS

Leafy spurge maps from the western, central, and eastern subsets of the coincident area of flight lines 1 and 3 were isolated and viewed in pairs to compare the spurge classifications that were produced from data collected from different view angles. Figure 8.1 shows diagrammatically the relationship between the view angles and classified areas from adjacent overlapping flight lines, including the location of the three subsets that were used to compare the high and low angle portions of the overlapping maps (the three colored regions in Figure 8.1).

SPECTRAL COMPARISONS

The spectral characteristics of spurge pixels within the coincident area from flight lines 1 and 3 were compared to evaluate the change in spectral response with view angle that were associated with the differences in spurge classification between flight lines. Maps from the original first order corrected images were used for the comparison.

The spectral characteristics of spurge pixels when viewed from low (flight line 1) versus high (flight line 3) angles were examined using identical subsets from the western third of the coincident area of flight lines 1 and 3 (magenta region in Figure 8.1). Recoding and band math operations were used to isolate pixels that mapped as spurge on both map subsets, as well as pixels that mapped as spurge on one flight line, but not the second. Four mean spectra were calculated: the mean of all pixels that classified as spurge on flight line 1 (low angle) and flight line 3 (high angle); and two additional mean spectra from the pixels that mapped as spurge in the low angle view map, and the equivalent pixels that mapped as another vegetation class from the high angle subset. All four mean spectra were plotted together for direct comparison of the differences in spectral response curves.

SECOND AND THIRD ORDER CROSS-TRACK CORRECTION MODELS

In addition to the linear first order model, second and third order polynomial cross-track models were calculated for the original NDVI-masked image from 2001 and plotted against the uncorrected data to visually evaluate the fit of the different models. Eight randomly selected wavelength bands spanning the spectral range of the data were used to demonstrate the different models and their effects on cross-track response. These included: 15 (509 nm); 38 (702 nm);

57 (884 nm); 81 (1117 nm); 82 (1126 nm); 124 (1523 nm); 176 (2030 nm); and 210 (2369 nm). The cross-track response of the data was plotted after each of the corrections was applied to compare the effects of the corrections on cross-track response and to determine the most appropriate correction for the THRO data set. The second and third order corrections were applied individually to the data, which were re-classified using the procedure from Chapter 5 to produce two new spurge maps. Map accuracies were calculated using the identical basic assessment methods and reference data described in Chapter 6.

The cross-track frequency of leafy spurge from the second order corrected map was plotted as described above. The cross-track distributions of leafy spurge from the first and second order corrected maps were compared to assess change in frequency when the different corrections were applied.

Spurge map subsets (western, central, and eastern areas) were produced and compared for the second order, coincident area maps from flight lines 1 and 3 using the procedure described above for the original, first-order corrected maps (Figure 8.1).

The mean spectra for the leafy spurge class were computed for the area of flight line 1 covered by 4.5° to 15.0° view angles, after each of the three corrections was applied to the flight line. Three additional mean spectra (one for each correction) were calculated using a subset of the high angle edge of flight line 1 only (approximate view angles of 11.5° to 15°).

RESULTS

LAND COVER CLASS FREQUENCY CHANGES WITH VIEW ANGLE

If the map procedure produced consistent results across the board, similar frequencies would be expected for all classes because the identical area was mapped from each flight line. When land cover class totals were calculated over the full coincident areas of flight lines 1 and 3, nine classes showed similar frequencies on both flight line maps, eleven classes mapped with a distinctly higher frequency with flight line 1, and eleven classes showed a higher frequency when mapped from flight line 3. The frequencies of the remaining classes were very low and were not included in these counts.

When the class frequencies were compared for *subsets* of the overlapping regions that included only the low view angle area from one flight line and high angle view from the second (e.g., the outer 1/3 of a coincident area, as indicated by the green or magenta subsets in Figure 8.1), the class frequencies were more variable for most classes (Figure 8.2). Nearly all classes showed a change in frequency with changing viewing angle, demonstrating the sensitivity of plant reflectance to view/illumination geometry. Class frequencies increased with the lower view angle for the majority of the land cover classes (Figure 8.3).

BINARY LEAFY SPURGE MAPS AND FREQUENCY CHANGE WITH VIEW ANGLE

The binary spurge maps from the coincident areas of flight lines 1 and 3 were isolated and visually compared. Subsets of the western, central, and eastern sections of the coincident area are shown for the two flight lines to allow the spurge maps produced from high, moderate, and low view angles from each flight line to be compared (Figure 8.4). High angle views included the outer edge of a flight line up to 15° degrees from nadir, while low angles views of the coincident area were mapped at a minimum of 4.5° from nadir. The extent of spurge cover varied over identical areas when viewed from different angles, with more spurge mapped when the sensor view angle was small and closer to nadir (compare Figure 8.4 A versus B, and E versus F; A and F are the low angle views showing apparent heavier spurge infestation). When the view angle was approximately identical, the maps were very similar (Figure 8.4, C and D). The percentage of the total mapped vegetation that was classified as spurge for both flight lines, for each 1/3 subset, is listed below; color refers to the diagrams in Figures 8.1 and 8.4:

Western third (magenta): fl 1E, west 3rd (low) = 4.4%; fl 3W, west 3rd (high) = 1.5%

Central third (blue): fl 1E, mid 3rd = 2.7%; fl 3W, mid 3rd = 2.7%

Eastern third (green): fl 1E, east 3rd (high) = 1.0%; fl 3W, east 3rd (low) = 3.5%

When mean frequency was plotted for leafy spurge across track, the frequency decreased as the view angle increased out to the maximum view angle of the sensor (Figure 8.5 A). This effect was seen for both east- and west-facing maximum view angles, in data that had been corrected with the first order polynomial model. The same pattern of decreasing frequency as a function of increasing view angle was seen in five of the six high/low view angle pairs from

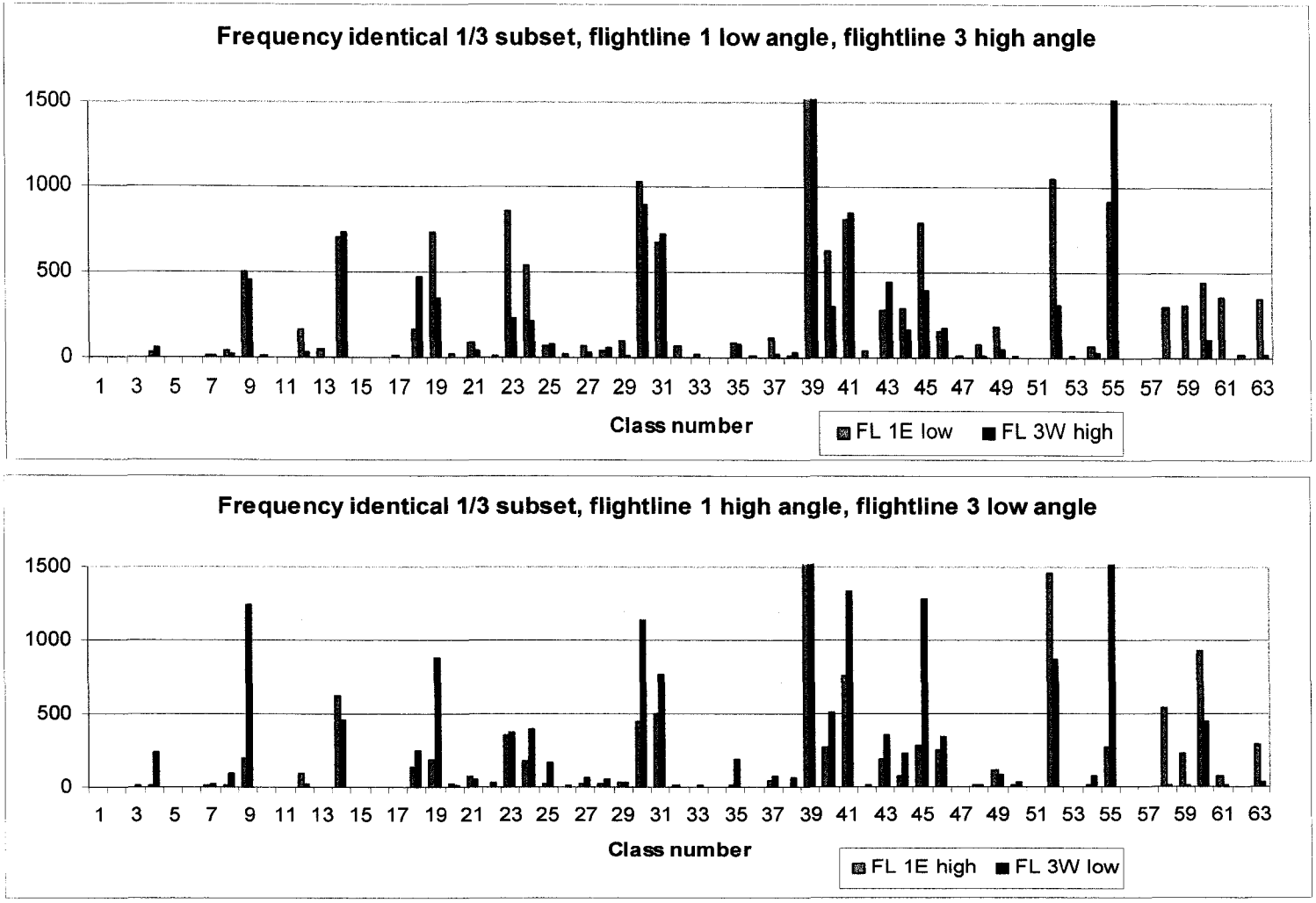

Figure 8.2. Class frequencies from high/low angle coincident area subsets. In A, flight line 1 is the *low* view angle (shown in blue), and the majority of classes show higher frequency when mapped with this low angle view than with the *high* angle view fro m flight line 3 (magenta). In B, flight line 3 (magenta) is the *low* angle view and the majority of class frequencies mapped with this flight line are greater than the *high* angle flight line 1.

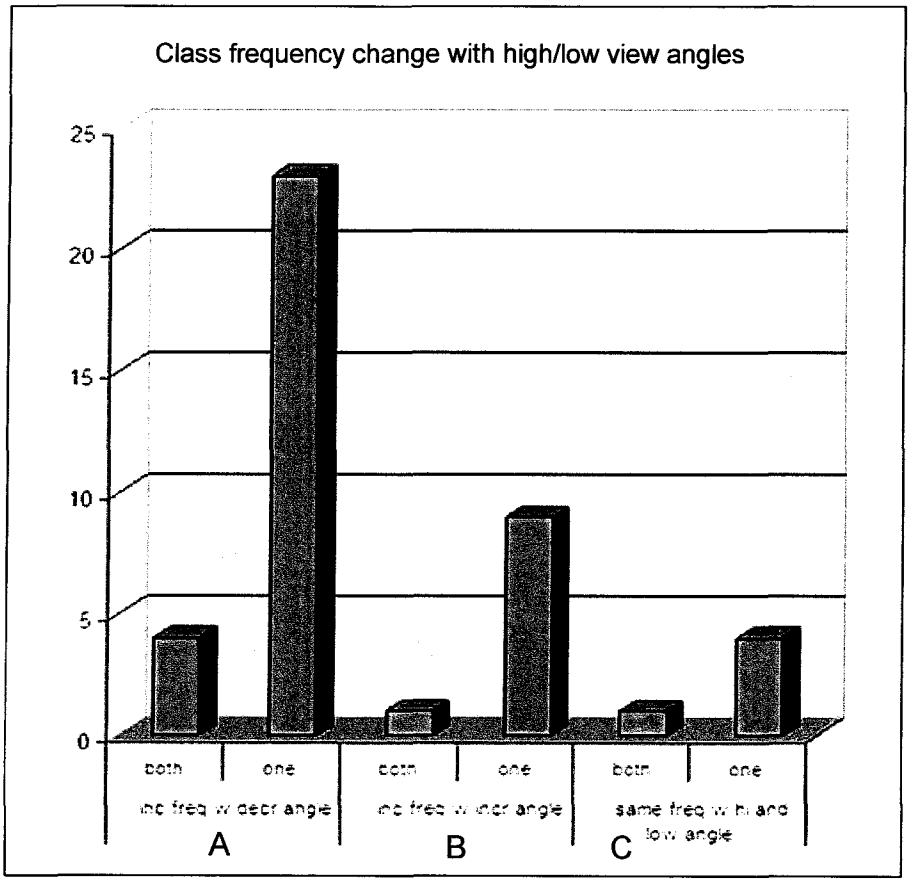

Figure 8.3. Class frequency change with high/low view angles. A: number of land cover classes showing increasing frequency with decreasing view angle with either one or both low view angles (from flight lines 1 or 3). B: number of classes showing increasing frequency with increasing view angle with either one or both high angle views. C: number of classes showing the same frequency with both high and low angles (no apparent relationship to view angle).

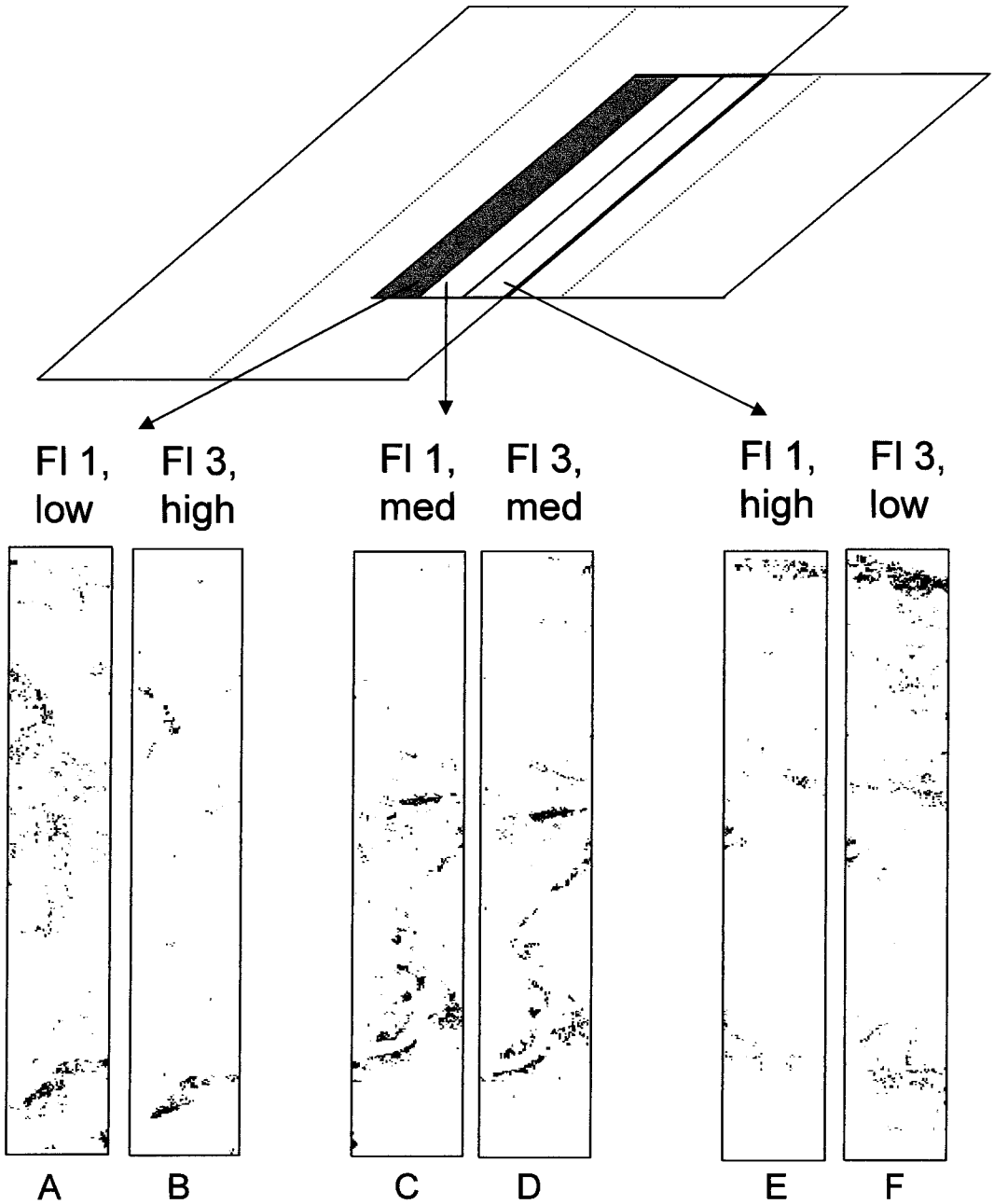

Figure 8.4. Differences between leafy spurge classifications due to sensor view angle. Each pair is an identical subset from each flight line map (from 2001). Colored strips at top represent the overlap between flight lines 1 and 3 that was mapped twice, using data from each flight line (also see Figure 8.1). More spurge is mapped with low than high view angles (A vs. B and F vs. E). The quantity of spurge that was mapped when the view angles were approximately the same for both flight lines is very similar (C vs. D, from the central overlapping region, shown in blue). Formal accuracy values were not calculated for the individual high/low angle subset pairs.

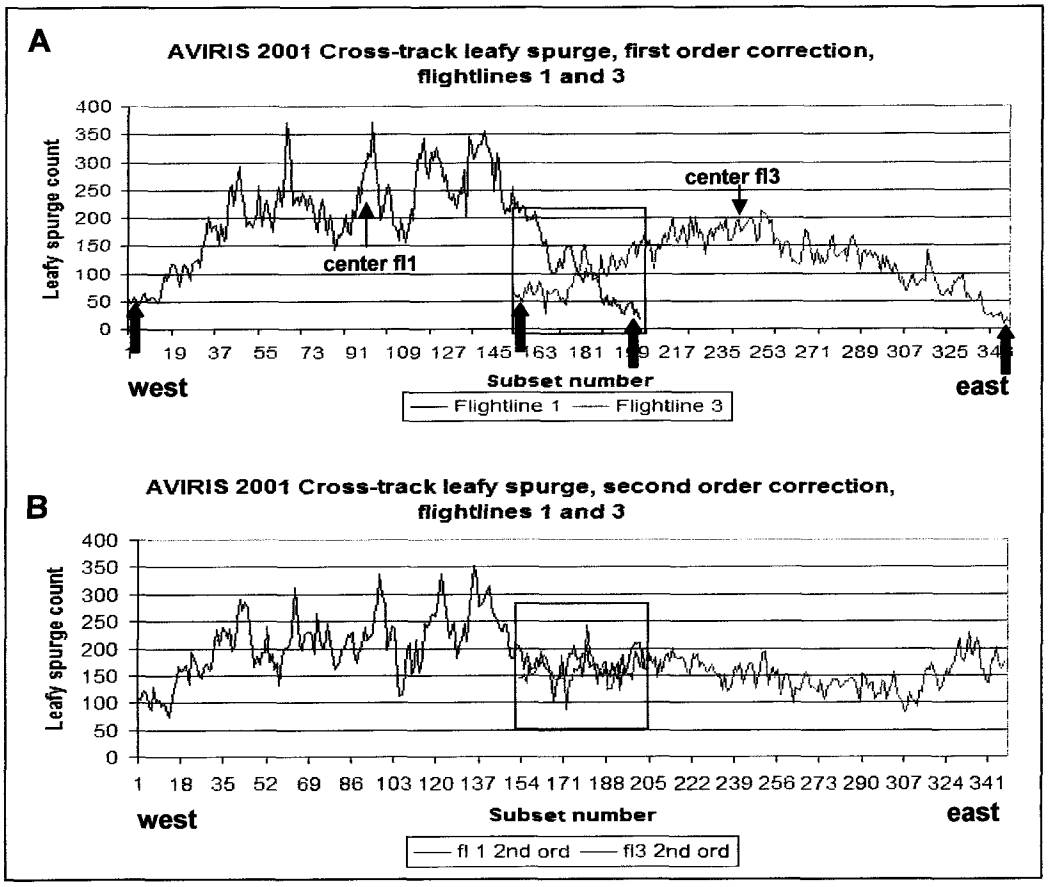

Figure 8.5. Cross-track frequency of mapped leafy spurge for flight lines 1 and 3; first order correction (A) and second order correction (B). In A and B, spurge frequency across the full width of both flight lines is shown. With the first order correction (A), low frequency is indicated at the 2 high angle edges of both flight lines (red arrows); with increasing frequency through the central portion of each scene. The distribution is more stable throughout the scene (and between the scenes) when the second order correction is used (B). The red boxes in A and B outline the coincident coverage area between the two flight lines.

the three overlapping flight lines from 2001 (Figure 8.6). In nearly every case, the view angle affect was seen, and was independent of view direction. The effects of varied illumination angle were eliminated, but not the effects of the magnitude of the view angle.

SPURGE SPECTRAL CHARACTERISTICS AND CHANGES WITH VIEW ANGLE

The average spectra from the westernmost subsets (i.e., the magenta region in Figure 8.1) of the coincident maps from flight lines 1 (low angle) and 3 (high angle) are plotted in Figure 8.7. Only pixels that classified as spurge in both flight line maps were included in the mean spectrum calculations shown in Figure 8.7 A. The high angle average spectrum shows somewhat shallower absorption features and slightly higher apparent reflectance in the visible, NIR, SWIR I, and SWIR II regions. These spectral differences were insufficient, however, to change the class assignment for these pixels when viewed from a high angle. Figure 8.7 B includes the average spectra over the same region for pixels that mapped as spurge with the low view angle (flight line 1), but were *not* classified as spurge with the high view angle (flight line 3). Similar but more pronounced differences were seen between the mean spectra of these pixels, including higher brightness throughout the spectral range for the high angle pixels. The high angle chlorophyll absorption feature is shallower and brighter, NIR brightness is variable but higher throughout, with a slightly steeper continuum (dotted lines in Figure 8.7). The brightness was noticeably higher in both the SWIR I and SWIR II for the high angle spectrum. The four mean spectra were plotted together in Figure 8.8 to facilitate comparison of brightness differences. The mean spectrum for pixels that did not classify as spurge with the high angle view is identified on the figure. The more pronounced spectral differences that were seen with a high view angle were sufficient to place these pixels into another land cover class. The changes in spectral response described above showed wavelength-dependant differences in the magnitude of the brightness variation across the spectrum with increasing view angle.

CROSS-TRACK CORRECTION TESTS: SECOND AND THIRD ORDER MODELS

Because of the variation in land cover frequency, including the reduction in classified spurge that was seen at high view angles regardless of direction, the average spectral response across the scene, and the modeled cross-track correction that was applied to normalize it, were

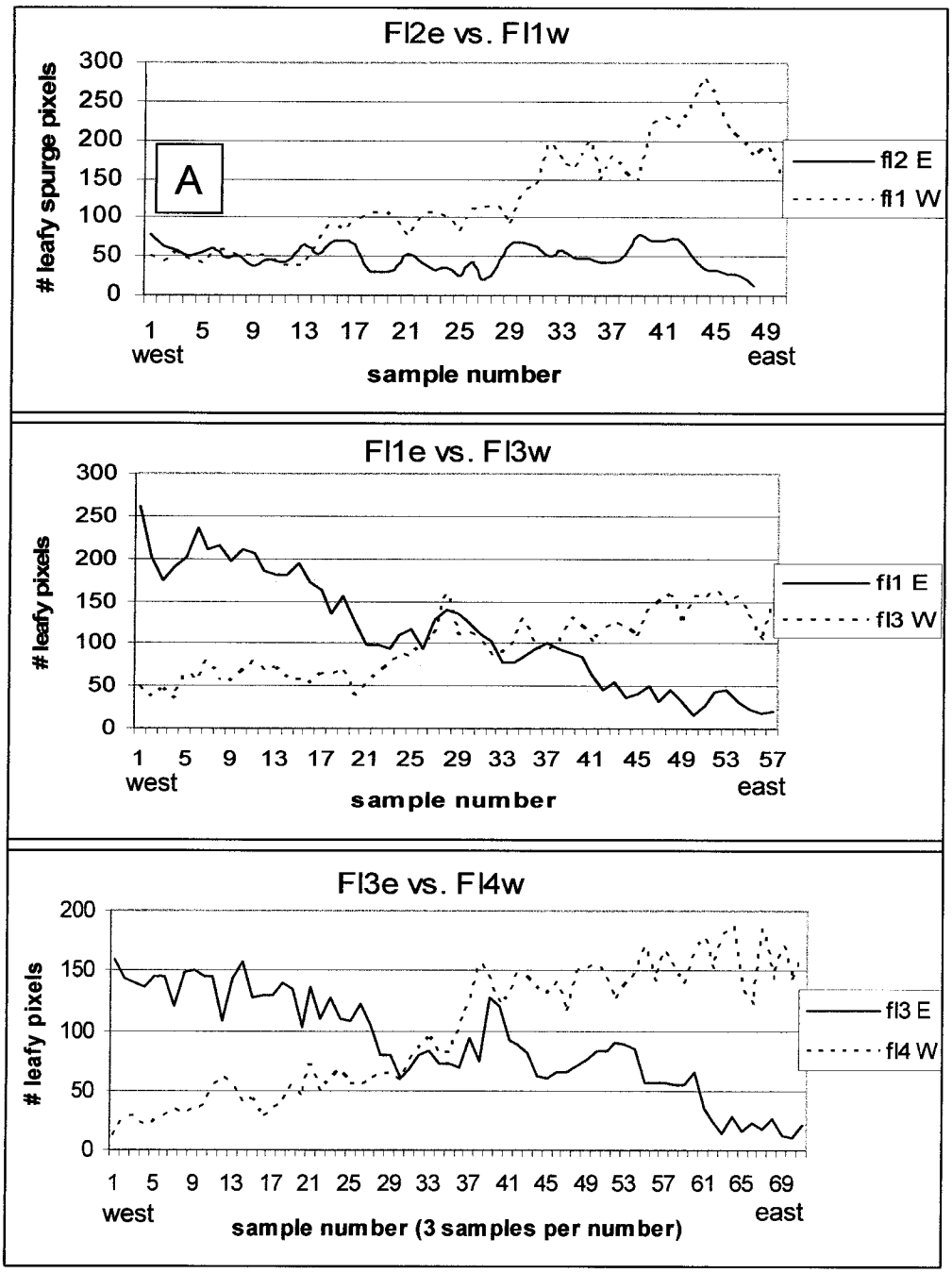

Figure 8.6. Spurge distribution from flight line pairs over three coincident areas from 2001 AVIRIS maps. The consistent influence of view angle on the frequency of classified spurge is shown. A (in top plot) shows the only case (out of the six high/low angle coincident regions-the western and eastern edges of each coincident area) where the spurge distribution was not clearly affected by viewing angle.

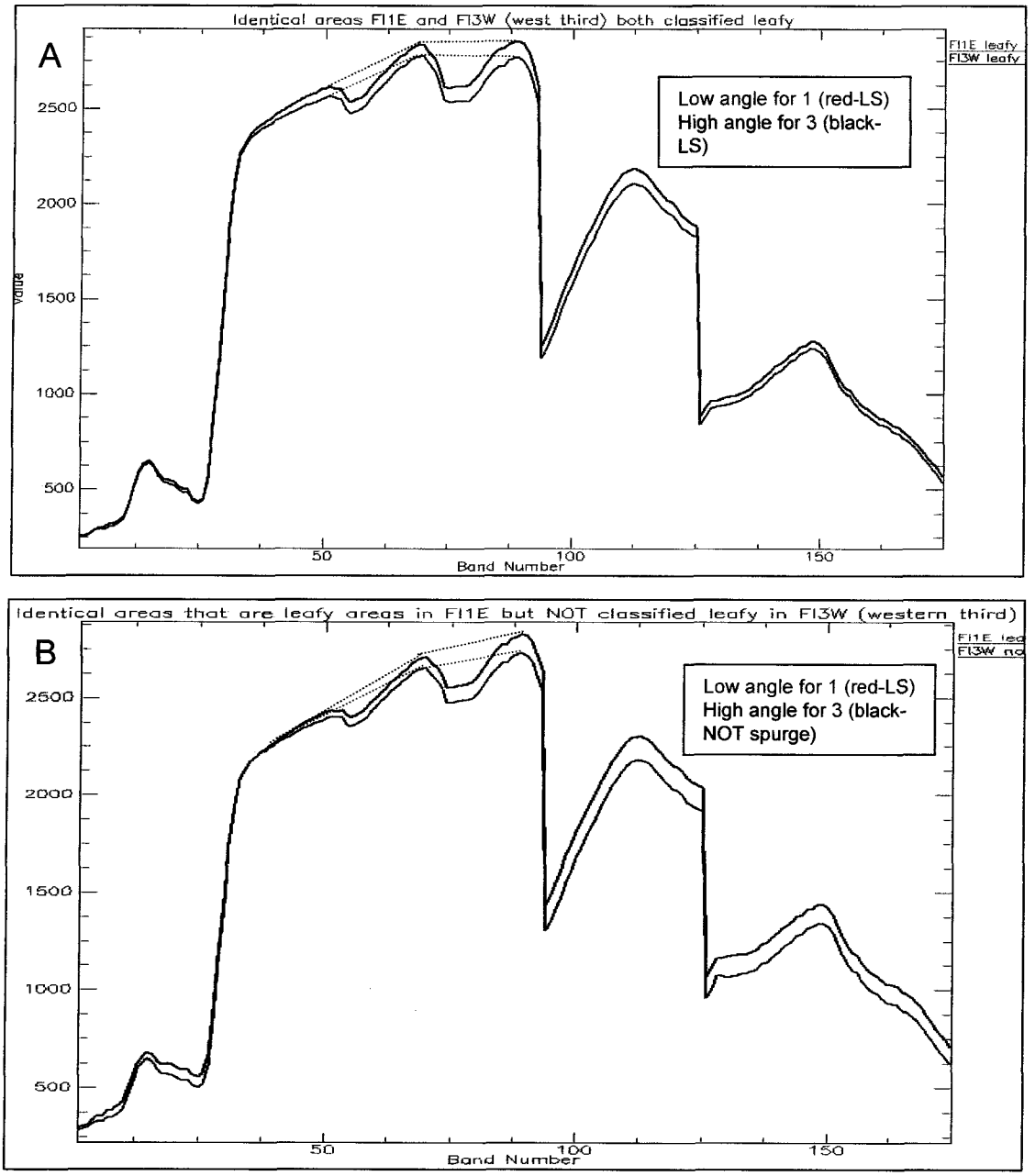

Figure 8.7. Mean spurge spectra from coincident high (flight line 3) and low (flight line 1) view angle areas. In A, mean spectra include only pixels that mapped as spurge with both high and low angle views. Both spectra are similar in the visible region, but show greater variation in albedo throughout the NIR, SWIR I and SWIR II. B shows the mean spectra from the same area for only pixels that mapped as spurge with the low view angle, but were *not* mapped as spurge with the high view angle. The high angle spectrum (black) shows a more pronounced increase in brightness in the SWIR I and II; variable, but higher reflectance in the NIR; and higher visible reflectance with decreased depth of the chlorophyll absorption feature. These differences were sufficient to place these pixels in another vegetation class when viewed from a high angle.

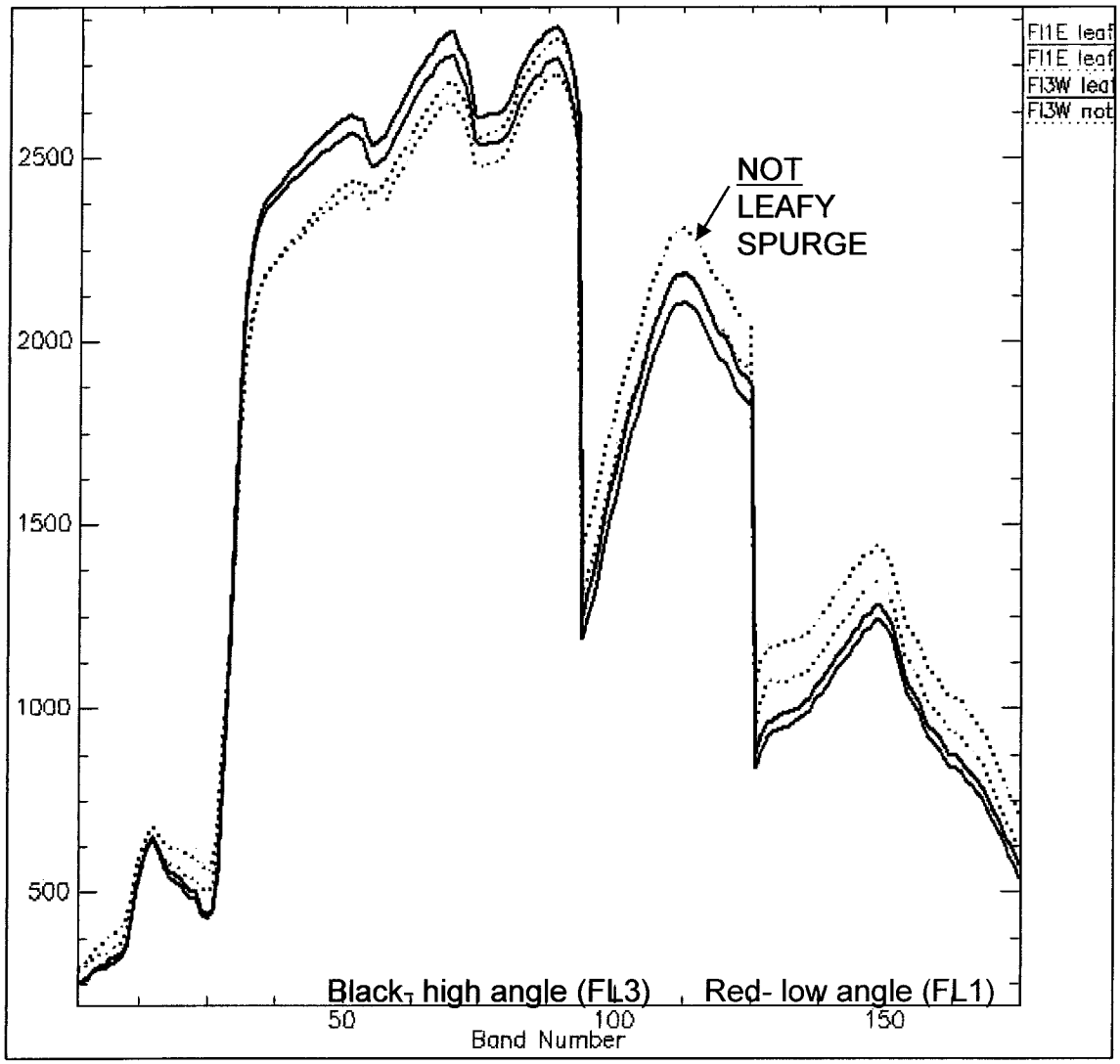

Figure 8.8. High vs. low angle "leafy spurge" mean spectra. Three of the four spectra represent the means of leafy spurge classified pixels; the black dotted line is the mean spectrum of pixels that did not map as spurge when viewed from a high angle (fl 3), but were classified spurge with the low angle view (fl 1). These are the combined spectra from Figure 8, A and B, with the solid lines from Figure 8 A (classified spurge from both flight lines); dotted lines from Figure 8 B (classified spurge only from low angle flight lines). In the non-spurge spectrum the shallower chlorophyll absorption feature, lower NIR brightness, higher SWIR I and SWIR II brightness, and lignin/cellulose features in the SWIR II region resulted in assignment of this set of pixels to another class when mapped from a high view angle.

re-examined in greater detail to determine whether the view angle effects on classification could be minimized or eliminated by applying a different model of the cross-track spectral response.

The first order modeled response across the scene initially appeared to be a good fit to the actual cross-track response. This was based on evaluation of the cross-track response of several randomly selected visible and NIR (near infrared) bands with the corresponding modeled response. In the sampled bands, the average cross-track response varied linearly, and the first order polynomial model (a linear function) appeared to model the response correctly (i.e., Figure 8.9, bands 15, 38, 57, 81, 82). When the actual and modeled responses were examined in greater detail and over a broader range of wavelengths, it was apparent that although the change in response in the visible and NIR wavelengths was linear throughout much of the scene, some dampening of the rate of change in brightness toward the edges of the flight line occurred (i.e., circled areas in Figure 8.9). In the SWIR I and SWIR II regions this was more pronounced, and the response was non-linear across most of the scene (Figure 8.9, bands 124, 176, and 210). The linear polynomial model was a poor fit for these wavelength bands. Second and third order polynomials were calculated for the cross-track spectral response using ENVI, and the fit of the models improved (Figure 8.10). The higher order models also provided a better fit for the shorter, visible wavelengths bands. An advantage of the higher order cross-track correction models is that the correction is not constrained to a linear model for those wavelengths where the cross-track variation in reflectance is non-linear. A unique model is fit to each wavelength, and the cross-track responses can be more correctly modeled.

Model comparisons. The first, second, and third order corrected cross-track responses for all wavelengths were notably different from the uncorrected cross-track responses (Figure 8.9 vs. Figure 8.11). The directional gradient in spectral response across track (i.e., decreasing reflectance from west to east) was removed with all three polynomial models; however, some differences were apparent between the three corrected responses (e.g., see arrows in Figure 8.11). For nearly all wavelength bands, increased brightness was apparent at the high angle edges of the flight line when the first order correction was applied. With the higher order correction the response was more stable across track. The increased stability of the mean cross-

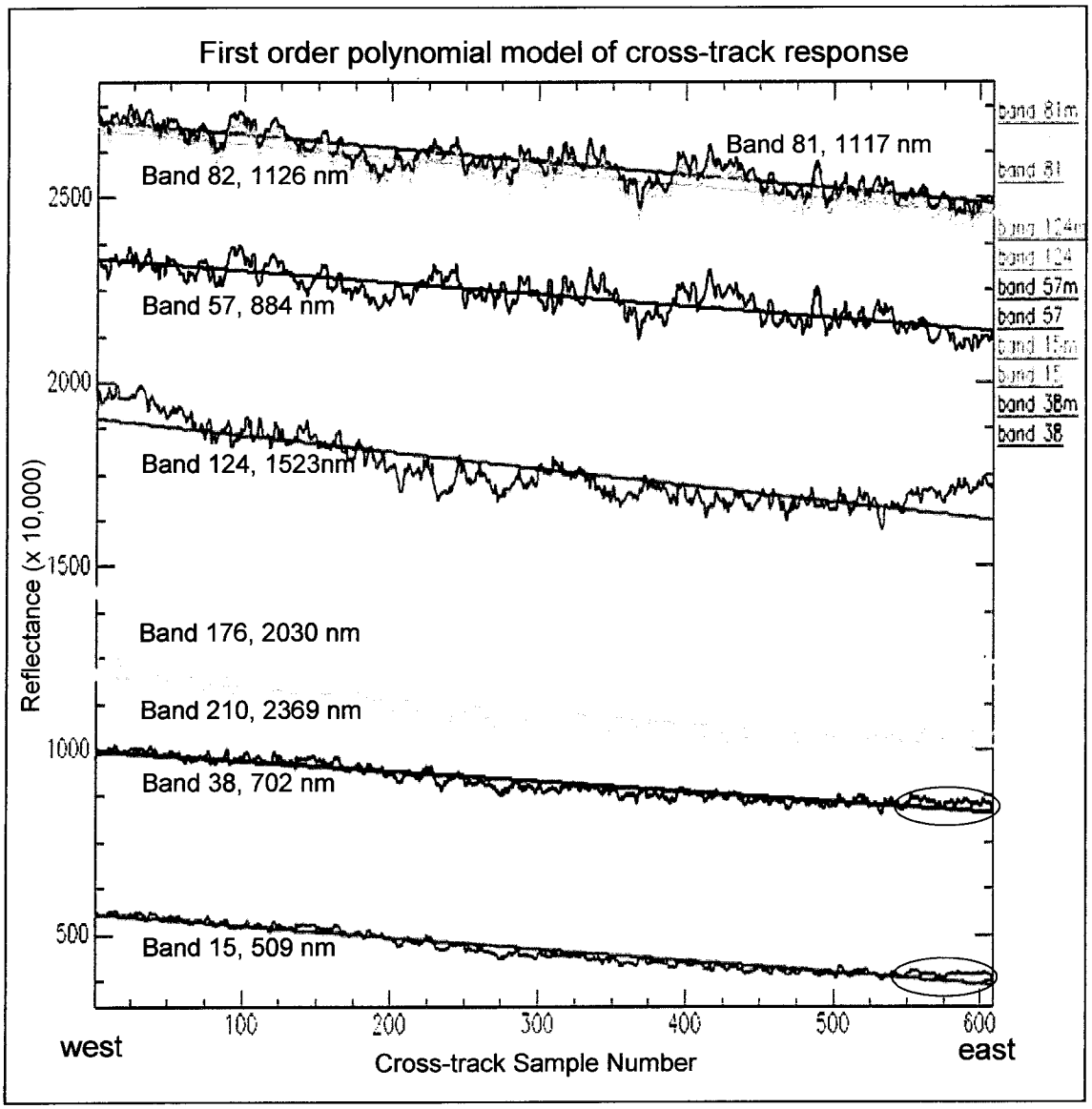

Figure 8.9. Modeled vs. actual cross-track spectral response for eight randomly sampled wavelength bands. The cross-track response for each band (irregular lines) and the corresponding first order polynomial modeled correction (straight lines) are indicated for each sampled band. Apparent reflectance decreases from west (left side) to east across the width of the flight line. The average response for each of 609 samples is plotted across the width of the full flight line. Initial comparison of the modeled and actual response from samples within the visible region (i.e., purple and blue bands 15 and 38) suggested the first order polynomial was an appropriate correction. Subsequent analysis of the response at longer wavelengths indicated the linear model was not appropriate for all wavelength bands.

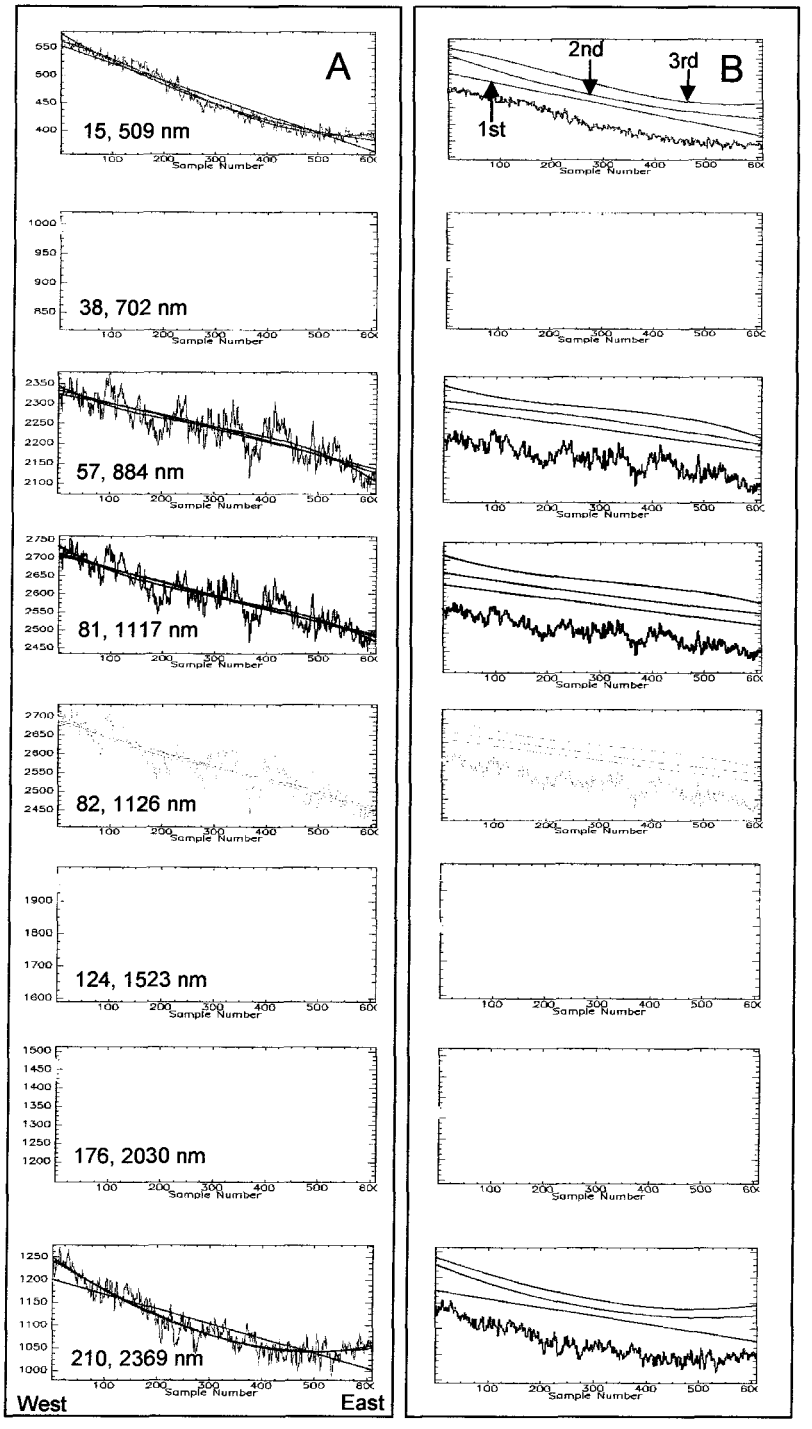

Figure 8.10. Cross-track response and first, second, and third order modeled response for each of the sampled wavelengths (A). Offset for clarity in B. Band number and wavelength are indicated for each sampled wavelength in A. The linear correction is appropriate for some wavelengths, but across the spectrum, the second or third order models will produce a better correction than the first order model. In B the graphs are arranged from bottom to top as follows: cross-track response; first order model; second order model; third order model. Y axes are reflectance x 10,000 in column A.

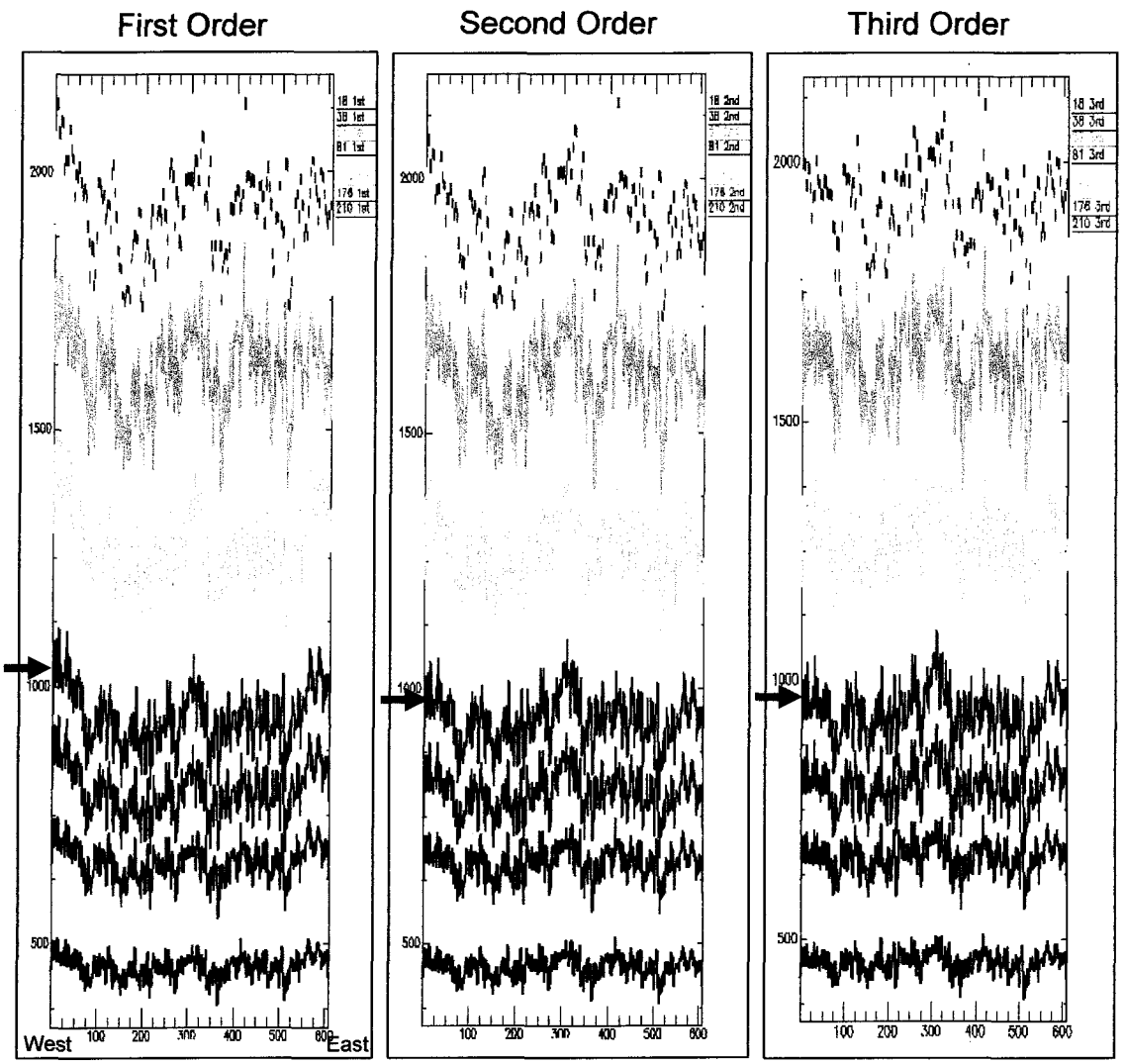

Figure 8.11. Cross-track spectral response for the 8 sampled wavelengths after first, second and third order corrections were applied. Some differences in brightness are evident (i.e., red arrows), predominantly along the high view angle edges of flight lines. The mean brightness across track is more linearly distributed with the second and third order corrections. The remnant spectral variation in the first order corrected data may account for the uneven distribution of classified spurge that was seen in maps produced with first order corrected data, but not evident in the second order spurge maps. The X axis is the cross-track sample number from west (left) to east across flight line 1; the Y axis is DN (brightness). Each color represents the average spectral response (brightness) from west to east over the full length of the flight line, for one wavelength band.

track responses for all wavelength bands with the higher order models indicated better corrections for geometric effects, which should result in more consistent class distributions throughout the entire image. In Figure 8.12, details of the differences in the first, second, and third order modeled cross-track responses for a single wavelength band (103, at 1313 nm) are shown. Greater fluctuation in the first order response is indicated with higher viewing angle near edges of the flight line. Second and third order responses vary somewhat at the edges of the flight line, where view angle differences are greatest, but are nearly identical across most of the coincident scene (i.e., central region in Figure 8.12).

Maps. New maps were produced after the second and third order corrections were applied to the original uncorrected data. Three map subsets are displayed for each of the first, second, and third order corrected maps (Figure 8.13) from areas where the spurge distribution was well-documented on the ground. The identical library was used for all classifications, and the spurge class is green in each map. The vegetation map produced with the first order correction is distinct from those produced after the second and third order corrections were applied. The second and third order maps were very similar.

All three maps were considered reasonable representations of leafy spurge, although the first order map omitted more low density spurge. With the second and third order corrected data, additional spurge was classified, and the spurge patches were a better match to the overlaid grid reference data (Figure 8.14). The grid coverage indicated any areas in which spurge was located within the measured grid network, and included very low density spurge and small spurge patches.

Accuracy. Accuracy assessments were run on the maps using the two-class confusion matrices discussed in Chapter 6. Accuracy values for the second and third order maps were essentially identical, with overall accuracy of 50%, 1 percentage point higher than the overall accuracy of the first order map (accuracies were calculated based on flight line 1 only). Second and third order spurge producer's accuracies were 1% *lower* than the first order map. User's accuracies for the spurge class, however, were 96% for both the second- and third-order corrected maps, an increase from 83% that was obtained with the first order correction. Overall,

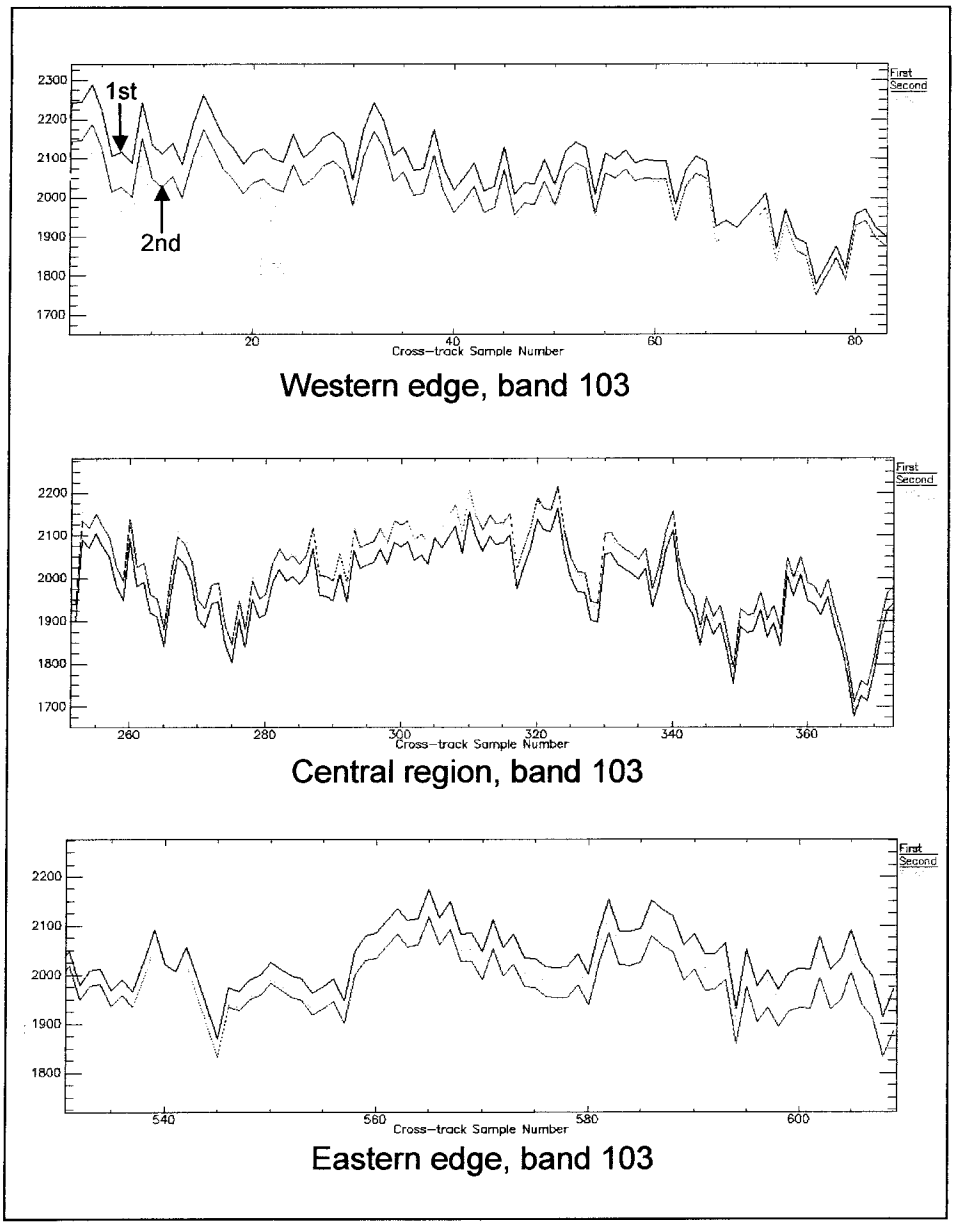

Figure 8.12. Cross-track brightness after first, second, and third order corrections applied; band 103 (1313 nm). Detail of cross-track response for band 103 from edges and center of flight line 1. Black is the first order corrected data; red, second order; green is the third order corrected data. Band 103 is a high amplitude (range of ~500), high reflectance NIR band. The first order response is higher near flight line edges, and lower through the central portion of the flight lines. Second and third order responses are similar through the central region but diverge near the high angle edges of the flight line.

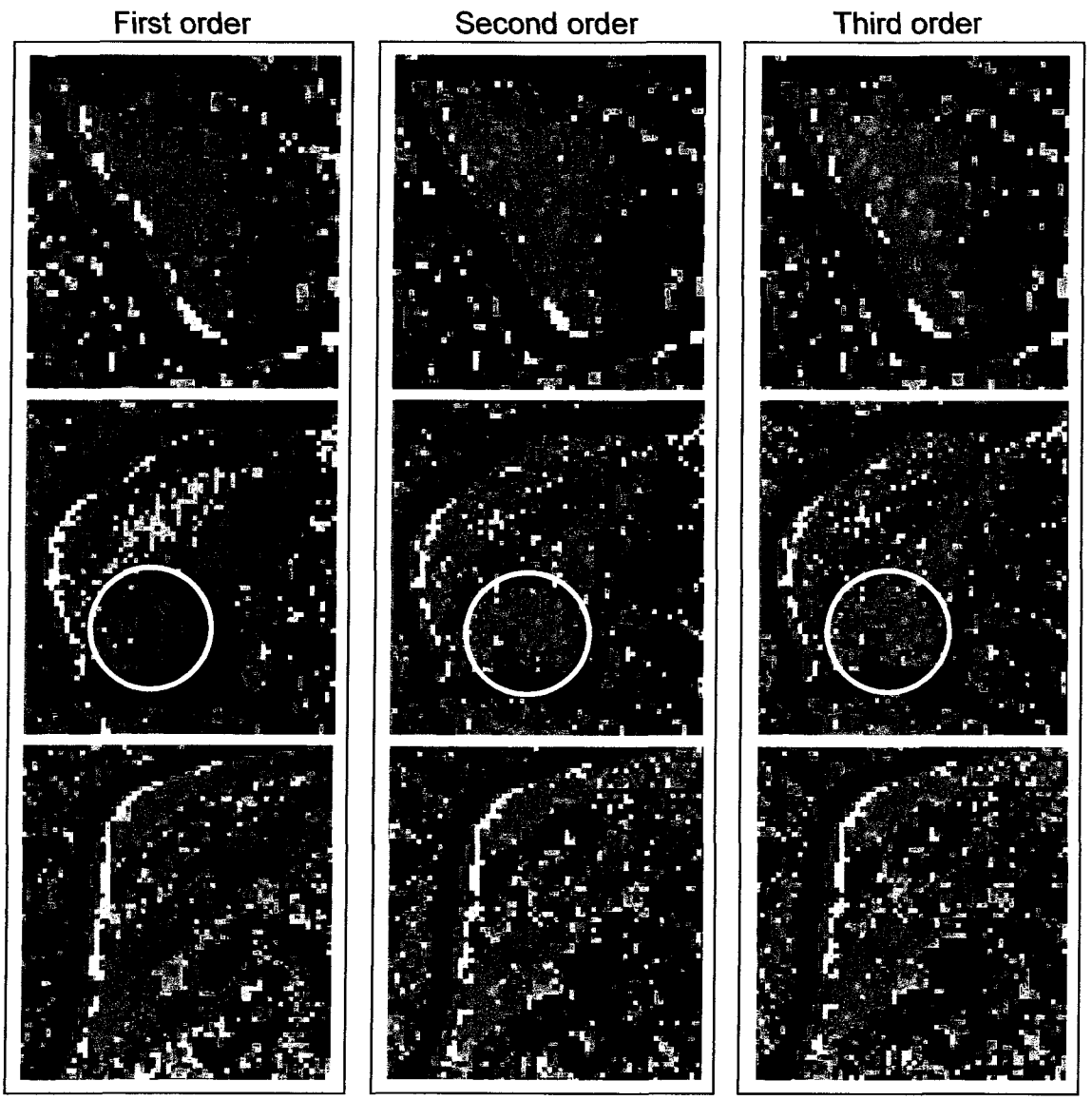

Figure 8.13. Cross-track polynomial correction comparisons for selected subsets from flight line 1 vegetation maps (1st, 2nd, 3rd order corrections applied). The first order map differs from the others, and has under-classified spurge somewhat (based on qualitative comparisons to field polygons and grids-see Figure 21 and circled areas above). The second and third order maps are nearly identical, and classified spurge matches field data more closely. The second and third order corrections appear to be interchangeable, and better than the first order correction.

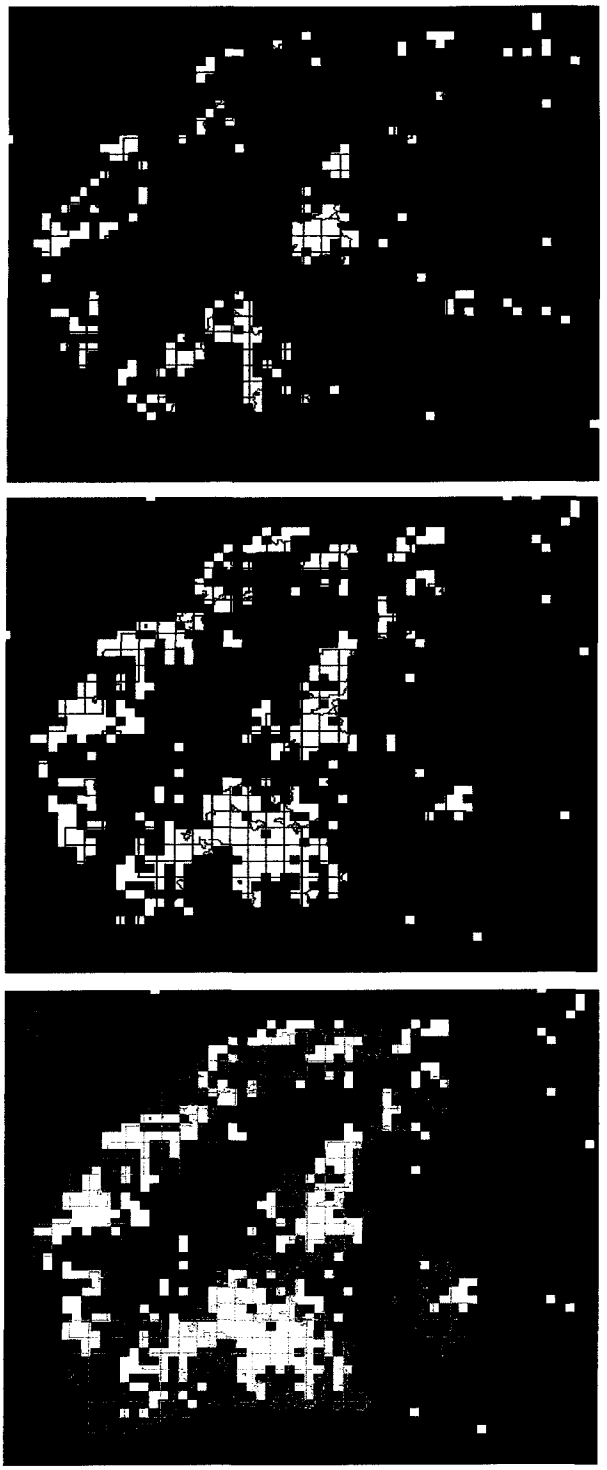

Figure 8.14. First (A), second (B), third (C) order corrected spurge maps (white) with overlaid field grids. Under-classification of spurge is indicated with the first order correction.

the second and third order polynomial corrections produced slightly more accurate maps based on the error matrices. The second and third order maps more accurately represented low density spurge (i.e., circled area in Figure 8.13, and Figure 8.14), but this was not reflected in the calculated producer's accuracy. The second and third order models appear to be interchangeable because the maps and accuracy results were nearly identical for the two corrections.

Classified spurge frequency. The average cross track frequency of spurge from the second order corrected map from flight line 3 (plotted across the full width of the flight line) was distributed more evenly than seen on the first order corrected map (Figure 8.15). The same change in frequency distribution is shown in Figure 8.5, where first and second order spurge frequencies are plotted across two adjacent flight lines. The reduction in classified spurge that was seen at high view angles with the first order corrected map was eliminated when the higher order correction was applied. When the spurge distribution over the overlapping region was plotted for second order maps from adjacent flight lines 1 and 3, the spatial distribution of the weed was more consistent between the high and low angle regions from the two flight lines (Figure 8.16 A versus B). The map subsets for the high and low angle views from the two flight lines were very similar as well after the second order correction was applied (Figure 8.17 A vwersus B, and E versus F).

Spectral characteristics. When the mean spectral response was calculated over the full coincident area for flight line 1, no significant differences were seen between the first, second, and third order corrected data (Figure 8.18); however, when only the outer (high angle) area of the flight line was used to calculate the average spectral response, differences were noted between the mean spectra depending on which correction was applied. The greatest difference was seen with the linear, first order correction (Figure 8.19). The spectral differences were subtle, but when the maps produced with the different corrections were compared, less low density spurge, and pixels with lower overall percent spurge cover were mapped with the first order correction. The relative spectral differences associated with the first order mean spectrum are similar to the differences seen for spurge when viewed from high versus low angle views.

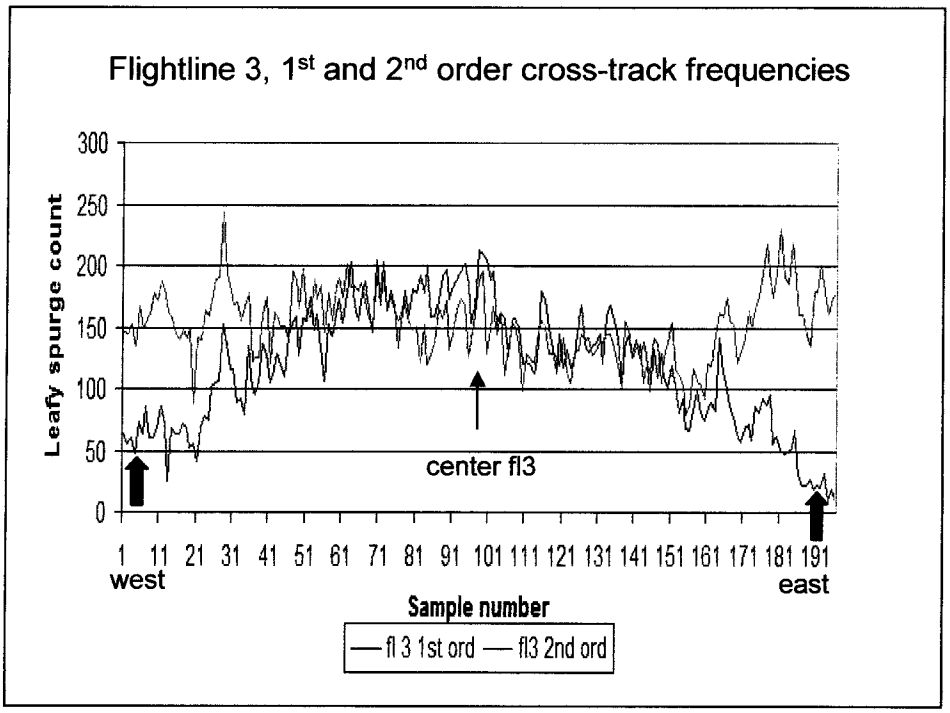

Figure 8.15. Cross-track frequency of mapped leafy spurge; first and second order correction differences, flight line 3. With the first order correction (blue graphs) lower spurge frequency is indicated at the high angle edges of both flight lines (red arrows), with increasing frequency away from the high angle edge of each scene. The distribution is more stable across the flight line when the second order correction was used (magenta). Plotted together, these emphasize the more even distribution of spurge when the second order correction is applied.

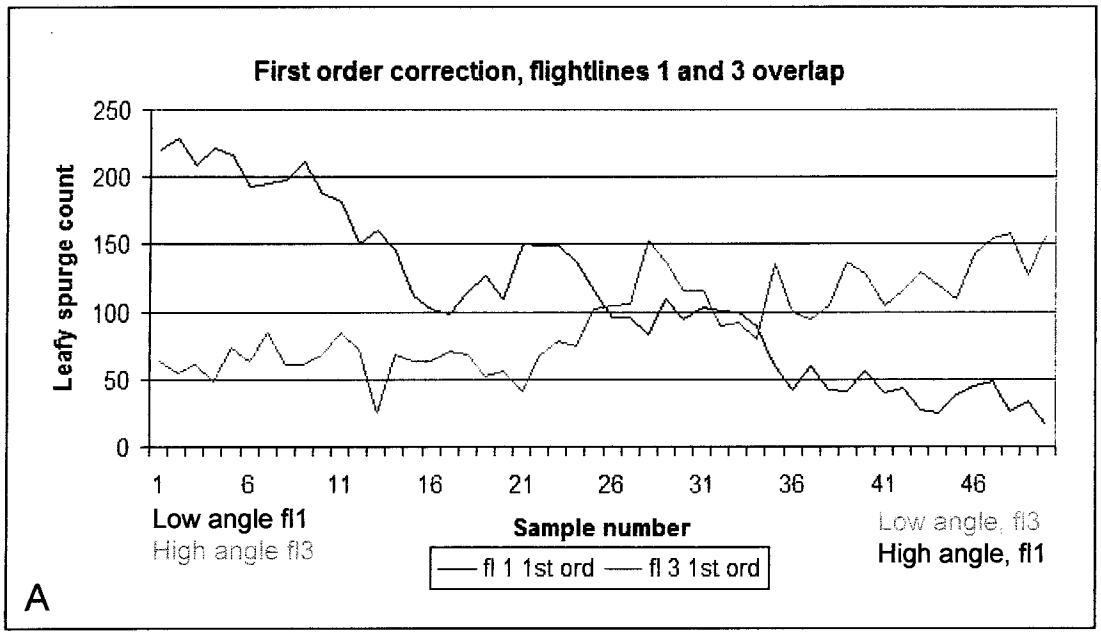

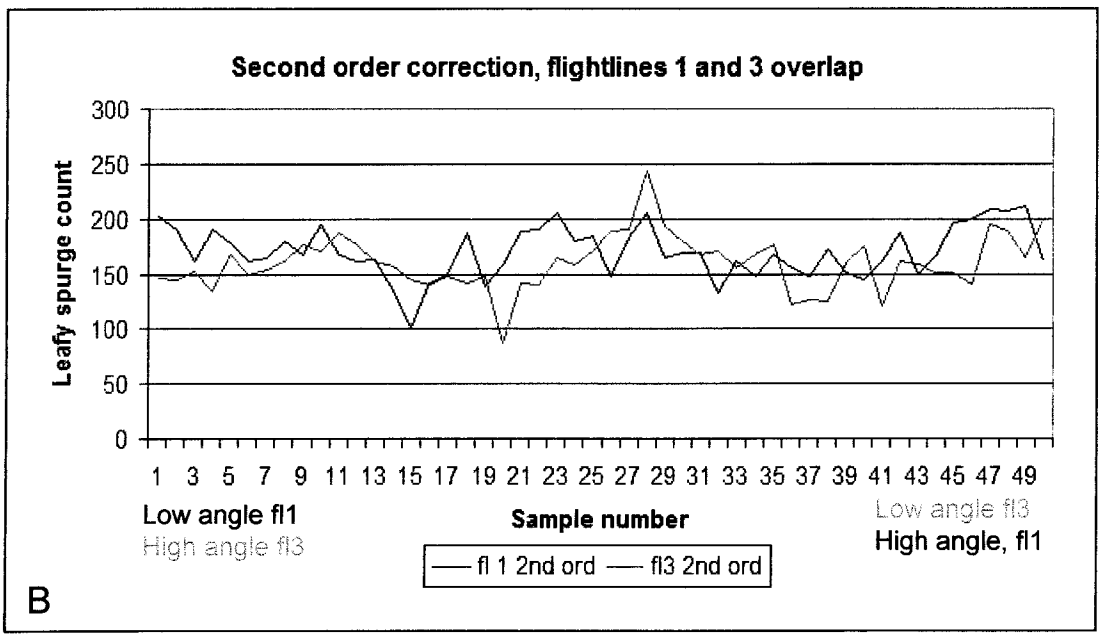

Figure 8.16. Change in spurge distribution with first and second order cross-track corrections from two flight lines across identical, coincident area. The first order map in A shows a decrease in spurge with increasing view angle. In B the distribution of spurge across the same area is shown for both flight lines after the second order correction was applied. The frequency of spurge mapped from the two flight lines is similar, and the affect of view angle has been eliminated.

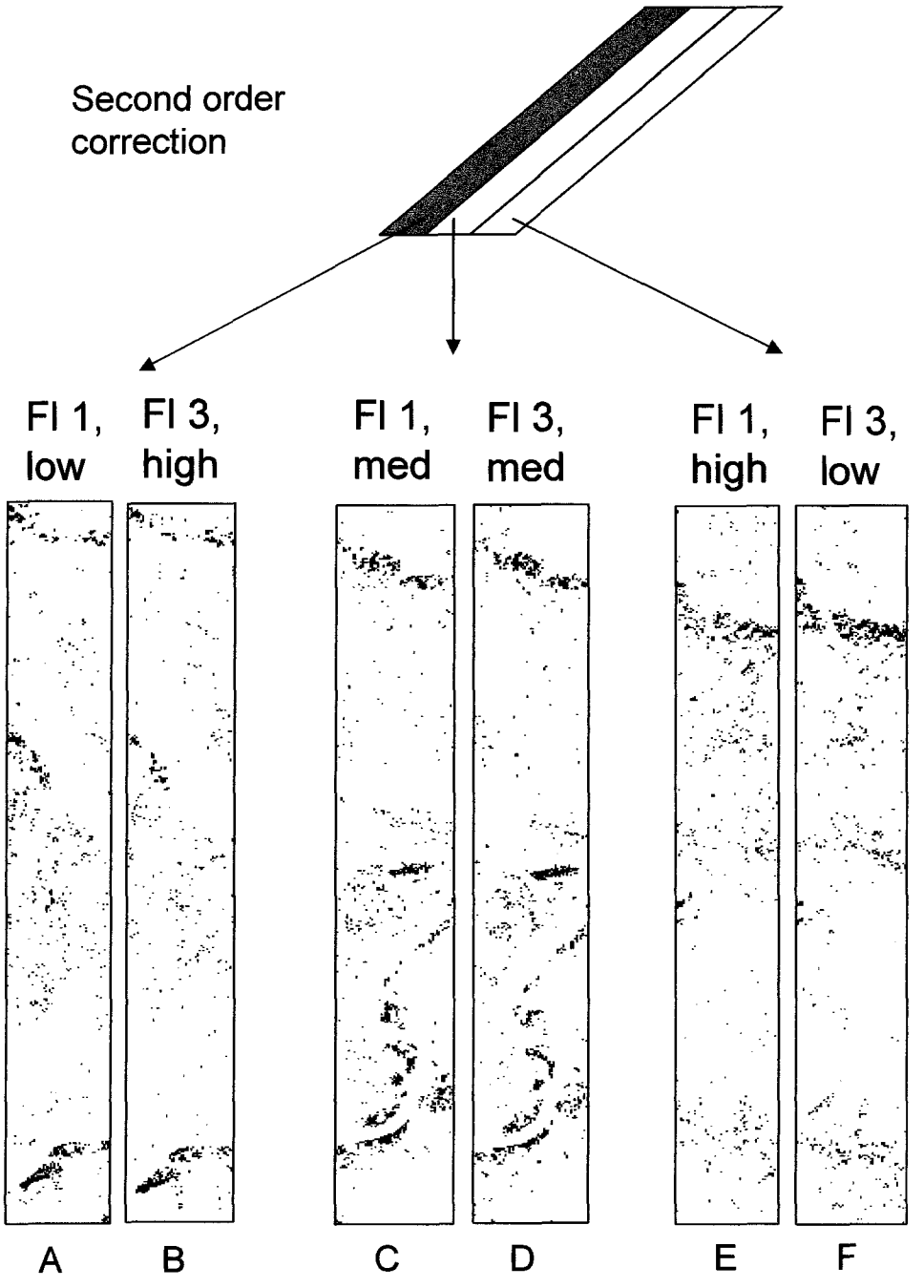

Figure 8.17. View angle affect on spurge classification is minimized with second order cross-track illumination correction. The high/low angle pairs (A,B and E,F) are more similarly mapped than the equivalent pairs in Figure 8.4, where a first order polynomial model was used for the cross-track correction.

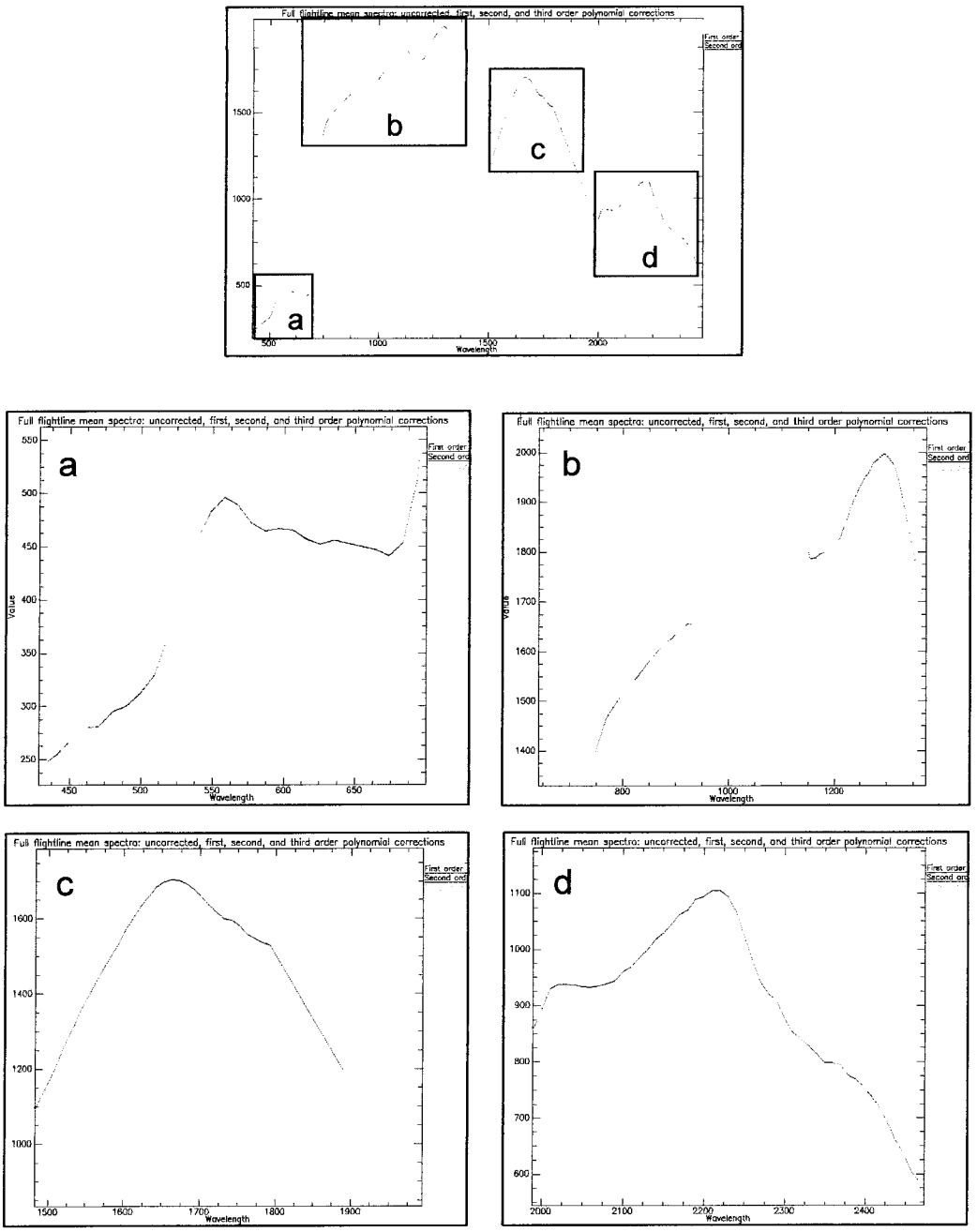

Figure 8.18. Full flight line 1 mean spectrum: and after first, second, and third order corrections applied. A single mean spectrum was produced from the mean response of *all* pixels from flight line 1. Non-vegetative materials were masked and not included in the mean calculation. The three mean spectra are virtually identical and do not show the variation that was seen for the high angle subset from flight line 1 (see Figure 8.19).

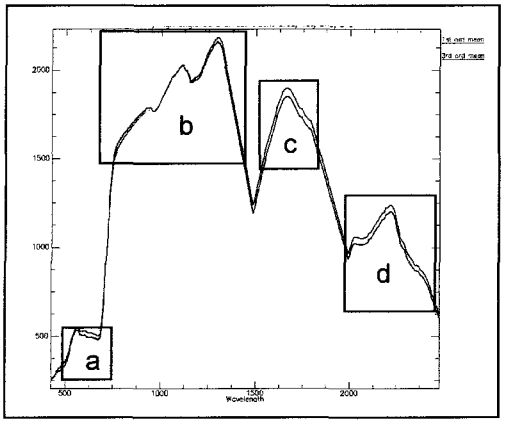

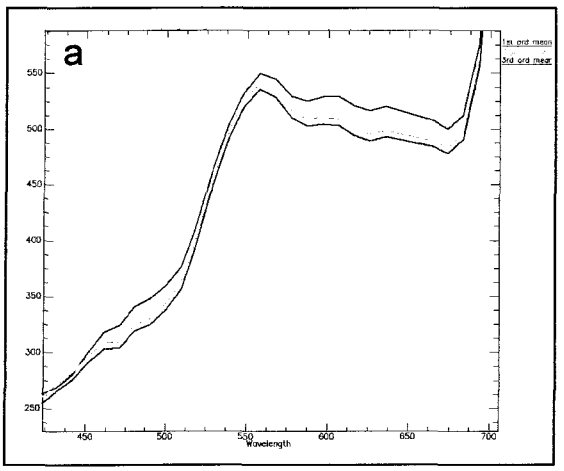

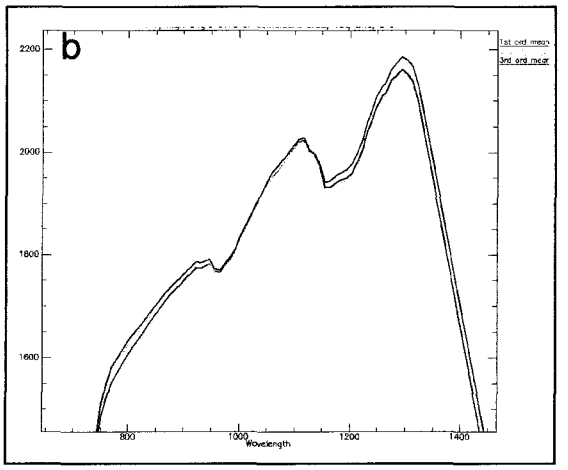

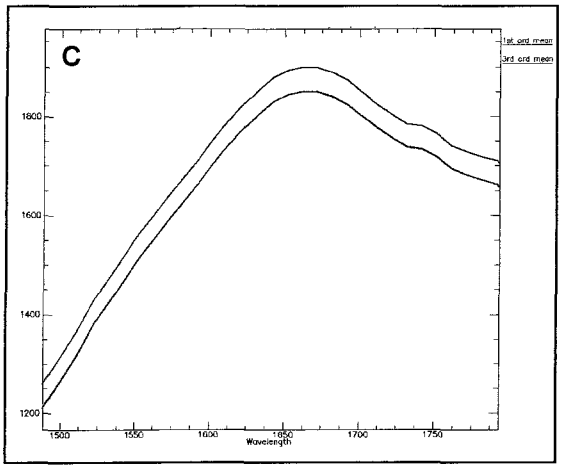

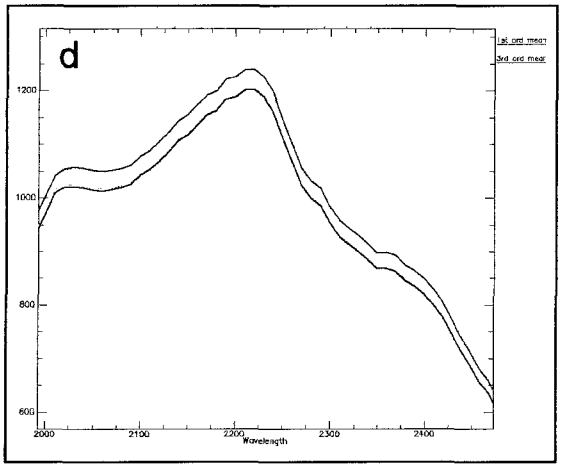

Figure 8.19. Mean spectral response over outer (high angle) third of coincident area for 1st, 2nd, and 3rd order corrected data, flight line 1 only. With the linear first order correction (in red), the response is higher throughout the visible, SWIR I, and SWIR II. The NIR plateau is steeper with the first order correction, showing lower reflectance at shorter NIR wavelengths, and higher at longer NIR wavelengths. Second order (green) and third order (blue) spectra are nearly identical in the NIR, SWIR I, and SWIR II, and differ only slightly in the visible region.

These included higher visible, SWIR I and SWIR II reflectance, and a steeper NIR plateau, showing both increased and decreased brightness (depending on wavelength) relative to the second and third order mean spectra. This suggests that the higher order corrections are eliminating the spectral effects (and by extrapolation classification effects) that are associated with higher viewing angle.

Overall results: cross-track model comparisons. Based on the maps, the stable frequency distribution of classified spurge across track, and the overall better fit of the model that stabilized the mean cross-track spectral response, the second order map was considered an improvement over the first order map with respect to view angle effects and consistency. Maps produced with the higher order corrections will be more consistent across the full width of a flight line with the elimination of the decrease in mapped spurge with high angle that was evident with the linear cross-track correction. These maps will be more appropriate for temporal change studies.

DISCUSSION

A detailed analysis of the first order polynomial cross-track correction model that was used to correct the data for the main mapping project, as well as an evaluation of the maps produced with this correction, indicated that view angle effects on albedo remained in the data following the linear correction for cross-track illumination variation. These residual geometric effects appeared to be related primarily to the sensor view angle. When the cross-track frequency of spurge was plotted, the distribution was non-linear, yet symmetrical across individual flight lines, and appeared to be related to the magnitude but not direction of the sensor view angle. This was supported by the differences in cross-track frequency for other vegetation classes as well, and by the differences in spurge frequency that were seen for identical areas mapped from different view angles (from adjacent flight lines).

In addition, the change in mean spectral characteristics for identical pixels extracted from high and low view angles from different flight lines varied. The general effects of increasing view angle on leafy spurge spectra included:

Increased visible reflectance;

Increased NIR reflectance;

Decreased depth of absorption features in the visible region;

Increased SWIR I and SWIR II reflectance;

Minor decrease in the NIR water absorption features (although inconclusive and requires additional measurements);

Minor steepening of the NIR continuum/plateau;

Minor strengthening of SWIR II lignin/cellulose features, in some cases.

With the exception of the increased NIR brightness, the spectral trends that were noted with high versus low view angle for leafy spurge were analogous to those that would occur with decreased plant vigor and/or increased senescence of vegetation. Alternatively, these spectral trends may result from viewing higher proportions of bright soil, stems, and litter at the expense of green biomass, characteristics that would be expected with higher viewing angles based on the morphology of the leafy spurge plant. Spurge stems are erect and often single, with branching only toward the top of the plant. Stems are relatively free of leaves. Leaves are long, linear, and sessile, and protrude horizontally from dominantly vertical stems, resulting in a larger proportion of stems, litter, and soil in the field of view with higher angles (Figure 8.20). At or close to nadir the IFOV of the sensor would be dominated by leaves and bracts, the vegetative components that produce the deep absorption features, high NIR, and low visible, SWIR I, and SWIR II reflectance. In some cases these apparent spectral differences with view angle were sufficient to force some pixels to map as a class other than spurge.

Second and third order polynomial models were calculated to determine whether additional geometric (view angle) effects could be reduced or eliminated. These were applied to the data and the average cross-track brightness variation decreased or was eliminated. Spurge frequency was stabilized and became more consistent across flight lines. Maps produced with the higher order corrections indicated fewer omission problems for low density and sparse leafy spurge patches in areas where the ground distribution had been well characterized.

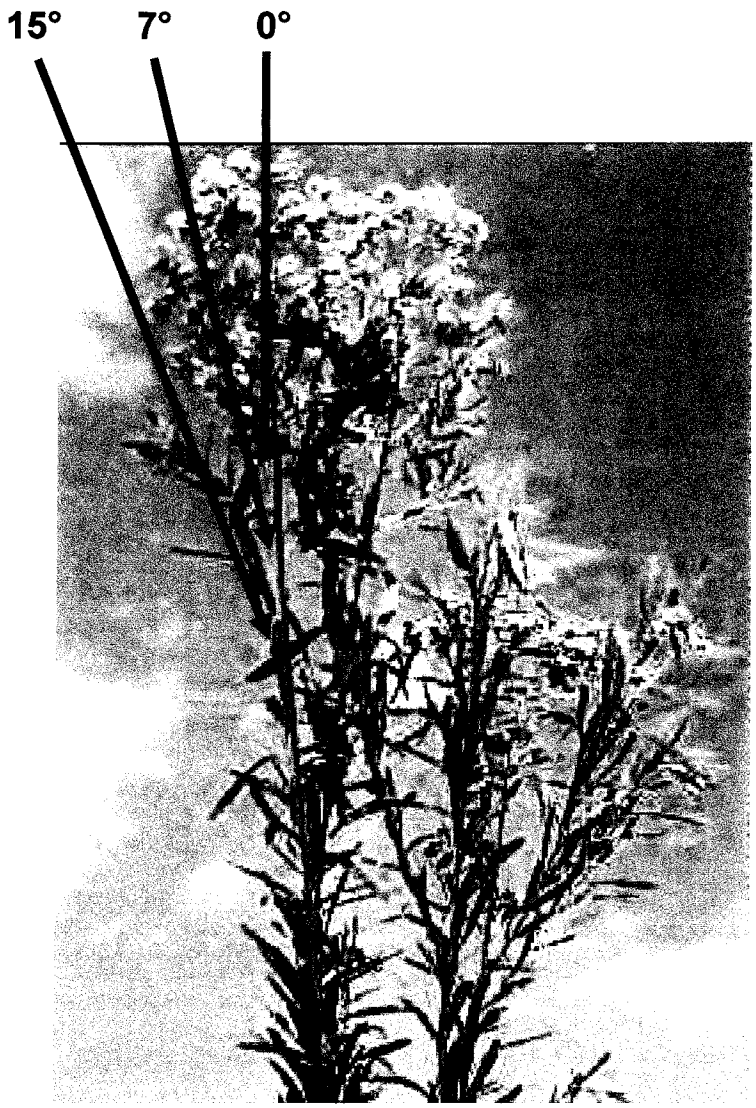

Figure 8.20. Leafy spurge morphology and view angle. With increasing angle, the sensor may view a higher proportion of stems, and less leaf, flower, and bract material. This can change the spectral response "seen" by the sensor, with possible classification consequences (although the proportion of plant components seen by the sensor with changing angles will vary with canopy density and bract density). View angles are approximated in this diagram. Spurge image from Anonymous, 1998.

If the change in spectral response with view angle is the result of viewing land cover or vegetation components in different proportions, these high angle differences could be considered "real" and simply accepted as a map artifact that is associated with airborne hyperspectral data. For practical mapping purposes, however, these changes can have a negative effect on class mapping that would be carried through and compounded in multi-temporal change maps. To produce reliable change maps it is necessary to minimize apparent change that is the result of the differences in classification between dates that are due to different sensor view angles rather than true land cover change. Applying a correction to standardize the spectral response across the scene will increase the consistency over time. In addition, inconsistent class assignments resulting from different view angles will introduce spatial errors when creating mosaics from multiple flight lines, and should be reduced for greater consistency of maps. Careful selection of the empirical cross-track correction model can successfully compensate for these effects when mapping leafy spurge.

Although the view angle effects appeared to be eliminated with the second order cross-track correction, the effects of the higher order correction on spurge or other vegetation spectra were not examined in detail, and the explanation for the elimination of the view angle effect on the frequency of classified spurge is not entirely clear (from a spectral perspective). Additional analysis of the spectral characteristics of higher-order corrected data is needed. This is an area that should be explored further to document the changes to spectra of spurge-classified pixels that resulted in the stable frequency distribution of spurge across the width of the flight lines.

Cross-track illumination and viewing geometry are known to affect apparent reflectance, but few studies have corrected for these effects when mapping vegetation species or associations with imaging spectroscopy. Directional effects on the reflectance of vegetation are well known and there has been considerable research on modeling these effects. It is difficult, however, to calculate and apply these BRDF models for practical correction of imagery during routine vegetation mapping. The models are species specific, wavelength dependant, and it requires considerable effort to characterize the change in apparent reflectance for every combination of illumination and viewing geometry when creating maps for monitoring purposes.

Many studies address the potential effect of view/illumination/target geometry when deriving biophysical parameters from an image, but little information was found regarding practical studies of the effects of viewing angle on class, or species mapping. Practical, applied corrections for vegetation mapping are rarely described in the literature. Kennedy et al. (1997) is an exception. This article describes a practical empirical correction for cross-track illumination changes in apparent reflectance. A similar correction has been incorporated into ENVI software. The cross-track correction proved to be important for map consistency based on the THRO study, and the cross-track correction may be more important for consistent vegetation mapping than is generally acknowledged in the literature. Although the ENVI cross-track correction is empirical and does not account for many of the theoretical arguments that are incorporated in detailed BRDF models, the spatial and temporal improvement in map consistency with this correction was notable for this data set. The empirical correction increased cross-track map consistency, and it was easily modeled and applied using ENVI software. The improvement in cross-track consistency has important consequences for temporal change studies.

A blanket application of a predefined correction model may not be appropriate in all situations, however, and the model used to correct the data should be carefully selected to avoid overcorrection of data that is poorly fit by the model. This is particularly important when the landscape is heterogeneous across the sensor track, to ensure that a cross-track change in spectral response associated with a change in dominant land cover is not confused with cross-track illumination and/or view angle effects.

Future work. It would be a useful extension of this project to examine the relationship between matched filter (MF) values and associated spectral characteristics to determine whether distinct spectral differences can be associated with the best and weakest matches for the leafy spurge class, and whether these share similarities to spectral changes associated with changing view angle. By correlating the spectral characteristics to mapped class, MF score, and the class endmember spectrum, it may be possible to determine whether changes in class assignment are a function of density, vegetation condition, geometric relationships between illumination, sensor, and target, or some combination of these and other factors. These spectral analyses could be

expanded beyond a single target of interest, to other species or classes, particularly those that exchange "identification" with spurge as view angle changes. The spectral analysis that was initiated in this study is very preliminary, and additional spectral information is available that has not been fully exploited to date.

Normalization of the data for the effects of sun/sensor/target geometry in addition to standardization of the processing methods (Chapter 5) will lead to more reliable and accurate change analysis. Because the empirical cross-track correction model can be calculated and applied quickly using ENVI software, it is well suited for applied mapping projects. The cross-track consistency of spurge maps in this study was improved with these methods, which are an important contribution to increased precision for temporal change studies that use hyperspectral imagery.

CHAPTER 9

OVERVIEW OF CHARACTERISTICS AND IMPROVEMENTS FOR INCREASED PRECISION OF MULTI-TEMPORAL HYPERSPECTRAL MAPS

INTRODUCTION

Since its inception in the late 1980s, imaging spectroscopy has been used predominantly in the research arena, but recently it is being used increasingly for applications-oriented work. This study was initiated to determine whether it is possible to accurately and precisely monitor leafy spurge with imaging spectroscopy, and to determine whether the results produced from AVIRIS data with current processing methods are sufficiently reliable and consistent to use for multi-temporal monitoring and change detection. The answer depends on several factors including: 1) economics; i.e., the resources are available to invest in the collection and processing of imaging spectroscopy data; and 2) the processing methods and decisions that are used during production of the maps.

The economic costs associated with end-to-end production of leafy spurge maps were not directly examined in this study; however, AVIRIS data is expensive in terms of both data acquisition and processing costs. This research focused on analysis and refinement of hyperspectral image processing methods, and the quality of the resulting maps. The repeatability and reliability of maps were concerns that were specifically explored. It was critical to determine whether the AVIRIS data provided significantly better maps that facilitated earlier detection of leafy spurge to evaluate whether the additional cost and effort of using imaging spectroscopy for monitoring purposes was justified.

Hyperspectral remote sensing is particularly suited to discriminating species, and the unmixing methods that are often used in hyperspectral processing are capable of detecting subpixel occurrences of a specific material. This capability is particularly important for locating

new and smaller weed infestations, as well as tracking low density infestations over larger areas. These methods are also useful for detecting changes in density that occur with expansion or decline in infestations over time.

In theory, imaging spectroscopy is not difficult to conceptualize; however, it can be challenging to successfully process and apply these data to specific questions. Hyperspectral sensors record the reflected electromagnetic radiation of materials, similar to multi-spectral sensors, but over a continuous spectral range using many small-width bands. Additional challenges are encountered when processing hundreds of wavelength bands. For example, hyperspectral signals are noisier than multi-spectral data, and require careful atmospheric correction to eliminate the effects of atmospheric absorption features that can confuse the interpretation of radiance from surface materials. A finite quantity of incoming solar irradiance, radiated from the target to sensor, must be spread over hundreds of detectors, resulting in a relatively small recorded radiance for each detector. This signal can be difficult to separate from the noise of the sensor.

Other factors have been an impediment to using imaging spectroscopy for regional and multi-temporal applied work. For example, inconsistencies in maps became apparent during the course of this study when multiple dates and multiple flight lines of AVIRIS data were used to map the change in leafy spurge distribution between 1999 and 2001. The inconsistencies resulted from differences in preprocessing steps, map algorithms, spectral libraries, decisions on thresholds for defining classes, and differences in view/illumination geometry. For multi-temporal applications, it became apparent that map outcome was highly sensitive to the processing method that was used to produce the maps.

Solutions were proposed to reduce the effects of processing methods and decisions on map accuracy and precision. By minimizing interactive steps and decisions that are required of the image analyst, the use of hyperspectral data was facilitated for those with limited experience in processing hyperspectral imagery. In addition, specific processing steps were standardized to increase consistency to improve the outcome of temporal studies. All processing was completed using only algorithms and techniques that are available in the commercial software package

ENVI. A goal of the modifications was to develop a method that would minimize or eliminate inconsistencies in maps and over-classification of leafy spurge, while simultaneously minimizing the omission of known leafy spurge patches, including low density occurrences that could represent newly established infestations.

METHOD COMPARISONS/SELECTION

In early leafy spurge test maps, the weed was typically over-classified to varying degrees and maps were highly variable. To determine which factors produced ideal results for temporal and spatial monitoring, multiple tests were completed to isolate the optimum procedures for producing accurate *and* precise results for the full temporal study.

Test classifications were run using several pre-processing strategies, spectral libraries, and mapping methods to determine which steps were responsible for the distinct differences that were seen in initial test maps, and to select the most consistent and accurate set of steps for further processing.

The following steps produced results that represented the best compromise between minimizing omission error, while still mapping low density and/or small infestations, and were therefore selected for the basic mapping procedure:

1) Cross-track correction to minimize the potential effects of the change in cross-track illumination seen in the original data;

2) Removal of "bad" and extraneous bands; liberal editing was used to eliminate several band anomalies that negatively impacted the maps;

3) NDVI-masking was used to isolate vegetation to facilitate extraction of detailed vegetation endmembers and improve vegetation maps;

4) Selection of the MTMF from several tested algorithms because the maps produced with this algorithm were high quality and could be refined and improved with the "infeasible" images that are produced when the algorithm is run;

5) Selection of image-derived over field-derived endmembers because a more complete library could be produced; remnant image anomalies would also be incorporated into the spectral library;

and maps, in general, were more accurate with the image library.

MODIFIED HYBRID MTMF METHOD

Maps produced with the selected processing steps appeared to be satisfactory for mapping single flight lines; however, inconsistencies were seen between maps when additional flight lines were processed. These inconsistencies were predominantly related to interactive threshold decisions by the analyst, and to the size and quality of the image-derived spectral library. Several modifications to the selected standard processing steps were developed in an effort to increase automation, decrease interactive processing, and minimize the threshold decisions required of the image analyst.

PREPROCESSING MODIFICATIONS

Before classification, the image-derived spectral library was selected in two-stages: 1) the full (unmasked) image was used to extract a set of general endmembers; and 2) an NDVI-masked image (masked for vegetation) was used to collect a more refined and detailed set of vegetation endmember classes.

An exhaustive endmember set was extracted by continuing class selection until no additional classes could reasonably be found. This resulted in the collection of more endmembers than the theoretical maximum, which is estimated based on the number of coherent MNF bands used in the analysis. Potential vegetation endmembers were selected from minor extensions from a centralized vegetation pixel cloud, rather than restricting the selection to obvious, isolated pixel clusters, the standard approach used in interactive endmember selection with ENVI software. By collecting and using all possible classes for mapping, critical endmembers (including the target of interest) were not inadvertently omitted. Detailed editing of the individual spectral endmembers classes as well as the final spectral library ensured that the library represented legitimate, spectrally distinct classes.

A single library was successfully used to map all four flight lines from a single date by using independent MNF transformations of the single spectral library prior to mapping each

additional flight line. The individual transformations were based on the MNF transformation statistics that were unique to each flight line.

MAPPING MODIFICATION

A modified, hybrid MTMF method was used to map leafy spurge. The algorithm was run, however, using all possible endmembers as input to the algorithm rather than a single target endmember spectrum. This approach is similar to the logic used with linear spectral mixture analysis. The modified MTMF program ran iteratively, however, and independently solved for each input class rather than a single, user-defined target class.

POST-CLASSIFICATION MODIFICATIONS

The standard method for producing a target map uses plots of the MF and infeasibility outputs from the MTMF algorithm to manually select appropriate thresholds, and the selection is at the discretion of the analyst. To remove the subjectivity of the manual/graphical selection of the thresholds, the MF boundary was selected automatically by allowing all classes to compete for best class assignment, which was based on the highest MF score for each pixel, using the post-classification "rule" classifier in ENVI. A single, image-wide MF threshold was not required, no selection was required of the image analyst to determine the threshold, and the threshold adjusted to the highest matched filter score on a pixel-by-pixel basis.

To assign the infeasible threshold, a standard boundary was set at one standard deviation above the mean infeasibility value (for the spurge class) and was applied over the entire image. Band math was used to link the pixels that mapped leafy spurge as the primary component of a pixel to the infeasible image scores. With this method no analyst decision was required, and the threshold assignment was standardized.

MODIFIED HYBRID MTMF SUMMARY

A summary of the critical modifications and refinements that resulted in increased automation, and increased quality and consistency of spurge maps included:

1) Using a two-step endmember collection (masked and unmasked), with a modified selection strategy for improved isolation of vegetation classes;

2) Selection of all possible endmembers (with no restriction or limit imposed by a theoretical

maximum number), followed by detailed editing of the spectral library;

3) MNF re-transformation of the spectral library prior to mapping each flight line;

4) Mapping with the MTMF algorithm using a hybrid approach that included all possible endmembers as input rather than a single target endmember;

5) Automatically assigning MF thresholds for maps on a pixel-by-pixel basis using the ENVI post-classification rule classifier to eliminate the manual MF threshold selection;

6) Assigning a +1 sigma above the mean score from the leafy spurge infeasibility image to standardize the infeasible threshold for refinement of the target map.

With the mapping method and modifications that were developed, several advantages and improvements to the mapping procedure and results were noted and are outlined below:

1) Processing was standardized and automation was increased;

2) Interpretive input and possible bias by the image analyst was reduced, particularly with respect to threshold placement for final map production;

3) Less ground support/reference data was necessary because no field reference data were needed for training (all spectral endmembers for matching or training were derived from the imagery);

4) Because all possible endmembers were used, no *a priori* decision on identification of the endmember target was required, where it can be difficult to select the most appropriate image-derived endmembers to represent target(s) of interest before mapping is completed; this effectively eliminated another interactive decision during the mapping process;

5) The method is not restricted to a theoretical maximum number of endmembers, therefore all subtly different classes can be collected for more successful plant species mapping, and no classes were omitted;

6) With the full image endmember library, classes were not restricted to those that could be characterized by ground-based spectral measurements, as when a field-based spectral library is used for classification; in the field it is difficult to collect representative spectra from all possible endmembers over a large region, and it can be difficult to find the "purest" areas in the field to best represent ideal endmembers;

7) Sub-pixel abundance measurements were retained, allowing a more detailed characterization of leafy spurge than with thematic, hard-classified maps;

8) The new method eliminates variability of the threshold over different subsets of the image that results when the graphical threshold selection method is used (separate threshold values must be collected over individual isolated blocks from large images that cannot be viewed entirely within the ENVI image window);

9) Because MF thresholds were established on a per-pixel basis, more accurate thresholds could be obtained, to avoid incorrect inclusion/exclusion that can occur when a single threshold value is applied;

10) The method allows simultaneous mapping to the best score class from all possible classes; individual mapping of each class of interest was not required;

11) Area-wide vegetation maps could be produced rapidly relative to standard photo-interpreted vegetation mapping methods;

12) All class coding was consistent, which allowed easier mosaicing and inter-flight line analyses;

13) By selecting specific processes, outlining the method in detail, and minimizing interactive steps requiring analyst decisions, complex technology and processing become more accessible for applied monitoring and management decisions; a decreased level of expertise would be required for data processing;

14) By increasing standardization and consistency of individual date maps, change maps will be more consistent, as variability in processing and decision-making are minimized;

15) All processing steps used software and algorithms that are commercially available, with no complex modifications of programs or software required;

16) The methods were not specific to the target class or location used in this project, and could easily be extended to additional vegetation classes, given sufficient ground data for unequivocal identification of the classes.

17) With this hybrid approach, information was available for *all* classes, and total land cover could be more thoroughly characterized without sacrificing the accuracy that can be obtained with the MTMF algorithm.

MAPS

Binary maps were produced to indicate the presence or absence of leafy spurge in 1999 and 2001. Additional fraction maps were produced by level slicing the binary spurge maps after combining classified spurge with matched filter scores to produce a map of estimated spurge fraction on a pixel-by-pixel basis. A full thematic vegetation map was also produced, based on the highest MF score from all classes, which was determined using the post-classification rule classifier in ENVI.

The above maps included material only when it represented the dominant component within a pixel. Secondary spurge maps were also produced that indicated the spurge fraction in pixels where spurge was not the dominant component. These were produced by isolating the non-spurge vegetation, attaching the MF scores, and applying the same level slice categories that were used for the primary map. The primary and secondary maps were combined, with separate color-coding schemes retained for the primary and secondary level slice categories to provide a more complete representation of spurge infestations.

A map of the change in leafy spurge between 1999 and 2001 was produced using the primary, binary maps from 1999 and 2001. A second change map was produced from the MF scores (i.e., fraction maps) from each year. This was and level sliced into categories that represented the magnitude of the change in fraction between 1999 and 2001.

In summary, the maps produced using 1999 and 2001 AVIRIS imagery included:

1) Binary (presence/absence), spurge dominant (primary);

2) Density-sliced, spurge dominant (primary);

3) Density-sliced, spurge non-dominant (secondary);

4) Primary/secondary combined maps;

5) Area-wide, all vegetation;

6) Change map (for spurge-dominant class only);

7) Fraction change map.

ACCURACY ASSESSMENT

Formal accuracy assessments have been notably absent in early imaging spectroscopy projects, although recent studies are increasingly reporting accuracy results. Accuracy was calculated for the THRO spurge maps using the error matrices that are routinely applied in multispectral map validation. In addition, regression between field-measured density and mean fraction for spurge patches was used to assess the accuracy of mapped fractions. Accuracy values based on confusion matrices varied widely. The variation was related primarily to registration errors between maps and reference data, and to the source and quality of the reference data. The primary reference set included centroid locations of small (3 m x 5 m) plots, and was not collected for validation of remote sensing maps. These reference data were inadequate for validation of 17 m AVIRIS data. When buffers were applied to the classified maps to accommodate registration offsets between maps and reference data, the overall accuracy increased by nearly 20 percentage points. Producer's accuracy for leafy spurge increased 72 percentage points (to 92%) with the largest buffer.

Several patches of spurge with densities ranging from 25% to effectively 100%, as well as representative patches of other common associated vegetation species, were collected within 2 weeks of the 2001 AVIRIS overflight. These were used in a regression of the mean fraction value within a polygon (from the imagery) to the density of the equivalent field-measured polygon. When field density for a patch was regressed against the mean MF score for the same area on the image, r^2 values up to 0.73 were obtained. The regression analysis added an additional component to the map assessment beyond the point-based error matrices, which were sensitive to registration problems, particularly where spurge distribution was fragmented and patches were small. Error matrices only measured the correct class assignment, while the regression provided additional validation of the assigned fraction (on a patch level).

Because flight lines were collected with 35% sidelap, the accuracy of maps of identical areas that were produced from different data sets could be compared, without the variables that are encountered between multi-temporal data collections, for example, atmospheric variability, phenological differences, and/or environmental conditions on the ground such as soil moisture.

Spurge accuracy results were very similar and the full thematic maps were comparable, indicating that the method produced maps that were suitable for change detection.

CHANGE DETECTION

Imaging spectroscopy has rarely been used to monitor change in classified land cover. By using the processing protocol described in this study, precise results were obtained that were suitable for change detection. The change maps that were produced with post-classification differencing indicated regional patterns in the change in spurge infestation, including areas that had been heavily infested and targeted for control in 1999, where spurge was eliminated by 2001. Other regions suggesting new outbreaks of spurge by 2001 were identified, as well as areas that indicated persistent spurge infestations over the two years. The occurrence of many small new infestations in a region that was believed to be relatively free of spurge, as well as heavy infestations in some riparian regions on the map that were originally believed to be incorrectly mapped, convinced land managers in the area to re-evaluate their control efforts in this region and target some of these areas for bio-control and aerial herbicide application.

Local change patterns were suggested by the maps as well. These included areas that indicated successful control, areas of rampant expansion in the absence of controls, and areas suggesting mixed success with controls where infestations were extremely heavy. These local changes should be interpreted cautiously, however, because the maps were affected by registration offsets between the 1999 and 2001 maps. Several of these local interpretations of change were verified by park personnel with extensive knowledge of the progress of these infestations in heavily monitored areas.

A map of the change in spurge fraction between 1999 and 2001 was produced but was difficult to interpret due to registration offsets between maps. This will be an area for further exploration, if registration can be improved significantly enough to allow pixel-to-pixel comparisons over time. Detailed information on the change in fraction would allow an analysis of intra-class trends in fraction, and facilitate earlier intervention in areas that were increasing in density, yet not infested severely enough to map spurge as the dominant material within a pixel.

VIEW ANGLE EFFECTS AND CROSS-TRACK CORRECTION

The maps from individual flight lines matched well visually, accuracy values were similar, and the maps were suitable for change detection; however, some inconsistencies in the final spurge maps were apparent between identical areas that were mapped from different flight lines. The inconsistencies were related to the magnitude of the sensor viewing angle, and indicated declining frequency of mapped spurge as view angle increased. A similar pattern was seen for several other vegetation classes as well. The first order polynomial cross-track correction model that was used to correct the data for the main mapping project was re-evaluated, and it was determined that additional cross-track variation in the mean spectral response remained following the illumination correction. Second and third-order polynomial models were calculated and applied to the data. With the higher order corrections, the response was more stable across track, and the maps produced after these corrections were applied indicated fewer omission problems for spurge. A plot of the frequency of mapped spurge across track also indicated that the change in frequency associated with the magnitude of the viewing angle had been minimized or eliminated. The results emphasize that the cross-track model used for correcting data for the effects of view and illumination angle should be selected carefully for maximum spatial and temporal consistency between maps.

A preliminary evaluation of the spectral characteristics of spurge mapped from high and low view angles was completed for the first order corrected map. Leafy spurge spectra from identical areas mapped with high and low angle views from adjacent flight lines showed changes in spectra with increasing view angle that were similar to the spectral characteristics that are associated with senescing or stressed vegetation, or an increased percentage of non-leafy biomass and other non-vegetative materials within a mixed pixel. These are characteristics that would be expected for low to moderate density spurge infestations viewed from higher angles based on the morphology of the plant. A similar evaluation of spectral characteristics of spurge is needed for different view angles from the higher order corrected data, as well as for additional

vegetation classes to fully understand the affects of these corrections on spectral responses and classification.

For leafy spurge mapping, the cross-track correction was an important factor in improving map consistency throughout entire scenes, yet similar corrections have not been applied routinely in other studies. Bidirectional effects on reflectance are well known, particularly for vegetation, and there has been considerable research on modeling these effects. There appear to be few investigations, however, of the effects of angular relationships on class or species mapping. Practically, it is difficult to apply BRDF models for routine correction of imagery. The models are species specific, wavelength dependant, and it is an effort to adequately characterize or model the change in apparent reflectance for every combination of illumination and viewing angle. Mixed pixels also complicate the correction of data using BRDF models. The empirical cross-track correction used in this study, when selected carefully, provided a rapid and simple method to compensate for geometric effects. For the leafy spurge class, the correction was important in standardizing cross-track reflectance and increasing the precision of the resulting maps. The cross-track correction may be more important for hyperspectral species mapping than is generally acknowledged in the literature.

FUTURE WORK

The modified, hybrid MTMF that was used to map multiple flight lines from two dates was evaluated and considered reliable and consistent enough to be used for temporal monitoring of leafy spurge. To be adopted as a routine protocol, however, the method should be tested in other locations and on additional vegetation species, assemblages, and other materials. With additional field characterization, binary and fraction maps could be produced for the other vegetation classes that were mapped over THRO, to test whether the method and data are suitable for general vegetation mapping.

With improved georeferencing it may be possible to complete more detailed analyses of the change in relative abundance of specific classes over time. The quality of spatial correction of airborne hyperspectral scanners currently lags behind the quality of the spectral information

that can be extracted from high quality sensors, including AVIRIS. If reliable pixel-scale maps of change in fraction can be produced, different treatments that were applied at fine scales could be correlated with response of infestations to specific controls, in order to determine the most effective method(s) for long-term weed management.

The AVIRIS data was collected within the period of peak inflorescence of spurge under the assumption that the weed would be more easily separated based on the spectral signatures associated with the unique yellow-green bracts that are associated with the spurge flowering stage. Tracking the spectral characteristics of spurge throughout a single season could provide additional insight regarding the effects of phenological stage on spectral characteristics of the weed, and the potential to remotely identify spurge throughout a growing season.

Additional spectral studies would be valuable to establish in greater detail: 1) the spectral characteristics of classified spurge pixels as a function of viewing angle; 2) the spectral changes that are responsible for class re-assignments with changing viewing angle; 3) spectral characteristics of the uncorrected data versus the first, second, and third order polynomial corrected data that may be responsible for differences in cross-track vegetation class assignment; 4) the relationship between view angle, spectral characteristics, and MF fraction values to determine whether changes in class assignment are a function of density, or are related to vegetation condition, or other factors including geometric illumination and view angle effects (or a combination of these factors); 5) to provide additional information regarding spectral differences that are associated with the best and weakest matches for a given land cover class; and 6) the characteristics of pixels that were eliminated from spurge maps with the infeasible refinement. These spectral analyses could be expanded beyond a single target of interest to other species or classes.

This study included only a very preliminary analysis of spectral characteristics, and considerable spectral information is available that has not been fully investigated.

CONCLUSION

Some would argue that the potential of remote sensing is not being realized, in part due to the nature of classes ("fuzzy boundaries") and the methods used for mapping, many of which assume pure pixels (Foody, 1999). Hyperspectral image analysis can address these problems. Unmixing algorithms used in processing are specifically designed to analyze partial class membership within mixed pixels. Fraction maps, which indicate the relative abundance of target materials, can be produced as well as hard-classified maps, allowing class "fuzziness" and mixed pixels to be addressed.

To "realize the full potential" of hyperspectral remote sensing, however, additional problems with these data that have precluded more widespread use must be addressed. These include practical issues such as the expense and availability of the data. Currently, the highest quality hyperspectral data is collected from airborne platforms that are affected by view angle, as well as inherent instability that may create problems with registration. In addition, the strength of hyperspectral (i.e., high spectral resolution) can also be a weakness, as the data are sensitive to processing methods and are easily affected by noise. The data are also very sensitive to atmospheric effects, which must be eliminated to successfully isolate the surface radiance.

In this study, potential solutions were presented for sensitivity to processing methods, and for view angle effects. A detailed calibration successfully minimized atmospheric interference. AVIRIS instrument noise has been significantly reduced in recent years and noise issues were minimal in the THRO data set. Registration remained problematic, however, and precluded successful pixel-level analysis of temporal change, as well as assessment of different spurge controls, which were applied at a scale finer than the estimated magnitude of the registration shifts. The development of a high quality, widely available rectification algorithm for airborne scanners would significantly improve the potential of hyperspectral remote sensing.

Over the course of this project several maps were created that are not frequently associated with hyperspectral data, yet may prove valuable due to exploitation of the high spectral resolution. These included: primary (spurge dominant) *and* secondary (spurge subordinate) maps; level-sliced fraction maps; binary change maps; fraction change maps; and area-wide vegetation maps.

There have been few investigations that have evaluated or even applied imaging spectroscopy for multi-temporal studies, although this is a very common application of remote sensing in general. The primary focus of this study was to determine whether it was possible to produce consistent and accurate maps of leafy spurge from airborne imaging spectroscopy data that can be used effectively for temporal monitoring of the weed. After completing an analysis of hyperspectral processing methods and developing refinements and modifications, the results of this study indicate that it *is* possible to produce consistent leafy spurge maps that are suitable for temporal analyses. The mapping protocol is critical, however. Comparative analyses of hyperspectral processing methods and method refinements are not common, but are important, as shown by the variability in species maps that resulted solely from different processing techniques and decisions. Careful selection of a well-defined and adequately tested protocol that reduced interactive decisions and standardized threshold selection, resulted in fewer processing artifacts that could be misinterpreted as change (or lack thereof). The methods described in this paper resulted in greater precision of maps, and therefore more reliable change maps. High spectral resolution data are potentially very valuable for detailed land cover mapping within many environments. The enhanced separation of materials with high spectral resolution data and the ability to map fractions within mixed pixels, coupled with the increased precision from the method refinements introduced in this project will make imaging spectroscopy a potentially powerful tool for remote temporal analyses. If processing is completed cautiously and consistently throughout all mapping steps, using the most appropriate methods and high quality calibrated data, then temporal change maps of leafy spurge infestations can be successfully produced, and imaging spectroscopy can be used as an integral part of a weed management program.

APPENDIX 1: ACRONYMS

ACORN: Atmospheric Correction Now

AIS: Airborne Imaging Spectrometer

AISA: Airborne Imaging Spectrometer for Applications

ANN: Artificial neural network

AP: Accumulated precipitation

APAR: Absorbed photosynthetically active radiation

ASCII: American Standard Code for Information Interchange

ASD FR: Analytical Spectral Devices, full range

AVIRIS: Airborne Visible Infrared Imaging Spectrometer

BRDF: Bidirectional reflectance distribution function

CASI: Compact Airborne Spectrographic Imager

CEM: Constrained energy minimization

DN: Digital number

DOQ: Digital orthophoto quadrangle

ENVI: Environment for Visualizing Images

EO-1: Earth Observer 1

ER-2: Earth Resources # 2 (NASA jet)

ETM+: Enhanced Thematic Mapper Plus

***f*APAR**: Fraction of absorbed photosynthetically active radiation

FWHM: Full width at half maximum depth

GDD: Growing degree days

GIS: Geographic information systems

GIFOV: Ground instantaneous field of view

GPS: Global positioning system

GV: Green vegetation

IFOV: Instantaneous field of view

IR: Infrared

ISODATA: Iterative self-organizing data analysis technique

JPL: Jet Propulsion Laboratory

LAD: Leaf angle distribution

LAI: Leaf area index

MESMA: Multiple endmember spectral mixture analysis

MF: Matched filter

MNF: Minimum noise fraction

MTMF: Mixture-tuned matched filtering

NAPC: Noise-adjusted principal components

NASA: National Aeronautics and Space Administration

NDWI: Normalized difference water index

NDVI: Normalized difference vegetation index

NIR: Near infrared

NPV: Non-photosynthetic vegetation

PAR: Incident light intensity

PCA: Principal components analysis

PPI: Pixel purity index

RGB: Red, green, blue

RMS: Root mean square

ROI: Region of interest

RSI: Research Systems, Inc.

RTGC: Radiative transfer ground calibration

SAIL: Scattering by Arbitrarily Inclined Leaves

SAM: Spectral angle mapper

SFF: Spectral feature fitting

SMA: Spectral mixture analysis

SNR: Signal-to-noise ratio

SPOT: Systeme Probatoire d'Observation de la Terre

SWIR I: Short wave infrared one

SWIR II: Short wave infrared two

THRO: Theodore Roosevelt National Park

USGS: United States Geological Survey

UTM: Universal transverse mercator

UV: Ultraviolet

WTC: World Trade Center

REFERENCES

Adams, J.B., M.O. Smith, and A.R. Gillespie, 1993. Imaging spectroscopy: interpretation based on spectral mixture analysis. In: *Remote geochemical analysis: elemental and mineralogical composition,* C.M. Pieters and P.A.J. Englert, eds., Cambridge University Press, New York, NY, pp. 145-166.

ACORN Quick Start Guide, 2001. ACORN version 3.12, ImSpec, LLC, distributed by Analytical Imaging and Geophysics, LLC, Boulder, CO.

Anderson, G.L., 1995. Using remote sensing and geographic information systems for mapping noxious weed infestations within North Dakota. *Proceedings of the Alien Plant Invasions: Increasing Deterioration of Rangeland Ecosystem Health Symposium,* 1995, Bureau of Land Management http://www.mt.blm.gov/, pp. 28-32.

Anderson, G.L., E.S. Delfosse, N.R. Spencer, C.W. Prosser, and R.D. Richard, 2000. Biological control of leafy spurge: an emerging success story. *Proceedings of the Tenth International Symposium on Biological Control of Weeds*, 4-14 July, 1999, Montana State University, Bozeman, Montana, USA, N.R. Spencer, ed., pp.15-25.

Anderson, G.L., E.S. Delfosse, N.R. Spencer, C.W. Prosser, and R.D. Richard, 2003. Lessons in developing successful invasive weed control programs. *Journal of Range Management*, 56:2-12.

Anderson, G.L., J.H. Evert, D.E. Escobar, N.R. Spencer, and R.J. Andrascik, 1994. Mapping leafy spurge (*Euphorbia esula*) infestations within Theodore Roosevelt National Park using large format aerial photography and geographic information systems technology. *Proceedings: Leafy Spurge Strategic Planning Workshop,* Dickinson, North Dakota, March 29-30, 1994, pp. 42-56.

Anderson, G.L., J.H. Evert, D.E. Escobar, N.R. Spencer, and R.J. Andrascik, 1996. Mapping leafy spurge (*Euphorbia esula*) infestations using aerial photography and geographic information systems. *Geocarto International*, 11:81-89.

Anderson, G.L., J.H. Evert, A.J. Richardson, and D.E. Escobar, 1993. Using satellite data to map false broomweed (*Ericameria austrotexana*) infestations on South Texas rangelands. *Weed Technology* 7:865-871.

Anderson, G.L., C.W. Prosser, S. Hager, and B. Foster, 1999. Change detection of leafy spurge (*Euphorbia esula*) infestations using aerial photography and geographic information systems. *1999 Proceedings: Leafy Spurge Symposium*, Medora, North Dakota, North Dakota State University Cooperative Extension Service, Fargo, N.D.

Andrascik, R.J., 1994a. Process for developing a leafy spurge strategic management plan within Theodore Roosevelt National Park, *1994 Leafy Spurge Symposium*, Bozeman, MT. July 26-29, 1994, p.2.

Andrascik, R.J., 1994b. A post-workshop review: Discussion process and highlights for developing a leafy spurge strategic management plan within Theodore Roosevelt National Park. *Proceedings: Leafy Spurge Strategic Planning Workshop*, Dickinson, North Dakota, March 29-30, 1994, pp. 109-117.

Anger, C., 2003. Defense R & D, Canada, Military Engineering, Hyperspectral Imaging, http://www.dres.dnd.ca/ResearchTech/Products/MilEng_Products/RD20002_CASI/index_e.html

Anonymous, 1998. Leafy spurge. *Cooperative Extension Fact Sheet* 98-68, University of Nevada, Reno.

Asner, G.P., 1998. Biophysical and biochemical sources of variability in canopy reflectance. *Remote Sensing of Environment* 64:234-253.

Asner, G.P., 2004. Biophysical remote sensing signatures of arid and semiarid ecosystems. In: *Remote Sensing for Natural Resources Management and Environmental Monitoring, Manual of Remote Sensing, Third Edition, Volume 4*, S.L. Ustin, ed., John Wiley & Sons, Inc., Hoboken, New Jersey, pp. 53-109.

Asner, G.P., M.M.C. Bustamante, and A.R. Townsend, 2003. Scale dependence of biophysical structure in deforested areas bordering the Tapajós National Forest, Central Amazon. *Remote Sensing of Environment* 87:507-520.

Asner, G.P. and D.B. Lobell, 2000. AutoSWIR: a spectral endmember unmixing algorithm using 2000-2400 nm endmembers and Monte Carlo analysis. *Proceedings of the Ninth Airborne Geoscience Workshop*, NASA Jet Propulsion Laboratory Publication 00-18, Pasadena, CA, 29-38.

Asner, G., C. Wessman, and C, Bateson, 1998a. Sources of variability in plant canopy hyperspectral data in a savanna ecosystem. *Proceedings of the Seventh JPL Airborne Earth Science Workshop*, NASA Jet Propulsion Laboratory Publication 97-21, Pasadena, CA, 23-32.

Asner, G.P., C.A. Wessman, D.S. Schimel, and S. Archer, 1998b. Variability in leaf and litter optical properties: implications for BRDF model inversions using AVHRR, MODIS, and MISR. *Remote Sensing of Environment* 63:243-257.

Aspinall, R.J., 2002. Use of logistic regression for validation of maps of the spatial distribution of vegetation species derived from high spatial resolution hyperspectral remotely sensed data. *Ecological Modelling* 157:301-312.

Asrar, G., R.B. Myneni, Y. Li, and E.T. Kanemasu, 1989. Measuring and modeling spectral characteristics of a tallgrass prairie. *Remote Sensing of Environment* 27:143-155.

AVIRIS Data Facility web page: http://aviris.jpl.nasa.gov/html/aviris.datafacility.html

AVIRIS Proceedings web page: http://aviris.jpl.nasa.gov/html/aviris.documents.html

Bangsund, D.A., J.R. Baltezore, J.A. Leitch, and F.L. Leistritz, 1993. Economic impact of leafy spurge on wildland in Montana, South Dakota, and Wyoming. *NDSU Agricultural Economics Report* No.304, North Dakota Agricultural Experiment Station, North Dakota State University, Fargo, ND.

Barnsley, M.J., D. Allison, and P. Lewis, 1997. On the information content of multiple view angle (MVA) images. *International Journal of Remote Sensing* 18:1937-1960.

Beck, K.G., 1996. Leafy spurge, *Colorado State University Cooperative Extension* No. 3, 107, Natural Resources Series. http://www.colostate.edu/ds/

Biek, R.F. and M.A. Gonzalez, 2001. The geology of Theodore Roosevelt National Park; Billings and McKenzie Counties, North Dakota. *North Dakota Geological Survey Miscellaneous Series*, Grand Forks, ND.

Birdsall, J.L., P.C. Quimby, Jr., N.E. Rees, T.J. Svejcar, and B.F. Sowell, 1997. Image analysis of leafy spurge (*Euphorbia esula*) cover. *Weed Technology* 11:798-803.

Birdsall, J.L., P.C. Quimby, Jr., T. Svejcar, and B. Sowell, 1995. Image analysis to determine vegetative cover of leafy spurge. *1995 Leafy Spurge Symposium*, Fargo, North Dakota, July 25-27, 1995, pp.12-14.

Boardman, J.W., 1991. Sedimentary facies analysis using imaging spectrometry. *Proceedings of the Ninth Thematic Conference on Geologic Remote Sensing,* ERIM, Denver, CO, 29 April-2 May 1991, Ann Arbor, Environmental Research Institute of Michigan, 1189-1199.

Boardman, J.W., 1993. Automating spectral unmixing of AVIRIS data using convex geometry concepts. *Summaries of the Fourth Annual JPL Airborne Geosciences Workshop*, NASA Jet Propulsion Laboratory Special Publication 93-26, Pasadena, CA, 11-14.

Boardman, J.W., 1998. Leveraging the high dimensionality of AVIRIS data for improved sub-pixel target unmixing and rejection of false positives: mixture-tuned matched filtering. *Proceedings of the Seventh Airborne Earth Science Workshop*, NASA Jet Propulsion Laboratory Publication 97-21, Pasadena, CA.

Boardman, J.W. and R.O. Green, 2000. Exploring the spectral variability of the earth as measured by AVIRIS in 1999. *Proceedings of the Ninth Airborne Earth Science Workshop,* NASA Jet Propulsion Laboratory Publication 00-18, Pasadena, CA.

Boardman J. W., and F.A. Kruse, 1994. Automated spectral analysis: A geologic example using AVIRIS data, north Grapevine Mountains, Nevada, *Proceedings, Tenth Thematic Conference on Geologic Remote Sensing*, Environmental Research Institute of Michigan, Ann Arbor, MI, pp. I-407- I-418.

Boardman, J.W., F.A. Kruse, and R.O. Green, 1995. Mapping target signatures via partial unmixing of AVIRIS data. *Summaries of the Fifth JPL Airborne Earth Science Workshop*, NASA Jet Propulsion Laboratory Publication 95-1, Pasadena, CA, 23-26.

Borel, C.C. and S.A.W. Gerstl, 1994. Nonlinear spectral mixing models for vegetative and soil surfaces. *Remote Sensing of Environment* 47:403-416.

Callihan, R.H., J.P. McCaffrey, and V.J. Parker-Clark, 1990. Leafy spurge: biology and management. *The Service*, December 1990. (Series no. 877) 5p. Cooperative Extension System, Agricultural Experiment Station, University of Idaho, Moscow, Idaho.

Carmel, Y., D.J. Dean, and C.H. Flather, 2001. Combining location and classification error sources for estimating multi-temporal database accuracy. *Photogrammetric Engineering and Remote Sensing* 67:865-872.

Carter, G.A., 1993. Responses of leaf spectral reflectance to plant stress. *American Journal of Botany* 80:239-243.

Carter, G.A. and R.L. Miller, 1994. Early detection of plant stress by digital imaging within narrow stress-sensitive wavebands. *Remote Sensing of Environment* 50:295-302.

Chabrillat, S., A.F.H. Goetz, H.W. Olsen, L. Krosley, and D.C. Noe, 2000. The search for swelling clays along the Colorado Front Range: results from field spectrometry and hyperspectral

imagery. *Proceedings of the Ninth Airborne Earth Science Workshop,* NASA Jet Propulsion Laboratory Publication 00-18, Pasadena, CA, 93-100.

Champagne, C.M., K. Staenz, A. Bannari, H. McNairn, and J.-C. Deguise, 2003. Validation of a hyperspectral curve-fitting model for the estimation of plant water content of agricultural canopies. *Remote Sensing of Environment* 87:148-160.

Chen, Z., C.D. Elvidge, and D.P. Groenveld, 1998. Vegetation change detection using high spectral resolution vegetation indices. In: *Remote Sensing Change Detection: Environmental Monitoring Methods and Applications,* R.S. Lunetta and C.D. Elvidge, eds., Ann Arbor Press, Chelsea, Michigan, pp. 181-190.

Chicoine, T. K., P.K. Fay, and G.A. Nielsen, 1985. Predicting weed migration from soil and climate maps. *Weed Science* 34:57-61.

Chopping, M.J., A. Rango, K.M. Havstad, F.R. Schiebe, J.C. Ritchie, T.J. Schmugge, A.N. French, L.Su, L. McKee, and M.R. Davis, 2003. Canopy attributes of desert grassland and transition communities derived from multiangular airborne imagery. *Remote Sensing of Environment* 85:339-354.

Chrisman, N.R., 1989. Modelling error in overlaid categorical maps. In: *The accuracy of spatial databases*, M. Goodchild and S. Gopal, eds., Taylor and Francis, New York, NY, pp. 21-34.

Clark, R.N., 1995. Reflectance spectra. *AGU Handbook of Physical Constants,* pp. 178-188.

Clark, R.N., 1999. Spectroscopy of rocks and minerals, and principles of spectroscopy. In: *Manual of Remote Sensing, Volume 3, Remote Sensing for the Earth Sciences,* A.N. Rencz, ed., John Wiley & Sons, New York, NY, pp. 3-58.

Clark, R.N., T.M. Hoefen, G.A. Swayze, K.E. Livo, G.P. Meeker, S.J. Sutley, S. Wilson, I.K. Brownfield, and J.S. Vance, 2003. Reflectance spectroscopy as a rapid assessment tool for the detection of amphiboles from the Libby, Montana region. *U.S. Geological Survey Open File Report* 03-128.

Clark, R.N., A.J. Gallagher, and G.A. Swayze, 1990. Material absorption band depth mapping of imaging spectrometer data using the complete band shape least squares algorithm simultaneously fit to multiple spectral features from multiple materials. *Proceedings of the Airborne Visible/Infrared Imaging Spectrometer (AVIRIS) Workshop*, NASA Jet Propulsion Laboratory Publication 90-54, Pasadena, CA, 176-186.

Clark, R.N, R.O. Green, G.A. Swayze, G. Meeker, S. Sutley, T.M. Hoefen, K.E. Livo, G. Plumlee, B. Pavri, C. Sarture, S. Wilson, P. Hageman, P. Lamothe, J.S. Vance, J. Boardman, I. Brownfield, C. Gent, L.C. Morath, J. Taggart, P.M. Theodorakos, and M. Adams, 2001. Environmental studies of the World Trade Center area after the September 11, 2001 attack. *USGS Open-File Report* 01-0429, http://pubs.usgs.gov/of/2001/ofr-01-0429/

Clark, R.N., T.V. King, C. Ager, and G. Swayze, 1995. Initial vegetation species and senescence/stress mapping in the San Luis Valley, Colorado using imaging spectrometer data. *Proceedings: Summitville Forum '95*, H.H. Posey, J.A. Pendelton, and D. Van Zyl (eds.), Colorado Geological Survey Special Publication 38, p. 64-69.

Clark, R. N., and Swayze, G. A., 1995. Mapping minerals, amorphous materials, environmental materials, vegetation, water, ice, and snow, and other materials: the USGS Tricorder Algorithm. *Summaries of the Fifth Annual JPL Airborne Earth Science Workshop*, NASA Jet Propulsion Laboratory Publication 95-1, Pasadena, CA, 39-40.

Clark, R.N. and G.A. Swayze, 1996. Evolution in imaging spectroscopy analysis and sensor signal-to-noise: an examination of how far we have come. *Summaries of the Sixth Annual JPL Airborne Earth Science Workshop,* NASA Jet Propulsion Laboratory Publication 96-4, Pasadena, CA, 49-53.

Clark, R.N., G. Swayze, J. Boardman, and F. Kruse, 1993. Comparison of three methods for materials identification and mapping with imaging spectroscopy. *Proceedings of the Fourth Airborne Geoscience Workshop,* NASA Jet Propulsion Laboratory Publication 93-26, Pasadena, CA, 31-33.

Clark, R. N., G.A. Swayze, A. Gallagher, N. Gorelick, and F.A. Kruse, 1991. Mapping with imaging spectrometer data using the complete band shape least squares algorithm simultaneously fit to multiple spectral features from multiple materials. *Proceedings of the Second Airborne Visible/Infrared Imaging Spectrometer (AVIRIS) workshop*, NASA Jet Propulsion Laboratory Publication 91-28, Pasadena, CA, 2-3.

Clark, R.N., G.A. Swayze, K.E. Livo, R.F. Kokaly, T. V.V. King, J.B. Dalton, J.S. Vance, B. W. Rockwell, T. Hoefen, and R.R. McDougal, 2002. Surface reflectance calibration of terrestrial imaging spectroscopy data: a tutorial using AVIRIS data. *Proceedings of the Eleventh Airborne Earth Science Workshop,* JPL Publication 03-4, Pasadena, CA, and U.S. Geological Survey, http://speclab.cr.usgs.gov/PAPERS.calibration.tutorial

Clark, R.N., G.A. Swayze, K.E. Livo, R.F. Kokaly, S.J. Sutley, J.B. Dalton, R.R. McDougal, and C.A. Gent, 2003. Imaging Spectroscopy: Earth and planetary remote sensing with the USGS Tetracorder and expert systems. *Journal of Geophysical Research* 108 (E12):5-1 to 5-44.

Clarke, B., T.H. Painter, W.F. Manley, and E.J. Dixon, 2003. Field spectrometry, sub-pixel resolution of satellite imagery, and archeological potential of the cryosphere. *EOS Trans. American Geophysical Union, 84(46),* Fall Meeting Supplement, Abstract C12A-0871.

Cogan, D.R. and J.L. Butler, 1999. Impacts of leafy spurge on local and landscape patterns of plant species diversity in Theodore Roosevelt National Park. *Leafy Spurge Symposium Proceedings*, Medora, North Dakota, June 26-27, 1999. pp 20-21.

Cohen, W.B. and M. Fiorella, 1998. Comparison of methods for detecting conifer forest change with Thematic Mapper imagery. In: *Remote Sensing Change Detection: Environmental Monitoring Methods and Applications,* R.S. Lunetta and C.D. Elvidge, eds., Ann Arbor Press, Chelsea, Michigan, pp. 89-102.

Congalton, R.G. and K. Green, 1999. *Assessing the Accuracy of Remotely Sensed Data: Principles and Practices,* Lewis Publishers, Boca Raton, FL.

Coppin, P., I. Jonckheere, K. Nackaerts, B. Muys, and E. Lambin, 2004. Digital change detection methods in ecosystem monitoring: a review. *International Journal of Remote Sensing* 25:1565-1596.

Crowley, J.K., D.W. Brickey and L.C. Rowan, 1989. Airborne imaging spectrometer data of the Ruby Mountains, Montana: mineral discrimination using relative absorption band-depth images. *Remote Sensing of Environment* 29:121-134.

Crowley, J.K. and D.R. Zimbelman, 1997. Mapping hydrothermally altered rocks on Mount Rainier, Washington, with Airborne Visible/Infrared Imaging Spectrometer (AVIRIS) data. *Geology* 25:559-563.

CSES, 2000. *Hyperspectral Imaging and Data Analysis Short Course*, Center for the Study of Earth from Space, University of Colorado at Boulder, Boulder, CO.

Curran, P.J., 1989. Remote sensing of foliar chemistry. *Remote Sensing of Environment* 30:271-278.

Curran, P.J., J.L. Dungan, B.A. Macler, S.E. Plummer, and D.L. Peterson, 1992. Reflectance spectroscopy of fresh whole leaves for the estimation of chemical concentration. *Remote Sensing of Environment* 39:153-166.

Dalsted, K., J. Nelson, and J. McCord, 1988. Optimizing the use of aerial photography to map leafy spurge. *1988 Proceedings of Leafy Spurge Annual Meeting*, Rapid City, SD, July 13-14, pp 38-43.

Dalton, J.B., T.V.V. King, D.J. Bove, R.F. Kokaly, R.N. Clark, J.S. Vance, and G.A. Swayze, 1998. Mapping of acid-generating and acid-buffering minerals in the Animas Watershed by AVIRIS spectroscopy. *Proceedings of the Seventh Airborne Earth Science Workshop,* NASA Jet Propulsion Laboratory Publication 97-21, Pasadena, CA.

Demirican, A., B. Geiger, M. Radke, and M. Von Schönermark, 2000. Bi-directional reflectance measurements with the CCD line camera WAAC. *Remote Sensing Reviews* 19:95-110.

Dennison, P.E. and D.A. Roberts, 2003. The effects of vegetation phenology on endmember selection and species mapping in southern California chaparral. *Remote Sensing of Environment* 87:295-309.

Dennison, P.E. and D.A. Roberts, 2004. Examining seasonal changes in canopy moisture using AVIRIS time series data. *Proceedings of the Thirteenth Airborne Earth Science Workshop,* NASA Jet Propulsion Laboratory Publication ???, Pasadena, CA.

Dewey, S.A., K.P. Price, and D. Ramsey, 1991. Satellite remote sensing to predict potential distribution of Dyers wood (*Isatis finctoria*). *Weed Technology* 5:479-484.

DiPietro, D., S. Ustin, and E. Underwood, 2002. Mapping the invasive plant *Arundo donax* and associated riparian vegetation using AVIRIS. *Proceedings of the Eleventh JPL Airborne Earth Science Workshop*, NASA Jet Propulsion Laboratory Publication 03-4, Pasadena, CA, 65-74.

Dudek, K.B., 2002. Multi-temporal imaging spectroscopy of leafy spurge over Theodore Roosevelt National Park, North Dakota. *Spectral Remote Sensing of Vegetation Conference*, US Environmental Protection Agency, National Exposure Research Laboratory, Environmental Sciences Division, 3-5 December, 2002, Las Vegas , NV.

Dudek, K.B., 2005. Modifications of processing to improve the reliability of change maps produced from hyperspectral imagery: a case study using AVIRIS to identify change in leafy spurge between 1999 and 2001 within Theodore Roosevelt National Park, North Dakota. *2005 Annual Meeting of the Association of American Geographers,* April 5-9, 2005, Denver, CO.

Dudek, K.B., R.R. Root, R.F. Kokaly, G.L. Anderson, K.E. Brown, C.S. Mladinich, S.F. Stitt, S.N. Hager, and M.L. Lefsky, 2004. Temporal monitoring of leafy spurge: an example using 1999 and 2001 Airborne Visible/Infrared Imaging Spectrometer (AVIRIS) data over Theodore Roosevelt National Park. *TEAM Leafy Spurge Symposium, 57th Annual Meeting of the Society for Range Management*, January 24-30, 2004, Salt Lake City, UT.

Dudek, K.B., R.R. Root, R.F. Kokaly, G.L. Anderson, 2004. Increased spatial and temporal consistency of leafy spurge maps from multi-date AVIRIS imagery: a modified, hybrid linear spectral mixture analysis (SMA)/mixture-tuned matched filtering (MTMF) approach, *Proceedings of the Thirteenth Airborne Earth Science Workshop,* NASA Jet Propulsion Laboratory Publication, Pasadena, CA.

Dungan, J., L. Johnson, C. Billow, P. Matson, J. Mazzurco, J. Moen, and V. Vanderbilt, 1996. High spectral resolution reflectance of Douglas fir grown under different fertilization treatments: Experiment design and treatment effects. *Remote Sensing of Environment* 55:217-228.

Dunn, P.H., 1985. Origins of leafy spurge in North America. *Leafy Spurge, Monograph series of the Weed Science Society of America*, Alan K. Watson, ed., Chapter 2, 7-13.

Dury, S., B. Turner, B. Foley, and I. Wallis, 2001. Use of high spectral resolution remote sensing to determine leaf palatability of eucalypt trees for folivorous marsupials. JAG: 3, 4, 328-336.

Eastwood, M.L., R.O. Green, C.M. Sarture, B.J. Chippindale, C.J. Chovit, J.A. Faust, D.L. Johnson, S.P. Monacos, and J.J. Raney, 2000. Recent Improvements to the AVIRIS sensor: flight season 2000. *Proceedings of the Ninth Airborne Earth Science Workshop,* NASA Jet Propulsion Laboratory Publication 00-18, Pasadena, CA.

Elliston, R. and L.D. Miller, 1987. Mapping leafy spurge with color video and micro-computer image processing. *Proceedings of the Western Society of Weed Science* 40:61-63.

ENVI User's Guide, 2003. ENVI Version 4.0, September 2003 Edition, Research Systems, Inc., Boulder, CO.

Erickson, B.J., C.J. Johannsen, J.J. Vorst, and L.L. Biehl, 2004. Using remote sensing to assess stand loss and defoliation in maize. *Photogrammetric Engineering and Remote Sensing* 70:717-722.

Evans, J.O. and J.M. Torell, 1986. Leafy spurge: a threat to crops and rangelands in Utah. *Utah Science- Utah Agricultural Experiment Station*, Summer 1986, 47:63-66.

Everitt, J.H., M.A. Alaniz, D.E. Escobar, and M.R. Davis, 1992. Using remote sensing to distinguish common (*Isocoma coronopifolia*) and Drummond goldenweed (*Isocoma drummondii*). *Weed Science* 40:621-628.

Everitt, J.H., G.L. Anderson, D.E. Escobar, M.R. Davis, N.R. Spencer, and R.J. Andrascik, 1995. Use of remote sensing for detecting and mapping leafy spurge (*Euphorbia esula*). *Weed Technology* 9:599-609.

Everitt, J.H., D.E. Escobar, R. Villarreal, M.A. Alaniz, and M.R. Davis, 1993. Canopy light reflectance and remote sensing of shin oak (*Quercus havardii*) and associated vegetation. *Weed Science* 41:291-297.

Everitt, J.H., J.V. Richerson, M.A. Alaniz, D.E. Escobar, R. Villarreal, and M.R. Davis, 1994. Light reflectance characteristics and remote sensing of Big Bend loco (*Astragalus mollissimus* var. *earlei*) and Wooton loco (*Astragalus wootonii*). *Weed Science* 42:115-122.

Farrand, W.H., 2001. Analysis of AVIRIS data: a comparison of the performance of commercial software with published algorithms. *Proceedings of the Tenth Airborne Earth Science Workshop,* NASA Jet Propulsion Laboratory Publication 02-1, Pasadena, CA.

Farrand, W. and S. Blundell, 2004. *Hyperspectral Image Processing and Feature Extraction: Maximizing Geospatial Information Retrieval,* Workshop Twelve Manual, ASPRS 2004 Annual Meeting, Denver, CO.

Farrand, W.H. and J.C. Harsanyi, 1993. Mineralogic variation in fluvial sediments contaminated by mine tailings as determined from AVIRIS data, Coeur D'Alene River Valley, Idaho.

Proceedings of the Fourth Airborne Geoscience Workshop, NASA Jet Propulsion Laboratory Publication 93-26, Pasadena, CA, 47-50.

Farrand, W.H. and J.C. Harsanyi, 1994. Mapping distributed geological and botanical targets through constrained energy minimization. *Proceedings Tenth Thematic Conference on Geologic Remote Sensing*, 419-429.

Farrand, W.H. and J.C. Harsanyi, 1997. Mapping the distribution of mine tailings in the Coeur d'Alene River Valley, Idaho, through the used of a constrained energy minimization technique. *Remote Sensing of Environment* 59:64-76.

Fitzgerald, G.J., S.J. Maas, W.R. DeTar, 2002. Detecting spider mite damage in cotton through spectral mixture analysis of AVIRIS imagery. *Proceedings of the Eleventh Airborne Earth Science Workshop,* NASA Jet Propulsion Laboratory Publication 03-4, Pasadena, CA.

Foody, G.M., 1999. Image classification with a neural network: from completely-crisp to fully-fuzzy situations. In: *Advances in Remote Sensing and GIS Analysis*, P.M. Atkinson and N.J. Tate, eds., John Wiley & Sons, Chichester, England, pp. 17-38.

Foody, G.M., 2002. Status of land cover classification assessment. *Remote Sensing of Environment* 80:185-201.

Foody, G.M., 2004. Thematic map comparison: evaluating the statistical significance of differences in classification accuracy. *Photogrammetric Engineering and Remote Sensing* 70:627-633.

Foster, J.R. and P.A. Townsend, 2002. Mapping forest composition in the central Appalachians using AVIRIS: effects of topography and phenology. *Proceedings of the Eleventh Airborne Earth Science Workshop,* NASA Jet Propulsion Laboratory Publication 03-4, Pasadena, CA.

Frank, M. and M Canty, 2003. Unsupervised change detection for hyperspectral images. *Proceedings of the Twelfth Airborne Earth Science Workshop,* NASA Jet Propulsion Laboratory Publication, Pasadena, CA.

Gaffey, S.J., L.A. McFadden, D. Nash, and C.M. Pieters, 1993. Ultraviolet, visible, and near-infrared reflectance spectroscopy: laboratory spectra of geologic materials. In: *Remote Geochemical Analysis: Elemental and Mineralogical Composition,* C.M. Pieters, and P.A.J. Englert, eds., Cambridge University Press, Cambridge, pp. 43-78.

Galitz, Donald, 1994. The biology of leafy spurge. *Proceedings: Leafy Spurge Strategic Planning Workshop*, Dickinson, North Dakota, March 29-30, 1994. pp. 57-62.

Gamon, J., D. Fuentes, D. Sims, S. Houston, A. Moyes, H.L. Qui, and W. Oechel, 2002. Ecosystem carbon flux in a disturbed, fragmented southern California landscape. *Proceedings of the Eleventh Airborne Earth Science Workshop,* NASA Jet Propulsion Laboratory Publication 03-4, Pasadena, CA.

Gao, B.C., K.B. Heidebrecht, and A.F.H. Goetz, 1993. Derivation of scaled surface reflectances from AVIRIS data. *Remote Sensing of Environment* 44:165-178.

Gao, B., Y.J. Kaufman, and R.O. Green, 1993. Remote sensing of smoke, clouds, and fire using AVIRIS data. *Summaries of the Fourth Airborne Geoscience Workshop,* NASA Jet Propulsion Laboratory Publication 93-26, Pasadena, CA, 61-64.

Garcia, M. and S.L. Ustin, 2001. Detection of interannual vegetation responses to climatic variability using AVIRIS data in a coastal savanna in California. *IEEE Transactions on Geoscience and Remote Sensing* 39:1480-1490.

Gat, N., H. Erives, G.J. Fitzgerald, S.R. Kaffka, and S.J. Maas, 2000. Estimating sugar beet yield using AVIRIS-derived indices. *Proceedings of the Ninth Airborne Earth Science Workshop,* NASA Jet Propulsion Laboratory Publication 00-18, Pasadena, CA.

Gausman, H.W., R.M. Menges, D.E. Escobar, J.H. Everitt, and R.L. Bowen, 1977. Pubescence affects spectra and imagery of silverleaf sunflower (*Helianthus argophyllus*). *Weed Science* 25:437-440.

Geomatica version 9.0 OrthoEngine User Guide, 2003. PCI Geomatics Enterprises, Inc. Richmond Hill, Ontario, Canada.

Glenn, N.F., J.T.Mundt, K.T. Weber, T.S Prather, L.W. Lass, and J. Pettingill, 2005. Hyperspectral data processing for repeat detection of small infestations of leafy spurge. *Remote Sensing of Environment* 95:399-412.

Goetz, A.F.H., 1989. Spectral remote sensing in geology. In: *Theory and applications of Optical Remote Sensing,* G. Asrar, ed., John Wiley & Sons, New York, NY, pp. 491-526.

Goetz, A.F.H. and L.C. Rowan, 1981. Geologic remote sensing, *Science* 211:781-791.

Goetz, A. F. H., G. Vane, J. E. Solomon, and B.N. Rock, 1985. Imaging spectrometry for earth remote sensing. *Science* 228:1147-1153.

Goodman, J.A. and S.L. Ustin, 2001. Hyperspectral image analysis of coral reefs in the Hawaiian Islands. *Proceedings of the Tenth Airborne Earth Science Workshop,* NASA Jet Propulsion Laboratory Publication 02-1, Pasadena, CA.

Graetz, R.D., R.P. Pech, M.R. Gentle, and J.F. O'Callaghan, 1983. The application of Landsat image data to rangeland assessment and monitoring: the development and demonstration of a land image-based resource information system (LIBRIS). *Journal of Arid Environments* 10:53-80.

Green, A.A., M. Berman, P. Switzer, and M.D. Craig, 1988. A transformation for ordering multispectral data in terms of image quality with implications for noise removal. *IEEE Transactions on Geoscience and Remote Sensing* 26:65-74.

Green, R.O., 1996. Estimation of biomass fire temperature and areal extent from calibrated AVIRIS spectra. *Proceedings of the Seventh Annual Airborne Geoscience Workshop,* NASA Jet Propulsion Laboratory Publication 96-16, Pasadena, CA, 105-113.

Green, R.O., R.N. Clark, J. Boardman, B. Pavri, and C. Sarture, 2002. Initial estimates from AVIRIS of the temperature and fractional areas of fires at the World Trade Center disaster. *Proceedings of the Eleventh Airborne Earth Science Workshop,* NASA Jet Propulsion Laboratory Publication 03-4, Pasadena, CA.

Green, R.O., M.L. Eastwood, C.M. Sarture, T.G. Chrien, M. Aronsson, B.J. Chippendale. J.A. Faust, B.E. Pavri, C.J. Chovit, M. Solis, M.R. Olah, and O. Williams, 1998. Imaging spectroscopy and the Airborne Visible/Infrared Imaging Spectrometer. *Remote Sensing of Environment* 65:227-248.

Guinness, E.A., R.E. Arvidson, B.L. Jolliff, K.S. Deal, F.P. Seelos, R.V. Morris, D.W. Ming, and T.G. Graff, 2003. Mapping hydrothermal alteration zones on Mauna Kea using AVIRIS data: an

analog for Mars. *EOS Trans. American Geophysical Union, 84(46),* Fall Meeting Supplement, Abstract P11B-1043.

Han, L. and D.C. Rundquist, 1997. Comparison of NIR/RED ratio and first derivative of reflectance in estimating algal-chlorophyll concentration: a case study in a turbid reservoir. *Remote Sensing of Environment* 62:253-261.

Hapke, B.W., 1981. Bidirectional reflectance spectroscopy, 1. Theory. *Journal of Geophysical Research* 86:3039-3054.

Hapke, B.W., 1986. Bidirectional reflectance spectroscopy, 4. The extinction coefficient and the opposition effect. *Icarus* 67:264-280.

Harrison, L., 2001. Ground truthing remotely sensed leafy spurge infestations at Theodore Roosevelt National Park: methodology for mapping project using global positioning systems and geographic information systems. Unpublished article.

Hauff, P. L., D. W. Coulter, D. C. Peters, M. A. Sares, E. C. Prosh, F. B. Henderson III, and D. Bird, 2003. Using AVIRIS in the NASA BAA Project to evaluate the impact of natural acid drainage on Colorado watersheds. *Proceedings of the Twelfth JPL Airborne Earth Science Workshop*, NASA Jet Propulsion Laboratory Publication 04-6, Pasadena, CA, 121-130.

Hollister, J.W., M.C. Gonzalez, J.F. Paul, P.V. August, and J.L. Copeland, 2004. Assessing the accuracy of National Land Cover dataset area estimates at multiple spatial extents. *Photogrammetric Engineering and Remote Sensing* 70:405-414.

Hunt, Jr., E.R., and A.E. Parker Williams, 2004. Comparison of AVIRIS and multispectral remote sensing for detection of leafy spurge. *Proceedings of the Thirteenth Jet Propulsion Laboratory (JPL) Airborne Earth Science Workshop*, NASA Jet Propulsion Laboratory Publication, Pasadena, CA.

Hunt, G.R., 1980. Electromagnetic radiation: the communication link in remote sensing. In: *Remote Sensing in Geology,* B.S. Siegal and A.R. Gillespie, eds., Wiley, New York, NY, pp. 5-45.

Hurcom, S.J., A.R. Harrison, and M. Taberner, 1996. Assessment of biophysical vegetation properties through spectral decomposition techniques. *Remote Sensing of Environment* 56:203-214.

Hutsinpillar, A., 1988. Discrimination of hydrothermal alteration mineral assemblages at Virginia City, Nevada, using the Airborne Imaging Spectrometer. *Remote Sensing of Environment* 24:53-66.

Hyperspectral Data Analysis and Image Processing Workshop, 2000. Analytical Imaging and Geophysics, LLC, Boulder CO.

Hyperion website: http://eo1.usgs.gov/hyperion.php

Ingle, J.D., 1988. *Spectrochemical Analysis*, Prentice-Hall, Inc., Engelwood Cliffs, New Jersey.

Jacquemoud, S. and F. Baret, 1990. PROSPECT: a model of leaf optical properties spectra. *Remote Sensing of Environment* 34:75-91.

Jacquemoud, S., S.L. Ustin, J. Verdebout, G. Schmuck, G. Andreoli, and B. Hosgood, 1996. Estimating leaf biochemistry using the PROSPECT leaf optical properties model. *Remote Sensing of Environment* 56:94-202.

Jensen, J.R., 1996. *Introductory Digital Image Processing: A Remote Sensing Perspective,* Second Edition, Prentice Hall, New Jersey.

Jia, X. and J.A. Richards, 1993. Binary encoding of imaging spectrometer data for fast spectral matching and classification. *Remote Sensing of Environment* 43:47-53.

Johnson, H.K. and R.O. Green, 1995. AVIRIS user's guide. *Proceedings of the Fourth Airborne Geoscience Workshop,* NASA Jet Propulsion Laboratory Publication 93-26, Pasadena, CA, 105-108.

Karaska, M.A., R.L. Huguenin, J.L. Beacham, M. Wang, J.R. Jensen, and R.S. Kaufmann, 2004. AVIRIS measurements of chlorophyll, suspended minerals, dissolved organic carbon, and turbidity in the Neuse River, North Carolina. *Photogrammetric Engineering and Remote Sensing* 70:125-133.

Kennedy, R.E. and W.B. Cohen, 2002. Automated designation of tie-points for image-to-image coregistration. *International Journal of Remote Sensing* 24:3467-3490.

Kennedy, R. E., W. B. Cohen, and G. Takao, 1997. Empirical methods to compensate for a view-angle-dependent brightness gradient in AVIRIS imagery. *Remote Sensing of Environment* 62:277-291.

Kennedy, R. E., W. B. Cohen, and G. Takao, 1998. A BRDF-related brightness gradient in AVIRIS imagery: lessons learned from an empirical compensation method. *Proceedings of the Seventh Airborne Earth Science Workshop,* NASA Jet Propulsion Laboratory Publication 97-21, Pasadena, CA.

Kennedy-Bowdoin, T.J., E.A. Silver, B.A. Martini, and W.L. Pickles, 2003. Understanding the chemical and structural dynamics of a geothermal system using hyperspectral imaging and field observations, Dixie Meadows, Nevada. *EOS Trans. American Geophysical Union, 84(46),* Fall Meeting Supplement, Abstract V51H-0367.

Keshava, N., and J.F. Mustard, 2002. Spectral unmixing. *IEEE Signal Processing Magazine* 19: 44-57.

King, T.V.V., R.N. Clark, C. Ager, and G.A. Swayze, 1995. Remote mineral mapping using AVIRIS data at Summitville, Colorado and the adjacent San Juan Mountains. *Proceedings of the Fourth Airborne Geoscience Workshop,* NASA Jet Propulsion Laboratory Publication 93-26, Pasadena, CA, 113-116.

Kokaly, R.F., 2000. Investigating a physical basis for spectroscopic estimates of leaf nitrogen concentration. *Remote Sensing of Environment* 75:153-161.

Kokaly, R.F. and R.N. Clark, 1999. Spectroscopic determination of leaf biochemistry using band-depth analysis of absorption features and stepwise multiple linear regression. *Remote Sensing of Environment* 67:267-287.

Kokaly, R.F., R.N. Clark, and K.E. Livo, 1998. Mapping the biology and mineralogy of Yellowstone National Park using imaging spectroscopy. *Summaries of the Seventh Annual JPL Airborne Earth Science Workshop*, NASA Jet Propulsion Laboratory Publication 97-21, Pasadena, CA, 245-254.

Kokaly, R.F., R. Root, and K. Brown, 2001. Mapping the distribution of the invasive species leafy spurge (Euphorbia esula) in Theodore Roosevelt National Park using field measurements of vegetation spectra and CASI imaging spectroscopy data. *Third International Conference on Geospatial Information in Agriculture and Forestry*, Denver, CO, 5-7 November, 2001.

Kooistra, L., R. Wehrens, M.C. Lutgarde, R. Buydens, S.E.W. Leuven, and P.H. Nienhuis, 2001. Possibilities of soil spectroscopy for the classification of contaminated areas in river floodplains. *JAG* 3, 4:337-344.

Kruse, F.A., 1988. Use of airborne imaging spectrometer data to map minerals associated with hydrothermally altered rocks in the northern Grapevine Mountains, Nevada and California. *Remote Sensing of Environment* 24:31-52.

Kruse, F. A., 2003. Preliminary results- hyperspectral mapping of coral reef systems using EO-1 Hyperion, Buck Island, U.S. Virgin Islands. *Proceedings of the Twelfth JPL Airborne Earth Science Workshop*, NASA Jet Propulsion Laboratory Publication 04-6, Pasadena, CA, 157-174.

Kruse, F. A., Lefkoff, A. B., Boardman, J. B., Heidebrecht, K. B., Shapiro, A. T., Barloon, P. J., and Goetz, A. F. H., 1993a. The Spectral Image Processing System (SIPS) - Interactive Visualization and Analysis of Imaging Spectrometer Data. *Remote Sensing of Environment*, Special issue on AVIRIS, 44:145-163.

Kruse, F. A., Lefkoff, A. B., and Dietz, J. B., 1993b. Expert System-Based Mineral Mapping in northern Death Valley, California/Nevada using the Airborne Visible/Infrared Imaging Spectrometer (AVIRIS). *Remote Sensing of Environment,* Special issue on AVIRIS, 44:309 - 336.

Kupiec, J., G.M. Smith, and P.J. Curan, 1993. AVIRIS spectra correlated with the chlorophyll concentration of a forest canopy. *Proceedings of the Fourth Airborne Earth Science Workshop*, NASA Jet Propulsion Laboratory Publication 93-26, Pasadena, CA, 105-108.

Laba, M., F. Tsai, D. Ogurcak, S. Smith, and M.E. Richmond, 2005. Field determination of optimal dates for the discrimination of invasive wetland plant species using derivative spectral analysis. *Photogrammetric Engineering and Remote Sensing* 71:603-611.

Lajeunesse, S., R. Sheley, R. Lym, D. Cooksey, C. Duncan, J. Lacey, N. Rees, and M. Ferrell, 1997. Leafy spurge: biology, ecology, and management, July 1997, EB-134, 25p., Montana State University Extension Service.

Larson, D.L., and J.B. Grace, 2004. Temporal dynamics of leafy spurge (*Euphorbia esula*) and two species of flea beetles (*Aphthona* spp.) used as biological control agents. *Biological Control* 29:207-214.

Lee, J.B., A.S. Woodyatt, and M. Berman, 1990. Enhancement of high spectral resolution remote sensing data by a noise-adjusted principal components transform. *IEEE Transactions on Geoscience and Remote Sensing* 28:295-304.

Lee, K.-S. and W.B. Cohen, 2002. Comparison of AVIRIS and Landsat ETM+ for the estimation of leafy area index. *Proceedings of the Eleventh JPL Airborne Earth Science Workshop*, NASA Jet Propulsion Laboratory Publication 03-4, Pasadena, CA.

Legleiter, C.J., D.A. Roberts, W.A. Marcus, and M.A. Fonstad, 2004. Passive optical remote sensing of river channel morphology and in-stream habitat: physical basis and feasibility. *Remote Sensing of Environment* 93:493-510.

Leitch, J.A., L. Leistritz, and D.A. Bangsund, 1994. Economic effect of leafy spurge in the upper Great Plains: Methods, models, and results. Agricultural Economics Report No. 316, March 1994. Department of Agricultural Economics, Agricultural Experiment Station, North Dakota State University, Fargo, North Dakota.

Lillesand, T.M. and R.W. Kiefer, 2000. *Remote Sensing and Image Interpretation*, 4th edition, John Wiley & Sons, Inc., New York, NY.

Loveland, T.R., Z. Xhu, D.O. Ohlen, J.F. Braun, B.C. Reed, and L. Yang, 1999. An analysis of the IGBP global land cover characterization process. *Photogrammetric Engineering and Remote Sensing* 65:1021-1032.

Lunetta, R.S., 1998. Applications, project formulation, and analytical approach. In: *Remote Sensing Change Detection: Environmental Monitoring Methods and Applications*, R.S. Lunetta and C.D. Elvidge, eds., Ann Arbor Press, Chelsea, Michigan, pp. 1-19.

Lym, R.G., 1998. The biology and integrated management of leafy spurge (Euphorbia esula) on North Dakota rangeland. *Weed Technology* 12:367-373.

Lym, R.G. and C.G. Messersmith, 1984. Leafy spurge- a nemesis of the Great Plains. *Weeds Today* 15:8-10.

Lym, R.G. and R.K. Zollinger, 1995. Integrated management of leafy spurge. *North Dakota State University Extension Service W-866,* March, 1995, http://ndsuext.nodak.edu/extpubs/plantsci/weeds/w866w.htm.

Mackin, S., N. Drake, J. Settle, and S. Briggs, 1991. Curve shape matching, end-member selection and mixture modeling of AVIRIS and GER data for mapping surface mineralogy and vegetation communities. *Proceedings of the Third Airborne Geoscience Workshop,* NASA Jet Propulsion Laboratory Publication 92-41, Pasadena, CA, 158-162.

Manners, G.D.,1983. The chemistry and allelopathy of *Euphorbia esula*. *1983 Leafy Spurge Symposium Proceedings*, Sundance, WY, June 21-22. pp. 66-72.

Marcus, W.A., C.J. Legleiter, R.J. Aspinall, J.W. Boardman, and R.L. Crabtree, 2003. High spatial resolution hyperspectral mapping of in-stream habitats, depths, and woody debris in mountain streams. *Geomorphology* 55:363-380.

Martin, M.E. and J.D. Aber, 1993. Measurements of canopy chemistry with 1992 AVIRIS data at Blackhawk Island and Harvard Forest. *Proceedings of the Fourth JPL Airborne Earth Science Workshop*, NASA Jet Propulsion Laboratory Publication 93-26, Pasadena, CA, 113-116.

Martin, M.E. and J.D. Aber, 1997. High spectral resolution remote sensing of forest canopy lignin, nitrogen and ecosystem process. *Ecological Applications* 7:431-443.

Martin, M.E., S.D. Newman, J.D. Aber, and R.G. Congalton, 1998. Determining forest species composition using high spectral resolution remote sensing data. *Remote Sensing of Environment* 65:249-254.

Martini, B.A. and E.A Silver, 2002. The evolution and present state of tree-kills on Mammoth Mountain, California: tracking volcanogenic CO_2 and its lethal effects. *Proceedings of the Eleventh JPL Airborne Earth Science Workshop*, NASA Jet Propulsion Laboratory Publication 03-4, Pasadena, CA.

Mather, P.M., 1999. Land cover classification revisited. In: *Advances in Remote Sensing and GIS Analysis*, P.M. Atkinson and N.J. Tate, eds., John Wiley & Sons, Chichester, England, pp. 7-16.

Mazer, A. S., M. Martin, M. Lee, and J.E. Solomon, 1988. Image processing software for imaging spectrometry data analysis. *Remote Sensing of Environment* 24:201-210.

Meroni, M. R. Colombo, and C. Panigada, 2004. Inversion of a radiative transfer model with hyperspectral observations for LAI mapping in poplar plantations. *Remote Sensing of Environment* 92:195-206.

Merton, R.N. and E.A. Silver, 2000. Tracking vegetation spectral trajectories with multi-temporal hysteresis models. *Proceedings of the Ninth Airborne Earth Science Workshop,* NASA Jet Propulsion Laboratory Publication 00-18, Pasadena, CA, 309-318.

Messersmith, C.G., R.G. Lym, and D.S. Galitz, 1985. Biology of leafy spurge. *Leafy Spurge, Monograph series of the Weed Science Society of America.* Alan K. Watson, ed., Chapter 5 (3):42-56.

Metternicht, G.I. and J.A. Zinck, 2003. Remote sensing of soil salinity: potentials and constraints. *Remote Sensing of Environment* 85:1-20.

Miller, L.D. and R. Elliston, 1987. Mapping leafy spurge with airborne color video and microcomputer image processing. *1987 Leafy Spurge Annual Meeting*, Fargo, North Dakota, July 8-9, 1987, p.5.

Myhre, R.J., 1983. Mapping leafy spurge communities from aerial photography. *1983 Leafy Spurge Symposium Proceedings*, Sundance, WY, June 21-22, p.52.

Myhre, R.J., 1987. Applications of aerial photography to several new and unusual vegetation pest problems. *Proceedings Tenth Biennial Workshop on Color Aerial Photography in the Plant Sciences,* American Society for Photogrammetry and Remote Sensing, Falls Church, VA, 49-53.

Okada, K. and A. Iwashita, 1992. Hyper-multispectral image analysis based on waveform characteristics of spectral curve. *Advanced Space Research* 12:433-442.

O'Neill, M., S.L. Ustin, S. Hager, and R. Root, 2000. Mapping the distribution of leafy spurge at Theodore Roosevelt National Park using AVIRIS. *Proceedings of the Ninth JPL Airborne Earth Science Workshop*, NASA Jet Propulsion Laboratory Publication 00-18, Pasadena, CA, 339-347.

Ong, C. and T. Cudahy, 2002. Deriving quantitative monitoring data related to acid drainage using multi-temporal hyperspectral data. *Proceedings of the Eleventh Airborne Earth Science Workshop,* NASA Jet Propulsion Laboratory Publication 03-4, Pasadena, CA.

Painter, T.H., J. Dozier, D.A. Roberts, R.E. Davis, R.O. Green, 2003. Retrieval of subpixel snow-covered area and grain size from imaging spectrometer data. *Remote Sensing of Environment* 85:64-77.

Parker Williams, A. and E.R. Hunt, Jr., 2002a. Estimation of leafy spurge cover from hyperspectral imagery using mixture tuned matched filtering. *Remote Sensing of Environment* 82: 446-456.

Parker Williams, A. and E.R. Hunt, Jr., 2002b. Using AVIRIS imagery to map invasive plants on rangelands: Leafy spurge in northeastern Wyoming. *Proceedings of the Eleventh JPL Airborne Earth Science Workshop*, NASA Jet Propulsion Laboratory Publication 03-4, Pasadena, CA.

Parker Williams, A. and E.R. Hunt, Jr., 2004. Accuracy assessment for detection of leafy spurge with hyperspectral imagery. *Journal of Range Management* 57:106-112.

Pellikka, P., 1996. Illumination compensation for aerial video images to increase land cover classification accuracy in mountains. *Canadian Journal of Remote Sensing* 22:368-381.

Penn, B.S., 2001. Band ratios as a reconnaissance tool for hyperspectral data. *Proceedings of the Tenth Airborne Earth Science Workshop,* NASA Jet Propulsion Laboratory Publication 02-1, Pasadena, CA, 245-255.

Perry, E.M., M. Gardner, J. Tagestad, D. Roberts, P. Cassady, J. Smith, and D. Nichols, 2000. Effects of image resolution and uncertainties on reflectance-derived crop stress indicators. *Proceedings of the Ninth Airborne Earth Science Workshop,* NASA Jet Propulsion Laboratory Publication 00-18, Pasadena, CA.

Plaza, A., P. Martinez, R.M. Perez, and J. Plaza, 2002. A comparative analysis of endmember extraction algorithms using AVIRIS hyperspectral imagery. *Proceedings of the Eleventh Airborne Earth Science Workshop,* NASA Jet Propulsion Laboratory Publication 03-4, Pasadena, CA.

Price, J.C., 1997. Spectral band selection for visible-near infrared remote sensing: spectral-spatial resolution tradeoffs. *IEEE Transactions on Geoscience and Remote Sensing* 35:1277-1285.

Qi. J., M.S. Moran, F. Cabot, and G. Dedieu, 1995. Normalization of sun/view angle effects using spectral albedo-based vegetation indices. *Remote Sensing of Environment* 52:207-217.

Ragona, D.E., B. Minster, Y. Fialko, and T. Rockwell, 2003. Hyperspectral analysis of paleoseismic trench stratigraphy: toward improving the recognition and documentation of past earthquakes. *EOS Trans. American Geophysical Union, 84(46),* Fall Meeting Supplement, Abstract S12B-0393.

Rahman, A.F., J.A. Gamon, D.A. Fuentes, D. Roberts, D. Prentiss, and H. Qiu, 2000. Modelling CO_2 flux of boreal forests using narrow-band indices from AVIRIS imagery. *Proceedings of the Ninth Airborne Earth Science Workshop*, NASA Jet Propulsion Laboratory Publication 00-18, Pasadena, CA.

Ranson, K.J., Biehl, L.L., and M.E. Bauer, 1985a. Variation in spectral response of soybeans with respect to illumination, view, and canopy geometry. *International Journal of Remote Sensing* 6:1827-1842.

Ranson, K.J., C.S.T. Daughtry, L.L. Biehl, and M.E. Bauer, 1985b. Sun-view angle effects of reflectance factors of corn canopies. *Remote Sensing of Environment* 18:147-11.

Ray, T.W. and B.C. Murray, 1996. Nonlinear spectral mixing in desert vegetation. *Remote Sensing of Environment* 55:59-64.

Riaza, A., P. Strobl, U. Beisl, A. Hausold, and A. Muller, 2001. Spectral mapping of rock weathering degrees on granite using hyperspectral DAIS 7915 spectrometer data. *JAG* 3, 4:345-354.

Roberts, D.A., S.T. Batista, J.L.G. Pereira, E.K. Waller, and B.W. Nelson, 1998. Change identification using multitemporal spectral mixture analysis: applications in eastern Amazonia. In: *Remote Sensing Change Detection: Environmental Monitoring Methods and Applications,* R.S. Lunetta and C.D. Elvidge, eds., Ann Arbor Press, Chelsea, Michigan, pp. 137-161.

Roberts, D., K. Brown, R. Green, S. Ustin, and T. Hinckley, 1998. Investigating the relationship between liquid water and leaf area index in clonal *Populus*. *Proceedings of the Seventh Airborne Geoscience Workshop*, NASA Jet Propulsion Laboratory Publication 97-21, Pasadena, CA.

Roberts, D.A., M. Gardner, R. Church, S. Ustin, G. Scheer, and R.O. Green, 1998. Mapping chaparral in the Santa Monica Mountaina using multiple endmember spectral mixture models. *Remote Sensing of Environment* 65:267-279.

Roberts, D.A., R.O. Green, and J.B. Adams, 1997. Temporal and spatial patterns in vegetation and atmospheric properties from AVIRIS. *Remote Sensing of Environment* 62:223-240.

Root, R. and R. Kokaly, (in preparation). Calibration of 2001 AVIRIS data Theodore Roosevelt National Park and Little Missouri National Grassland.

Root, R., S. Ustin, P. Zarco-Tejada, C. Pinilla, R. Kokaly, G. Anderson, K. Brown, K. Dudek, S. Hager, and E. Holroyd, 2002. Comparison of AVIRIS and EO-1 Hyperion for classification and mapping of invasive leafy spurge in Theodore Roosevelt National Park. *Proceedings of the Eleventh Jet Propulsion Laboratory (JPL) Airborne Earth Science Workshop,* NASA Jet Propulsion Laboratory Publication 03-4, Pasadena, CA.

Root, R. and D. Wickland, 2001. Hyperspectral technology transfer to the U.S. Department of Interior: summary of results of the NASA/DOI Hyperspectral Technology Transfer Project. *Proceedings of the Tenth Airborne Earth Science Workshop,* NASA Jet Propulsion Laboratory Publication 02-1, Pasadena, CA.

Rowan, L.C., J.K. Crowley, R.G. Schmidt, J.C. Mars, and C.M. Ager, 1998. Mapping chestnut oak forest associated with silicified hydrothermally altered rocks in the Carolina slate belt using Airborne Visible/Infrared Imaging Spectrometer (AVIRIS) data. *Proceedings of the Seventh Airborne Geoscience Workshop,* NASA Jet Propulsion Laboratory Publication 97-21, Pasadena, CA.

RSI, 2002. *Spectral Analysis with ENVI,* Research Systems, Inc., Boulder, CO.

Sabol Jr., D.E., D.A. Roberts, J.B. Adams, M.O. Smith, 1993. Mapping and monitoring changes in vegetation communities of Jasper Ridge, CA, using spectral fractions derived from AVIRIS images. *Proceedings of the Fourth Airborne Geoscience Workshop,* NASA Jet Propulsion Laboratory Publication 93-26, Pasadena, CA, 157-160.

Sabol Jr., D.E., M.O. Smith, J.B. Adams, J.H. Zukin, C.J. Tucker, D.A. Roberts, and A.R. Gillespie, 1995. AVIRIS spectral trajectories for forested areas of the Gifford Pinchot National Forest. *Proceedings of the Fourth Airborne Geoscience Workshop,* NASA Jet Propulsion Laboratory Publication 93-26, Pasadena, CA, 133-136.

Sathyendranath, S., D.V. Subba Rao, Z. Chen, V. Stuart, T. Platt, G.L. Bugden, W. Jones, and P. Vass, 1997. Aircraft remote sensing of toxic phytoplankton blooms: a case study from Cardigan River, Prince Edward Island. *Canadian Journal of Remote Sensing* 23:15-23.

Scepan, J., 1999. Thematic validation of high-resolution global land-cover data sets. *Photogrammetric Engineering and Remote Sensing* 65:1051-1060.

Schmidt, K.S. and A.K. Skidmore, 2003. Spectral discrimination of vegetation types in a coastal wetland. *Remote Sensing of Environment* 85:92-108.

Schmidt, K.S., A.K. Skidmore, E.H. Kloosterman, H. van Oosten, L. Kumar, and J.A.M. Janssen, 2004. Mapping coastal vegetation using an expert system and hyperspectral imagery. *Photogrammetric Engineering and Remote Sensing* 70:703-715.

Schott, J.R., 1997. *Remote Sensing: The Image Chain Approach*, Oxford University Press, Inc., New York, NY.

Settle, J.J. and N.A. Drake, 1993. Linear mixing and the estimation of ground cover proportions. *International Journal of Remote Sensing* 14:1159-1177.

Sisk, Robert L., and Jan Tysdal-Sisk, 2000. *Common Plants of Theodore Roosevelt National Park.* Theodore Roosevelt Nature & History Association, Medora North Dakota.

Smith, K.L., M.D. Steven, and J.J. Colls, 2004. Use of derivative ratios in the red-edge region to identify plant stress responses to gas leaks. *Remote Sensing of Environment* 92:207-217.

Spruce, J.P., 2001. Low-altitude AVIRIS data for mapping land cover in Yellowstone National Park: use of ISODATA clustering techniques. *Proceedings of the Tenth Airborne Earth Science Workshop,* NASA Jet Propulsion Laboratory Publication 02-1, Pasadena, CA.

Spruce, J.P., E.G. Otvos, and M.J, Giardino, 2002. Low-altitude AVIRIS data for mapping landform types on west Ship Island, Mississippi. *Proceedings of the Eleventh Airborne Earth Science Workshop,* NASA Jet Propulsion Laboratory Publication 03-4, Pasadena, CA.

Swayze, G.A., R.N. Clark, R.M. Pearson, and K.E. Livo, 1996. Mapping acid-generating minerals at the California Gulch Superfund Site in Leadville, Colorado using imaging spectroscopy. *Proceedings of the Sixth Airborne Earth Science Workshop,* NASA Jet Propulsion Laboratory Publication 96-4, Pasadena, CA, 231-234.

Swayze, G.A., R.N. Clark, K.S. Smith, P.L. Hageman, S.J. Sutley, R.M. Pearson, G.S. Rust, P.H. Briggs, A.L. Meier, M.J. Singleton, and S. Roth, 1998. Using imaging spectroscopy to cost-effectively locate acid-generating minerals at mine sites: an example from the California Gulch Superfund Site in Leadville, Colorado. *Proceedings of the Seventh Airborne Earth Science Workshop,* NASA Jet Propulsion Laboratory Publication 97-21, Pasadena, CA.

Thenkabail, P.S., 2001. Strengths and limitations of hyperspectral and hyperspatial datasets in study of agricultural crops. *Proceedings Third International Conference on Geospatial Information in Agriculture and Forestry,* 5-6 November, 2001, Denver, CO, Veridian, Ann Arbor, MI.

Thenkabail, P.S., R.B. Smith, and E. De Pauw, 2000. Hyperspectral vegetation indices and their relationships with agricultural crop characteristics. *Remote Sensing of Environment* 71:158-182.

THRO Natural History Page: http://www.theodore.roosevelt.national-park.com/nat.htm

Townsend, J.R.G., C.O. Justice, C. Gurney, and J. McManus, 1992. The impact of misregistration on change detection. *IEEE Transactions on Geoscience and Remote Sensing* 30:1054-1060.

Townsend, P. A. and J. R. Foster, 2002. Terrain normalization of AVIRIS and Hyperion imagery in forested landscapes. *Proceedings of the Eleventh JPL Airborne Earth Science Workshop,* NASA Jet Propulsion Laboratory Publication 03-4, Pasadena, CA.

Tueller, P.T., 1982. Remote sensing for range management. In: *Remote Sensing for Resource Management,* C.J. Johannsen and J.L. Sanders, eds., Soil Conservation Society of America, Ankeny, IO, 125-140.

Underwood, E., S. Ustin, and D. Dipietro, 2002. Mapping non-native plants using hyperspectral imagery. *Proceedings of the Eleventh Airborne Earth Science Workshop,* NASA Jet Propulsion Laboratory Publication 03-4, Pasadena, CA.

Ustin, S.L., D.A. Roberts, and Q.J. Hart, 1998b. Seasonal vegetation patterns in a California coastal savanna derived from Advanced Visible/Infrared Imaging Spectrometer (AVIRIS) data. In: *Remote Sensing Change Detection: Environmental Monitoring Methods and Applications,* R.S. Lunetta and C.D. Elvidge, eds., Ann Arbor Press, Chelsea, Michigan, pp. 163-180.

Ustin, S.L., R.A. Roberts, J Pinzón, S. Jacquemoud, M. Gardner, G. Scheer, C.M. Castañeda, and A. Palacios-Orueta, 1998a. Estimating canopy water content of chaparral shrubs using optical methods. *Remote Sensing of Environment* 65:280-291.

Ustin, S.L., M.O. Smith, and J.B. Adams, 1992. Multitemporal diurnal AVIRIS images of a forested ecosystem. *Proceedings of the Third Annual Airborne Geoscience Workshop*, NASA Jet Propulsion Laboratory Publication 92-41, Pasadena CA, 141-143.

van Aardt, J.A.N. and R.H. Wynne, 2001. Spectral separability among six southern tree species. *Photogrammetric Engineering and Remote Sensing* 67:1367-1375.

Van Bruggen, Theodore, 1992. *Wildflowers Grasses and Other Plants of the Northern Plains and Black Hills*. Badlands Natural History Association, Interior, South Dakota.

Vanderbilt, V.C., V.G. Ambrosia, and S.L. Ustin, 1998. Diurnal reflectance changes in vegetation observed with AVIRIS. *Proceedings of the Seventh Airborne Geoscience Workshop,* NASA Jet Propulsion Laboratory Publication 97-21, Pasadena, CA.

van der Meer, F., 1994a. Extraction of mineral absorption features from high-spectral resolution data using non-parametric geostatistical techniques. *International Journal of Remote Sensing* 15:2193-2214.

van der Meer, F., 1994b. Sequential indicator conditional simulation and indicator kriging applied to discrimination of dolomitization in GER 63-channel Imaging Spectrometer data. *Nonrenewable Resources* 3:146-164.

van der Meer, F., 1996. Performance characteristics of the Indicator Classifier tested on simulated image data. *International Journal of Remote Sensing* 17:621-627.

van der Meer, F., 1999. Geostatistical approaches for image classification and assessment of uncertaintiy in geologic processing. In: *Advances in Remote Sensing and GIS Analysis,* P.M. Atkinson and N.J. Tate, eds., John Wiley & Sons Ltd, Chichester, England, pp. 147-166.

Vane, G., A.F.H. Goetz, and J.B. Wellman, 1984. Airborne imaging spectrometer - A new tool for remote sensing. *IEEE Transactions on Geoscience and Remote Sensing*, 22:546-549.

Vane, G., and A.F.H. Goetz, 1988. Terrestrial imaging spectroscopy. *Remote Sensing of Environment* 24:1-29.

Vane, G. and A.F.H. Goetz, 1993. Terrestrial imaging spectrometry: current status, future trends. *Remote Sensing of Environment* 44:117-126.

Viers, J.H., C.T. Sailer, C.M. Ramirez, J.F. Quinn, and M.L. Johnson, 2002. An integrated approach to the discrimination of riparian vegetation in the Navarro River watershed, Mendocino County, California, USA. *Proceedings of the Eleventh JPL Airborne Earth Science Workshop*, NASA Jet Propulsion Laboratory Publication 03-4, Pasadena, CA.

Wallace, N. M., J.A. Leitch, and F.L. Leistritz, 1992. Economic impact of leafy spurge on North Dakota wildland. *NDSU Agricultural Economics Report* No. 281, 23 p., North Dakota Agricultural Experiment Station, North Dakota State University, Fargo, ND.

Wang, H. and E.C. Ellis, 2005. Image misregistration error in change measurements. *Photogrammetric Engineering and Remote Sensing* 71:1037-1044.

Wass, P.D., S.D. Marks, J.W. Finch, G.J.L. Leeks, and J.K. Ingram, 1997. Monitoring and preliminary interpretation of in-river turbidity and remote sensed imagery for suspended sediment transport studies in the Humber catchment. *The Science of the Total Environment* 194/195:263-283.

Watson, A.K., 1985. Introduction- The leafy spurge problem. *Leafy spurge, Monograph series of the Weed Science Society of America*, Alan K. Watson, ed., Chapter 1 (3):1-6.

Weber, K.T., 2001. A method to incorporate phenology into land cover change analysis. *Journal of Range Management* 54:A1-A7.

Wessman, C.A., J.D. Aber, and D.L. Peterson, 1989. An evaluation of imaging spectroscopy for estimating forest canopy chemistry. *International Journal of Remote Sensing* 10:1293-1316.

Wessman, C.A., C.A. Bateson, B. Curtis, and T.L. Benning, 1993. A comparison of spectral mixture analysis and NDVI for ascertaining ecological variables. *Proceedings of the Fourth Annual Airborne Geoscience Workshop,* NASA Jet Propulsion Laboratory Publication 93-26, Pasadena, CA, 193-196.

Whiting, M.L. and S.L. Ustin, 1999. Use of low altitude AVIRIS data for identifying salt affected soil surfaces in western Fresno County, California. *Proceedings of the Eighth JPL Airborne Earth Science Workshop,* NASA Jet Propulsion Laboratory Publication 99-17, Pasadena, CA, 443-450.

Yuan, D., C.D. Elvidge, and R.S. Lunetta, 1998. Survey of multispectral methods for land cover change analysis. In: *Remote Sensing Change Detection: Environmental Monitoring Methods and Applications,* R.S. Lunetta and C.D. Elvidge, eds., Ann Arbor Press, Chelsea, Michigan, pp. 21-39.

Yuhas, R.H., J.W. Boardman, and A.F.H. Goetz, 1993. Determination of semi-arid landscape endmembers and seasonal trends using convex geometry spectral unmixing techniques. *Summaries of the Fourth Annual JPL Airborne Geoscience Workshop,* NASA Jet Propulsion Laboratory Publication 93-26, Pasadena, CA, 205-208.

Yuhas, R., A. Goetz, and J.W. Boardman, 1992. Discrimination among semi-arid landscape endmembers using the spectral angle mapper (SAM) algorithm. *Summaries of the Third Annual JPL Airborne Geoscience Workshop,* NASA Jet Propulsion Laboratory Publication 92-41, Pasadena, CA, 147-149.